HENRIK SCHULZE
CHRISTIAN LÜDERS

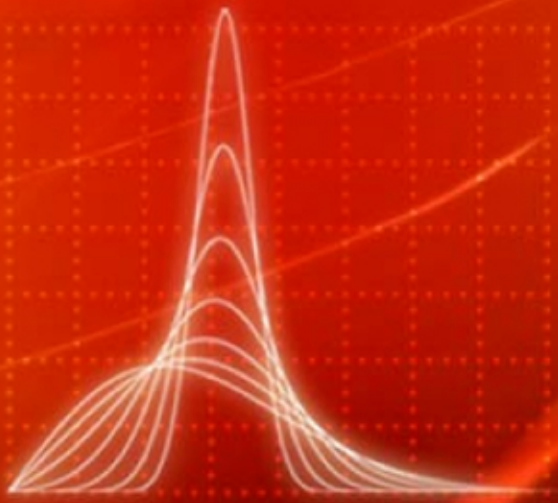

THEORY AND APPLICATIONS OF OFDM AND CDMA

WIDEBAND WIRELESS COMMUNICATIONS

WILEY

Companion Website

Theory and Applications of OFDM and CDMA

Theory and Applications of OFDM and CDMA

Wideband Wireless Communications

Henrik Schulze
and
Christian Lüders

Both of
Fachhochschule Südwestfalen
Meschede, Germany

John Wiley & Sons, Ltd

John Wiley & Sons Ltd, The Atrium, Southern Gate, Chichester,
West Sussex PO19 8SQ, England

Telephone (+44) 1243 779777

Email (for orders and customer service enquiries): cs-books@wiley.co.uk
Visit our Home Page on www.wiley.com

Other Wiley Editorial Offices

John Wiley & Sons Inc., 111 River Street, Hoboken, NJ 07030, USA

Jossey-Bass, 989 Market Street, San Francisco, CA 94103-1741, USA

Wiley-VCH Verlag GmbH, Boschstr. 12, D-69469 Weinheim, Germany

John Wiley & Sons Australia Ltd, 42 McDougall Street, Milton, Queensland 4064, Australia

John Wiley & Sons (Asia) Pte Ltd, 2 Clementi Loop #02-01, Jin Xing Distripark, Singapore 129809

John Wiley & Sons Canada Ltd, 22 Worcester Road, Etobicoke, Ontario, Canada M9W 1L1

Wiley also publishes its books in a variety of electronic formats. Some content that appears in print may not be available in electronic books.

British Library Cataloguing in Publication Data

A catalogue record for this book is available from the British Library

ISBN-13 978-0-470-85069-5 (HB)
ISBN-10 0-470-85069-8 (HB)

Typeset in 10/12pt Times by Laserwords Private Limited, Chennai, India.
Printed and bound in Great Britain by Antony Rowe Ltd, Chippenham, Wiltshire.
This book is printed on acid-free paper responsibly manufactured from sustainable forestry in which at least two trees are planted for each one used for paper production.

Contents

Preface

Wireless communication has become increasingly important not only for professional applications but also for many fields in our daily routine and in consumer electronics. In 1990, a mobile telephone was still quite expensive, whereas today most teenagers have one, and they use it not only for calls but also for data transmission. More and more computers use wireless local area networks (WLANs), and audio and television broadcasting has become digital.

Many of the above-mentioned communication systems make use of one of two sophisticated techniques that are known as *orthogonal frequency division multiplexing* (OFDM) and *code division multiple access* (CDMA).

The first, OFDM, is a digital multicarrier transmission technique that distributes the digitally encoded symbols over several *subcarrier* frequencies in order to reduce the symbol clock rate to achieve robustness against long echoes in a multipath radio channel. Even though the spectra of the individual subcarriers overlap, the information can be completely recovered without any interference from other subcarriers. This may be surprising, but from a mathematical point of view, this is a consequence of the *orthogonality* of the base functions of the Fourier series.

The second, CDMA, is a multiple access scheme where several users share the same physical medium, that is, the same frequency band at the same time. In an ideal case, the signals of the individual users are *orthogonal* and the information can be recovered without interference from other users. Even though this is only approximately the case, the concept of *orthogonality* is quite important to understand why CDMA works. It is due to the fact that pseudorandom sequences are approximately orthogonal to each other or, in other words, they show good correlation properties. CDMA is based on *spread spectrum*, that is, the spectral band is *spread* by multiplying the signal with such a pseudorandom sequence. One advantage of the enhancement of the bandwidth is that the receiver can take benefit from the multipath properties of the mobile radio channel.

OFDM transmission is used in several digital audio and video broadcasting systems. The pioneer was the European DAB (Digital Audio Broadcasting) system. At the time when the project started in 1987, hardly any communication engineers had heard about OFDM. One author (Henrik Schulze) remembers well that many practical engineers were very suspicious of these rather abstract and theoretical underlying ideas of OFDM. However, only a few years later, the DAB system became the leading example for the development of the digital terrestrial video broadcasting system, DVB-T. Here, in contrast to DAB, coherent higher-level modulation schemes together with a sophisticated and powerful channel estimation technique are utilized in a multipath-fading channel. High-speed WLAN systems like IEEE 802.11a and IEEE 802.11g use OFDM together with very similar channel coding

and modulation. The European standard HIPERLAN/2 (High Performance Local Area Network, Type 2) has the same OFDM parameters as these IEEE systems and differs only in a few options concerning channel coding and modulation. Recently, a broadcasting system called DRM (Digital Radio Mondiale) has been developed to replace the antiquated analog AM radio transmission in the frequency bands below 30 MHz. DRM uses OFDM together with a sophisticated multilevel coding technique.

The idea of spread spectrum systems goes back to military applications, which arose during World War II, and were the main field for spread spectrum techniques in the following decades. Within these applications, the main benefits of spreading are to hide a signal, to protect it against eavesdropping and to achieve a high robustness against intended interference, that is, to be able to separate the useful signal from the strong interfering one. Furthermore, correlating to a spreading sequence may be used within radar systems to obtain reliable and precise values of propagation delay for deriving the position of an object.

A system where different (nearly orthogonal) spreading sequences are used to separate the signals transmitted from different sources is the Global Positioning System (GPS) developed in about 1970. Hence, GPS is the first important system where code division multiple access (CDMA) is applied. Within the last 10 years, CDMA has emerged as the most important multiple access technique for mobile communications. The first concept for a CDMA mobile communication system was developed by Qualcomm Incorporated in approx 1988. This system proposal was subsequently refined and released as the so-called IS-95 standard in North America. In the meantime, the system has been rebranded as cdmaOne, and there are more than 100 millions of cdmaOne subscribers in more than 40 countries. Furthermore, cdmaOne has been the starting point for cdma2000, a third-generation mobile communication system offering data rates of up to some Mbit/s. Another very important third-generation system using CDMA is the Universal Mobile Telecommunications System (UMTS); UMTS is based on system proposals developed within a number of European research projects. Hence, CDMA is the dominating multiple access technique for third generation mobile communication systems.

This book has both theoretical and practical aspects. It is intended to provide the reader with a deeper understanding of the concepts of OFDM and CDMA. Thus, the theoretical basics are analyzed and presented in some detail. Both of the concepts are widely applied in practice. Therefore, a considerable part of the book is devoted to system design and implementation aspects and to the presentation of existing communication systems.

The book is organized as follows. In Chapter 1, we give a brief overview of the basic principles of digital communications and introduce our notation. We represent signals as vectors, which often leads to a straightforward geometrical visualization of many seemingly abstract mathematical facts. The concept of orthogonality between signal vectors is a key to the understanding of OFDM and CDMA, and the Euclidean distance between signal vectors is an important concept to analyze the performance of a digital transmission system. Wireless communication systems often have to cope with severe multipath fading in a mobile radio channel. Chapter 2 treats these aspects. First, the physical situation of multipath propagation is analyzed and statistical models of the mobile radio channel are presented. Then, the problems of digital transmission over these channels are discussed and the basic principles of Chapter 1 are extended for those channels. Digital wireless communication over fading channels is hardly possible without using some kind of error protection or channel coding. Chapter 3 gives a brief overview of the most important channel coding

techniques that are used in the above-mentioned communication systems. Convolutional codes are typically used in these systems, and many of the systems have very closely related (or even identical) channel coding options. Thus, the major part of Chapter 3 is dedicated to convolutional codes as they are applied in these systems. A short presentation of Reed–Solomon Codes is also included because they are used as outer codes in the DVB-T system, together with inner convolutional codes. Chapter 4 is devoted to OFDM. First, the underlying ideas and the basic principles are explained by using the basic principles presented in Chapter 1. Then implementation aspects are discussed as well as channel estimation and synchronization aspects that are relevant for the above-mentioned systems. All these systems are designed for mobile radio channels and use channel coding. Therefore, we give a comprehensive discussion of system design aspects and how to fit all these things together in an optimal way for a given channel. Last but not least, the transmission schemes for DAB, DVB-T and WLAN systems are presented and discussed. Chapter 5 is devoted to CDMA, focusing on its main application area – mobile communications. This application area requires not only sophisticated digital transmission techniques and receiver structures but also some additional methods as, for example, a soft handover, a fast and exact power control mechanism as well as some special planning techniques to achieve an acceptable radio network performance. Therefore, the first section of Chapter 5 discusses these methods and some general principles of CDMA and mobile radio networks. CDMA receivers may be simple or quite sophisticated, thereby making use of knowledge about other users. These theoretically involved topics are treated in the following three subsections. As examples of CDMA applications we discuss the most important systems already mentioned, namely, GPS, cdmaOne (IS-95), cdma2000 and UMTS with its two transmission modes called Wideband CDMA and Time Division CDMA. Furthermore, Wireless LAN systems conforming to the standard IEEE 802.11 are also included in this section as some transmission modes of these systems are based on spreading.

This book is supported by a companion website on which lecturers and instructors can find electronic versions of the figures contained within the book, a solutions manual to the problems at the end of each chapter and also chapter summaries. Please go to ftp://ftp.wiley.co.uk/pub/books/schulze

1

Basics of Digital Communications

1.1 Orthogonal Signals and Vectors

The concept of *orthogonal signals* is essential for the understanding of OFDM (orthogonal frequency division multiplexing) and CDMA (code division multiple access) systems. In the normal sense, it may look like a miracle that one can separately demodulate overlapping carriers (for OFDM) or detect a signal among other signals that share the same frequency band (for CDMA). The concept of orthogonality unveils this miracle. To understand these concepts, it is very helpful to interpret signals as vectors. Like vectors, signals can be added, multiplied by a scalar, and they can be expanded into a base. In fact, signals fit into the mathematical structure of a vector space. This concept may look a little bit abstract. However, vectors can be visualized by geometrical objects, and many conclusions can be drawn by simple geometrical arguments without lengthy formal derivations. So it is worthwhile to become familiar with this point of view.

1.1.1 The Fourier base signals

To visualize signals as vectors, we start with the familiar example of a Fourier series. For reasons that will become obvious later, we do not deal with a periodic signal, but cut off outside the time interval of one period of length T. This means that we consider a well-behaved (e.g. integrable) real signal $x(t)$ inside the time interval $0 \le t \le T$ and set $x(t) = 0$ outside. Inside the interval, the signal can be written as a Fourier series

$$x(t) = \frac{a_0}{2} + \sum_{k=1}^{\infty} a_k \cos\left(2\pi \frac{k}{T} t\right) - \sum_{k=1}^{\infty} b_k \sin\left(2\pi \frac{k}{T} t\right). \tag{1.1}$$

The Fourier coefficients a_k and b_k are given by

$$a_k = \frac{2}{T} \int_0^T \cos\left(2\pi \frac{k}{T} t\right) x(t)\, \mathrm{d}t \tag{1.2}$$

Theory and Applications of OFDM and CDMA Henrik Schulze and Christian Lüders

and

$$b_k = -\frac{2}{T}\int_0^T \sin\left(2\pi\frac{k}{T}t\right) x(t)\,\mathrm{d}t. \tag{1.3}$$

These coefficients are the amplitudes of the cosine and (negative) sine waves at the respective frequencies $f_k = k/T$. The cosine and (negative) sine waves are interpreted as a *base* for the (well-behaved) signals inside the time interval of length T. Every such signal can be expanded into that base according to Equation (1.1) inside that interval. The underlying mathematical structure of the Fourier series is similar to the expansion of an N-dimensional vector $\mathbf{x} \in \mathcal{R}^N$ into a base $\{\mathbf{v}_i\}_{i=1}^N$ according to

$$\mathbf{x} = \sum_{i=1}^{N} \alpha_i \mathbf{v}_i. \tag{1.4}$$

The base $\{\mathbf{v}_i\}_{i=1}^N$ is called *orthonormal* if two different vectors are orthogonal (perpendicular) to each other and if they are normalized to length one, that is,

$$\mathbf{v}_i \cdot \mathbf{v}_k = \delta_{ik},$$

where δ_{ik} is the Kronecker Delta ($\delta_{ik} = 1$ for $i = k$ and $\delta_{ik} = 0$ otherwise) and the dot denotes the usual scalar product

$$\mathbf{x} \cdot \mathbf{y} = \sum_{i=1}^{N} x_i y_i = \mathbf{x}^T \mathbf{y}$$

for real N-dimensional vectors. In that case, the coefficients α_i are given by

$$\alpha_i = \mathbf{v}_i \cdot \mathbf{x}.$$

For an orthonormal base, the coefficients α_i can thus be interpreted as the projections of the vector $\mathbf{x}$ onto the base vectors, as depicted in Figure 1.1 for $N = 2$. Thus, α_i can be interpreted as the *amplitude* of $\mathbf{x}$ in the direction of $\mathbf{v}_i$.

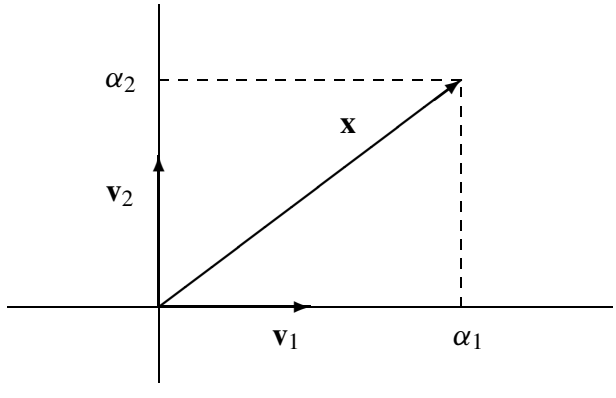

Figure 1.1 A signal vector in two dimensions.

The Fourier expansion (1.1) is of the same type as the expansion (1.4), except that the sum is infinite. For a better comparison, we may write

$$x(t) = \sum_{i=0}^{\infty} \alpha_i v_i(t)$$

with the normalized base signal vectors $v_i(t)$ defined by

$$v_0(t) = \sqrt{\frac{1}{T}}\, \Pi\left(\frac{t}{T} - \frac{1}{2}\right)$$

and

$$v_{2k}(t) = \sqrt{\frac{2}{T}}\, \cos\left(2\pi \frac{k}{T} t\right) \Pi\left(\frac{t}{T} - \frac{1}{2}\right)$$

for even $i > 0$ and

$$v_{2k+1}(t) = -\sqrt{\frac{2}{T}}\, \sin\left(2\pi \frac{k}{T} t\right) \Pi\left(\frac{t}{T} - \frac{1}{2}\right)$$

for odd i with coefficients given by

$$\alpha_i = \int_{-\infty}^{\infty} v_i(t) x(t)\, \mathrm{d}t,$$

that is,

$$\alpha_{2k} = \sqrt{T/2} a_k$$

and

$$\alpha_{2k+1} = \sqrt{T/2} b_k.$$

Here we have introduced the notation $\Pi(x)$ for the rectangular function, which takes the value one between $x = -1/2$ and $x = 1/2$ and zero outside. Thus, $\Pi(x - 1/2)$ is the rectangle between $x = 0$ and $x = 1$. The base of signals $v_i(t)$ fulfills the orthonormality condition

$$\int_{-\infty}^{\infty} v_i(t) v_k(t)\, \mathrm{d}t = \delta_{ik}. \tag{1.5}$$

We will see in the following text that this just means that the Fourier base forms a set of orthogonal signals. With this interpretation, Equation (1.5) says that the base signals for different frequencies are orthogonal and, for the same frequency $f_k = k/T$, the sine and cosine waves are orthogonal.

We note that the orthonormality condition and the formula for α_i are very similar to the case of finite-dimensional vectors. One just has to replace sums by integrals. A similar geometrical interpretation is also possible; one has to regard signals as vectors, that is, identify $v_i(t)$ with $\mathbf{v}_i$ and $x(t)$ with $\mathbf{x}$. The interpretation of α_i as a projection on $\mathbf{v}_i$ is obvious. For only two dimensions, we have $x(t) = \alpha_1 v_1(t) + \alpha_2 v_2(t)$, and the signals can be adequately described by Figure 1.1. In this special case, where $v_1(t)$ is a cosine signal and $v_2(t)$ is a (negative) sine signal, the figure depicts nothing else but the familiar phasor diagram. However, this is just a special case of a very general concept that applies to many other scenarios in communications.

Before we further discuss this concept for signals by introducing a scalar product for signals, we continue with the complex Fourier transform. This is because complex signals are a common tool in communications engineering.

Consider a well-behaved complex signal $s(t)$ inside the time interval $[0, T]$ that vanishes outside that interval. The complex Fourier series for that signal can be written as

$$s(t) = \sum_{k=-\infty}^{\infty} \alpha_k v_k(t) \tag{1.6}$$

with the (normalized) complex Fourier base functions

$$v_k(t) = \sqrt{\frac{1}{T}} \exp\left(j2\pi \frac{k}{T} t\right) \Pi\left(\frac{t}{T} - \frac{1}{2}\right). \tag{1.7}$$

The base functions are orthonormal in the sense that

$$\int_{-\infty}^{\infty} v_i^*(t) v_k(t)\, \mathrm{d}t = \delta_{ik}. \tag{1.8}$$

holds. The Fourier coefficient α_k will be obtained from the signal by the Fourier analyzer. This is a detection device that performs the operation

$$\alpha_k = \int_{-\infty}^{\infty} v_i^*(t) s(t)\, \mathrm{d}t. \tag{1.9}$$

This coefficient is the complex amplitude (i.e. amplitude and phase) of the wave at frequency f_k. It can be interpreted as the component of the signal vector $s(t)$ in the direction of the base signal vector $v_k(t)$, that is, we interpret frequency components as vector components or vector *coordinates*.

Example 1 (OFDM Transmission) *Given a finite set of complex numbers s_k that carry digitally encoded information to be transmitted, we may use the complex Fourier series for this purpose and transmit the signal*

$$s(t) = \sum_{k=0}^{K} s_k v_k(t). \tag{1.10}$$

The transmitter performs a Fourier synthesis. *In an ideal transmission channel with perfect synchronization and no disturbances, the transmit symbols s_k can be completely recovered at the receiver by the Fourier analyzer that plays the role of the detector. One may send K new complex symbols during every time slot of length T by performing the Fourier synthesis for that time slot. At the receiver, the Fourier analysis is done for every time slot. This method is called* orthogonal frequency division multiplexing (OFDM). *This name is due to the fact that the transmit signals form an orthogonal base belonging to different frequencies f_k. We will see in the following text that other – even more familiar – transmission setups use orthogonal bases.*

1.1.2 The signal space

A few mathematical concepts are needed to extend the concept of orthogonal signals to other applications and to represent the underlying structure more clearly. We consider (real or complex) signals of finite energy, that is, signals $s(t)$ with the property

$$\int_{-\infty}^{\infty} |s(t)|^2 \, \mathrm{d}t < \infty. \tag{1.11}$$

The assumption that our signals should have finite energy is physically reasonable and leads to desired mathematical properties. We note that this set of signals has the property of a vector space, because finite-energy signals can be added or multiplied by a scalar, resulting in a finite-energy signal. For this vector space, a scalar product is given by the following:

Definition 1.1.1 (Scalar product of signals) *In the vector space of signals with finite energy, the scalar product of two signals $s(t)$ and $r(t)$ is defined as*

$$\langle s, r \rangle = \int_{-\infty}^{\infty} s^*(t) r(t) \, \mathrm{d}t. \tag{1.12}$$

Two signals are called orthogonal if their scalar product equals zero. The Euclidean norm of the signal is defined by $\|s\| = \sqrt{\langle s, s \rangle}$, and $\|s\|^2 = \langle s, s \rangle$ is the signal energy. $\|s - r\|^2$ is called the squared Euclidean distance *between $s(t)$ and $r(t)$.*

We add the following remarks:

- This scalar product has a structure similar to the scalar product of vectors $\mathbf{s} = (s_1, \ldots, s_K)^T$ and $\mathbf{r} = (r_1, \ldots, r_K)^T$ in a K-dimensional complex vector space given by
$$\mathbf{s}^\dagger \mathbf{r} = \sum_{k=1}^{K} s_k^* r_k,$$
where the dagger (†) means conjugate transpose. Comparing this expression with the definition of the scalar product for continuous signals, we see that the sum has to be replaced by the integral.

- It is a common use of notation in communications engineering to write a function with an argument for the function, that is, to write $s(t)$ for a signal (which is a function of the time) instead of s, which would be the mathematically correct notation. In most cases, we will use the engineer's notation, but we write, for example, $\langle s, r \rangle$ and not $\langle s(t), r(t) \rangle$, because this quantity does not depend on t. However, sometimes we write s instead of $s(t)$ when it makes the notation simpler.

- In mathematics, the vector space of square integrable functions (i.e. finite-energy signals) with the scalar product as defined above is called the *Hilbert space* $L^2(\mathcal{R})$. It is interesting to note that the Hilbert space of finite-energy signals is the same as the Hilbert space of wave functions in quantum mechanics. For the reader who is interested in details, we refer to standard text books in mathematical physics (see e.g. (Reed and Simon 1980)).

Without proof, we refer to some mathematical facts about that space of signals with finite energy (see e.g. (Reed and Simon 1980)).

- Each signal $s(t)$ of finite energy can be expanded into an orthonormal base, that is, it can be written as
$$s(t) = \sum_{k=1}^{\infty} \alpha_k v_k(t) \tag{1.13}$$
with properly chosen orthonormal base signals $v_k(t)$. The coefficients can be obtained from the signal as
$$\alpha_k = \langle v_k, s \rangle . \tag{1.14}$$
The coefficient α_k can be interpreted as the component of the signal vector s in the direction of the base vector v_k.

- For any two finite energy signals $s(t)$ and $r(t)$, the Schwarz inequality
$$|\langle s, r \rangle| \leq \|s\| \ \|r\|$$
holds. Equality holds if and only if $s(t)$ is proportional to $r(t)$.

- The Fourier transform is well defined for finite-energy signals. Now, let $s(t)$ and $r(t)$ be two signals of finite energy, and $S(f)$ and $R(f)$ denote their Fourier transforms. Then,
$$\langle s, r \rangle = \langle S, R \rangle$$
holds. This fact is called *Plancherel theorem* or *Rayleigh theorem* in the mathematical literature (Bracewell 2000). The above equality is often called *Parseval's equation*. As an important special case, we note that the signal energy can be expressed either in the time or in the frequency domain as
$$E = \int_{-\infty}^{\infty} |s(t)|^2 \, \mathrm{d}t = \int_{-\infty}^{\infty} |S(f)|^2 \, \mathrm{d}f.$$
Thus, $|S(f)|^2 \, \mathrm{d}f$ is the energy in an infinitesimal frequency interval of width $\mathrm{d}f$, and $|S(f)|^2$ can be interpreted as the spectral density of the signal energy.

In communications, we often deal with subspaces of the vector space of finite-energy signals. The signals of finite duration form such a subspace. An appropriate base of that subspace is the Fourier base. The Fourier series is then just a special case of Equation (1.13) and the Fourier coefficients are given by Equation (1.14). Another subspace is the space of strictly band-limited signals of finite energy. From the sampling theorem we know that each such signal $s(t)$ that is concentrated inside the frequency interval between $-B/2$ and $B/2$ can be written as a series
$$s(t) = \sum_{k=-\infty}^{\infty} s(k/B) \mathrm{sinc}\,(Bt - k) \tag{1.15}$$
with $\mathrm{sinc}\,(x) = \sin(\pi x)/(\pi x)$.

We define a base as follows:

Definition 1.1.2 (Normalized sinc base) *The orthonormal sinc base for the bandwidth $B/2$ is given by the signals*

$$\psi_k(t) = \sqrt{B}\,\mathrm{sinc}\,(Bt - k)\,. \tag{1.16}$$

We note that $\sqrt{B}\,\psi_0(t)$ is the impulse response of an ideal low-pass filter of bandwidth $B/2$, so that the sinc base consists of delayed and normalized versions of that impulse response. From the sampling theorem, we conclude that these $\psi_k(t)$ are a base of the subspace of strictly band-limited functions. By looking at them in the frequency domain, we easily see that they are orthonormal. From standard Fourier transform relations, we see that the Fourier transform $\Psi_k(f)$ of $\psi_k(t)$ is given by

$$\Psi_k(f) = \frac{1}{\sqrt{B}}\Pi\,(f/B)\,\mathrm{e}^{-j2\pi kf/B}.$$

Thus, $\Psi_k(f)$ is just a Fourier base function for signals concentrated inside the frequency interval between $-B/2$ and $B/2$. This base is known to be orthogonal. Thus, we rewrite the statement of the sampling theorem as the expansion

$$s(t) = \sum_{k=-\infty}^{\infty} s_k \psi_k(t)$$

into the orthonormal base $\psi_k(t)$. From the sampling theorem, we know that

$$s_k = \frac{1}{\sqrt{B}} s(k/B)$$

holds. The Fourier transform of this signal is given by

$$S(f) = \sum_{k=-\infty}^{\infty} s_k \Psi_k(f).$$

This is just a Fourier series for the spectral function that is concentrated inside the frequency interval between $-B/2$ and $B/2$. The coefficients are given by

$$s_k = \langle \psi_k, s \rangle = \langle \Psi_k, S \rangle\,.$$

This relates the coefficients of a Fourier expansion of a signal $S(f)$ in the frequency domain to the samples of the corresponding signal $s(t)$ in the time domain. As we have seen from this discussion, the Fourier base and the sinc base are related to each other by interchanging the role of time and frequency.

1.1.3 Transmitters and detectors

Any linear digital transmission setup can be characterized as follows: As in the OFDM Example 1, for each transmission system we have to deal with a synthesis of a signal (at the transmitter site) and the analysis of a signal (at the receiver site). Given a finite set $\{s_k\}_{k=1}^{K}$ of coefficients that carry the information to be transmitted, we choose a base $g_k(t)$ to transmit the information by the signal

$$s(t) = \sum_{k=1}^{K} s_k g_k(t). \tag{1.17}$$

Definition 1.1.3 (Transmit base, pulses and symbols) *In the above sum, each signal $g_k(t)$ is called a transmit pulse, the set of signals $\{g_k(t)\}_{k=1}^K$ is called the transmit base, and s_k is called a transmit symbol. The vector $\mathbf{s} = (s_1, \ldots, s_K)^T$ is called the transmit symbol vector.*

Note that in the terminology of vectors, the transmit symbols s_k are the *coordinates* of the signal vector $s(t)$ corresponding to the base $g_k(t)$.

If the transmit base is orthonormal, then, for an ideal transmission channel, the information symbols s_k can be recovered completely as the projections onto the base. These scalar products

$$s_k = \langle g_k, s \rangle = \int_{-\infty}^{\infty} g_k^*(t) s(t)\, \mathrm{d}t \tag{1.18}$$

can also be written as

$$s_k = \left[\int_{-\infty}^{\infty} g_k^*(\tau - t) s(\tau)\, \mathrm{d}\tau \right]_{t=0} = \left[g_k^*(-t) * s(t) \right]_{t=0}. \tag{1.19}$$

This means that the *detection* of the information s_k transmitted by $g_k(t)$ is the output of the filter with impulse response $g_k^*(-t)$ sampled at $t = 0$. This filter is usually called *matched filter*, because it is matched to the transmit pulse $g(t)$.

Definition 1.1.4 (Detector and matched filter) *Given a transmit pulse $g(t)$, the corresponding matched filter is the filter with the impulse response $g^*(-t)$. The detector $\mathcal{D}_g$ for $g(t)$ is defined by the matched filter output sampled at $t = 0$, that is, by the detector output $\mathcal{D}_g[r]$ given by*

$$\mathcal{D}_g[r] = \int_{-\infty}^{\infty} g^*(t) r(t)\, \mathrm{d}t \tag{1.20}$$

for any receive signal $r(t)$. If two transmit pulses $g_1(t)$ and $g_2(t)$ are orthogonal, then the corresponding detectors are called orthogonal.

Thus, a detector extracts a (real or complex) number. This number carries the information. The detector may be visualized as depicted in Figure 1.2.

The matched filter has an interesting property: if a transmit pulse is corrupted by white (not necessarily Gaussian) noise, then the matched filter is the one that maximizes the signal-to-noise ratio (SNR) for $t = 0$ at the receiver end (see Problem 6).

We add the following remarks:

- For a finite-energy receive signal $r(t)$, $\mathcal{D}_g[r] = \langle g, r \rangle$ holds. However, we usually have additive noise components in the signal at the receiver, which are typically not of finite energy, so that the scalar product is not defined.

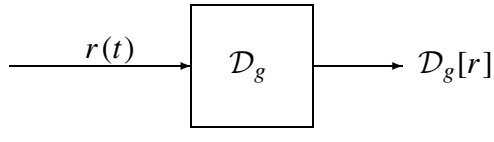

Figure 1.2 Detector.

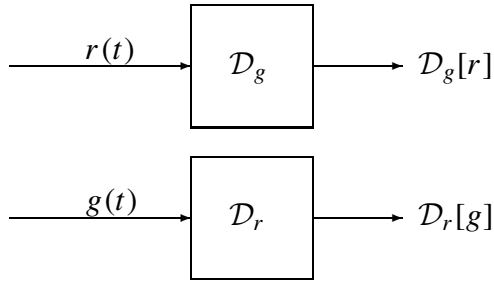

Figure 1.3 Input and detector pulses.

- The detector $\mathcal{D}_g[r]$ compares two signals: in principle, it answers the question 'How much of $r(t)$ looks like $g(t)$?'. The role of receive signal and the pulse can be interchanged according to
$$\mathcal{D}_g[r] = \mathcal{D}_r^*[g],$$
as Figure 1.3 depicts.
- The Fourier analyzer given by Equation (1.9) is a set of orthogonal detectors. The sinc base is another set of orthogonal detectors.
- For an orthonormal base, the energy of the transmit signal equals the energy of the vector of transmit symbols, that is,
$$E = \int_{-\infty}^{\infty} |s(t)|^2 \, \mathrm{d}t = \sum_{k=1}^{K} |s_k|^2,$$
or more compactly written as $E = \|s\|^2 = \|\mathbf{s}\|^2$. For the proof, we refer to Problem 1.

The following example shows that the familiar Nyquist pulse shaping can be understood as an orthogonality condition.

Example 2 (The Nyquist Base) *Consider a transmission pulse $g(t)$ with the property*

$$\int_{-\infty}^{\infty} g^*(t) g(t - kT_S) \, \mathrm{d}t = \delta[k] \tag{1.21}$$

for a certain time interval T_S, that is, the pulse $g(t)$ and its versions time-shifted by kT_S build an orthonormal base. This property also means that the pulse shape $h(t) = g^*(-t) * g(t)$ is a so-called Nyquist pulse that satisfies the first Nyquist criterion $h(kT_S) = \delta[k]$ and allows a transmission that is free of intersymbol interference (ISI). For the Fourier transforms $G(f)$ and $H(f)$ of $g(t)$ and $h(t)$, the relation $H(f) = |G(f)|^2$ holds. Therefore, $g(t)$ is often called a sqrt-Nyquist pulse. If we define $g_k(t) = g(t - kT_S)$ as the pulse transmitted at time kT_S, the condition (1.21) is equivalent to

$$\langle g_i, g_k \rangle = \delta_{ik}. \tag{1.22}$$

We then call the base formed by the signals $g_k(t)$ a (sqrt-) Nyquist base. Equation (1.22) means that if the pulse is transmitted at time kT_S, the detector for the pulse transmitted at time iT_S has output zero unless $i = k$. Thus, the pulses do not interfere with each other.

We note that in practice the pulse $g(t)$ is the impulse response of the transmit filter, that is, the pulse-shaping filter that will be excited by the transmit symbols s_k. The corresponding matched filter $g^*(-t)$ is the receive filter. Its output will be sampled once in every symbol clock T_S to recover the symbols s_k. The impulse response of the whole transmission chain $h(t) = g^*(-t) * g(t)$ must be a Nyquist pulse to ensure symbol recovery without intersymbol interference.

The Nyquist criterion

$$h(kT_S) = \delta[k]$$

in the time domain can be equivalently written in the frequency domain as

$$\sum_{k=-\infty}^{\infty} H\left(f - \frac{k}{T_S}\right) = T_S,$$

where $H(f)$ is the Fourier transform of $h(t)$. Familiar Nyquist pulses like *raised cosine* (RC) pulses are usually derived from this criterion in the frequency domain (see e.g. (Proakis 2001)). In the following text, we shall show a simple method to construct Nyquist pulses in the time domain.

Obviously, every pulse of the shape

$$h(t) = u(t) \cdot \operatorname{sinc}(t/T_S)$$

satisfies the Nyquist criterion in the time domain. $u(t)$ should be a function that improves the decay of the pulse. In the frequency domain, this is equivalent to

$$H(f) = T_S\, U(f) * \Pi(fT_S),$$

where $U(f)$ is the Fourier transform of $u(t)$. The convolution with $U(f)$ smoothens the sharp flank of the rectangle. Writing out the convolution integral leads to

$$H(f) = T_S \left(V\left(f + \frac{1}{2T_S}\right) - V\left(f - \frac{1}{2T_S}\right)\right)$$

with

$$V(f) = \int_{-\infty}^{f} U(x)\,\mathrm{d}x.$$

$V(f)$ is a function that describes the flank of the filter given by $H(f)$.

One possible choice for $U(f)$ is

$$U(f) = \frac{\pi}{2\alpha} T_S \cos\left(\frac{\pi}{\alpha} f T_S\right) \Pi\left(\frac{1}{\alpha} f T_S\right), \quad 0 \le \alpha \le 1$$

with a constant α between that we call the *rolloff factor*. The corresponding time domain function obviously given by

$$u(t) = \frac{\pi}{4}\left(\operatorname{sinc}\left(\alpha \frac{t}{T_S} + \frac{1}{2}\right) + \operatorname{sinc}\left(\alpha \frac{t}{T_S} - \frac{1}{2}\right)\right),$$

which equals the expression

$$u(t) = \frac{\cos(\pi\alpha t/T_S)}{1-(2\alpha t/T_S)^2}.$$

The filter flank is obtained by integration as

$$V(f) = \begin{cases} 0 & : \quad fT_S \le -\alpha/2 \\ \frac{1}{2}\left(1+\sin\left(\frac{\pi}{\alpha}fT_S\right)\right) & : \quad -\alpha/2 \le fT_S \le \alpha/2 \\ 1 & : \quad fT_S \ge \alpha/2. \end{cases} \tag{1.23}$$

The shape of the filter is then given by the familiar expression

$$H(f) = \begin{cases} T_S & : \quad 2|f|T_S \le 1-\alpha \\ \frac{T_S}{2}\left(1-\sin\left(\frac{\pi}{\alpha}\left(|f|T_S-\frac{1}{2}\right)\right)\right) & : \quad 1-\alpha \le 2|f|T_S \le 1+\alpha \\ 0 & : \quad 2|f|T_S \ge 1+\alpha. \end{cases} \tag{1.24}$$

The corresponding pulse is

$$h(t) = \mathrm{sinc}(t/T_S)\cdot\frac{\cos(\pi\alpha t/T_S)}{1-(2\alpha t/T_S)^2}. \tag{1.25}$$

Other Nyquist pulses than these so-called *raised cosine* (RC) pulses are possible. A Gaussian

$$u(t) = \exp\left(-(\beta t/T_S)^2\right)$$

guarantees an exponential decay in both the time and the frequency domain. β is a shaping parameter similar to the rolloff factor α. The Fourier transform $U(f)$ of $u(t)$ is given by

$$U(f) = \sqrt{\pi T_S^2/\beta^2}\,\exp\left(-(\pi T_S f/\beta)^2\right),$$

and the filter flank is

$$V(f) = \frac{1}{2}\left(1+\mathrm{erf}\left(\frac{\pi}{\beta}T_S f\right)\right).$$

The filter curve is then given by

$$H(f) = \frac{1}{2}T_S\left(\mathrm{erf}\left(\frac{\pi}{\beta}\left(T_S f+\frac{1}{2}\right)\right)-\mathrm{erf}\left(\frac{\pi}{\beta}\left(T_S f-\frac{1}{2}\right)\right)\right). \tag{1.26}$$

The RC pulse and the Gaussian Nyquist pulse

$$h(t) = \mathrm{sinc}(t/T_S)\cdot\exp\left(-(\beta t/T_S)^2\right) \tag{1.27}$$

have a very similar shape if we relate α and β in such a way that their flanks $V(f)$ have the same first derivative at $f=0$. This is the case for

$$\beta = \frac{2\alpha}{\pi}.$$

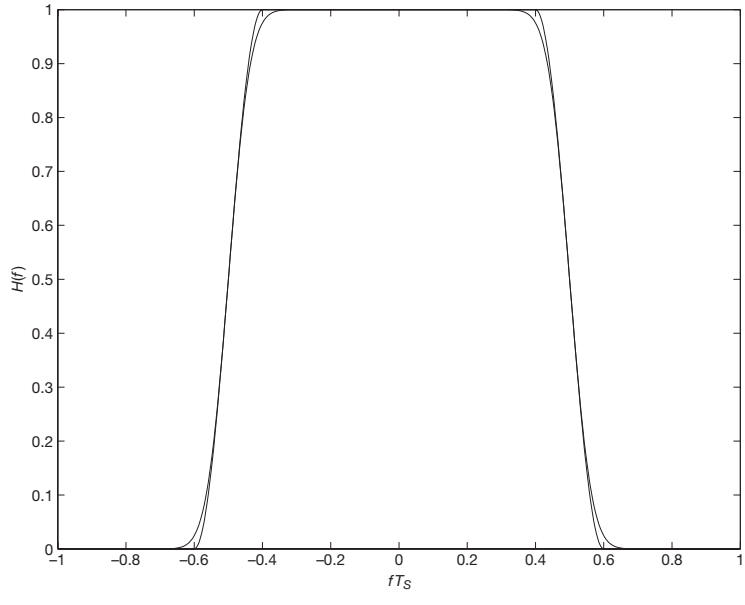

Figure 1.4 RC and Gaussian Nyquist filter shape for $\alpha = 0.2$.

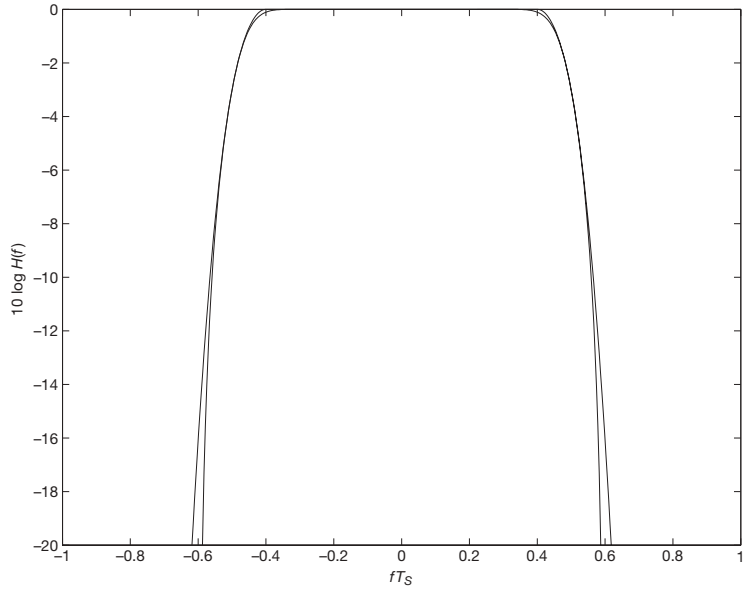

Figure 1.5 RC and Gaussian Nyquist filter shape for $\alpha = 0.2$ (decibel scale).

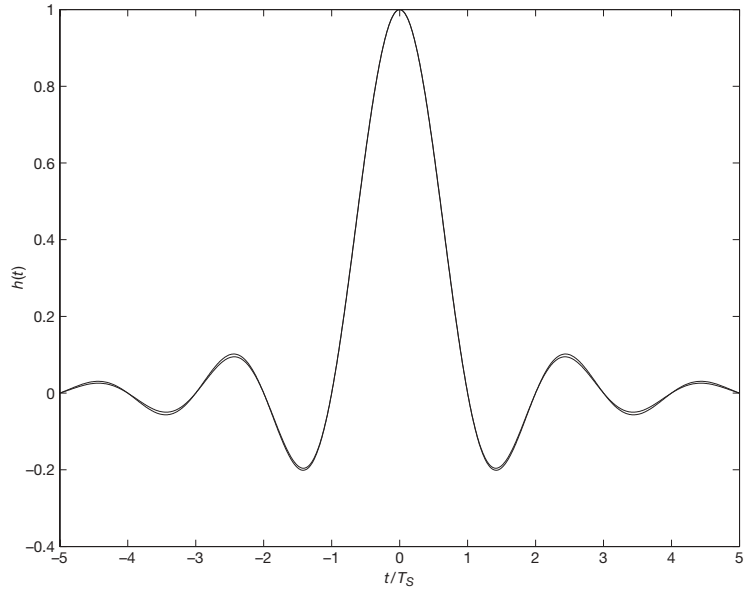

Figure 1.6 RC and Gaussian Nyquist pulse shape for $\alpha = 0.2$.

For this case and $\alpha = 0.2$, both filter shapes are depicted in Figure 1.4, and with a logarithmic scale, in Figure 1.5. The Gaussian shaping is slightly broader at the outer flanks, but the difference is very small even on the logarithmic scale. Figure 1.6 shows the corresponding pulses. The Gaussian pulse has slightly smaller amplitudes, but the difference is very small. Of course, both curves differ significantly in their asymptotic behavior (which can be seen on a logarithmic scale), but this is in a region where pulses are practically zero.

1.1.4 Walsh functions and orthonormal transmit bases

In this subsection, we introduce the Walsh functions that play an important role in CDMA signaling. We regard them as an example to discuss an orthonormal base that can be interpreted as a base of signals or as a base in an Euclidean space.

The $M \times M$ Walsh–Hadamard (WH) matrices $\mathbf{H}_M$, where M is a power of two, are defined by $\mathbf{H}_1 = 1$ and the recursive relation

$$\mathbf{H}_M = \begin{bmatrix} \mathbf{H}_{M/2} & \mathbf{H}_{M/2} \\ \mathbf{H}_{M/2} & -\mathbf{H}_{M/2} \end{bmatrix}.$$

For example, the matrix $\mathbf{H}_4$ is given by

$$\mathbf{H}_4 = \begin{bmatrix} 1 & 1 & 1 & 1 \\ 1 & -1 & 1 & -1 \\ 1 & 1 & -1 & -1 \\ 1 & -1 & -1 & 1 \end{bmatrix}.$$

The column vectors of the WH matrix are pairwise orthogonal but not normalized to one. We may divide them by their length $\sqrt{M}$ to obtain the normalized WH vectors $\mathbf{g}_k$ related to $\mathbf{H}_M$ by

$$\sqrt{M}\,\mathbf{H}_M = \mathbf{G} = \left[\mathbf{g}_1, \ldots, \mathbf{g}_M\right]. \tag{1.28}$$

The column vectors are orthonormal, that is,

$$\mathbf{g}_i \cdot \mathbf{g}_k = \delta_{ik}.$$

For a given value of M, the Walsh functions $g_k(t)$, $k = 1, \ldots, M$ are functions defined on a time interval $t \in [0, T_S]$ that are piecewise constant on time sub-intervals (called *chips*) of duration $T_c = T_S/M$. The sign of the function on the ith time sub-interval ($i = 1, \ldots, M$) is given by the ith component h_{ik} of the kth column vector in the WH matrix $\mathbf{H}_M$. The absolute value is normalized to $1/\sqrt{T_S}$ to obtain an orthonormal signal base, that is,

$$\langle g_i, g_k \rangle = \delta_{ik}.$$

Outside the interval $t \in [0, T_S]$, the Walsh functions vanish. For $M = 8$, the Walsh functions are depicted in Figure 1.7.

We can write the normalized Walsh functions as

$$g_k(t) = \sum_{i=1}^{M} g_{ik} c_i(t), \tag{1.29}$$

where $g_{ik} = h_{ik}/\sqrt{M}$, and the chip pulse $c_i(t)$ is defined by $c_i(t) = 1/\sqrt{T_c}$ in the ith chip interval and zero outside. Obviously

$$\langle c_i, c_k \rangle = \delta_{ik}$$

holds, that is, the chip pulses are orthonormal. Given the transmit base $\{g_k(t)\}_{k=1}^{M}$, we may transmit information carried by the symbols $\{s_k\}_{k=1}^{M}$ by using the signal

$$s(t) = \sum_{k=1}^{M} s_k g_k(t). \tag{1.30}$$

Instead of $\{g_k(t)\}_{k=1}^{M}$, we can use the equivalent discrete base $\{\mathbf{g}_k\}_{k=1}^{M}$ and transmit the vector

$$\mathbf{s} = \sum_{k=1}^{M} s_k \mathbf{g}_k. \tag{1.31}$$

This representation allows the geometrical interpretation of the transmit signal as a vector $\mathbf{s}$ in an M-dimensional Euclidean space. The transmit symbols s_k are the components of the vector $\mathbf{s}$ in the orthonormal Walsh–Hadamard base $\{\mathbf{g}_k\}_{k=1}^{M}$, which is a rotated version of the canonical Euclidean base $\mathbf{e}_1 = (1, 0, 0, \ldots, 0)^T$, $\mathbf{e}_2 = (0, 1, 0, \ldots, 0)^T, \ldots, \mathbf{e}_M = (0, \ldots, 0, 1)^T$ with the rotation given by the matrix $\mathbf{G}$. Equation (1.29) is the coordinate transform corresponding to the base transform from the base of chip pulses to the base of normalized Walsh functions. Thus, the chip pulse base can be identified with the canonical Euclidean base. For an ideal channel, the components s_k of the vector $\mathbf{s}$ can be completely

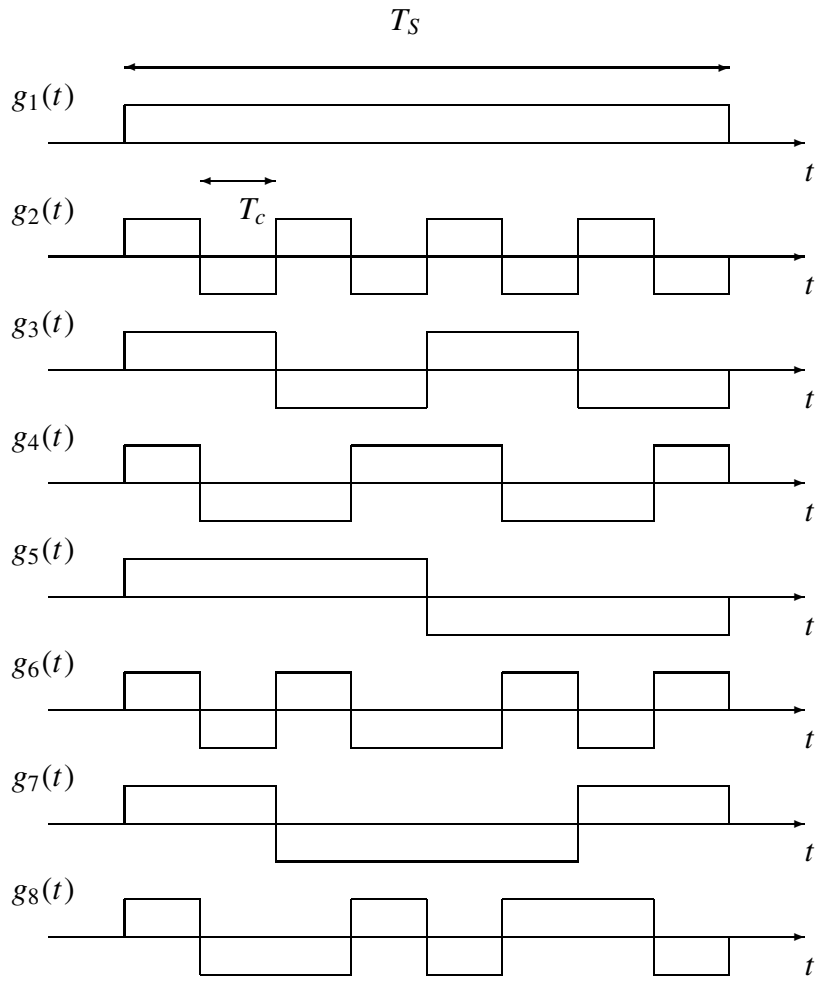

Figure 1.7 Walsh functions for $M = 8$.

recovered by projecting the receive vector on the base vectors $\mathbf{g_k}$. For $M = 2$, the situation is depicted in Figure 1.8.

The orthogonality of the base can be interpreted as the existence of M independent channels without cross talk as illustrated in Figure 1.9 for $M = 2$. The orthogonal detectors $\mathcal{D}_{g_i}$ correspond to the projections on the base vectors. If the symbols $\{s_k\}_{k=1}^{M}$ are part of the same data stream, M symbols are transmitted in parallel via M channels during the time interval T_S. Orthogonality means absence of ISI between these channels. Another possibility is to use the M channels to transmit M independent data streams, each of them with the rate of one symbol transmitted during the time interval T_S . In that case, the orthogonality is used for *multiplexing* or *multiple access*, as it is the situation in CDMA (code division multiple access). Each Walsh function corresponds to another code that may be allocated to

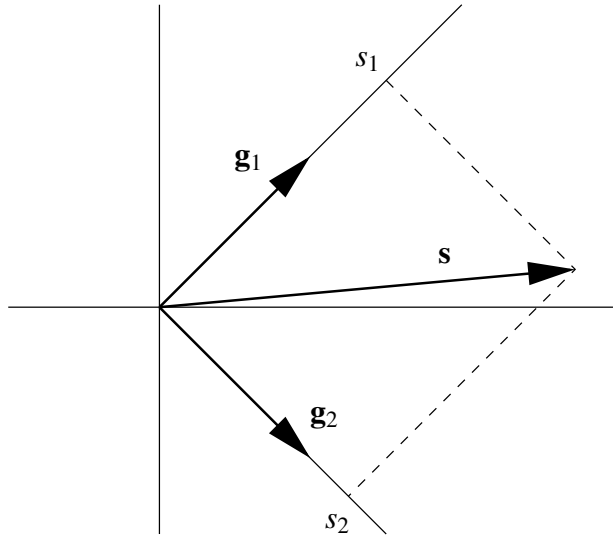

Figure 1.8 The orthonormal Walsh–Hadamard base.

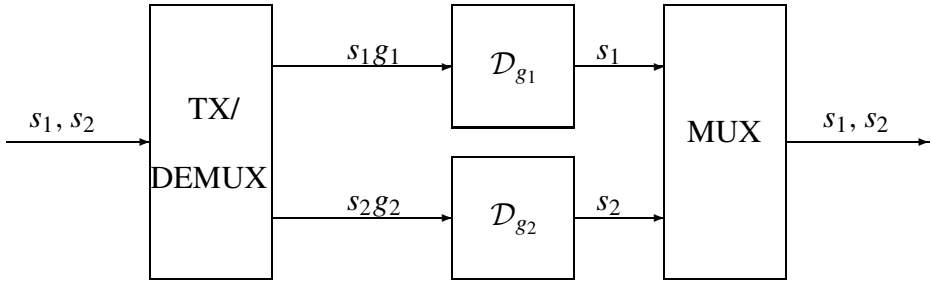

Figure 1.9 Orthogonal channels.

a certain user in a mobile radio scenario. The downlink of the Qualcomm CDMA system IS-95 (now called cdmaOne, see Subsection 5.5.6) is an example for such a setup (see the discussion in Chapter 5).

Walsh functions may also be used for orthogonal signaling. In that case the term *Walsh modulation* is often used. This transmission scheme is very robust against noise, but it leads to a significant spreading of the bandwidth. For CDMA systems, both properties together are desirable. This modulation scheme is used in the uplink of the Qualcomm system IS-95. In a setup with orthogonal Walsh modulation, only one base pulse $g_k(t)$ will be transmitted during the time period T_S. One can transmit $\log_2(M)$ bits during T_S by selecting one of the M base pulses. The transmit signal during this time period is simply given by

$$s(t) = \sqrt{E_S}\, g_k(t)$$

or

$$\mathbf{s} = \sqrt{E_S}\,\mathbf{g}_k,$$

where $\sqrt{E_S}$ is the energy of the signal in the time period of length T_S.

We note that all the properties discussed in this subsection hold not only for the piecewise constant chip pulse but also for any set of chip pulses $c_i(t)$ that satisfies the orthonormality condition $\langle c_i, c_k\rangle = \delta_{ik}$, and the base signal given by Equation (1.30) holds. One may, for example, choose any Nyquist base for the pulses $c_i(t)$ with smoother pulse shape than the rectangular pulses in order to get better spectral properties. It is also possible to use the Fourier base pulse for $c_i(t)$ in Equation (1.30), resulting in multicarrier (MC-) CDMA. Then, a chip may be interpreted as a frequency pulse rather than a time pulse.

1.1.5 Nonorthogonal bases

Orthonormal transmit bases have desirable properties for simple detection. However, sometimes it is necessary to deal with nonorthogonal bases. This may be the case when a transmission channel corrupts the orthogonality. For example, the channel may introduce ISI, so the ISI-free Nyquist base used for transmission will be convolved by the channel impulse response resulting in nonorthogonal base vectors. In such a case, the channel must be regarded as a part of the transmit setup.

Now, let the pulses $b_k(t)$ be such a base of nonorthogonal, but linearly independent, transmit pulses and let x_k, $k = 1, \ldots, K$ be the finite set of transmit symbols. The transmitted signal is then given by

$$s(t) = \sum_{k=1}^{K} x_k b_k(t). \tag{1.32}$$

There exists an orthonormal base $\{\psi_k\}_{k=1}^{K}$ for the finite-dimensional vector space spanned by the transmit pulses $b_k(t)$, which can be obtained using the Gram–Schmidt algorithm. The two bases are related by the base transform

$$b_k(t) = \sum_{i=1}^{K} b_{ik}\psi_i(t) \tag{1.33}$$

with $b_{ik} = \langle \psi_i, b_k\rangle$. We take the scalar product of Equation (1.32) with the vector $\psi_i(t)$ and obtain

$$s_i = \sum_{k=1}^{K} x_k b_{ik},$$

where we have defined $s_i = \langle \psi_i, s\rangle$. This is a coordinate transform of the coordinates x_k of the signal corresponding to the nonorthogonal base $b_k(t)$ to the coordinates s_k corresponding to the orthonormal base $\psi_k(t)$ by writing

$$s(t) = \sum_{k=1}^{K} s_k \psi_k(t).$$

Defining $\mathbf{x} = (x_1, \ldots, x_k)^T$ and $\mathbf{s} = (s_1, \ldots, s_k)^T$, the coordinate transform can be written in the more compact matrix notation as

$$\mathbf{s} = \mathbf{B}\mathbf{x}$$

with the matrix $\mathbf{B}$ of entries b_{ik}. Because this coordinate transform is invertible, the transmit symbols x_k can be recovered from the s_k by $\mathbf{x} = \mathbf{B}^{-1}\mathbf{s}$. Thus, in a channel without noise, the receiver may use the detector outputs corresponding to the orthonormal base and transform them by using the inverse matrix. However, in a noisy channel, this inversion is not optimal for the detection, because it causes noise enhancement.

For a receive signal $r(t)$, the detector outputs in the nonorthogonal base

$$y_k = \mathcal{D}_{b_k}[r] = \int_{-\infty}^{\infty} b_k^*(t) r(t)\,\mathrm{d}t$$

are related to the detector outputs

$$r_k = \mathcal{D}_{\psi_k}[r] = \int_{-\infty}^{\infty} \psi_k^*(t) r(t)\,\mathrm{d}t$$

in the orthogonal base by

$$y_k = \sum_{i=1}^{K} b_{ik}^* r_i$$

or, in matrix notation, by

$$\mathbf{y} = \mathbf{B}^{\dagger}\mathbf{r}.$$

Because this transform is invertible, the detector outputs r_k can be recovered from the y_k by $\mathbf{r} = \left(\mathbf{B}^{\dagger}\right)^{-1}\mathbf{y}$.

1.2 Baseband and Passband Transmission

It is convenient to describe a digitally modulated passband signal by a so-called *complex equivalent low-pass* or *complex baseband* signal. Let $\tilde{s}(t)$ be a strictly band-limited[1] passband signal of bandwidth B centered around a carrier frequency f_0. We have chosen the sign $\tilde{}$ for the signal $\tilde{s}(t)$ to indicate a wave for the RF signal. It is possible to completely describe $\tilde{s}(t)$ by its equivalent low-pass signal $s(t)$ of bandwidth $B/2$. Both signals are related by

$$\tilde{s}(t) = \sqrt{2}\,\Re\{s(t)\mathrm{e}^{j2\pi f_0 t}\}. \tag{1.34}$$

This one-to-one correspondence between both signals $\tilde{s}(t)$ and $s(t)$ is easy to visualize if we look at them in the frequency domain. Writing $\tilde{S}(f)$ and $S(f)$ for their respective Fourier transforms, Equation (1.34) is equivalent to

$$\tilde{S}(f) = \frac{1}{\sqrt{2}}\left(S\left(f - f_0\right) + S^*\left(-f - f_0\right)\right).$$

This is because, in Equation (1.34), multiplication with the exponential corresponds to a frequency shift by f_0, and taking the real part corresponds (up to a factor of 2) to adding

[1] We note that strictly band-limited signals do not exist in reality. This is due to the fact that a strictly band-limited signal cannot be time limited, which should be the case for signals in reality. However, it is mathematically convenient to make this assumption, always keeping in mind that this is only an approximation and the accuracy of this model has to be discussed for any practical case.

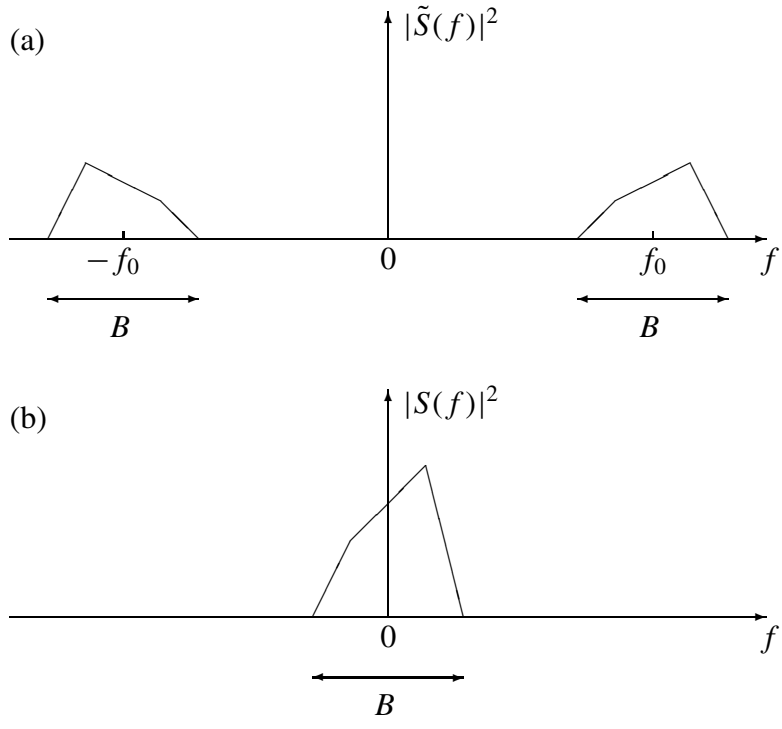

Figure 1.10 Equivalence of (a) passband and (b) complex baseband representation of the same signal.

the negative spectral component (see Problem 2). Figure 1.10 shows the energy spectral densities $|\tilde{S}(f)|^2$ and $|S(f)|^2$ for both signals. We have chosen a normalization such that the total energy of both signals is the same, that is,

$$\int_{-\infty}^{\infty} |s(t)|^2 \, \mathrm{d}t = \int_{-\infty}^{\infty} |\tilde{s}(t)|^2 \, \mathrm{d}t$$

and

$$\int_{-\infty}^{\infty} |S(f)|^2 \, \mathrm{d}f = \int_{-\infty}^{\infty} |\tilde{S}(f)|^2 \, \mathrm{d}f.$$

It is obvious from the figure that both signals $\tilde{S}(f)$ and $S(f)$ are only located at different frequencies, but they carry the same information. The signal $S(f)$ can be obtained from $\tilde{S}(f)$ by a frequency shift by $-f_0$ followed by an ideal low-pass filter of bandwidth $B/2$, and a scaling by the factor $\sqrt{2}$. Denoting the low-pass filter impulse response by $\Phi(t)$, this operation can be written in the time domain as

$$s(t) = \Phi(t) * \left[\sqrt{2} \exp(-j2\pi f_0 t) \; \tilde{s}(t)\right]. \tag{1.35}$$

We note that the upconversion from $s(t)$ to $\tilde{s}(t)$ as described by Equation (1.34) doubles the bandwidth of the two components (real and imaginary part) of the baseband signal,

resulting in one signal of bandwidth B instead of two (real) signals of bandwidth $B/2$. We write $s(t) = x(t) + jy(t)$ and call the real part, $x(t)$, the I- *(inphase)* and the imaginary part $y(t)$ the Q- *(quadrature)* component. Both components together are called *quadrature components*. Equation (1.34) can then be written as

$$\tilde{s}(t) = \sqrt{2}\, x(t) \cos(2\pi f_0 t) - \sqrt{2}\, y(t) \sin(2\pi f_0 t)\,, \tag{1.36}$$

which is the superposition of the cosine-modulated I-component and the (negative) sine-modulated Q-component. It is an important fact that the passband of width B is shared by two separable channels: one is the *cosine* and the other is the *sine* channel. We shall see that the I-component modulated by the cosine is orthogonal to the Q-component modulated by the sine. Thus, they behave like two different channels (without cross talk) that can be individually used for transmission. We will further see that both the I-modulation and the Q-modulation leave scalar products invariant. To make the following treatment simpler, we first introduce a formal shorthand notation for the quadrature modulator and demodulator.

1.2.1 Quadrature modulator

First we define the quadrature modulator as given by Equation (1.36), but separately for both components.

Definition 1.2.1 (I- and Q-modulator) *Let $x(t)$ and $y(t)$ be some arbitrary real signals. Let $\Phi(t)$ denote the impulse response of an ideal low-pass filter of bandwidth $B/2$. Let $f_0 > B/2$. We then define the modulated signals $\tilde{x}(t)$ and $\tilde{y}(t)$ as*

$$\tilde{x}(t) = \sqrt{2}\, \cos(2\pi f_0 t)\ [\Phi(t) * x(t)] \tag{1.37}$$

and

$$\tilde{y}(t) = -\sqrt{2}\, \sin(2\pi f_0 t)\ \big[\Phi(t) * y(t)\big]\,. \tag{1.38}$$

We write $\tilde{x}(t) = I\{x(t)\}$ and $\tilde{y}(t) = Q\{y(t)\}$ or, shorthand, $\tilde{x} = Ix$ and $\tilde{y} = Qy$ and call the time-variant systems given by I and Q the I-modulator *and the* Q-modulator*, respectively. The time-variant system that converts the pair of signals $x(t)$ and $y(t)$ to the passband signal $\tilde{s} = Ix + Qy$ is called* quadrature modulator.

In a practical setup, the signals $x(t)$ and $y(t)$ are already low-pass signals, and thus the convolution with $\Phi(t)$ at the input is obsolete. For mathematical convenience, we prefer to define this time-variant system for arbitrary (not only low-pass) signals as inputs.

The following theorem states the orthogonality of the outputs of the I- and Q-modulator and that both modulators leave scalar products invariant for band-limited signals.

Theorem 1.2.2 *Let $x(t)$ and $y(t)$ be arbitrary real signals of finite energy and let $\tilde{x}(t) = I\{x(t)\}$ and $\tilde{y}(t) = Q\{y(t)\}$. Then,*

$$\langle \tilde{x}, \tilde{y} \rangle = 0. \tag{1.39}$$

Furthermore, let $\tilde{u}(t) = I\{u(t)\}$ and $\tilde{v}(t) = Q\{v(t)\}$ be two other signals of finite energy. If x, y, u, v are real low-pass signals strictly band-limited to $B/2$, then

$$\langle \tilde{u}, \tilde{x} \rangle = \langle u, x \rangle\,,\ \langle \tilde{v}, \tilde{y} \rangle = \langle v, y \rangle \tag{1.40}$$

holds. As a special case, we observe that both I- and Q-modulator leave the signal energy unchanged, that is, $\|x\|^2 = \|\tilde{x}\|^2$ and $\|y\|^2 = \|\tilde{y}\|^2$.

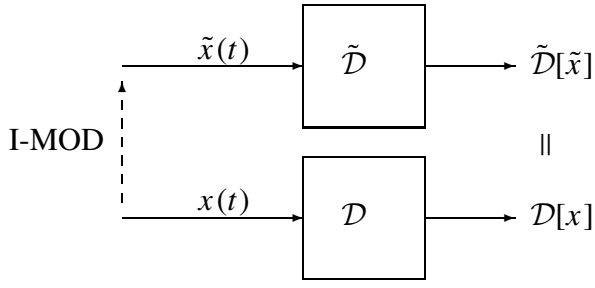

Figure 1.11 Equivalence of baseband and passband detection.

The proof of the theorem is left to Problem 3. Equation (1.39) states that the sine and the cosine channels are orthogonal. In particular, it means that a detector for a Q-modulated sine wave detects zero if only an I-modulated cosine wave has been transmitted and vice versa. For strictly band-limited baseband signals, Equation (1.40) states the following equivalence between baseband and passband transmission: we consider the detector for the baseband pulse $u(t)$ and denote it shorthand by $\mathcal{D} = \mathcal{D}_u$. For the passband detector corresponding to the I-modulated pulse $\tilde{u}(t) = I\{u(t)\}$, we write shorthand $\tilde{\mathcal{D}} = \mathcal{D}_{\tilde{u}}$. Then, as depicted in Figure 1.11, the baseband detector output for the baseband signal $x(t)$ is the same as the passband detector output for the I-modulated signal $\tilde{x}(t) = I\{x(t)\}$:

$$\tilde{\mathcal{D}}[\tilde{x}] = \mathcal{D}[x].$$

The same holds for the Q-modulation.

Now let $s(t) = x(t) + jy(t)$ and $z(t) = u(t) + jv(t)$ be strictly band-limited complex low-pass signals. The corresponding passband signals can be written as $\tilde{s} = Ix + Qy$ and $\tilde{z} = Iu + Qv$. Their scalar product is

$$\langle \tilde{z}, \tilde{s} \rangle = \langle Iu, Ix \rangle + \langle Qv, Qy \rangle + \langle Iu, Qy \rangle + \langle Qv, Ix \rangle .$$

As a consequence of the above theorem, the last two terms vanish and the first two can be converted, resulting in

$$\langle \tilde{z}, \tilde{s} \rangle = \langle u, x \rangle + \langle v, y \rangle .$$

We compare this expression with the scalar product of the two complex baseband signals

$$\langle z, s \rangle = \langle u, x \rangle + \langle v, y \rangle + j(\langle u, y \rangle - \langle v, x \rangle)$$

and find the relation

$$\langle \tilde{z}, \tilde{s} \rangle = \Re\{\langle z, s \rangle\}. \tag{1.41}$$

We note that there is a similar relation between the scalar products of vectors in the complex N-dimensional vector space $\mathcal{C}^N$ and in the real $2N$-dimensional space $\mathcal{R}^{2N}$. Let $\mathbf{s} = \mathbf{x} + j\mathbf{y}$ and $\mathbf{z} = \mathbf{u} + j\mathbf{v}$ be vectors in $\mathcal{C}^N$ and define the real vectors

$$\tilde{\mathbf{s}} = \begin{bmatrix} \mathbf{x} \\ \mathbf{y} \end{bmatrix}, \ \tilde{\mathbf{z}} = \begin{bmatrix} \mathbf{u} \\ \mathbf{v} \end{bmatrix}.$$

Then,

$$\tilde{\mathbf{z}} \cdot \tilde{\mathbf{s}} = \mathbf{u} \cdot \mathbf{x} + \mathbf{v} \cdot \mathbf{y}$$

and

$$\mathbf{z}^{\dagger}\mathbf{s} = \mathbf{u} \cdot \mathbf{x} + \mathbf{v} \cdot \mathbf{y} + j(\mathbf{u} \cdot \mathbf{y} - \mathbf{v} \cdot \mathbf{x})$$

and thus,

$$\tilde{\mathbf{z}} \cdot \tilde{\mathbf{s}} = \Re\{\mathbf{z}^{\dagger}\mathbf{s}\} \tag{1.42}$$

hold.

1.2.2 Quadrature demodulator

Consider again the detector $\mathcal{D} = \mathcal{D}_u$ and the detector $\tilde{\mathcal{D}} = \mathcal{D}_{\tilde{u}}$ for an I-modulated pulse $\tilde{u}(t) = I\{u(t)\}$. The detector output to an input signal $\tilde{s}(t)$ is given by $\tilde{\mathcal{D}}[\tilde{s}]$. We may ask for a time-variant system I^D called I-demodulator that maps $\tilde{s}(t)$ to a low-pass signal $x(t) = I^D\{\tilde{s}(t)\}$ which is defined by the property

$$\mathcal{D}[x] = \tilde{\mathcal{D}}[\tilde{s}],$$

(see Figure 1.12). Using simple integral manipulations, one can derive the explicit form of the I- (and similarly for the Q-) demodulator from this condition (see Problem 4). It turns out that I^D and Q^D are just given by the real and imaginary part of the Equation (1.35). We summarize the result in the following definition and theorem.

Definition 1.2.3 (I- and Q-demodulator) *Let $\tilde{s}(t)$ be a real signal. Let $\Phi(t)$ denote the impulse response of an ideal low-pass filter of bandwidth $B/2$. Let $f_0 > B/2$. We define the demodulated signals $x(t)$ and $y(t)$ as*

$$x(t) = \Phi(t) * \left[\sqrt{2}\,\cos(2\pi f_0 t)\;\tilde{s}(t)\right] \tag{1.43}$$

and

$$y(t) = -\Phi(t) * \left[\sqrt{2}\,\sin(2\pi f_0 t)\;\tilde{s}(t)\right] \tag{1.44}$$

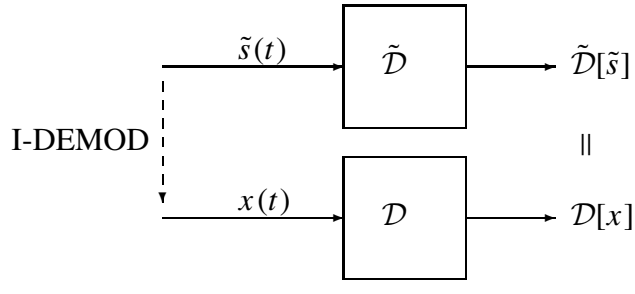

Figure 1.12 Characterization of the I-demodulator.

and write $x(t) = I^D\{\tilde{s}(t)\}$ *and* $y(t) = Q^D\{\tilde{s}(t)\}$ *or, using shorthand,* $x = I^D\tilde{s}$ *and* $y = Q^D\tilde{s}$. *We call the time-variant systems given by* I^D *and* Q^D *the I-demodulator and the Q-demodulator, respectively. The time-variant system given by* $I^D + jQ^D$ *that converts* $\tilde{s}$ *to the complex signal*

$$s(t) = \Phi(t) * \left[\sqrt{2}\,\exp(-j2\pi f_0 t)\;\tilde{s}(t)\right] \tag{1.45}$$

is called quadrature demodulator.

Theorem 1.2.4 *For real signals of finite energy, the I- and Q-demodulator have the following properties:*

$$\langle Iu, \tilde{s}\rangle = \left\langle u, I^D\tilde{s}\right\rangle, \quad \langle Qv, \tilde{s}\rangle = \left\langle v, Q^D\tilde{s}\right\rangle, \tag{1.46}$$
$$Q^D Ix = 0, \quad I^D Qy = 0.$$

Conversely, Equation (1.46) uniquely determines the I- and Q-demodulation given by the above definition. Furthermore, let $x(t)$ *and* $y(t)$ *be real signals of finite energy that are strictly band-limited to* $B/2$. *Then,*

$$I^D Ix = x, \quad Q^D Qy = y$$

holds. Thus, for band-limited signals, the I- (Q-)demodulator inverts the I- (Q-)modulator.

We may also write Equation (1.46) in the detector notation as

$$\mathcal{D}_{\tilde{u}}[\tilde{s}] = D_u[I^D\tilde{s}], \quad \mathcal{D}_{\tilde{v}}[\tilde{s}] = D_v[Q^D\tilde{s}] \tag{1.47}$$

with $\tilde{u}(t) = I\{u(t)\}$ and $\tilde{v}(t) = Q\{v(t)\}$. Without going into mathematical details, we note that if the detection pulses $u(t)$ and $v(t)$ are sufficiently well behaved, these equations – written as integrals – still make sense if the input signal is no longer of finite energy. This is the case, for example, for a sine wave, for a Dirac impulse, or for white noise, which is the topic of the next section.

1.3 The AWGN Channel

In reality, transmission is always corrupted by noise. The usual mathematical model is the AWGN (Additive White Gaussian Noise) channel. It is a very good model for the physical reality as long as the thermal noise at the receiver is the only source of disturbance. Nevertheless, because of its simplicity, it is often used to model man-made noise or multiuser interference. The AWGN channel model can be characterized as follows:

- The noise $w(t)$ is an *additive* random disturbance of the useful signal $s(t)$, that is, the receive signal is given by

$$r(t) = s(t) + w(t).$$

- The noise is *white*, that is, it has a constant power spectral density (psd). The one-sided psd is usually denoted by N_0, so $N_0/2$ is the two-sided psd, and BN_0 is the noise inside the (noise) bandwidth B, see part (a) of Figure 1.13. For thermal resistor noise, $N_0 = kT_0$, where k is the Boltzmann constant and T_0 is the absolute temperature. The

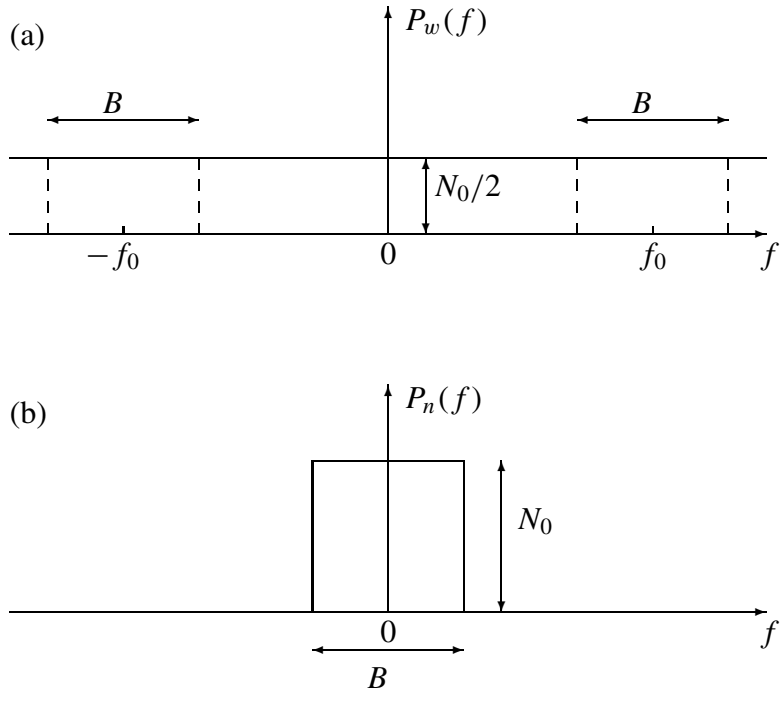

Figure 1.13 Equivalence of (a) wideband and (b) complex baseband AWGN for band-limited detection.

unit of N_0 is [W/Hz], which is the same as the unit [J] for the energy. Usually, N_0 is written as dBm/Hz. For $T_0 = 290$ K, $N_0 \approx -174$ dBm/Hz. However, this is only the ideal physical limit for an ideal receiver. In practice, some decibels according to the so-called *noise figure* have to be added. Typically, N_0 will be a value slightly above -170 dBm/Hz.

- The noise is a stationary and zero mean *Gaussian* random process. This means that the output of every (linear) noise measurement is a zero mean Gaussian random variable that does not depend on the time instant when the measurement is done.

One must keep in mind that the AWGN model is a mathematical fiction, because it implies that the total power (i.e. the psd integrated over all frequencies) is infinite. Thus, a time sample of the white noise has infinite average power, which is certainly not a physically reasonable property. It is known from statistical physics that the thermal noise density decreases exponentially at (very!) high frequencies. But to understand the physical situation in communications engineering it is better to keep in mind that every receiver limits the bandwidth as well as every physical noise measurement. So it makes sense to think of the noise process to be white, but it cannot be sampled directly without an input device. Each input device filters the noise and leads to a finite power.

1.3.1 Mathematical wideband AWGN

The mathematical AWGN random process $w(t)$ can be characterized as a zero mean Gaussian process with the autocorrelation function

$$\mathrm{E}\{w(t_1)w(t_2)\} = \frac{N_0}{2}\delta(t_1 - t_2). \tag{1.48}$$

We see that for $t_1 = t_2$, this expression is not well defined, because $\delta(t)$ is not well defined for $t = 0$. As for the δ-impulse, we must understand white noise as a *generalized function* that cannot be sampled directly, but it can be measured by a proper set of linear detectors. These linear detectors are the sampled outputs of linear filters. Thus, formally we can write the output of the detector for the (real) signal $\phi(t)$ of such a white noise measurement as $\mathcal{D}_\phi[w] = [\phi(-t) * w(t)]_{t=0}$ or

$$\mathcal{D}_\phi[w] = \int_{-\infty}^{\infty} \phi(t)w(t)\,\mathrm{d}t, \tag{1.49}$$

that is, $\phi(-t)$ is the impulse response of the measuring device. In the mathematical literature, $\phi(t)$ is called a *test function* (Reed and Simon 1980). Note that the integral in Equation (1.49) formally looks like the scalar product $\langle \phi, w \rangle$. Keeping in mind that the scalar product is well defined only for finite-energy signals, we have avoided such a notation. We can now characterize the white noise by the statistical properties of the outputs of linear detectors.

Definition 1.3.1 (White Gaussian Noise) *White Gaussian noise $w(t)$ is a random signal, characterized by the following properties: the output of a (finite-energy) linear detector $\mathcal{D}_\phi[w]$ is a Gaussian random variable with zero mean. Any two detector outputs $\mathcal{D}_{\phi_1}[w]$ and $\mathcal{D}_{\phi_2}[w]$ are jointly Gaussian with cross-correlation*

$$\mathrm{E}\left\{\mathcal{D}_{\phi_1}[w]\mathcal{D}_{\phi_2}[w]\right\} = \frac{N_0}{2}\langle \phi_1, \phi_2 \rangle . \tag{1.50}$$

Since Gaussian random variables are completely characterized by their second-order properties (Papoulis 1991), all the statistical properties of $w(t)$ are fixed by this definition. Using the integral representation (1.49), it is easy to show that the characterization by detector outputs (1.50) is equivalent to (1.48) (see Problem 5).

Note that the AWGN outputs of orthogonal detectors are uncorrelated and thus, as Gaussian random variables, even statistically independent. In many transmission setups as discussed in the above examples, the transmission base and therefore the corresponding detectors are orthogonal. Thus, for an orthonormal transmission base, the detector outputs are both ISI-free and independent. Orthogonality thus means complete separability, which will lead us to the concept of *sufficient statistics* (see Subsection 1.4.1).

1.3.2 Complex baseband AWGN

Up to now, we have only considered wideband white Gaussian noise. The question now is what happens at the receiver when this additive disturbance of the useful signal is converted (together with the signal) to the complex baseband.

Consider a baseband detector for the real low-pass signal $\phi(t)$ and the detector that corresponds to the I-modulated version for the signal, $\tilde{\phi} = I\phi$. We know from Equation (1.47) that the output of the detector for $\tilde{\phi}$ for any signal r is the same as the output of ϕ for the I-demodulated version $I^D r$ of that signal. This same property also holds for white noise, that is, $\mathcal{D}_{\tilde{\phi}}[w] = \mathcal{D}_{\phi}[I^D w]$. Similarly, for the Q-demodulated noise, we have the property $\mathcal{D}_{\tilde{\psi}}[w] = \mathcal{D}_{\psi}[Q^D w]$ with $\tilde{\psi} = Q\psi$. Using this fact, together with the definition of AWGN and Theorem 1.2.2, we get the following Proposition.

Proposition 1.3.2 *Let $w(t)$ be additive white Gaussian noise and its I- and Q-demodulated versions be denoted by $I^D w$ and $Q^D w$. Let ϕ_1 and ϕ_2 be two strictly band-limited low-pass detectors. Then, the following properties hold:*

$$\mathrm{E}\left\{\mathcal{D}_{\phi_1}[I^D w]\mathcal{D}_{\phi_2}[I^D w]\right\} = \frac{N_0}{2}\langle\phi_1, \phi_2\rangle \tag{1.51}$$

$$\mathrm{E}\left\{\mathcal{D}_{\phi_1}[Q^D w]\mathcal{D}_{\phi_2}[Q^D w]\right\} = \frac{N_0}{2}\langle\phi_1, \phi_2\rangle \tag{1.52}$$

$$\mathrm{E}\left\{\mathcal{D}_{\phi_1}[I^D w]\mathcal{D}_{\phi_2}[Q^D w]\right\} = 0. \tag{1.53}$$

The last equation means that the I- and the Q-demodulator produce statistically independent outputs[2]. Since both demodulators include a low-pass filter, both $I^D w$ and $Q^D w$ are well-behaved random processes having finite average power $BN_0/2$. The samples (with sampling frequency B) of the low-pass white noise are given by the outputs of the detector corresponding to $\Phi(t)$, the impulse response of the ideal low-pass filter of bandwidth $B/2$. Thus, the low-pass white noise can be characterized by its detector outputs and by its samples as well.

We now define the complex baseband noise process $n(t)$ as the IQ-demodulated white noise

$$n = (I^D + jQ^D)w. \tag{1.54}$$

From the above proposition, we conclude

$$\mathrm{E}\{\mathcal{D}_{\phi_1}[n]\,\mathcal{D}^*_{\phi_2}[n]\} = N_0\langle\phi_1, \phi_2\rangle \tag{1.55}$$

and

$$\mathrm{E}\{\mathcal{D}_{\phi_1}[n]\,\mathcal{D}_{\phi_2}[n]\} = 0. \tag{1.56}$$

Complex random variables are characterized by these two types of covariances. Here the second one, the so-called *pseudocovariance,* has vanished. Gaussian processes with this property are called *proper* Gaussian. Nonproper Gaussian random variables have undesired properties for describing communication systems (Neeser and Massey 1993). The autocorrelation properties of $n(t)$ can simply be obtained by setting $\phi_1(t) = \Phi_{t_1}(t) = \Phi(t - t_1)$ and $\phi_2(t) = \Phi_{t_2}(t) = \Phi(t - t_2)$, where $\Phi(t)$ is the impulse response of the ideal low-pass filter of bandwidth $B/2$. Using $\left\langle\Phi_{t_1}, \Phi_{t_2}\right\rangle = \Phi(t_1 - t_2)$ we easily derive the following properties

$$\mathrm{E}\{n(t_1)\,n^*(t_2)\} = N_0\Phi(t_1 - t_2) \tag{1.57}$$

[2]Equivalently, we may say that the I- and the Q-component of the noise are statistically independent.

and

$$\mathrm{E}\{n(t_1)\, n(t_2)\} = 0. \tag{1.58}$$

$n(t)$ has similar properties as $w(t)$. It is white, but restricted to a bandwidth B, and the constant psd is N_0 instead of $N_0/2$. This can be understood because $n(t)$ is complex and the total power is the sum of the powers of the real and the imaginary part. Passband and complex baseband white noise psd is depicted in Figure 1.13.

Instead of dealing with complex white Gaussian noise with psd N_0 band-limited to $B/2$, many authors regard it as convenient to perform the limit $B \to \infty$, so that Equation (1.57) turns into

$$\mathrm{E}\{n(t_1)\, n^*(t_2)\} = N_0 \delta(t_1 - t_2),$$

that is, $n(t)$ becomes complex infinite-bandwidth white noise with *one*- sided psd N_0 (see e.g. (Kammeyer 2004; Proakis 2001)). This is reasonable if we think of downconverting with a low-pass filter of bandwidth much larger than the signal bandwidth. We wish to point out that the limit $B \to \infty$, that is, the wideband complex white noise does not reflect the physical reality but is only a mathematically convenient model. The equivalence between passband and baseband is only true for band-limited signals, especially $B/2 < f_0$ must hold.

Proposition 1.3.3 (Baseband stochastic processes) *Consider a (real-valued) stochastic process $\tilde{z}(t)$ that influences the useful signal in the air. We want to characterize the IQ-demodulator output*

$$z(t) = \Phi(t) * \left[\sqrt{2}\, \exp\left(-j2\pi f_0 t\right) \tilde{z}(t)\right]$$

by its second-order properties, that is, an autocorrelation function. Here $\Phi(t) = B\, \mathrm{sinc}\,(Bt)$ is the impulse response of the ideal low-pass filter of bandwidth $B/2$. We may think of white noise $w(t)$ as such a process, but also of an RF carrier that is broadened by the Doppler effect in a mobile radio environment (see Chapter 2). The following treatment is very general. We only assume that the random RF signal $\tilde{z}(t)$ has zero mean and it is wide-sense stationary (WSS), which means that the autocorrelation function

$$\tilde{\mathcal{R}}(\tau) = \mathrm{E}\left\{\tilde{z}(t+\tau)\tilde{z}(t)\right\}$$

of the process does not depend on t. We want to show that

$$\mathrm{E}\left\{z(t+\tau)z^*(t)\right\} = \Phi(\tau) * \left[2\, \exp\left(-j2\pi f_0 \tau\right)\, \tilde{\mathcal{R}}(\tau)\right] \tag{1.59}$$

and

$$\mathrm{E}\left\{z(t+\tau)z(t)\right\} = 0. \tag{1.60}$$

Obviously, for the special case of AWGN, this property is just given by the two Equations (1.57, 1.58) above.

To prove Equation (1.59), we apply the convolution in the definition of $z(t)$

$$\begin{aligned}
&\mathrm{E}\left\{z(t+\tau)z^*(t)\right\} \\
&\quad = 2\,\mathrm{E}\left\{\int_{-\infty}^{\infty} \mathrm{d}t_1 \Phi(t+\tau-t_1)\mathrm{e}^{-j2\pi f_0 t_1}\tilde{z}(t_1)\int_{-\infty}^{\infty} \mathrm{d}t_2 \Phi(t-t_2)\mathrm{e}^{j2\pi f_0 t_2}\tilde{z}(t_2)\right\} \\
&\quad = 2\,\mathrm{E}\left\{\int_{-\infty}^{\infty} \mathrm{d}t_1 \int_{-\infty}^{\infty} \mathrm{d}t_2 \Phi(t+\tau-t_1)\Phi(t-t_2)\mathrm{e}^{-j2\pi f_0(t_1-t_2)}\tilde{\mathcal{R}}(t_1-t_2)\right\} \\
&\quad = 2\,\mathrm{E}\left\{\int_{-\infty}^{\infty} \mathrm{d}t_1 \int_{-\infty}^{\infty} \mathrm{d}t_2 \int_{-\infty}^{\infty} \mathrm{d}f\ \Phi(t+\tau-t_1)\Phi(t-t_2)\mathrm{e}^{j2\pi(f-f_0)(t_1-t_2)}\tilde{\mathcal{S}}(f)\right\},
\end{aligned}$$

where we have expressed $\tilde{\mathcal{R}}(\tau)$ by means of its Fourier transform, that is, the power spectral density $\tilde{\mathcal{S}}(f)$ of the process. We have used the simpler notation $\int \mathrm{d}x \int \mathrm{d}y f(x, y)$ instead of $\int \left(\int f(x, y)\,\mathrm{d}y\right) \mathrm{d}x$. Substituting the time integration variables according to $t_1' = t + \tau - t_1$ and $t_2' = t - t_2$ and noting that $t_1 - t_2 = \tau - t_1' + t_2'$, we get the expression

$$\begin{aligned}
&2\,\mathrm{E}\left\{\int_{-\infty}^{\infty} \mathrm{d}f\ \tilde{\mathcal{S}}(f)\int_{-\infty}^{\infty} \mathrm{d}t_1' \Phi(t_1')\mathrm{e}^{j2\pi(f-f_0)(\tau-t_1')}\int_{-\infty}^{\infty} \mathrm{d}t_2' \Phi(t_2')\mathrm{e}^{+j2\pi(f-f_0)t_2'}\right\} \\
&\quad = 2\,\mathrm{E}\left\{\int_{-\infty}^{\infty} \mathrm{d}f\ \mathrm{e}^{j2\pi(f-f_0)\tau}\tilde{\mathcal{S}}(f)\,\Pi\left(\frac{f-f_0}{B}\right)\right\} \\
&\quad = 2\,\mathrm{E}\left\{\int_{-\infty}^{\infty} \mathrm{d}f\ \mathrm{e}^{j2\pi f\tau}\tilde{\mathcal{S}}(f+f_0)\,\Pi\left(\frac{f}{B}\right)\right\},
\end{aligned}$$

which completes the proof. We note that

$$\mathcal{S}(f) = 2\,\tilde{S}(f+f_0)\,\Pi\left(\frac{f}{B}\right),$$

the power spectral density of the process in the complex baseband, is the Fourier transform of the complex baseband autocorrelation function

$$\mathcal{R}(\tau) = \Phi(\tau) * \left[2\,\exp\left(-j2\pi f_0\tau\right)\,\tilde{\mathcal{R}}(\tau)\right].$$

The proof of Equation (1.60) is similar. Applying again the convolution in the definition of $z(t)$ leads to

$$\begin{aligned}
&\mathrm{E}\left\{z(t+\tau)z(t)\right\} \\
&\quad = 2\,\mathrm{E}\left\{\int_{-\infty}^{\infty} \mathrm{d}t_1 \Phi(t+\tau-t_1)\mathrm{e}^{-j2\pi f_0 t_1}\tilde{z}(t_1)\int_{-\infty}^{\infty} \mathrm{d}t_2 \Phi(t-t_2)\mathrm{e}^{-j2\pi f_0 t_2}\tilde{z}(t_2)\right\} \\
&\quad = 2\,\mathrm{E}\left\{\int_{-\infty}^{\infty} \mathrm{d}t_1 \int_{-\infty}^{\infty} \mathrm{d}t_2 \Phi(t+\tau-t_1)\Phi(t-t_2)\mathrm{e}^{-j2\pi f_0(t_1+t_2)}\tilde{\mathcal{R}}(t_1-t_2)\right\} \\
&\quad = 2\,\mathrm{E}\left\{\int_{-\infty}^{\infty} \mathrm{d}t_1 \int_{-\infty}^{\infty} \mathrm{d}t_2 \int_{-\infty}^{\infty} \mathrm{d}f\ \Phi(t+\tau-t_1)\Phi(t-t_2)\mathrm{e}^{-j2\pi f_0(t_1+t_2)}\mathrm{e}^{j2\pi f(t_1-t_2)}\tilde{\mathcal{S}}(f)\right\}.
\end{aligned}$$

We now substitute the time integration variables according to $t_1' = t + \tau - t_1$ and $t_2' = t - t_2$ and get the expression

$$2\,\mathrm{E}\left\{\int_{-\infty}^{\infty} \mathrm{d}f\, \tilde{\mathcal{S}}(f) \int_{-\infty}^{\infty} \mathrm{d}t_1' \Phi(t_1') \mathrm{e}^{j2\pi(f-f_0)(t+\tau-t_1')} \int_{-\infty}^{\infty} \mathrm{d}t_2' \Phi(t_2') \mathrm{e}^{-j2\pi(f+f_0)(t_2'-t)}\right\}$$
$$= 2\,\mathrm{E}\left\{\int_{-\infty}^{\infty} \mathrm{d}f\, \tilde{\mathcal{S}}(f)\, \mathrm{e}^{j2\pi(f-f_0)(t+\tau)}\, \Pi\left(\frac{f-f_0}{B}\right) \mathrm{e}^{j2\pi(f+f_0)t}\, \Pi\left(\frac{f+f_0}{B}\right)\right\}.$$

We note that

$$\Pi\left(\frac{f-f_0}{B}\right) \Pi\left(\frac{f+f_0}{B}\right) = 0,$$

which completes the proof.

1.3.3 The discrete AWGN channel

Consider a complex baseband signal $s(t)$ band limited to $B/2$ to be transmitted at the carrier frequency f_0. The corresponding passband transmit signal $\tilde{s}(t)$ given by Equation (1.34) is corrupted by AWGN, resulting in the receive signal

$$\tilde{r}(t) = \tilde{s}(t) + w(t).$$

The IQ-demodulated complex baseband receive signal is then given by

$$r(t) = s(t) + n(t), \tag{1.61}$$

where $n(t)$ is complex baseband AWGN as introduced in the preceding subsection. Let $\{g_k(t)\}_{k=1}^{K}$ be an orthogonal transmit base, for example, a Nyquist base, and

$$s(t) = \sum_{k=1}^{K} s_k g_k(t). \tag{1.62}$$

Let $n_k = \mathcal{D}_{g_k}[n]$ be the detector outputs of the noise for the detector $g_k(t)$. The detector outputs at the receiver $r_k = \mathcal{D}_{g_k}[r]$ are then given by

$$r_k = s_k + n_k. \tag{1.63}$$

We conclude from Equations (1.55) and (1.56) that n_k is discrete complex AWGN characterized by

$$\mathrm{E}\{n_i\, n_k^*\} = N_0 \delta_{ik} \tag{1.64}$$

and

$$\mathrm{E}\{n_i\, n_k\} = 0. \tag{1.65}$$

For $n_k = x_k + j\, y_k$, these two equations are equivalent to

$$\mathrm{E}\{x_i\, x_k\} = \frac{N_0}{2}\delta_{ik}, \tag{1.66}$$

$$\mathrm{E}\{y_i\, y_k\} = \frac{N_0}{2}\delta_{ik}, \tag{1.67}$$

and

$$\mathrm{E}\{x_i\, y_k\} = 0. \tag{1.68}$$

The random variables x_k have the joint pdf

$$p(x_1, \ldots, x_K) = \frac{1}{\sqrt{2\pi\sigma^2}^K} \exp\left(-\frac{1}{2\sigma^2}\left(x_1^2 + \cdots + x_K^2\right)\right)$$

for $\sigma^2 = N_0/2$. The random variables y_k have the same pdf. Defining the vectors

$$\mathbf{x} = (x_1, \ldots, x_K)^T,\ \mathbf{y} = (y_1, \ldots, y_K)^T$$

results in

$$p(\mathbf{x}) = \frac{1}{\sqrt{2\pi\sigma^2}^K} \exp\left(-\frac{1}{2\sigma^2}\|\mathbf{x}\|^2\right),$$

$$p(\mathbf{y}) = \frac{1}{\sqrt{2\pi\sigma^2}^K} \exp\left(-\frac{1}{2\sigma^2}\|\mathbf{y}\|^2\right).$$

The joint pdf for the x_k, y_k is the product of both. We define the complex noise vector

$$\mathbf{n} = (n_1, \ldots, n_K)^T,$$

and write, with $p(\mathbf{n}) = p(\mathbf{x}, \mathbf{y}) = p(\mathbf{x})p(\mathbf{y})$,

$$p(\mathbf{n}) = \frac{1}{\sqrt{2\pi\sigma^2}^{2K}} \exp\left(-\frac{1}{2\sigma^2}\|\mathbf{n}\|^2\right).$$

Using the vector notation $\mathbf{s} = (s_1, \ldots, s_K)^T$ and $\mathbf{r} = (r_1, \ldots, r_K)^T$ for the transmit symbols and the detector outputs, we write the discrete AWGN transmission channel (1.63) as

$$\mathbf{r} = \mathbf{s} + \mathbf{n}. \tag{1.69}$$

If the symbols s_k are real numbers, one can depict this as a transmission mission of a vector in the K-dimensional real Euclidean space with the canonical base $\mathbf{e}_1 = (1, 0, 0, \ldots, 0)^T$, $\mathbf{e}_2 = (0, 1, 0, \ldots, 0)^T, \ldots$. For complex s_k, one may think of a $2K$-dimensional real Euclidean space, because it has the same distance structure as a K-dimensional complex space.

We have assumed that the transmit base is orthonormal. This is not a fundamental restriction, because one can always perform a base transform to an orthonormal base. In that case, the symbols s_i are related to the original transmit symbols x_k by a transform $\mathbf{s} = \mathbf{B}\mathbf{x}$, where $\mathbf{B}$ is the matrix that describes the coordinate transform.

1.4 Detection of Signals in Noise

1.4.1 Sufficient statistics

For the sake of simplicity, consider the model of Equations (1.63) and (1.69) for only three real dimensions as illustrated in Figure 1.14. Assume that two real symbols s_1, s_2

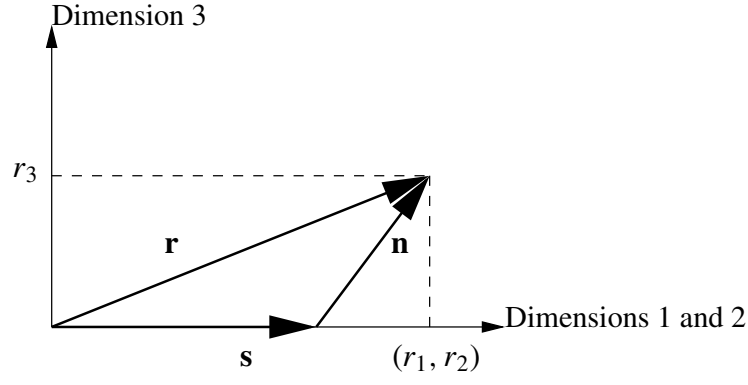

Figure 1.14 The noise in dimension 3 is irrelevant for the decision.

chosen from a finite alphabet are transmitted, while nothing is transmitted ($s_3 = 0$) in the third dimension. At the receiver, the detector outputs r_1, r_2, r_3 for three real dimensions are available. We can assume that the signal and the noise are statistically independent. We know that the Gaussian noise samples n_1, n_2, n_3, as outputs of orthogonal detectors, are statistically independent. It follows that the detector outputs r_1, r_2, r_3 are statistically independent. We argue that only the receiver outputs for those dimensions where a symbol has been transmitted are relevant for the decision and the others can be ignored because they are statistically independent, too. In our example, this means that we can ignore the receiver output r_3. Thus, we expect that

$$P(s_1, s_2|r_1, r_2, r_3) = P(s_1, s_2|r_1, r_2) \tag{1.70}$$

holds, that is, the probability that s_1, s_2 was transmitted conditioned by the observation of r_1, r_2, r_3 is the same as conditioned by the observation of only r_1, r_2. We now show that this equation follows from the independence of the detector outputs. From Bayes rule (Feller 1970), we get

$$P(s_1, s_2|r_1, r_2, r_3) = \frac{p(s_1, s_2, r_1, r_2, r_3)}{p(r_1, r_2, r_3)}, \tag{1.71}$$

where $p(a, b, \ldots)$ denotes the joint pdf for the random variable $a, b, \ldots$. Since r_3 is statistically independent from the other random variables s_1, s_2, r_1, r_2, it follows that

$$P(s_1, s_2|r_1, r_2, r_3) = \frac{p(s_1, s_2, r_1, r_2)p(r_3)}{p(r_1, r_2)p(r_3)}. \tag{1.72}$$

From

$$P(s_1, s_2|r_1, r_2) = \frac{p(s_1, s_2, r_1, r_2)}{p(r_1, r_2)}, \tag{1.73}$$

we obtain the desired property given by Equation (1.70). Note that, even though this property is seemingly intuitively obvious, we have made use of the fact that the noise is Gaussian. White noise outputs of orthogonal detectors are uncorrelated, but the Gaussian property ensures that they are statistically independent, so that their pdfs can be factorized.

The above argument can obviously be generalized to more dimensions. We only need to detect in those dimensions where the signal has been transmitted. The corresponding detector outputs are then called a *set of sufficient statistics*. For a more detailed discussion, see (Benedetto and Biglieri 1999; Blahut 1990; Wozencraft and Jacobs 1965).

1.4.2 Maximum likelihood sequence estimation

Again we consider the discrete-time model of Equations (1.63) and (1.69) and assume a finite alphabet for the transmit symbols s_k , so that there is a finite set of possible transmit vectors $\mathbf{s}$. Given a receive vector $\mathbf{r}$, we ask for the most probable transmit vector $\hat{\mathbf{s}}$, that is, the one for which the conditional probability $P(\mathbf{s}|\mathbf{r})$ that $\mathbf{s}$ was transmitted given that $\mathbf{r}$ has been received becomes maximal. The estimate of the symbol is

$$\hat{\mathbf{s}} = \arg\max_{\mathbf{s}} P(\mathbf{s}|\mathbf{r}). \tag{1.74}$$

From Bayes law, we have

$$P(\mathbf{s}|\mathbf{r})\,p(\mathbf{r}) = p(\mathbf{r}|\mathbf{s})\,P(\mathbf{s}), \tag{1.75}$$

where $p(\mathbf{r})$ is the pdf for the receive vector $\mathbf{r}$, $p(\mathbf{r}|\mathbf{s})$ is the pdf for the receive vector $\mathbf{r}$ given a fixed transmit vector $\mathbf{s}$, and $P(\mathbf{s})$ is the *a priori* probability for $\mathbf{s}$. We assume that all transmit sequences have equal *a priori* probability. Then, from

$$p(\mathbf{r}|\mathbf{s}) \propto \exp\left(-\frac{1}{2\sigma^2}\,\|\mathbf{r}-\mathbf{s}\|^2\right), \tag{1.76}$$

we conclude that

$$\hat{\mathbf{s}} = \arg\min_{\mathbf{s}} \|\mathbf{r}-\mathbf{s}\|^2 . \tag{1.77}$$

Thus, the most likely transmit vector minimizes the squared Euclidean distance. From

$$\|\mathbf{r}-\mathbf{s}\|^2 = \|\mathbf{r}\|^2 + \|\mathbf{s}\|^2 - 2\Re\left\{\mathbf{s}^\dagger\mathbf{r}\right\},$$

we obtain the alternative condition

$$\hat{\mathbf{s}} = \arg\max_{\mathbf{s}} \left(\Re\left\{\mathbf{s}^\dagger\mathbf{r}\right\} - \frac{1}{2}\,\|\mathbf{s}\|^2\right). \tag{1.78}$$

The first (scalar product) term can be interpreted as a cross correlation between the transmit and the receive signal. The second term is half the signal energy. Thus, the most likely transmit signal is the one that maximizes the cross correlation with the receive signal, thereby taking into account a correction term for the energy. If all transmit signals have the same energy, this term can be ignored.

The receiver technique described above, which finds the most likely transmit vector, is called *maximum likelihood sequence estimation* (MLSE). It is of fundamental importance in communication theory, and we will often need it in the following chapters.

A continuous analog to Equation (1.78) can be established. We recall that the continuous transmit signal $s(t)$ and the components s_k of the discrete transmit signal vector $\mathbf{s}$ are related by

$$s(t) = \sum_{k=1}^{K} s_k g_k(t),$$

and the continuous receive signal $r(t)$ and the components r_k of the discrete transmit signal vector $\mathbf{r}$ are related by

$$r_k = \mathcal{D}_{g_k}[r] = \int_{-\infty}^{\infty} g_k^*(t) r(t)\, \mathrm{d}t.$$

From these relations, we easily conclude that

$$\mathbf{s}^\dagger \mathbf{r} = \int_{-\infty}^{\infty} s^*(t) r(t)\, \mathrm{d}t$$

holds. Equation (1.78) is then equivalent to

$$\hat{s} = \arg\max_s \left(\Re\{\mathcal{D}_s[r]\} - \frac{1}{2}\|s\|^2 \right) \tag{1.79}$$

for finding the maximum likelihood (ML) transmit signal $\hat{s}(t)$. In the first term of this expression,

$$\mathcal{D}_s[r] = \int_{-\infty}^{\infty} s^*(t) r(t)\, \mathrm{d}t$$

means that the detector outputs (= sampled MF outputs) for all possible transmit signals $s(t)$ must be taken. For all these signals, half of their energy

$$\|s\|^2 = \int_{-\infty}^{\infty} |s(t)|^2\, \mathrm{d}t$$

must be subtracted from the real part of the detector output to obtain the likelihood of each signal.

Example 3 (Walsh Demodulator) *Consider a transmission with four possible transmit vectors* $\mathbf{s}_1$, $\mathbf{s}_2$, $\mathbf{s}_3$ *and* $\mathbf{s}_4$ *given by the columns of the matrix*

$$[\mathbf{s}_1,\ \mathbf{s}_2,\ \mathbf{s}_3,\ \mathbf{s}_4] = \begin{bmatrix} 1 & 1 & 1 & 1 \\ 1 & -1 & 1 & -1 \\ 1 & 1 & -1 & -1 \\ 1 & -1 & -1 & 1 \end{bmatrix},$$

each being transmitted with the same probability. This is just orthogonal Walsh modulation for $M = 4$. *We ask for the most probable transmit vector* $\hat{\mathbf{s}}$ *on the condition that the vector* $\mathbf{r} = (1.5,\ -0.8,\ 1.1,\ -0.2)^T$ *has been received. Since all transmit vectors have equal energy, the most probable transmit vector is the one that maximizes the scalar product with* $\mathbf{r}$. *We calculated the scalar products as*

$$\mathbf{s}_1 \cdot \mathbf{r} = 2.0, \quad \mathbf{s}_2 \cdot \mathbf{r} = 3.2, \quad \mathbf{s}_3 \cdot \mathbf{r} = 0.4, \quad \mathbf{s}_4 \cdot \mathbf{r} = 1.4.$$

We conclude that $\mathbf{s}_2$ *has most probably been transmitted.*

1.4.3 Pairwise error probabilities

Consider again a discrete AWGN channel as given by Equation (1.69). We write

$$\mathbf{r} = \mathbf{s} + \mathbf{n}_c,$$

where $\mathbf{n}_c$ is the complex AWGN vector. For the geometrical interpretation of the following derivation of error probabilities, it is convenient to deal with real vectors instead of complex ones. By defining

$$\mathbf{y} = \begin{bmatrix} \Re\{\mathbf{r}\} \\ \Im\{\mathbf{r}\} \end{bmatrix}, \quad \mathbf{x} = \begin{bmatrix} \Re\{\mathbf{s}\} \\ \Im\{\mathbf{s}\} \end{bmatrix},$$

and

$$\mathbf{n} = \begin{bmatrix} \Re\{\mathbf{n}_c\} \\ \Im\{\mathbf{n}_c\} \end{bmatrix},$$

we can investigate the equivalent discrete real AWGN channel

$$\mathbf{y} = \mathbf{x} + \mathbf{n}. \tag{1.80}$$

Consider the case that $\mathbf{x}$ has been transmitted, but the receiver decides for another symbol $\hat{\mathbf{x}}$. The probability for this event (excluding all other possibilities) is called the *pairwise error probability* (PEP) $P(\mathbf{x} \mapsto \hat{\mathbf{x}})$. Define the decision variable

$$X = \|\mathbf{y} - \mathbf{x}\|^2 - \|\mathbf{y} - \hat{\mathbf{x}}\|^2$$

as the difference of squared Euclidean distances. If $X > 0$, the receiver will take an erroneous decision for $\hat{\mathbf{x}}$. Then, using simple vector algebra (see Problem 7), we obtain

$$X = 2\left[\left(\mathbf{y} - \frac{\mathbf{x} + \hat{\mathbf{x}}}{2}\right)(\hat{\mathbf{x}} - \mathbf{x})\right].$$

The geometrical interpretation is depicted in Figure 1.15. The decision variable is (up to a factor) the projection of the difference between the receive vector $\mathbf{y}$ and the center point $\frac{1}{2}(\mathbf{x} + \hat{\mathbf{x}})$ between the two possible transmit vectors on the line between them. The decision threshold is a plane perpendicular to that line. Define $\mathbf{d} = \frac{1}{2}(\hat{\mathbf{x}} - \mathbf{x})$ as the difference vector between $\hat{\mathbf{x}}$ and the center point, that is, $d = \|\mathbf{d}\|$ is the distance of the two possible transmit signals from the threshold. Writing $\mathbf{y} = \mathbf{x} + \mathbf{n}$ and using $\mathbf{x} = \frac{1}{2}(\mathbf{x} + \hat{\mathbf{x}}) - \mathbf{d}$, the scaled decision variable $\tilde{X} = \frac{1}{4d}X$ can be written as

$$\tilde{X} = (-\mathbf{d} + \mathbf{n}) \cdot \frac{\mathbf{d}}{d}.$$

It can easily be shown that

$$n = \mathbf{n} \cdot \frac{\mathbf{d}}{d},$$

the projection of the noise onto the relevant dimension, is a Gaussian random variable with zero mean and variance $\sigma^2 = N_0/2$ (see Problem 8). Since $\tilde{X} = -d + n$, the error probability is given by

$$P(\tilde{X}) > 0) = P(n > \mathbf{d}).$$

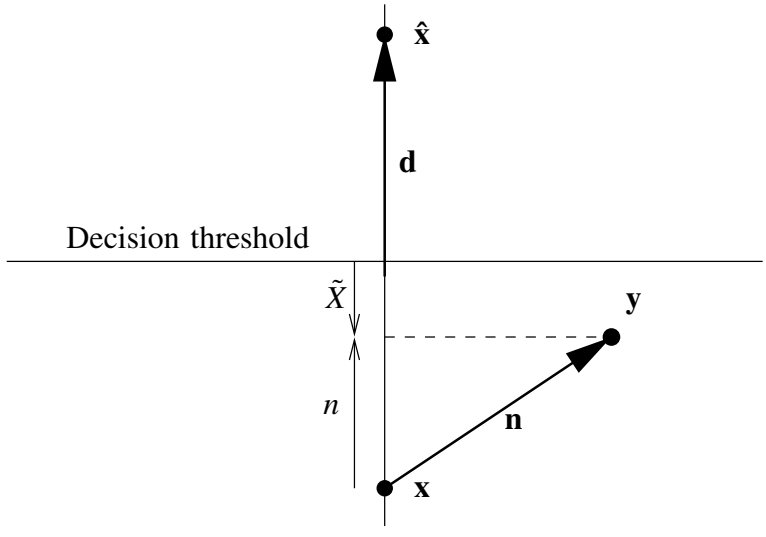

Figure 1.15 Decision threshold.

This equals

$$P(n > \mathbf{d}) = Q\left(\frac{\mathbf{d}}{\sigma}\right), \tag{1.81}$$

where the Gaussian probability integral is defined by

$$Q(x) = \frac{1}{\sqrt{2\pi}} \int_x^\infty e^{-\frac{1}{2}\xi^2} \, \mathrm{d}\xi$$

The Q-function defined above can be expressed by the complementary Gaussian error function $\mathrm{erfc}(x) = 1 - \mathrm{erf}(x)$, where $\mathrm{erf}(x)$ is the Gaussian error function, as

$$Q\,(x) = \frac{1}{2}\mathrm{erfc}\left(\frac{x}{\sqrt{2}}\right). \tag{1.82}$$

The pairwise error probability can then be expressed by

$$P(\mathbf{x} \mapsto \hat{\mathbf{x}}) = \frac{1}{2}\mathrm{erfc}\left(\sqrt{\frac{1}{4N_0}\|\mathbf{x} - \hat{\mathbf{x}}\|^2}\right). \tag{1.83}$$

Since the norms of complex vectors and the equivalent real vectors are identical, we can also write

$$P(\mathbf{s} \mapsto \hat{\mathbf{s}}) = \frac{1}{2}\mathrm{erfc}\left(\sqrt{\frac{1}{4N_0}\|\mathbf{s} - \hat{\mathbf{s}}\|^2}\right). \tag{1.84}$$

For the continuous signal,

$$s(t) = \sum_{k=1}^{K} s_k g_k(t), \tag{1.85}$$

this is equivalent to

$$P\left(s(t) \mapsto \hat{s}(t)\right) = \frac{1}{2}\mathrm{erfc}\left(\sqrt{\frac{1}{4N_0}\int_{-\infty}^{\infty} |s(t) - \hat{s}(t)|^2 \, \mathrm{d}t}\right). \tag{1.86}$$

It has been pointed out by Simon and Divsalar (Simon and Divsalar 1998) that, for many applications, the following polar representation of the complementary Gaussian error function provides a simpler treatment of many problems, especially for fading channels.

Proposition 1.4.1 (Polar representation of the Gaussian erfc function)

$$\frac{1}{2}\mathrm{erfc}(x) = \frac{1}{\pi}\int_0^{\pi/2} \exp\left(-\frac{x^2}{\sin^2\theta}\right) \mathrm{d}\theta. \tag{1.87}$$

Proof. The idea of the proof is to view the one-dimensional problem of pairwise error probability as two-dimensional and introduce polar coordinates. AWGN is a Gaussian random variable with mean zero and variance $\sigma^2 = 1$. The probability that the random variable exceeds a positive real value, x, is given by the Gaussian probability integral

$$Q(x) = \int_x^{\infty} \frac{1}{\sqrt{2\pi}} \exp\left(-\frac{1}{2}\xi^2\right) \mathrm{d}\xi. \tag{1.88}$$

This probability does not change if noise of the same variance is introduced in the second dimension. The error threshold is now a straight line parallel to the axis of the second dimension, and the probability is given by

$$Q(x) = \int_x^{\infty} \left(\int_{-\infty}^{\infty} \frac{1}{2\pi} \exp\left(-\frac{1}{2}(\xi^2 + \eta^2)\right) \mathrm{d}\eta\right) \mathrm{d}\xi. \tag{1.89}$$

This integral can be written in polar coordinates (r, ϕ) as

$$Q(x) = \int_{-\pi/2}^{\pi/2} \left(\int_{x/\cos\phi}^{\infty} \frac{r}{2\pi} \exp\left(-\frac{1}{2}r^2\right) \mathrm{d}r\right) \mathrm{d}\phi. \tag{1.90}$$

The integral over r can immediately be solved to give

$$Q(x) = \int_{-\pi/2}^{\pi/2} \frac{1}{2\pi} \exp\left(-\frac{1}{2}\frac{x^2}{\cos^2\phi}\right) \mathrm{d}\phi. \tag{1.91}$$

A simple symmetry argument now leads to the desired form of $\frac{1}{2}\mathrm{erfc}(x) = Q(\sqrt{2}x)$.

An upper bound of the erfc function can easily be obtained from this expression by upper bounding the integrand by its maximum value,

$$\frac{1}{2}\mathrm{erfc}(x) \leq \frac{1}{2}\mathrm{e}^{-x^2}. \tag{1.92}$$

Example 4 (PEP for Antipodal Modulation) *Consider the case of only two possible transmit signals $s_1(t)$ and $s_2(t)$ given by*

$$s_{1,2}(t) = \pm\sqrt{E_S}\, g(t),$$

where $g(t)$ is a pulse normalized to $\|g\|^2 = 1$, and E_S is the energy of the transmitted signal. To obtain the PEP, according to Equation (1.86), we calculate the squared Euclidean distance

$$\|s_1 - s_2\|^2 = \int_{-\infty}^{\infty} |s_1(t) - s_2(t)|^2 \, \mathrm{d}t$$

between two possible transmit signals $s_1(t)$ and $s_2(t)$ and obtain

$$\|s_1 - s_2\|^2 = \left\| \sqrt{E_s}\, g - \left(-\sqrt{E_s}\, g \right) \right\|^2 = 4E_S.$$

The PEP is then given by Equation (1.86) as

$$P\left(s_1(t) \mapsto s_2(t)\right) = \frac{1}{2}\mathrm{erfc}\left(\sqrt{\frac{E_S}{N_0}}\right).$$

One can transmit one bit by selecting one of the two possible signals. Therefore, the energy per bit is given by $E_b = E_S$ leading to the PEP

$$P\left(s_1(t) \mapsto s_2(t)\right) = \frac{1}{2}\mathrm{erfc}\left(\sqrt{\frac{E_b}{N_0}}\right).$$

Example 5 (PEP for Orthogonal Modulation) *Consider an orthonormal transmit base $g_k(t)$, $k = 1, \ldots, M$. We may think of the Walsh base or the Fourier base as an example, but any other choice is possible. Assume that one of the M possible signals*

$$s_k(t) = \sqrt{E_S}\, g_k(t)$$

is transmitted, where E_S is again the signal energy. In case of the Walsh base, this is just Walsh modulation. In case of the Fourier base, this is just (orthogonal) FSK (frequency shift keying). To obtain the PEP, we have to calculate the squared Euclidean distance

$$\|s_i - s_k\|^2 = \int_{-\infty}^{\infty} |s_i(t) - s_k(t)|^2 \, \mathrm{d}t$$

between two possible transmit signals $s_i(t)$ and $s_k(t)$ with $i \neq k$. Because the base is orthonormal, we obtain

$$\|s_i - s_k\|^2 = E_S \, \|g_i - g_k\|^2 = 2E_S.$$

The PEP is then given by

$$P\left(s_i(t) \mapsto s_k(t)\right) = \frac{1}{2}\mathrm{erfc}\left(\sqrt{\frac{E_S}{2N_0}}\right).$$

One can transmit $\log_2(M)$ bits by selecting one of M possible signals. Therefore, the energy per bit is given by $E_b = E_S/\log_2(M)$, leading to the PEP

$$P\left(s_i(t) \mapsto s_k(t)\right) = \frac{1}{2}\mathrm{erfc}\left(\sqrt{\log_2(M)\frac{E_b}{2N_0}}\right).$$

Concerning the PEP, we see that for $M = 2$, orthogonal modulation is inferior compared to antipodal modulation, but it is superior if more than two bits per signal are transmitted. The price for that robustness of high-level orthogonal modulation is that the number of the required signal dimensions and thus the required bandwidth increases exponentially with the number of bits.

1.5 Linear Modulation Schemes

Consider some digital information that is given by a finite bit sequence. To transmit this information over a physical channel by a passband signal $\tilde{s}(t) = \Re\left\{s(t)\mathrm{e}^{j2\pi f_0 t}\right\}$, we need a mapping rule between the set of bit sequences and the set of possible signals. We call such a mapping rule a *digital modulation scheme*. A *linear* digital modulation scheme is characterized by the complex baseband signal

$$s(t) = \sum_{k=1}^{K} s_k g_k(t),$$

where the information is carried by the complex transmit symbols s_k. The modulation scheme is called *linear*, because this is a *linear mapping* from the vector $\mathbf{s} = (s_1, \ldots, s_K)^T$ of transmit symbols to the continuous transmit signal $s(t)$. In the following subsections, we will briefly discuss the most popular *signal constellations* for the modulation symbols s_k that are used to transmit information by choosing one of M possible points of that constellation. We assume that M is a power of two, so each complex symbol s_k carries $\log_2(M)$ bits of the information. Although it is possible to combine several symbols to a higher-dimensional constellation, the following discussion is restricted to the case where each symbol s_k is modulated separately by a tuple of $m = \log_2(M)$ bits. The rule how this is done is called the *symbol mapping* and the corresponding device is called the symbol mapper. In this section, we always deal with orthonormal base pulses $g_k(t)$. Then, as discussed in the preceding sections, we can restrict ourselves to a discrete-time transmission setup where the complex modulation symbols

$$s_k = x_k + jy_k$$

are corrupted by complex discrete-time white Gaussian noise n_k.

1.5.1 Signal-to-noise ratio and power efficiency

Since we have assumed orthonormal transmit pulses $g_k(t)$, the corresponding detector outputs are given by

$$r_k = s_k + n_k,$$

where n_k is discrete complex AWGN. We note that, because the pulses are normalized according to

$$\int_{-\infty}^{\infty} g_i^*(t) g_k(t)\,\mathrm{d}t = \delta_{ik},$$

the detector changes the dimension of the signal; the squared continuous signals have the dimension of a power, but the squared discrete detector output signals have the dimension of an energy.

The average signal energy is given by

$$E = \mathrm{E}\left\{\int_{-\infty}^{\infty} |s(t)|^2 \, \mathrm{d}t\right\} = \mathrm{E}\left\{\sum_{k=1}^{K} |s_k|^2\right\} = K \, \mathrm{E}\left\{|s_k|^2\right\},$$

where we have assumed that all the K symbols s_k have identical statistical properties. The energy per symbol $E_S = E/K$ is given by

$$E_S = \mathrm{E}\left\{|s_k|^2\right\}.$$

The energy of the detector output of the noise is

$$E_N = \mathrm{E}\left\{|n_k|^2\right\} = N_0,$$

so the signal-to-noise ratio, *SNR*, defined as the ratio between the signal energy and the relevant noise, results in

$$SNR = \frac{E_S}{N_0}.$$

When thinking of practical receivers, it may be confusing that a detector changes the dimension of the signal, because we have interpreted it as a matched filter together with a sampling device. To avoid this confusion, we may introduce a proper constant. For signaling with the Nyquist base, $g_k(t) = g(t - kT_S)$, one symbol s_k is transmitted in each time interval of length T_S. We then define the matched filter by its impulse response

$$h(t) = \frac{1}{\sqrt{T_S}} \, g^*(-t)$$

so that the matched filter output $h(t) * r(t)$ has the same dimension as the input signal $r(t)$. The samples of the matched filter output are given by

$$\frac{1}{\sqrt{T_S}} r_k = \frac{1}{\sqrt{T_S}} s_k + \frac{1}{\sqrt{T_S}} n_k.$$

Then, the power of the sampled useful signal is given by

$$P_S = \mathrm{E}\left\{\left|\frac{1}{\sqrt{T_S}} s_k\right|^2\right\} = \frac{E_S}{T_S},$$

and the noise power is

$$P_N = \mathrm{E}\left\{\left|\frac{1}{\sqrt{T_S}} n_k\right|^2\right\} = \frac{N_0}{T_S}.$$

Thus, the SNR may equivalently be defined as

$$SNR = \frac{P_S}{P_N},$$

which is the more natural definition for practical measurements.

The SNR is a physical quantity that can easily be measured, but it does not say anything about the power efficiency. To evaluate the power efficiency, one must know the

average energy E_b per useful bit at the receiver that is needed for a reliable recovery of the information. If $\log_2(M)$ useful bits are transmitted by each symbol s_k, the relation

$$E_S = \log_2(M)\, E_b$$

holds, which relates both quantities by

$$SNR = \log_2(M)\, \frac{E_b}{N_0}.$$

We note the important fact that $E_b = P_S/R_b$ is just the average signal power P_S needed per useful bit rate R_b. Therefore, a modulation that needs less E_b/N_0 to achieve a reliable transmission is more *power efficient* .

In the following sections, we discuss the most popular symbol mappings and their properties.

1.5.2 ASK and QAM

For M-ASK (*amplitude-shift keying*), a tuple of $m = \log_2(M)$ bits will be mapped only on the real part x_k of s_k, while the imaginary part y_k will be set to zero. The M points will be placed equidistant and symmetrically about zero. Denoting the distance between two points by $2d$, the signal constellation for 2-ASK is given by $x_l \in \{\pm d\}$, for 4-ASK by $x_l \in \{\pm d, \pm 3d\}$ and for 8-ASK by $x_l \in \{\pm d, \pm 3d, \pm 5d, \pm 7d\}$. We consider *Gray mapping*, that is, two neighboring points differ only in one bit. In Figure 1.16, the M-ASK signal constellations are depicted for $M = 2,\ 4,\ 8$.

Assuming the same *a priori* probability for each signal point, we easily calculate the symbol energies as $E_S = \mathrm{E}\left\{|s_k|^2\right\} = d^2,\ 5d^2,\ 21d^2$ for these constellations, leading to the respective energies per bit $E_b = E_S/\log_2(M) = d^2,\ 2.5d^2,\ 7d^2$.

Adjacent points have the distance $2d$, so the distance to the corresponding decision threshold is given by d. If a certain point of the constellation is transmitted, the probability that an error occurs because the discrete noise with variance $\sigma^2 = N_0/2$ (per real dimension) exceeds the distance to the decision threshold with distance d is given by

$$P_{err} = \mathrm{Q}\left(\frac{\mathbf{d}}{\sigma}\right) = \frac{1}{2}\,\mathrm{erfc}\left(\sqrt{\frac{d^2}{N_0}}\right), \tag{1.93}$$

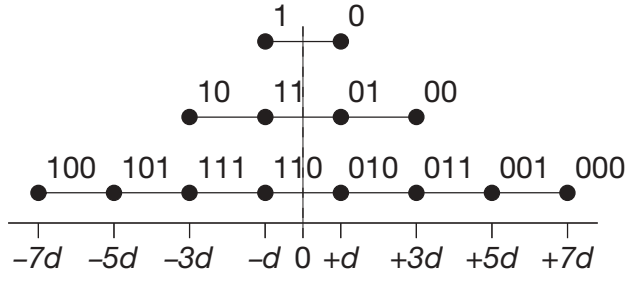

Figure 1.16 M-ASK Constellation for $M = 2, 4, 8$.

see Equation (1.81). For the two outer points of the constellation, this is just the probability that a symbol error occurs. In contrast, for $M > 2$, each inner point has two neighbors, leading to a symbol error probability of $2P_{err}$ for these points. Averaging over the symbol error probabilities for all points of each constellation, we get the symbol error probabilities

$$P_S^{2-ASK} = \mathrm{Q}\left(\frac{\mathbf{d}}{\sigma}\right), \quad P_S^{4-ASK} = \frac{3}{2}\mathrm{Q}\left(\frac{\mathbf{d}}{\sigma}\right), \quad P_S^{8-ASK} = \frac{7}{4}\mathrm{Q}\left(\frac{\mathbf{d}}{\sigma}\right).$$

For Gray mapping, we can make the approximation that each symbol error leads only to one bit error. Thus, we readily obtain the bit error probabilities expressed by the bit energy for $M = 2, 4, 8$ as

$$P_b^{2-ASK} = \frac{1}{2}\,\mathrm{erfc}\left(\sqrt{\frac{E_b}{N_0}}\right),$$

and

$$P_b^{4-ASK} \approx \frac{3}{8}\,\mathrm{erfc}\left(\sqrt{\frac{2}{5}\frac{E_b}{N_0}}\right), \tag{1.94}$$

$$P_b^{8-ASK} \approx \frac{7}{24}\,\mathrm{erfc}\left(\sqrt{\frac{1}{7}\frac{E_b}{N_0}}\right).$$

For ASK constellations, only the I-component, corresponding to the cosine wave, will be modulated, while the sine wave will not be present in the passband signal. Since, in general, every passband signal of a certain bandwidth may have both components, 50% of the bandwidth resources remain unused. A simple way to use these resources is to apply the same ASK modulation for the Q-component too. We thus have complex modulation symbols $s_k = x_k + jy_k$, where both x_k and y_k are taken from an M-ASK constellation. The result is a square constellation of M^2 signal points in the complex plane, as depicted in Figure 1.17 for $M^2 = 64$. We call this an M^2-QAM (quadrature amplitude modulation). The bit error performance of M^2-QAM as a function of E_b/N_0 is the same as for M-ASK, that is,

$$P_b^{4-QAM} = \frac{1}{2}\,\mathrm{erfc}\left(\sqrt{\frac{E_b}{N_0}}\right),$$

$$P_b^{16-QAM} \approx \frac{3}{8}\,\mathrm{erfc}\left(\sqrt{\frac{2}{5}\frac{E_b}{N_0}}\right) \tag{1.95}$$

and

$$P_b^{64-QAM} \approx \frac{7}{24}\,\mathrm{erfc}\left(\sqrt{\frac{1}{7}\frac{E_b}{N_0}}\right).$$

This is because the I- and the Q-component can be regarded as completely independent channels that do not influence each other. Thus, M^2-QAM can be regarded as M-ASK multiplexed to the orthogonal I- and Q-channel. Note that the bit error rates are not identical if they are plotted as a function of the signal-to-noise ratio. The bit error probabilities of Equations (1.95) are depicted in Figure 1.18. For high values of E_b/N_0, 16-QAM shows

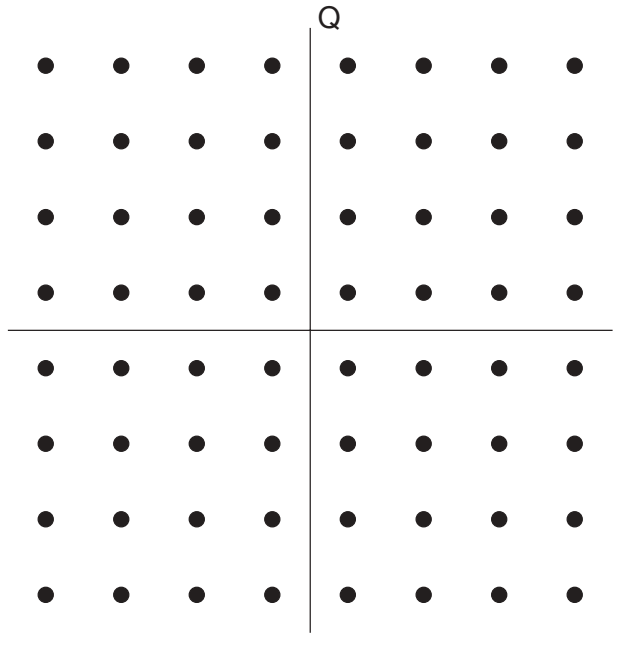

Figure 1.17 The 64-QAM constellation.

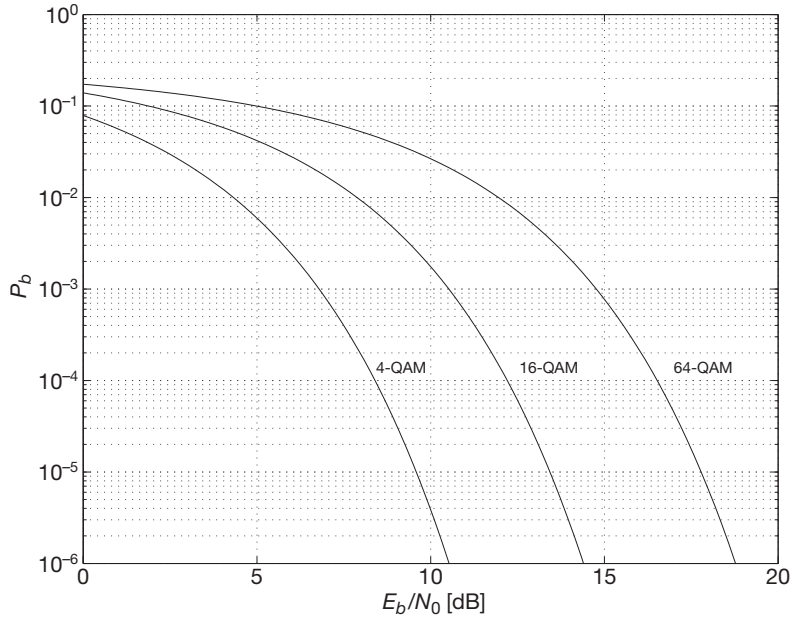

Figure 1.18 Bit error probabilities for 4-QAM, 16-QAM, and 64-QAM.

a performance loss of $10\lg(2.5) \approx 4$ dB compared to 4-QAM, while 64-QAM shows a performance loss of $10\lg(7) \approx 8.5$ dB. This is the price that has to be paid for transmitting twice, respectively three times the data rate in the same bandwidth.

We finally note that nonsquare QAM constellations are also possible like, for example, 8-QAM, 32-QAM and 128-QAM, but we will not discuss these constellations in this text.

1.5.3 PSK

For M-PSK (phase-shift keying), the modulation symbols s_k can be written as

$$s_k = \sqrt{E_S}\, e^{j\phi_k},$$

that is, all the information is contained in the M possible phase values ϕ_k of the symbol. Two adjacent points of the constellation have the phase difference $2\pi/M$. It is a matter of convenience whether $\phi = 0$ is a point of the constellation or not. For 2-PSK – often called *BPSK* (binary PSK) – the phase may take the two values $\phi_k \in \{0, \pi\}$ and thus 2-PSK is just the same as 2-ASK. For 4-PSK – often called QPSK (quaternary PSK) – the phase may take the four values $\phi_k \in \left\{\pm\frac{\pi}{4}, \pm\frac{3\pi}{4}\right\}$ and thus 4-PSK is just the same as 4-QAM. The constellation for 8-PSK with Gray mapping, as an example, is depicted in Figure 1.19.

The approximate error probabilities for M-PSK with Gray mapping can be easily obtained. Let the distance between two adjacent points be $2d$. From elementary geometrical consideration, we get

$$\mathbf{d} = \sqrt{E_S}\, \sin\left(\frac{\pi}{M}\right).$$

For $M > 2$, each constellation point has two nearest neighbors. All the other signal points corresponding to symbol errors lie beyond the two corresponding decision thresholds. By

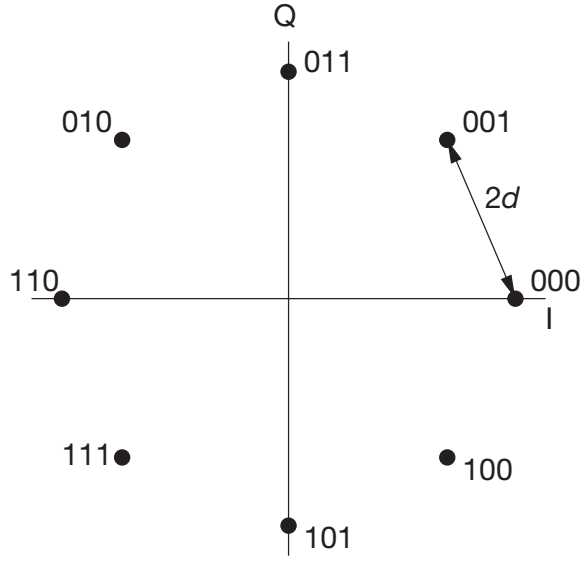

Figure 1.19 Signal constellation for 8-PSK.

a simple union-bound argument, we find that the symbol error probability can be tightly upper bounded by

$$P_S \leq 2\mathrm{Q}\left(\frac{\mathbf{d}}{\sigma}\right) = \mathrm{erfc}\left(\sqrt{\sin^2\left(\frac{\pi}{M}\right)\frac{E_S}{N_0}}\right).$$

By assuming that only one bit error occurs for each symbol error and taking into account the relation $E_S = \log_2(M)\, E_b$, we get the approximate expression

$$P_b \approx \frac{1}{\log_2(M)}\mathrm{erfc}\left(\sqrt{\log_2(M)\,\sin^2\left(\frac{\pi}{M}\right)\frac{E_b}{N_0}}\right) \tag{1.96}$$

for the bit error probability. The bit error probabilities of Equation (1.96) are depicted in Figure 1.20. For high values of E_b/N_0, 8-PSK shows a performance loss of $10\lg(3\sin^2(\pi/8)) \approx 3.6$ dB compared to 4-PSK, while 16-PSK shows a performance loss of $10\lg(4\sin^2(\pi/16)) \approx 8.2$ dB. Thus, higher-level PSK modulation leads to a considerable loss in power efficiency compared to higher-level QAM at the same spectral efficiency.

1.5.4 DPSK

For DPSK (differential PSK), the phase *difference* between two adjacent transmit symbols carries the information, not the phase of the transmit symbol itself. This means that for a sequence of transmit symbols

$$s_k = \sqrt{E_S}\,\mathrm{e}^{j\phi_k},$$

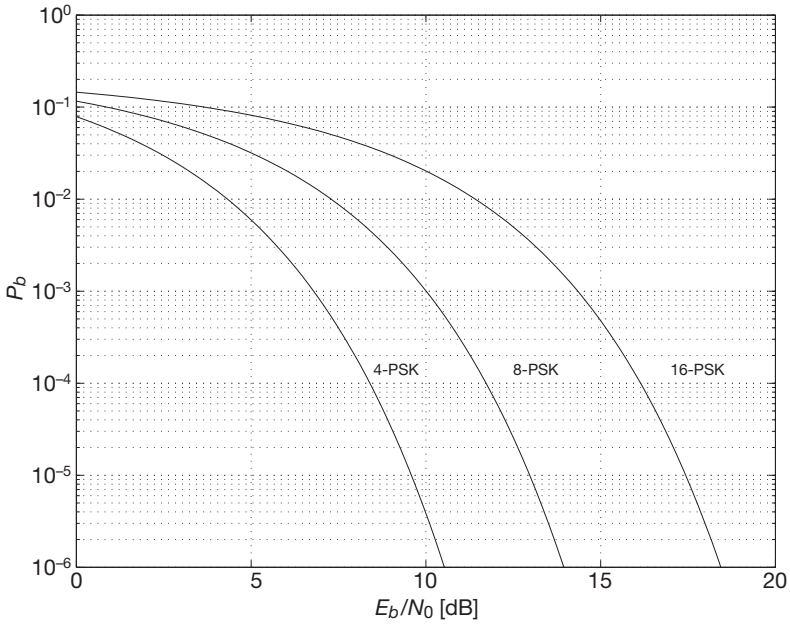

Figure 1.20 Bit error probabilities for 4-PSK, 8-PSK and 16-PSK.

the information is carried by

$$\Delta\phi_k = \phi_k - \phi_{k-1},$$

and

$$z_k = \mathrm{e}^{j\,\Delta\phi_k}$$

is a symbol taken from an M-PSK constellation with energy one. The transmit symbols are then given by the recursion

$$s_k = z_k \cdot s_{k-1}$$

with a start symbol s_0 that may have some arbitrary reference phase ϕ_0. We may set this phase equal to zero and write

$$s_0 = \sqrt{E_S}.$$

Because of this phase reference symbol, the transmit signal

$$s(t) = \sum_{k=0}^{K} s_k g_k(t)$$

carries $K+1$ transmit symbols s_k, but only K useful PSK symbols z_k. Typically, the phase reference symbol will be transmitted at the beginning of a frame, and the frame length is large enough so that the loss in data rate due to the reference symbol can be neglected.

Again it is a matter of convenience whether the PSK constellation for z_k contains the phase (difference) $\Delta\phi_k = 0$ or not. For the most popular QPSK constellation, $\Delta\phi_k \in \left\{\pm\frac{\pi}{4}, \pm\frac{3\pi}{4}\right\}$ or

$$z_k \in \left\{\frac{1}{\sqrt{2}}\,(\pm 1 \pm j)\right\}.$$

Obviously, this leads to eight possible values of the transmit symbol s_k, corresponding to the absolute phase values

$$\phi_k \in \left\{0, \pm\frac{\pi}{4}, \pm\frac{\pi}{2}, \pm\frac{3\pi}{4}, \pi\right\},$$

see Figure 1.21, where the possible transitions are marked by arrows.

For even values of k,

$$\phi_k \in \left\{0, \pm\frac{\pi}{2}, \pi\right\}$$

and for odd values of k,

$$\phi_k \in \left\{\pm\frac{\pi}{4}, \pm\frac{3\pi}{4}\right\}.$$

We thus have two different constellations for s_k, which are phase shifted by $\pi/4$. This modulation scheme is therefore called $\pi/4$-*DQPSK*.

Differential PSK is often used because it does not require an absolute phase reference. In practice, the channel introduces an unknown phase θ, that is, the receive signal is

$$r_k = \mathrm{e}^{j\theta} s_k + n_k.$$

In a coherent PSK receiver, the phase must be estimated and back- rotated. A differential receiver compares the phase of two adjacent symbols by calculating

$$u_k = r_k r_{k-1}^* = s_k s_{k-1}^* + \mathrm{e}^{j\theta} s_k n_{k-1}^* + n_k \mathrm{e}^{-j\theta} s_{k-1}^* + n_k n_{k-1}^*.$$

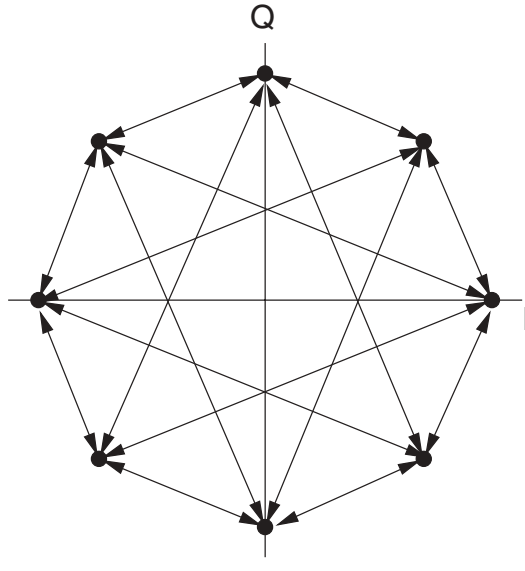

Figure 1.21 Transmit symbols for $\frac{\pi}{4}$-DQPSK.

In the noise-free case, $u_k/\sqrt{E_S} = z_k$ represents original PSK symbols that carry the information. However, we see from the above equation that we have additional noise terms that do not occur for coherent signaling and that degrade the performance. The performance analysis of DPSK is more complicated than for coherent PSK (see e.g. (Proakis 2001)). We will later refer to the results when we need them for the applications.

1.6 Bibliographical Notes

This chapter is intended to give a brief overview of the basics that are needed in the following chapters and to introduce some concepts and notations. A more detailed introduction into digital communication and detection theory can be found in many text books (see e.g. (Benedetto and Biglieri 1999; Blahut 1990; Kammeyer 2004; Lee and Messerschmidt 1994; Proakis 2001; Van Trees 1967; Wozencraft and Jacobs 1965)). We assume that the reader is familiar with Fourier theory and has some basic knowledge of probability and stochastic processes. We will not define these concepts further; one may refer to standard text books (see e.g. (Bracewell 2000; Feller 1970; Papoulis 1991)).

We have emphasized the vector space properties of signals. This allows a geometrical interpretation that makes the solution of many detection problems intuitively obvious. The interpretation of signals as vectors is not new. We refer to the excellent classical text books (Van Trees 1967; Wozencraft and Jacobs 1965).

We have emphasized the concept of a detector as an integral operation that performs a measurement. A Fourier analyzer is such a device that may be interpreted as a set of detectors, one for each frequency. The integral operation is given by a scalar product if the signal

is well behaved (i.e. of finite energy). If not, the signal has to be understood as a generalized function (which is called *distribution* or *functional* in mathematical literature (Reed and Simon 1980)), and the detection is the action of this signal on a well-behaved *test function.* It is interesting to note that this is the same situation as in quantum theory, where such a test function is interpreted as a detection device for the quantum state of a physical system. In this context it is worth noting that $\delta(t)$, the most important generalized function in communication theory, has been introduced by one of the quantum theory pioneers, P.A.M. Dirac.

1.7 Problems

1. Let $\{g_k(t)\}_{k=1}^K$ be an orthonormal transmit base and

$$\mathbf{s} = (s_1, \ldots, s_K)^T$$

and

$$\mathbf{x} = (x_1, \ldots, x_K)^T$$

two transmit symbol vectors. Let

$$s(t) = \sum_{k=1}^{K} s_k g_k(t)$$

and

$$x(t) = \sum_{k=1}^{K} x_k g_k(t).$$

Show that

$$\langle s, x \rangle = \mathbf{s}^{\dagger}\mathbf{x}.$$

2. Let $S(f)$ denote the Fourier transform of the signal $s(t)$ and define

$$\tilde{s}(t) = \sqrt{2}\,\Re\{s(t)\mathrm{e}^{j2\pi f_0 t}\}.$$

Show that the Fourier transform of that signal is given by

$$\tilde{S}(f) = \frac{1}{\sqrt{2}}\left(S\left(f - f_0\right) + S^*\left(-f - f_0\right)\right).$$

3. Let $x(t)$ and $y(t)$ be finite-energy low-pass signals strictly band- limited to $B/2$ and let $f_0 > B/2$. Show that the two signals

$$\tilde{x}(t) = \sqrt{2}\,\cos\left(2\pi f_0 t\right)\,x(t)$$

and

$$\tilde{y}(t) = -\sqrt{2}\,\sin\left(2\pi f_0 t\right)\,y(t)$$

are orthogonal. Let $u(t)$ and $v(t)$ be two other finite-energy signals strictly band-limited to $B/2$ and define

$$\tilde{u}(t) = \sqrt{2}\cos(2\pi f_0 t)\ u(t)$$

and

$$\tilde{v}(t) = -\sqrt{2}\sin(2\pi f_0 t)\ v(t).$$

Show that

$$\langle \tilde{u}, \tilde{x} \rangle = \langle u, x \rangle$$

and

$$\langle \tilde{v}, \tilde{y} \rangle = \langle v, y \rangle$$

hold. Hint: Transform all the signals into the frequency domain and use Parseval's equation.

4. Show that, from the definition of the time-variant linear systems I and Q, the definitions (given in Subsection 1.2.2) of the time-variant linear systems I^D and Q^D are uniquely determined by

$$\langle \tilde{u}, Iv \rangle = \left\langle I^D \tilde{u}, v \right\rangle$$

and

$$\langle \tilde{u}, Qv \rangle = \left\langle Q^D \tilde{u}, v \right\rangle$$

for any (real-valued) finite-energy signal $\tilde{u}(t)$ and $v(t)$. Mathematically speaking, this means that I^D and Q^D are defined as the *adjoints* of the linear operators I and Q. For the theory of linear operators, see for example (Reed and Simon 1980).

5. Show that the definitions

$$\mathrm{E}\{w(t_1)w(t_2)\} = \frac{N_0}{2}\delta(t_1 - t_2)$$

and

$$\mathrm{E}\left\{\mathcal{D}_{\phi_1}[w]\mathcal{D}_{\phi_2}[w]\right\} = \frac{N_0}{2}\langle \phi_1, \phi_2 \rangle$$

are equivalent conditions for the *whiteness* of the (real-valued) noise $w(t)$.

6. Let $g(t)$ be a transmit pulse and $n(t)$ complex baseband white (not necessarily Gaussian) noise. Let

$$\mathcal{D}_h[r] = \int_{-\infty}^{\infty} h^*(t) r(t)\,\mathrm{d}t$$

be a detector for a (finite-energy) pulse $h(t)$ and $r(t) = g(t) + n(t)$ be the transmit pulse corrupted by the noise. Show that the signal-to-noise ratio after the detector defined by

$$SNR = \frac{|\mathcal{D}_h[g]|^2}{\mathrm{E}\left\{|\mathcal{D}_h[n]|^2\right\}}$$

becomes maximal if $h(t)$ is chosen to be proportional to $g(t)$.

7. Show the equality

$$\|\mathbf{y}-\mathbf{x}\|^2 - \|\mathbf{y}-\hat{\mathbf{x}}\|^2 = 2\left[\left(\mathbf{y}-\frac{\mathbf{x}+\hat{\mathbf{x}}}{2}\right)(\hat{\mathbf{x}}-\mathbf{x})\right].$$

8. Let $\mathbf{n} = (n_1, \ldots, n_K)^T$ be a K-dimensional real-valued AWGN with variance $\sigma^2 = N_0/2$ in each dimension and $\mathbf{u} = (u_1, \ldots, u_K)^T$ be a vector of length $|\mathbf{u}| = 1$ in the K-dimensional Euclidean space. Show that $n = \mathbf{n} \cdot \mathbf{u}$ is a Gaussian random variable with mean zero and variance $\sigma^2 = N_0/2$.

9. We consider a digital data transmission from the Moon to the Earth. Assume that the digital modulation scheme (e.g. QPSK) requires $E_b/N_0 = 10$ dB at the receiver for a sufficiently low bit error rate of, for example, $BER = 10^{-5}$. For free-space propagation, the power at the receiver is given by

$$P_r = G_t G_r \frac{\lambda^2}{(4\pi R)^2} P_t.$$

   We assume $G_t = G_r = 10$ dB for the antenna gains at the receiver and the transmitter, respectively, and $\lambda = 40$ cm for the wavelength. The distance of the moon is approximately given by $R = 400\,000$ km. The receiver noise (including a noise figure of 4 dB) is given by $N_0 = -170$ dBm/Hz. How much transmit power is necessary for a bit rate of $R_b = 1$ bit/s?

2

Mobile Radio Channels

2.1 Multipath Propagation

Mobile radio reception is severely affected by multipath propagation; the electromagnetic wave is scattered, diffracted and reflected, and reaches the antenna via various ways as an incoherent superposition of many signals with different delay times that are caused by the different path lengths of these signals. This leads to an interference pattern that depends on the frequency and the location or – for a mobile receiver – the time. The mobile receiver moves through an interference pattern that may change within milliseconds and that varies over the transmission bandwidth. One says that the mobile radio channel is characterized by *time variance* and *frequency selectivity*.

The time variance is determined by the relative speed v between receiver and transmitter and the wavelength $\lambda = c/f_0$, where f_0 is the transmit frequency and c is the velocity of light. The relevant physical quantity is the maximum Doppler frequency shift given by

$$\nu_{\max} = \frac{v}{c} f_0 \approx \frac{1}{1080} \frac{f_0}{\text{MHz}} \frac{v}{\text{km/h}} \text{Hz}.$$

Table 2.1 shows some practically relevant figures for $\nu_{\max}$ for speeds from a slowly moving person (2.4 km/h) to a high-speed train or car (192 km/h).

For an angle α between the direction of the received signal and the direction of motion, the Doppler shift ν is given by

$$\nu = \nu_{\max} \cos \alpha.$$

Consider a carrier wave transmitted at frequency f_0. Typically, the received signal is a superposition of many scattered and reflected signals from different directions resulting in a spatial interference pattern. For a vehicle moving through this interference pattern, the received signal amplitude fluctuates in time, which is called *fading*. In the frequency domain, we see a superposition of many Doppler shifts corresponding to different directions resulting in a Doppler spectrum instead of a sharp spectral line located at f_0. Figure 2.1 shows an example of the amplitude fluctuations of the received time signal for $\nu_{\max} = 50$ Hz, corresponding for example, to a transmit signal at 900 MHz for a vehicle

Theory and Applications of OFDM and CDMA Henrik Schulze and Christian Lüders

Table 2.1 Doppler frequencies

Radio frequency	Doppler frequency for a speed of			
	$v = 2.4$ km/h	$v = 48$ km/h	$v = 120$ km/h	$v = 192$ km/h
$f_0 = 225$ MHz	0.5 Hz	10 Hz	25 Hz	40 Hz
$f_0 = 900$ MHz	2.0 Hz	40 Hz	100 Hz	160 Hz
$f_0 = 2025$ MHz	4.5 Hz	90 Hz	225 Hz	360 Hz

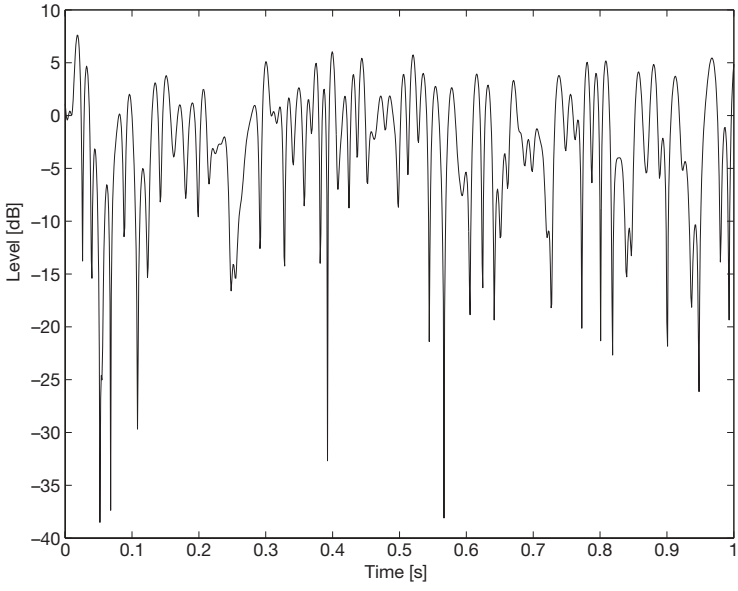

Figure 2.1 Time variance (selectivity) of the fading amplitude for 50 Hz maximum Doppler frequency.

speed $v = 60$ km/h. The figure shows deep amplitude fades up to -40 dB. If a car stands still at the corresponding location (e.g. at a traffic light), the reception breaks down. If the car moves half a wavelength, it may get out of the deep fade.

The superposition of Doppler-shifted carrier waves leads to a fluctuation of the carrier amplitude and phase. This means that the received signal is amplitude and phase modulated by the channel.

Figure 2.2 shows the trace of the phasor in the complex plane for the same channel parameters as above. For digital phase modulation, these rapid phase fluctuations cause severe problems if the carrier phase changes too much during the time T_S that is needed to transmit one digitally modulated symbol. The amplitude and the phase fluctuate randomly. The typical frequency of the variation is of the order of $\nu_{\max}$ corresponding to a timescale of the variations given by

$$t_{\text{corr}} = \nu_{\max}^{-1},$$

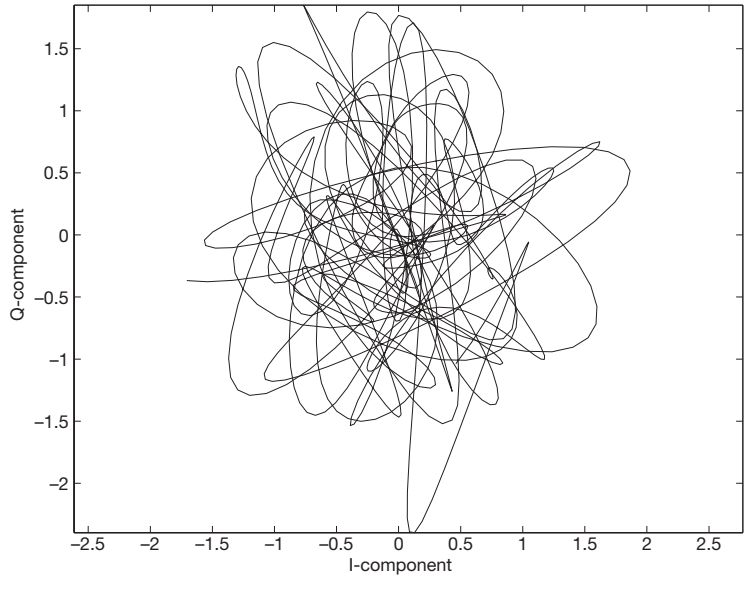

Figure 2.2 Time variance (selectivity) shown above as a curve in the complex plane.

which we call the correlation time. Digital transmission with symbol period T_S is only possible if the channel remains nearly constant during that period, which requires $T_S \ll t_{\text{corr}}$ or, equivalently, the condition

$$\nu_{\max} T_S \ll 1$$

must hold.

The frequency selectivity of the channel is determined by the different delay times of the signals. They can be calculated as the ratio between the traveling distances and the velocity of light. 1 μs delay time difference corresponds to 300 m of path difference. A few microseconds are typical for cellular mobile radio. For a broadcasting system for a large area, echoes up to 100 μs are possible in a hilly or mountainous region. In a so-called *single frequency network* (see Section 4.6), the system must cope with even longer echoes. Longer echoes correspond to more fades within the transmission bandwidth. Figure 2.3 shows an example for a received signal level as a function of the frequency (relative to the center frequency) at a fixed location in a situation with delay time differences of the signals corresponding to a few kilometers. In the time domain, intersymbol interference disturbs the transmission if the delay time differences are not much smaller than the symbol duration T_S. A data rate of 200 kbit/s leads to $T_S = 10$ μs for the QPSK modulation. This is of the same order as the echoes for such a scenario. This means that digital transmission of that data rate is not possible without using more sophisticated methods such as equalizers, spread spectrum techniques, or multicarrier modulation. We define a correlation frequency

$$f_{\text{corr}} = \Delta\tau^{-1},$$

where $\Delta\tau$ is the square root of the variance of the power distribution of the echoes, which we call the *delay spread*. f_{corr} is often called *coherence* (or *coherency*) *bandwidth* because the

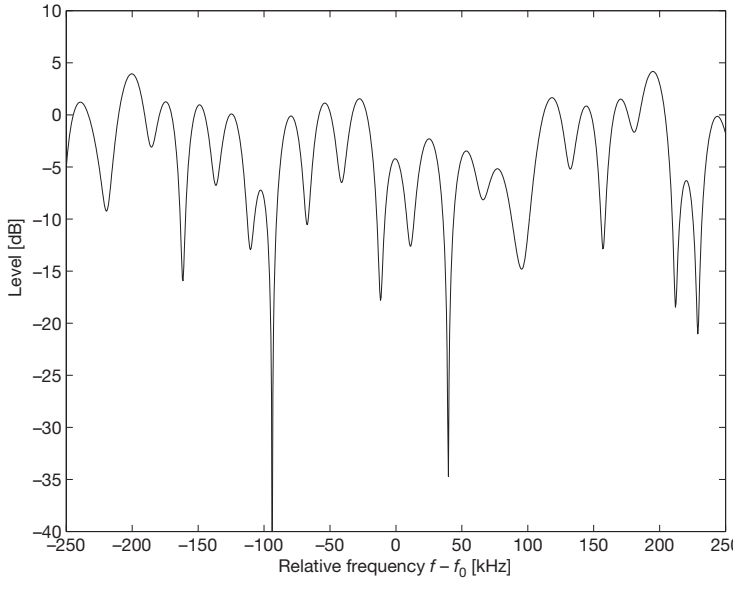

Figure 2.3 Frequency selectivity (variance) of the fading amplitude for a broadcasting channel with long echoes.

channel can be regarded as frequency-nonselective within a bandwidth B with $B \ll f_{\text{corr}}$. If B is in the order of T_s^{-1} as it is the case for signaling with the Nyquist base, this is equivalent to the condition

$$\Delta\tau \ll T_S$$

that intersymbol interference can be neglected.

2.2 Characterization of Fading Channels

2.2.1 Time variance and Doppler spread

Consider a modulated carrier wave

$$\tilde{s}(t) = \sqrt{2}\,\Re\left\{s(t)\mathrm{e}^{j2\pi f_0 t}\right\} \tag{2.1}$$

at frequency f_0 that is modulated by a complex baseband signal $s(t)$. For a moving receiver with velocity v and an incoming wave with an angle of incidence α relative to the direction of motion, the carrier frequency will be shifted by the Doppler frequency given by

$$\nu = \nu_{\max}\cos\alpha. \tag{2.2}$$

The same Doppler shift occurs for a fixed receiver and a transmitter moving with velocity v. Because the angle α from the left-hand side causes the same Doppler shift as the angle

$-\alpha$ from the right-hand side, we identify both cases and let the angle run from 0 to π. The Doppler-shifted receive signal is given by

$$\tilde{r}(t) = \sqrt{2}\,\Re\left\{a\mathrm{e}^{j\theta}\mathrm{e}^{j2\pi\nu t}s(t)\mathrm{e}^{j2\pi f_0 t}\right\}, \tag{2.3}$$

where a is an attenuation factor and θ the phase of the carrier wave at the receiver. Here, we have made some reasonable assumptions that simplify the treatment:

- The angle α is constant during the time of consideration. This is true if the distance between transmitter and receiver is sufficiently large and we can assume that many bits are transmitted during a very small change of the angle. This is in contrast to the case of the acoustic Doppler shift of an ambulance car, where the angle runs from 0 to π during the observation time and the listener hears a tone decreasing in frequency from $f_0 + v_{\max}$ to $f_0 - v_{\max}$.
- The signal is of sufficiently small bandwidth so that the Doppler shift can be assumed to be the same for all spectral components.

Furthermore, we have only taken into account that the delay of the RF signal results in a phase delay, ignoring the group delay of the complex baseband signal $s(t)$. We will study the effect of such a delay in the following subsection. Here, we assume that these delays are so small that they can be ignored. Typically, the received signal is the superposition of several signals, scattered from different obstacles, with attenuation factors a_k, carrier phases θ_k and Doppler shifts $\nu_k = \nu_{\max}\cos\alpha_k$, resulting in

$$\tilde{r}(t) = \sqrt{2}\sum_{k=1}^{N}\Re\left\{a_k\mathrm{e}^{j\theta_k}\mathrm{e}^{j2\pi\nu_k t}s(t)\mathrm{e}^{j2\pi f_0 t}\right\}. \tag{2.4}$$

The complex baseband transmit and receive signals $s(t)$ and $r(t)$ are thus related by

$$r(t) = c(t)s(t), \tag{2.5}$$

where

$$c(t) = \sum_{k=1}^{N} a_k\mathrm{e}^{j\theta_k}\mathrm{e}^{j2\pi\nu_k t} \tag{2.6}$$

is the time-variant complex fading amplitude of the channel. Typically, this complex fading amplitude looks as shown in Figures 2.1 and 2.2. In the special case of two-path channels ($N = 2$), the fading amplitude shows a more regular behavior. In this case, the time-variant power gain $|c(t)|^2$ of the channel can be calculated as

$$|c(t)|^2 = a_1^2 + a_2^2 + 2a_1a_2\cos\left(2\pi\left(\nu_1 - \nu_2\right)t + \theta_1 - \theta_2\right).$$

Figure 2.4 shows $|c(t)|^2$ for $a_1 = 0.75$ and $a_2 = \sqrt{7}/4$. The average power is normalized to one, the maximum power is $(a_1 + a_2)^2 \approx 1.99$, the minimum power is $(a_1 - a_2)^2 \approx 0.008$, resulting in level fluctuations of about 24 dB. The fading amplitude is periodic with period $|\nu_1 - \nu_2|^{-1}$. Such a two-path channel can occur in reality, for instance, in the special situation where the received signal is a superposition of a direct signal and

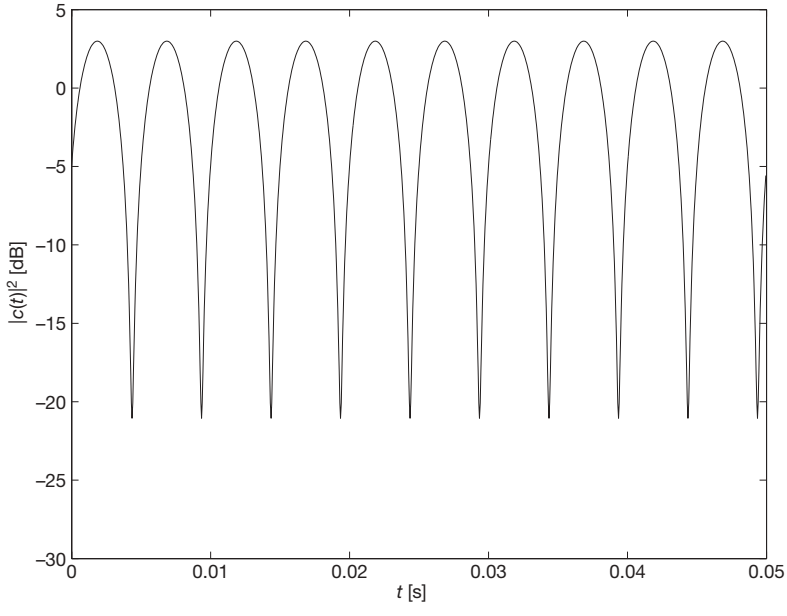

Figure 2.4 Time variance of a two-path channel.

a strong reflection. If, for example, $\nu_1 = \nu_{\max}$ and $\nu_2 = -\nu_{\max}$, that is, one signal from the front and one from the back, then the period is $(2\nu_{\max})^{-1}$. Since $\nu_{\max} = v/\lambda$, the spatial separation of two power maxima (or minima) is $\lambda/2$. This interference pattern is well known in physics as a standing wave. In the example, we have chosen $\nu_1 = 100$ Hz and $\nu_2 = -100$ Hz, which corresponds to 120 km/h at 900 MHz. For that frequency, $\lambda/2 \approx 16.7$ cm.

It is a usual assumption to think of a general complex fading amplitude $c(t)$ given by Equation (2.6) as a *stationary* random signal. This is a convenient assumption, but one should keep in mind that this introduces a simplified mathematical model for the physical reality. We therefore add the following remarks:

- The real physical $c(t)$ is deterministic because a_k, ν_k, and θ_k are deterministic. But at least the phases θ_k are completely unknown. It is reasonable and a common practice in communications engineering to model unknown phases as random variables. Philosophically speaking, statistics is not due to the randomness of nature, but to our lack of knowledge. This is also a common practice in physics, for example, in statistical thermodynamics (Landau and Lifshitz 1958).

- Strictly speaking, stationarity cannot be true because the environment changes. This slow change of the channel is called *long-term fading*, in contrast to the short-term fading considered here. Long-term fading is of primary interest for network planning (see Subsection 5.1.2), but for the performance analysis of communication systems we have to focus on the short-term fading, thereby assuming that the environment

is constant during the time period that is necessary to measure, for example, the bit error rate.

- Because mathematical modeling of physical reality is a coarse procedure, we regard it as splitting hairs to distinguish between wide-sense stationary (WSS) and strict-sense stationary (SSS) stochastic processes. For SSS processes, time-shift invariance is given for all statistical properties, while for WSS this is only true up to the second-order properties (covariances). For a theoretical analysis, for example, to identify bit error probabilities with bit error rates, we need to assume even some ergodic properties (which is a stronger assumption than SSS) that are mathematically necessary but physically not given.

The random process $c(t)$ given by Equation (2.6) has a discrete power spectral density (psd) $\mathcal{S}_c(\nu)$ as shown in Figure 2.5(a) for $N = 5$. We call $\mathcal{S}_c(\nu)$ the *Doppler spectrum.* However, in most real situations, the received signal is a continuous rather than a discrete superposition of Doppler-shifted signals, resulting in a continuous psd $\mathcal{S}_c(\nu)$ as shown in Figure 2.5(b).

As a result of Equation (2.2), each Doppler frequency corresponds to an angle $\alpha \in [0, \pi]$. Therefore, the Doppler spectrum is related to the angular power density $\mathcal{S}_{\text{angle}}(\alpha)$ by

$$-\mathcal{S}_c(\nu)\,\mathrm{d}\nu = \mathcal{S}_{\text{angle}}(\alpha)\,\mathrm{d}\alpha.$$

The negative sign is due to the fact that, because the cosine is a decreasing function over the relevant interval, a positive infinitesimal $\mathrm{d}\alpha$ corresponds to a negative infinitesimal $\mathrm{d}\nu$. By Equation (2.2), we get

$$\mathrm{d}\nu = -\nu_{\max}\sin\alpha\,\mathrm{d}\alpha = -\nu_{\max}\sqrt{1 - \frac{\nu^2}{\nu_{\max}^2}}\,\mathrm{d}\alpha$$

resulting in

$$\mathcal{S}_c(\nu)\sqrt{\nu_{\max}^2 - \nu^2} = \mathcal{S}_{\text{angle}}\left(\arccos\left(\frac{\nu}{\nu_{\max}}\right)\right),\ -\nu_{\max} < \nu < \nu_{\max}.$$

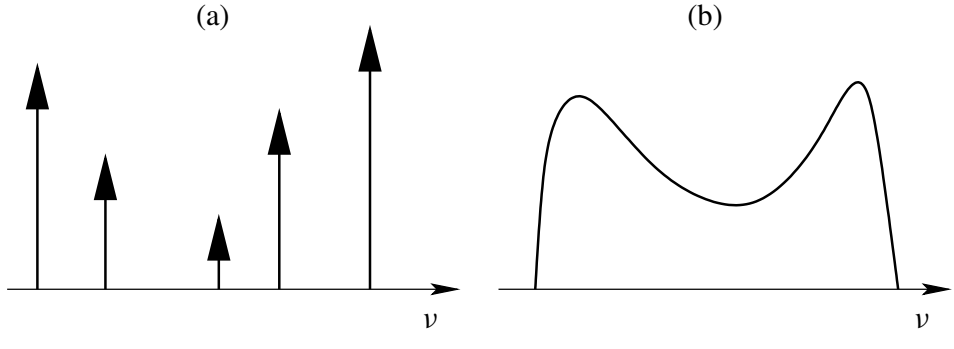

Figure 2.5 Example of a discrete (a) and continuous (b) Doppler spectrum.

A simple model – and also a kind of worst case – is the isotropic angular power distribution $\mathcal{S}_{\text{angle}}(\alpha) = \pi^{-1}$. In that case, we obtain the power spectral density

$$\mathcal{S}_c(\nu) = \frac{1}{\pi \nu_{\max} \sqrt{1 - \frac{\nu^2}{\nu_{\max}^2}}} \tag{2.7}$$

for $-\nu_{\max} < \nu < \nu_{\max}$ and zero outside that interval. This spectral shape is sometimes called the *isotropic* or *Jakes* Doppler spectrum (Jakes 1975). Figure 2.6 shows this (normalized) Doppler spectrum $\nu_{\max}\mathcal{S}_c(\nu)$. Note the singularities at the edges that have their origin in geometry.

We assumed that $c(t)$ is the complex baseband signal corresponding to a (wide-sense) stationary stochastic process, which is the carrier wave affected by the Doppler spread. The autocorrelation function (ACF) of such a process is given by

$$\mathcal{R}_c(t) = \mathrm{E}\left\{c(t_1 + t)c^*(t_1)\right\}$$

(see Proposition 1.3.3). The power spectrum is the Fourier transform of the ACF, that is,

$$\mathcal{S}_c(\nu) = \int_{-\infty}^{\infty} \mathrm{e}^{-j2\pi\nu t}\mathcal{R}_c(t)\,\mathrm{d}t.$$

For the Jakes spectrum, the ACF given by

$$\mathcal{R}_c(t) = \mathrm{J}_0\left(2\pi\nu_{\max}t\right), \tag{2.8}$$

where $\mathrm{J}_0(x)$ is the Bessel function of the first kind of order 0.

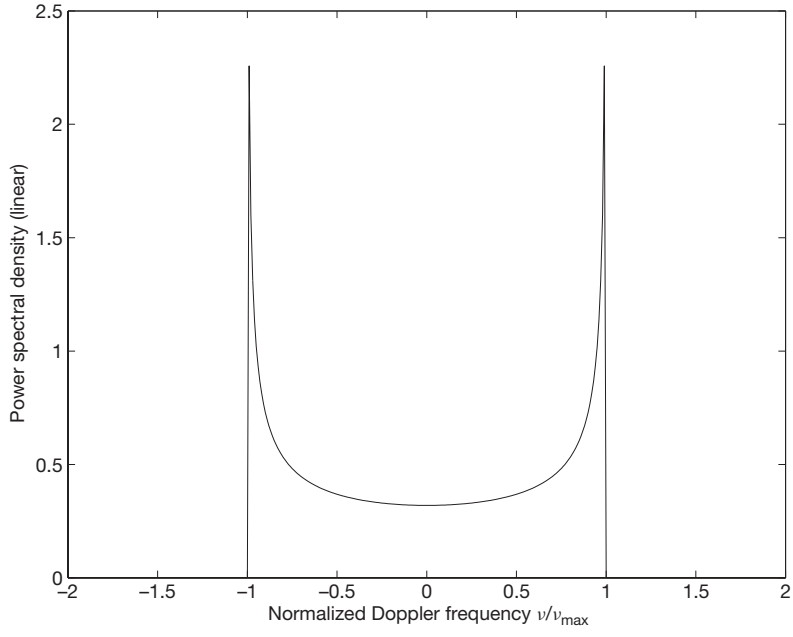

Figure 2.6 The Jakes Doppler spectrum corresponding to the isotropic power distribution.

Because of the coarse modeling of reality, relevant quantities like error probabilities should not strongly depend on the shape of the Doppler spectrum, and in fact, they do not for all known examples. We will illustrate this by the following consideration. As discussed above, digital transmission is only possible if the channel does not vary too fast relative to the symbol duration, which can be expressed by the condition $\nu_{\max} T_S \ll 1$ over relevant times (of the order T_S). The correlation time $t_{\text{corr}} = \nu_{\max}^{-1}$ must be large enough so that the channel samples are highly correlated. These correlations are characterized by the ACF $\mathcal{R}_c(t)$. Thus, only $\mathcal{R}_c(t)$ for small values $|t| \ll t_{\text{corr}}$ is relevant for the performance and we may approximate $\mathcal{R}_c(t)$ by a Taylor series. We note that

$$\frac{\mathrm{d}^n}{\mathrm{d}t^n}\mathcal{R}_c(t)\bigg|_{t=0} = (2\pi j)^n \mu_n\{\mathcal{S}_c(\nu)\},$$

where

$$\mu_n\{\mathcal{S}_c(\nu)\} = \int_{-\infty}^{\infty} \nu^n \mathcal{S}_c(\nu)\,\mathrm{d}\nu$$

is the nth moment of the power spectral density. $\mathcal{R}_c(t)$ can thus be expanded into the Taylor series

$$\mathcal{R}_c(t) = \sum_{n=0}^{\infty} \frac{1}{n!}(2\pi j)^n \mu_n\{\mathcal{S}_c(\nu)\}\, t^n.$$

Note that $\mu_0\{\mathcal{S}_c(\nu)\} = 1$ due to energy normalization and $\mu_1\{\mathcal{S}_c(\nu)\} = 0$ can always be achieved by a frequency shift. Since $\mu_n\{\mathcal{S}_c(\nu)\} \le (2\nu_{\max})^n$, the absolute value of the nth term in the Taylor series is bounded by

$$\frac{1}{n!}|4\pi\,\nu_{\max} t|^n,$$

which is very small for $|t| \ll t_{\text{corr}} = \nu_{\max}^{-1}$. We thus approximate $\mathcal{R}_c(t)$ by the lowest non-trivial order of the Taylor series

$$\mathcal{R}_c(t) \approx 1 - \frac{1}{2}(2\pi)^2 \mu_2\{\mathcal{S}_c(\nu)\}\, t^2.$$

Thus, one should expect that only the second moment of the Doppler spectrum – rather than the exact shape – is relevant for the performance of the system. We will see later in Subsection 2.4.6 that the bit error rate of differential QPSK (DQPSK) in a time-variant fading channel depends on the time variance through $\mathcal{R}_c(T_S)$.

Thus, it is therefore not important to use the real shape of the Doppler spectrum. We may use, for example, the Jakes spectrum as a coarse reflection of reality. We note that the second moment typically becomes smaller if the angles of receive signals are not isotropically distributed.

Furthermore, we should always keep in mind that the assumed stationarity (or wide-sense stationarity) is, strictly speaking, not true. We can only say that $c(t)$ cannot be distinguished from a stationary process when observed over a relatively short time of, say, a few seconds. This makes it reasonable to treat it like a stationary process, because this is mathematically convenient.

Finally, we state that for the Jakes spectrum the second moment can easily be calculated as

$$\mu_2\{\mathcal{S}_c(\nu)\} = \frac{\nu_{\max}^2}{2}$$

(see Problem 2).

The inverse of the variance

$$\Delta\nu = \sqrt{\mu_2\{\mathcal{S}_c(\nu)\}}$$

also appears to be a reasonable choice for the definition of the correlation time t_{corr}. However, $\nu_{\max}$ is easy to obtain from the carrier frequency and the vehicle speed and is therefore a better choice for the practice. For typical shapes as the Jakes spectrum, both quantities are of the same order.

2.2.2 Frequency selectivity and delay spread

Consider again a transmit signal as given by Equation (2.1). We now assume that both transmitter and receiver are at rest (or the time variance is so slow that it can be neglected for the time period under consideration) and we can ignore any Doppler shifts. But, unlike in the above treatment, we do not ignore the delays $\tau_k = l_k/c$ of the complex baseband signal $s(t) \mapsto s(t-\tau_k)$ for the different propagation paths of length l_k. Instead of Equation (2.4), we now get for the received signal

$$\tilde{r}(t) = \sqrt{2}\sum_{k=1}^{N} \Re\left\{a_k e^{j\theta_k}\, s(t-\tau_k) e^{j2\pi f_0 t}\right\}. \tag{2.9}$$

The delays of the carrier are already included in the phases θ_k. The complex baseband transmit and receive signals $s(t)$ and $r(t)$ are related by

$$r(t) = h(t) * s(t), \tag{2.10}$$

where

$$h(t) = \sum_{k=1}^{N} a_k e^{j\theta_k}\delta(t-\tau_k) \tag{2.11}$$

is the impulse response of the channel. The corresponding channel transfer function is given by

$$H(f) = \sum_{k=1}^{N} a_k e^{j\theta_k} e^{-j2\pi f\tau_k}. \tag{2.12}$$

We note the strong similarity to Equation (2.6). Typically, the frequency response looks as shown in Figure 2.3. In the special case of two-path channels ($N = 2$), the transfer function shows a more regular behavior. In this case, the power gain $|H(f)|^2$ of the channel can be calculated as

$$|H(f)|^2 = a_1^2 + a_2^2 + 2a_1a_2\cos\left(2\pi f\,(\tau_1-\tau_2) + \theta_2 - \theta_1\right).$$

The picture is similar to the one depicted in Figure 2.4, where time is replaced by frequency. The transfer function is periodic with period $|\tau_1 - \tau_2|^{-1}$.

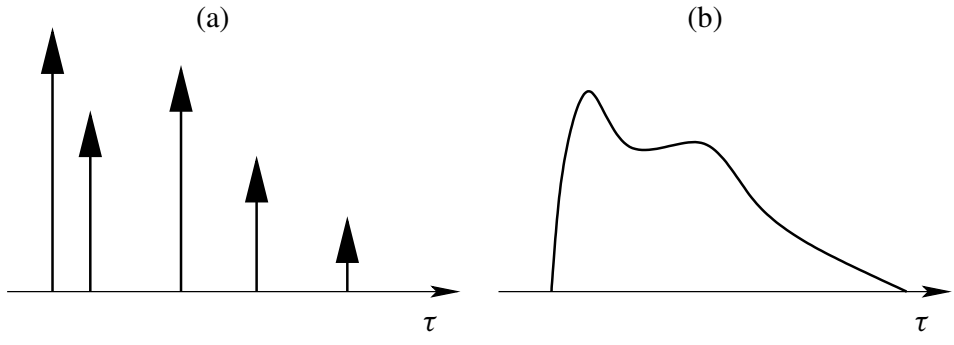

Figure 2.7 Example of a discrete (a) and continuous (b) delay power spectrum.

With the same arguments as for the treatment of the time-variant fading amplitude $c(t)$, we may regard $H(f)$ as a random transfer function, or – more formally – as a stochastic process in a frequency variable. Frequency-shift invariance (corresponding to stationarity for the time variable) can only be an approximation. The same remarks about modeling the reality as made in the preceding subsection apply here. Since the variable for this process is a frequency, there is a power density distribution as a function of a time variable τ that can be identified as the delay time. Figure 2.7(a) illustrates such a *delay power spectrum* $\mathcal{S}_H(\tau)$ corresponding to the process given by the Equations (2.11) and (2.12). However, in most real situations, the received signal is a continuous rather than a discrete superposition of delayed signal components, resulting in a continuous delay power spectrum $\mathcal{S}_H(\tau)$ as shown in Figure 2.7(b). Note that the delay power spectrum reflects the distribution of path length. We identify the delay spread as

$$\Delta\tau = \sqrt{\mu_2\{\mathcal{S}_H(\tau)\} - \mu_1^2\{\mathcal{S}_H(\tau)\}}.$$

Here, in contrast to the Doppler spectrum, we do not set the first moment to zero because this would lead to negative delay times τ. However, with similar arguments as for the Doppler spectrum, we expect that typically the performance of a communication system in a frequency selective fading channel will not depend on the shape of $\mathcal{S}_H(\tau)$, but only on the second moment.

One popular model for $\mathcal{S}_H(\tau)$ is an exponential distribution

$$\mathcal{S}_H(\tau) = \frac{1}{\tau_m} \mathrm{e}^{-\tau/\tau_m}$$

for $\tau > 0$ and zero elsewhere. The mean value τ_m of this distribution equals the delay spread $\Delta\tau$. The exponential power delay spectrum reflects the idea that the power of the paths decreases strongly with their delay. This is of course a very rough model, but it can be refined by adding components due to significant distant reflectors.

We have assumed frequency-shift invariance (which is similar to what is called *wide-sense stationarity* for the time variable). The (frequency) ACF is given by

$$\mathcal{R}_H(f) = \mathrm{E}\left\{H(f_1 + f)H^*(f_1)\right\}.$$

The delay power spectrum is the inverse Fourier transform of the ACF, that is,

$$\mathcal{S}_H(\tau) = \int_{-\infty}^{\infty} \mathrm{e}^{j2\pi f\tau} \mathcal{R}_H(f)\,\mathrm{d}f.$$

For the exponential delay power spectrum, the ACF given by

$$\mathcal{R}_H(f) = \frac{1}{1 + j2\pi f\tau_m}.$$

2.2.3 Time- and frequency-variant channels

We now consider a channel that is both time and frequency selective. We combine the effects of the Equations (2.4) and (2.9) and obtain a receive signal given by

$$\tilde{r}(t) = \sqrt{2} \sum_{k=1}^{N} \Re\left\{a_k \mathrm{e}^{j\theta_k} \mathrm{e}^{j2\pi\nu_k t} s(t-\tau_k) \mathrm{e}^{j2\pi f_0 t}\right\}. \tag{2.13}$$

The complex baseband transmit and receive signals $s(t)$ and $r(t)$ are related by

$$r(t) = \int_{-\infty}^{\infty} h(\tau, t) s(t-\tau)\,\mathrm{d}\tau, \tag{2.14}$$

where

$$h(\tau, t) = \sum_{k=1}^{N} a_k \mathrm{e}^{j\theta_k} \mathrm{e}^{j2\pi\nu_k t} \delta(t-\tau_k) \tag{2.15}$$

is the time-variant impulse response of the channel. Note that Equation (2.14) contains Equations (2.5) and (2.10) as special cases by setting either $h(\tau, t) = c(t)\delta(\tau)$ or $h(\tau, t) = h(\tau)$. We note that $h(\tau, t)$ is the channel response of an impulse with travel time τ received at time t, that is, transmitted at time $t - \tau$.

The time-variant channel transfer function will now be defined as the Fourier transform in the delay variable τ of the time-variant impulse response

$$H(f, t) = \int_{-\infty}^{\infty} \mathrm{e}^{-j2\pi f\tau} h(\tau, t)\,\mathrm{d}\tau$$

which equals

$$H(f, t) = \sum_{k=1}^{N} a_k \mathrm{e}^{j\theta_k} \mathrm{e}^{j2\pi\nu_k t} \mathrm{e}^{-j2\pi f\tau_k}$$

in our special case. The receive signal $r(t)$ is related to the Fourier transform $S(f)$ of the transmit signal $s(t)$ by

$$r(t) = \int_{-\infty}^{\infty} \mathrm{e}^{-j2\pi f\tau} H(f, t) S(f)\,\mathrm{d}\tau.$$

The power density with respect to Doppler and delay is now given by a common power density function $\mathcal{S}(\tau, \nu)$ called *scattering function* with the properties

$$\mathcal{S}_c(\nu) = \int_{-\infty}^{\infty} \mathcal{S}(\tau, \nu)\,\mathrm{d}\tau$$

and

$$\mathcal{S}_H(\tau) = \int_{-\infty}^{\infty} \mathcal{S}(\tau, \nu)\, \mathrm{d}\nu.$$

Since the Doppler frequency is related to the angle of the incoming wave by $\nu = \nu_{\max} \cos\alpha$, and the delay is related to the echo path length l by $\tau = l/c$, the scattering function reflects the geometrical distribution of the scatterers and their corresponding power contributions. Like the Doppler and the delay power spectrum, the scattering function is typically a continuous rather than a discrete superposition of Doppler-shifted and delayed components.

The ACF of the two-dimensional random process is defined by

$$\mathcal{R}(f, t) = \mathrm{E}\left\{H(f_1 + f, t_1 + t)H^*(f_1, t_1)\right\}.$$

It is related to the scattering function by a two-dimensional Fourier (back) transform

$$\mathcal{S}(\tau, \nu) = \int_{-\infty}^{\infty} \mathrm{d}f \int_{-\infty}^{\infty} \mathrm{d}t\, \mathrm{e}^{j2\pi f\tau} \mathrm{e}^{-j2\pi\nu t} \mathcal{R}(f, t).$$

Here, we have used the simpler notation $\int \mathrm{d}x \int \mathrm{d}y f(x, y)$ instead of $\int \left(\int f(x, y)\, \mathrm{d}y\right) \mathrm{d}x$. We note that

$$\mathcal{R}(0, t) = \mathcal{R}_c(t)$$

and

$$\mathcal{R}(f, 0) = \mathcal{R}_H(f)$$

hold.

Up to now, the treatment was mainly heuristic, which seems to be adequate for a channel that can only be modeled roughly. However, formally we have to deal with time-variant random systems. In the following section, we characterize such systems and give more formal definitions. However, these are formal mathematical concepts and their relation to reality must be argued as done above.

2.2.4 Time-variant random systems: the WSSUS model

Consider a linear, but typically not time-invariant system. The output $r(t)$ for an input $s(t)$ of such a system can formally be written as

$$r(t) = \int_{-\infty}^{\infty} k(t, t')\mathrm{s}(t')\, \mathrm{d}t', \tag{2.16}$$

where $k(t, t')$ is the so-called *integral kernel* of the system. This means that the output at time t is a continuous superposition of the input signal taken at time instants t' multiplied by a weight factor $k(t, t')$. We add the following remarks:

- For (finite-dimensional) vectors, every linear mapping is given by a matrix multiplication. Equation (2.16) is just a natural generalization of a matrix multiplication to the continuous case.
- In the case in which the kernel depends only on the difference argument $t - t'$, that is $k(t, t') = \tilde{k}(t - t')$, the system is time invariant, and Equation (2.16) reduces to a convolution.

- Equation (2.16) is a formal notation. The integral kernel $k(t, t')$ may contain singularities, for example, terms like δ-functions. But this is not really a problem in practice.

We now substitute the integration variable by $\tau = t - t'$, which can be interpreted as the delay between the input time t' and the output time t, resulting in

$$r(t) = \int_{-\infty}^{\infty} k(t, t-\tau)\mathrm{s}(t-\tau)\,\mathrm{d}\tau.$$

Furthermore, we define the time-variant impulse response as

$$h(\tau, t) = k(t, t-\tau)$$

and obtain

$$r(t) = \int_{-\infty}^{\infty} h(\tau, t)s(t-\tau)\,\mathrm{d}\tau.$$

The time-variant channel transfer function is defined as the Fourier transform in the delay variable τ of the time-variant impulse response

$$H(f, t) = \int_{-\infty}^{\infty} \mathrm{e}^{-j2\pi f\tau} h(\tau, t)\,\mathrm{d}\tau.$$

The receive signal $r(t)$ is related to the Fourier transform $S(f)$ of the transmit signal $s(t)$ by

$$r(t) = \int_{-\infty}^{\infty} \mathrm{e}^{j2\pi f\tau} H(f, t)S(f)\tau,$$

where $H(f, t)$ is the time-variant transfer function of the channel.

We now assume that the time-variant transfer function $H(f, t)$ is a two-dimensional random process, and, without losing generality, that the mean value is zero[1]. We further assume that the two-dimensional autocorrelation is time- and frequency-shift invariant, that is,

$$\mathrm{E}\left\{H(f_1 + f, t_1 + t)H^*(f_1, t_1)\right\} = \mathrm{E}\left\{H(f_2 + f, t_2 + t)H^*(f_2, t_2)\right\}. \tag{2.17}$$

Such a process is called a *wide-sense stationary uncorrelated scattering* (WSSUS) process. Wide-sense stationarity means time-shift invariance only up to second-order statistical expectation values. This is weaker than SSS, where all statistical expectation values must be time-shift invariant. Frequency-shift invariance up to the second order is named uncorrelated scattering for reasons that will become obvious soon. The two-dimensional ACF of the two-dimensional random process is defined by

$$\mathcal{R}(f, t) = \mathrm{E}\left\{H(f_1 + f, t_1 + t)H^*(f_1, t_1)\right\} \tag{2.18}$$

and the scattering function by the two-dimensional (2-D) Fourier (back) transform

$$\mathcal{S}(\tau, \nu) = \int_{-\infty}^{\infty} \mathrm{d}f \int_{-\infty}^{\infty} \mathrm{d}t\, \mathrm{e}^{j2\pi f\tau} \mathrm{e}^{-j2\pi\nu t} \mathcal{R}(f, t). \tag{2.19}$$

[1] If the mean value does not equal zero, we may consider the stochastic process of the difference to the mean value.

Because $H(f,t)$ is the complex baseband process for a WSSUS process, we have the property

$$\mathrm{E}\{H(f_1+f,t_1+t)H(f_1,t_1)\}=0,$$

which is the generalization of the result of Proposition 1.3.3. to two-dimensional stochastic processes.

We define the 2-D Fourier transform of the time-variant transfer function as

$$G(\tau,\nu)=\int_{-\infty}^{\infty}\mathrm{d}f\int_{-\infty}^{\infty}\mathrm{d}t\,\mathrm{e}^{j2\pi f\tau}\mathrm{e}^{-j2\pi\nu t}H(f,t). \tag{2.20}$$

The inverse is given by

$$H(f,t)=\int_{-\infty}^{\infty}\mathrm{d}\tau\int_{-\infty}^{\infty}\mathrm{d}\nu\,\mathrm{e}^{-j2\pi f\tau}\mathrm{e}^{j2\pi\nu t}G(\tau,\nu). \tag{2.21}$$

The term *uncorrelated scattering* stems from the following.

Proposition 2.2.1 (Uncorrelated scattering) *The condition (2.17) is equivalent to the condition*

$$\mathrm{E}\left\{G(\tau_1,\nu_1)G^*(\tau_2,\nu_2)\right\}=\delta(\tau_1-\tau_2)\delta(\nu_1-\nu_2)\mathcal{S}(\tau_1,\nu_2)$$

with $\mathcal{S}(\tau,\nu)$ defined by Equations (2.19) and (2.18).

Proof. From Equations (2.20) and (2.18), we conclude that the left-hand side equals the fourfold integral

$$\int_{-\infty}^{\infty}\mathrm{d}f_1\,\mathrm{d}t_1\,\mathrm{d}f_2\,\mathrm{d}t_2\,\mathrm{e}^{j2\pi f_1\tau_1}\mathrm{e}^{-j2\pi\nu_1 t_1}\mathrm{e}^{-j2\pi f_2\tau_2}\mathrm{e}^{j2\pi\nu_2 t_2}\cdot\mathrm{E}\left\{H(f_1,t_1)H^*(f_2,t_2)\right\}$$

$$=\int_{-\infty}^{\infty}\mathrm{d}f_1\int_{-\infty}^{\infty}\mathrm{d}t_1\int_{-\infty}^{\infty}\mathrm{d}f_2\int_{-\infty}^{\infty}\mathrm{d}t_2\,\mathrm{e}^{j2\pi(f_1\tau_1-f_2\tau_2)}\mathrm{e}^{-j2\pi(\nu_1 t_1-\nu_2 t_2)}\mathcal{R}(f_1-f_2,t_1-t_2).$$

We change the order of integration and substitute $f=f_1-f_2$ for f_1 and $t=t_1-t_2$ for t_1 to obtain

$$\int_{-\infty}^{\infty}\mathrm{d}f_2\int_{-\infty}^{\infty}\mathrm{d}t_2\int_{-\infty}^{\infty}\mathrm{d}f\int_{-\infty}^{\infty}\mathrm{d}t\,\mathrm{e}^{j2\pi(f+f_2)\tau_1}\mathrm{e}^{-j2\pi\nu_1(t+t_2)}\mathrm{e}^{-j2\pi f_2\tau_2}\mathrm{e}^{j2\pi\nu_2 t_2}\mathcal{R}(f,t)$$

$$=\int_{-\infty}^{\infty}\mathrm{d}f_2\mathrm{e}^{j2\pi f_2(\tau_1-\tau_2)}\int_{-\infty}^{\infty}\mathrm{d}t_2\mathrm{e}^{-j2\pi(\nu_1-\nu_2)t_2}\int_{-\infty}^{\infty}\mathrm{d}f\int_{-\infty}^{\infty}\mathrm{d}t\,\mathrm{e}^{j2\pi f\tau_1}\mathrm{e}^{-j2\pi\nu_1 t}\mathcal{R}(f,t).$$

The first integral equals $\delta(\tau_1-\tau_2)$, the second equals $\delta(\nu_1-\nu_2)$ and the third (twofold) integral equals $\mathcal{S}(\tau_1,\nu_2)$.

We add the following remarks:

- This is a generalization of a known property for WSS processes to two dimensions: The Fourier transform $X(f)$ of a WSS process $x(t)$ has the property that its values $X(f_1)$ and $X(f_2)$ for different frequencies f_1 and f_2 are uncorrelated (see e.g. (Papoulis 1991)). The proposition says that the values of $G(\tau,\nu)$ for different Doppler frequencies and for different delays are uncorrelated.

- We must note that in a real transmission setup, uncorrelated scattering will no longer be given because any receive filter will introduce a correlation between delays τ_1 and τ_2.

2.2.5 Rayleigh and Ricean channels

To apply the WSSUS model to concrete problems in digital communications (e.g. to calculate or simulate bit error rates), the statistics of the two-dimensional fading process $H(f,t)$ has to be specified. In many typical situations without line of sight (LOS), the received signal is a superposition of many scattered components. Owing to the central limit theorem (Feller 1970; Papoulis 1991; van Kampen 1981), it is reasonable in this case to model $H(f,t)$ by a Gaussian process with zero mean. If a LOS component is present, this can be taken into account simply by adding a constant mean value. A WSSUS process that is Gaussian is sometimes called a *GWSSUS* process. We note that a wide-sense stationary Gaussian process is already a strict-sense stationary (see e.g. (Feller 1970; Papoulis 1991)). Gaussian processes are completely characterized by their properties up to second order, that is, the mean and the autocorrelation (one can take this as a definition of a Gaussian process). For a GWSSUS process with zero mean, every sample $H(f_1,t_1)$ for fixed frequency and time is a complex Gaussian random variable that we write as

$$H(f_1,t_1) = X + jY.$$

From the property

$$\mathrm{E}\{H(f_1+f,t_1+t)H(f_1,t_1)\} = 0$$

we conclude that X and Y are uncorrelated and have the same variance (see Problem 1). Because these random variables are Gaussian, they are even statistically independent, identically distributed real Gaussian random variables . We normalize the average power gain of the channel to one so that

$$\mathrm{E}\left\{X^2\right\} = \mathrm{E}\left\{Y^2\right\} = \frac{1}{2}.$$

The probability density functions of X and Y are then given by

$$p_X(x) = \frac{1}{\sqrt{\pi}}\mathrm{e}^{-x^2},\ p_Y(y) = \frac{1}{\sqrt{\pi}}\mathrm{e}^{-y^2}.$$

We introduce polar coordinates $X = A\cos\Phi,\ Y = A\sin\Phi$ to calculate the joint pdf $p_{A,\Phi}(a,\phi)$ of amplitude and phase. From the condition

$$p_{A,\Phi}(a,\phi)\,\mathrm{d}a\,\mathrm{d}\phi = p_X(x)p_Y(y)\,\mathrm{d}x\,\mathrm{d}y$$

and $\mathrm{d}x\,\mathrm{d}y = a\,\mathrm{d}a\,\mathrm{d}\phi$, we obtain

$$p_{A,\Phi}(a,\phi) = \frac{1}{2\pi}2a\mathrm{e}^{-a^2}.$$

Thus, $p_{A,\Phi}(a,\phi) = p_A(a)p_\Phi(\phi)$ with

$$p_\Phi(\phi) = \frac{1}{2\pi}$$

and

$$p_A(a) = 2a\mathrm{e}^{-a^2}. \tag{2.22}$$

This probability density function for the amplitude is called *Rayleigh distribution.* We therefore call this mean-zero GWSSUS channel a *Rayleigh fading channel.* It is interesting to ask for the pdf $p_{\text{power}}(\gamma)$ of the power A^2. From the condition

$$p_{\text{power}}(\gamma)\,\mathrm{d}\gamma = p_A(a)\,\mathrm{d}a$$

we easily obtain

$$p_{\text{power}}(\gamma) = \mathrm{e}^{-\gamma},$$

that is, the power is exponentially distributed for a Rayleigh fading channel. The probability $\mathrm{P}(A^2 < \gamma)$ that the power falls below a certain value γ is given by

$$\mathrm{P}(A^2 < \gamma) = \int_0^{\gamma} \mathrm{e}^{-x}\,\mathrm{d}x = 1 - \mathrm{e}^{-\gamma} = \gamma - \frac{1}{2}\gamma^2 + \cdots .$$

For small values of γ, the approximation $\mathrm{P}(A^2 < \gamma) \approx \gamma$ is allowed. We can now easily conclude that, in a Rayleigh fading channel, the probability for a deep fade of -20 dB (relative to the mean power) is approximately 1%, the probability for a deep fade below -30 dB is approximately 0.1% and so on.

For a LOS channel, we assume a GWSSUS channel with a constant mean value, that is, the Doppler shift of the LOS is assumed to be zero. This can always be achieved by a proper choice of the carrier frequency f_0, that is, each Doppler shift is defined as the shift relative to the LOS. The probability density function for the amplitude is now a Gaussian distribution with nonzero mean. It can be shown to be (Proakis 2001)

$$p_A(a) = 2a\,(1+K)\,\mathrm{e}^{-\left(K+a^2(1+K)\right)} \cdot \mathrm{I}_0\left(2a\sqrt{K\,(1+K)}\right),$$

where $\mathrm{I}_0\,(x)$ is the modified Bessel function of the first kind and order zero. This pdf is called the *Rice distribution* and the GWSSUS channel is called a *Ricean channel*. The parameter K called *Rice factor* is the power ratio between the LOS component and the scattering components. The special case $K = 0$ corresponds to the absence of a LOS and leads to a Rayleigh channel. The special case $K \to \infty$ corresponds to the absence of scattering and leads to an AWGN channel. Figure 2.8 shows the Ricean pdf for different values of K. For large K, it approaches a δ function. The pdf for the power can be obtained as

$$p_{\text{power}}(\gamma) = (1+K)\,\mathrm{e}^{-(K+\gamma(1+K))} \cdot \mathrm{I}_0\left(2\sqrt{\gamma\,K\,(1+K)}\right).$$

The probability $\mathrm{P}(A^2 < \gamma)$ that the power falls below a certain value γ must be calculated by numerical integration. Figure 2.9 shows this quantity for different values of K.

2.3 Channel Simulation

To evaluate the performance of a digital communication system in a mobile radio channel by means of computer simulations, we need a simulation method that can be implemented in a computer program and that reflects the relevant statistical properties of the channels discussed above. In this section, we introduce a practical simulation method that is quite simple to implement and has been adopted by many authors because of its computational efficiency.

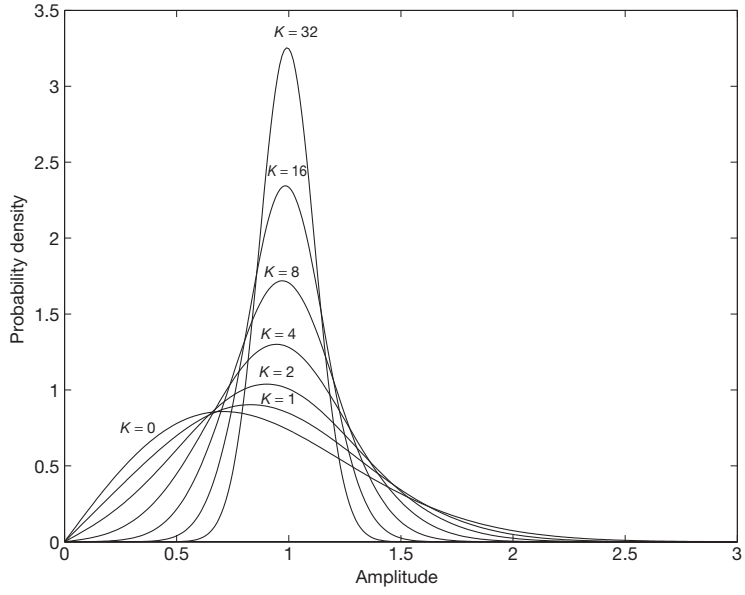

Figure 2.8 The Ricean pdf for $K = 0$ (Rayleigh), and $K = 1, 2, 4, 8, 16, 32$.

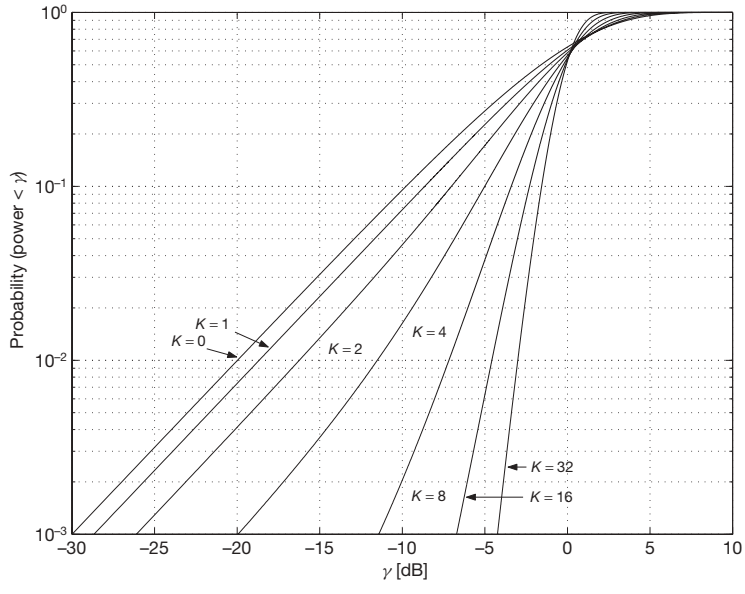

Figure 2.9 The probability $\mathrm{P}(A^2 < \gamma)$ that the power below a certain value γ for the Ricean channel with $K = 0$ (Rayleigh), and $K = 1, 2, 4, 8, 16, 32$.

The main idea of this simulation model is to reverse the line of thought that leads to the statistical Gaussian WSSUS model to reflect the physical reality. The central limit theorem gives the justification to apply the mathematical model of a Gaussian process for a physical signal that is the superposition of many unknown, that is, (pseudo-) random components. On the other hand, owing to the central limit theorem, a superposition of sufficiently many independent random signal components should be a good approximation for a Gaussian process and should thus be a good model for computer simulations. The remaining task is to find out what statistical properties of the components are needed to achieve the appropriate statistical properties of the composed process. For a zero mean GWSSUS channel, we make the following *ansatz* for the process of the simulation model

$$H_N(f,t) = \frac{1}{\sqrt{N}} \sum_{k=1}^{N} \mathrm{e}^{j\theta_k} \mathrm{e}^{j2\pi\nu_k t} \mathrm{e}^{-j2\pi f \tau_k}, \tag{2.23}$$

where θ_k, ν_k, τ_k are random variables that are statistically independent and identically distributed for different values of k. To be more specific, the random phase θ_k is assumed to be independent of ν_k and τ_k and it is uniformly distributed over the unit circle. The random variables ν_k and τ_k have a joint pdf $p(\tau, \nu)$ that needs to be adjusted to the statistical properties of the mathematical GWSSUS channel, which is completely characterized by the autocorrelation $\mathcal{R}(f,t)$ or, alternatively, by the scattering function $\mathcal{S}(\tau, \nu)$. The factor $1/\sqrt{N}$ in Equation (2.23) has been introduced to normalize the average power to one. Note that we did not introduce different amplitudes for the different fading paths. It turns out that this is not necessary. Because of the central limit theorem, in the limit $N \to \infty$, $H_N(f,t)$ approaches a Gaussian process. The following theorem states that $H_N(f,t)$ is WSSUS for any finite value of N.

Theorem 2.3.1 *For any value of N,*

$$\mathrm{E}\left\{H_N(f_1+f, t_1+t) H_N^*(f_1,t_1)\right\} = \mathrm{E}\left\{H_N(f_2+f, t_2+t) H_N^*(f_2,t_2)\right\}$$

is independent of f_1 *and* t_1 *and*

$$\mathrm{E}\left\{H_N(f_1+f, t_1+t) H_N^*(f_1,t_1)\right\} = \int_{-\infty}^{\infty} \mathrm{d}\tau \int_{-\infty}^{\infty} \mathrm{d}\nu\, \mathrm{e}^{-j2\pi f\tau} \mathrm{e}^{j2\pi\nu t} p(\tau,\nu)$$

holds. Furthermore

$$\mathrm{E}\{H_N(f,t)\} = 0.$$

Proof. We insert Equation (2.23) into the left-hand side of the above equation and obtain the expression

$$\begin{aligned} &\frac{1}{N} \sum_{k=1}^{N} \sum_{l=1}^{N} \mathrm{E}\left\{\mathrm{e}^{j(\theta_k-\theta_l)} \mathrm{e}^{j2\pi(\nu_k(t_1+t)-\nu_l t_1)} \mathrm{e}^{-j2\pi((f_1+f)\tau_k - f_1\tau_l)}\right\} \\ &\quad = \frac{1}{N} \sum_{k=1}^{N} \sum_{l=1}^{N} \mathrm{E}\left\{\mathrm{e}^{j(\theta_k-\theta_l)}\right\} \mathrm{E}\left\{\mathrm{e}^{j2\pi(\nu_k(t_1+t)-\nu_l t_1)} \mathrm{e}^{-j2\pi((f_1+f)\tau_k - f_1\tau_l)}\right\}. \end{aligned}$$

The last equality holds because θ_k is independent of all other random variables. For $k \neq l$, $\mathrm{E}\left\{\mathrm{e}^{j(\theta_k - \theta_l)}\right\} = \mathrm{E}\left\{\mathrm{e}^{j\theta_k}\right\}\mathrm{E}\left\{\mathrm{e}^{j\theta_l}\right\} = 0$. Therefore, all terms with $k \neq l$ in the double sum vanish and we obtain the single sum

$$\frac{1}{N}\sum_{k=1}^{N}\mathrm{E}\left\{\mathrm{e}^{j2\pi\nu_k t}\mathrm{e}^{-j2\pi f\tau_k}\right\},$$

which is obviously independent of f_1 and t_1. Because the random variables ν_k and τ_k have the same statistics for all values of k with joint pdf $p(\tau, \nu)$, we eventually obtain for the sum

$$\mathrm{E}\left\{\mathrm{e}^{j2\pi\nu_k t}\mathrm{e}^{-j2\pi f\tau_k}\right\} = \int_{-\infty}^{\infty}\mathrm{d}\tau\int_{-\infty}^{\infty}\mathrm{d}\nu\,\mathrm{e}^{-j2\pi f\tau}\mathrm{e}^{j2\pi\nu t}\,p(\tau, \nu).$$

The second property follows from $\mathrm{E}\left\{\mathrm{e}^{j\theta_l}\right\} = 0$.

The theorem states that $H_N(f, t)$ is a WSSUS process with an ACF

$$\mathcal{R}_{\mathrm{model}}(f, t) = \mathrm{E}\left\{H_N(f_1 + f, t_1 + t)H_N^*(f_1, t_1)\right\}$$

and a scattering function given by

$$\mathcal{S}_{\mathrm{model}}(\tau, \nu) = \int_{-\infty}^{\infty}\mathrm{d}f\int_{-\infty}^{\infty}\mathrm{d}t\,\mathrm{e}^{j2\pi f\tau}\mathrm{e}^{-j2\pi\nu t}\mathcal{R}_{\mathrm{model}}(f, t).$$

The inverse relation is

$$\mathcal{R}_{\mathrm{model}}(f, t) = \int_{-\infty}^{\infty}\mathrm{d}\tau\int_{-\infty}^{\infty}\mathrm{d}\nu\,\mathrm{e}^{-j2\pi f\tau}\mathrm{e}^{j2\pi\nu t}\mathcal{S}_{\mathrm{model}}(\tau, \nu).$$

Comparing this equation with the statement

$$\mathcal{R}_{\mathrm{model}}(f, t) = \int_{-\infty}^{\infty}\mathrm{d}\tau\int_{-\infty}^{\infty}\mathrm{d}\nu\,\mathrm{e}^{-j2\pi f\tau}\mathrm{e}^{j2\pi\nu t}\,p(\tau, \nu)$$

of the theorem, we find that

$$\mathcal{S}_{\mathrm{model}}(\tau, \nu) = p(\tau, \nu).$$

We thus have found that for the model channel, the scattering function can be interpreted as a probability density function of the delays and Doppler frequencies.

We add the following remarks:

- The statement of the theorem and the interpretation is true for any N, even for $N = 1$. However, the model is a reasonable approximation only if N is sufficiently large.
- For finite values of N, the model process is not ergodic.
- The model process is Gaussian only in the limit $N \to \infty$. Thus, it only approximates the GWSSUS process, and it does so in a similar manner, as the GWSSUS process is only a model of the physical reality.

- For bit error simulations, it is not necessary to choose N extremely large. For small amplitudes, only a moderately large number of superposed random variables already approximates a Gaussian distribution quite well. Bit errors in a Rayleigh fading channel occur mainly during deep fades, that is, at small channel amplitudes. For many practical simulations, $N = 100$ has proven to be a good choice.

Channel simulations will be done in the time domain. The fading channel model is then given by the receive signal

$$r(t) = \frac{1}{\sqrt{N}} \sum_{k=1}^{N} e^{i\theta_k} e^{i2\pi \nu_k t} s(t - \tau_k) + n(t), \tag{2.24}$$

where $s(t)$ is the transmit signal and $n(t)$ is AWGN. The random variables ν_k and τ_k will be generated by a random number generator matched to the scattering function. Approximations are allowed. As discussed above, the exact structure of the scattering function is not important, and it can be expected that the model is quite good if the second moments agree.

An additional direct component to simulate Ricean fading can easily be included into the model by writing

$$r(t) = \frac{K}{1+K} \cdot s(t) + \frac{1}{1+K} \frac{1}{\sqrt{N}} \sum_{k=1}^{N} e^{i\theta_k} e^{i2\pi \nu_k t} s(t - \tau_k) + n(t) \tag{2.25}$$

for a direct component with Doppler shift zero. K is the Rice factor.

The tapped delay line model

Another kind of model, which is widely used for simulations of mobile communication systems, is called the *tapped delay line model*. This model may be interpreted as a superposition of a certain number M of discrete fading paths (taps) corresponding to propagation delay values τ_m, $m = 1, 2, \ldots, M$. To fix such a model, the Doppler spectrum of each tap, the delay values (relative to the first tap) and the corresponding mean relative amplitudes or power values of each tap have to be specified. The channel according to such a model may be generated using Equation (2.23) by inserting the fixed delay values τ_m of the taps instead of choosing random delay values. The number of summands corresponding to one tap has to be selected proportional to the relative amplitude of that tap.

Some important tapped delay line models used for Global System for Mobile Communication (GSM) and Universal Mobile Telecommunication System (UMTS) simulations are illustrated in Figure 2.10: the GSM models for a typical urban (TU) and a hilly terrain (HT) as well as the International Telecommunication Union (ITU) channel models for the so-called *vehicular* (V) and *indoor-to-outdoor-pedestrian* (IOP) environment. For each environment, two channel models have been specified by the ITU (see e.g. (ETSI TR 101 112 1998)) – one with a low delay spread (channel A) and one with a higher delay spread (channel B). For the evaluation of the system proposals of UMTS, mainly the low delay spread models (channel A) have been used.

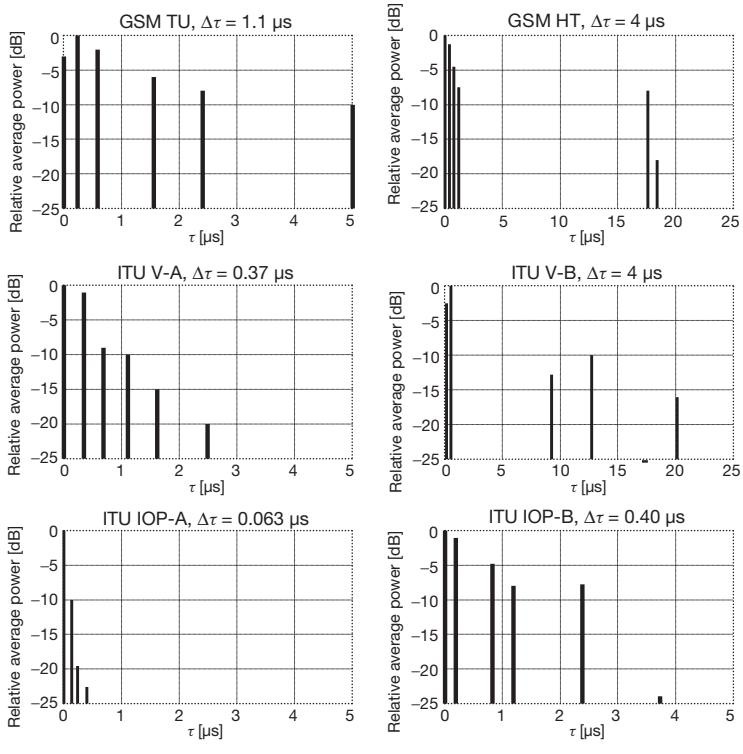

Figure 2.10 Tapped delay line models for GSM, UMTS simulations.

2.4 Digital Transmission over Fading Channels

2.4.1 The MLSE receiver for frequency nonselective and slowly fading channels

Consider a time variant, but frequency nonselective fading channel as discussed in Subsection 2.2.1 with a complex baseband receive signal given by

$$r(t) = c(t)s(t) + n(t),$$

where $c(t)$ is the complex fading amplitude of the channel, $n(t)$ is complex baseband AWGN and the transmit signal $s(t)$ is given by

$$s(t) = \sum_{k=1}^{K} s_k g_k(t)$$

with an orthonormal transmit base $g_k(t)$ and transmit symbols s_k. The assumption that the fading is frequency nonselective – resulting only in a multiplicative fading amplitude – is justified if the symbol duration T_S is much longer than the delay spread $\Delta\tau$ of the channel. The fading channel transforms the transmit base to a new base with pulses given by $h_k(t) =$

$c(t)g_k(t)$ that must be taken as detector pulses at the receiver. In general, these pulses are not orthogonal and the treatment becomes more involved. However, it can be simplified for the important special case that the fading amplitude varies slowly compared to the duration of the pulse $g_k(t)$ (which is typically of the order T_S) and can thus be treated as a constant c_k for the transmission of s_k. This means that the pulse $g_k(t)$ is concentrated in time compared to the variation of the channel so that the approximation $h_k(t) = c(t)g_k(t) \approx c_k g_k(t)$ can be made and

$$\int_{-\infty}^{\infty} g_i^*(t)c(t)g_k(t)\,\mathrm{d}t \approx \int_{-\infty}^{\infty} g_i^*(t)c_k g_k(t)\,\mathrm{d}t = c_k\delta_{ik}$$

holds. Because the channel only changes the transmit base vectors by a multiplicative factor, the outputs r_k of the detectors for the base $g_k(t)$ are a set of sufficient statistics and the treatment is similar to the one described in Section 1.4 with s_k replaced by $c_k s_k$, resulting in discrete-time channel model with receive symbols given by

$$r_k = c_k s_k + n_k,\ k = 1, \ldots, K. \tag{2.26}$$

We can write this in vector notation as

$$\mathbf{r} = \mathbf{C}\mathbf{s} + \mathbf{n}, \tag{2.27}$$

where $\mathbf{C} = \mathrm{diag}(c_1, \ldots, c_K)$ is the diagonal matrix of the complex fading amplitudes.

We note that the discrete channel model also applies to frequency selective channels as long as the channel is frequency-flat for one transmission pulse. Such a situation may occur if the transmit pulses $g_k(t)$ are located at different frequencies, for example, for multicarrier transmission (OFDM), frequency hopping or frequency diversity, when the same information is repeated at another frequency. Let $G_k(f)$ be the Fourier transform of $g_k(t)$. The fading channel transforms the transmit base to a new base with pulses given by

$$h_k(t) = \int_{-\infty}^{\infty} \mathrm{e}^{j2\pi f t} H(f,t)G_k(f)\,\mathrm{d}f$$

that have to be taken as detector pulses at the receiver. We first assume that $G_k(f)$ is concentrated at the frequency f_k so that $H(f,t)$ can be replaced by $H(f_k,t)$ under the integral. Then, we can write $h_k(t) \approx H(f_k,t)g_k(t)$. We then assume that $g_k(t)$ is concentrated at the frequency t_k so that $H(f_k,t) \approx H(f_k,t_k)$ during the pulse duration. We can then write

$$h_k(t) \approx c_k g_k(t)$$

with $c_k = H(f_k,t_k)$.

Given a receive vector $\mathbf{r}$, we now ask for the maximum likelihood transmit vector $\hat{\mathbf{s}}$. If we assume that the complex fading amplitudes are known at the receiver, we can apply the analysis of Subsection 1.4.2, only replacing the vector $\mathbf{s}$ by $\mathbf{C}\mathbf{s}$. Modifying Equation (1.77) in this way, we obtain the most likely transmit vector $\hat{\mathbf{s}}$ as

$$\hat{\mathbf{s}} = \arg\min_{\mathbf{s}} \|\mathbf{r} - \mathbf{C}\mathbf{s}\|^2, \tag{2.28}$$

where

$$\|\mathbf{r} - \mathbf{C}\mathbf{s}\|^2 = \sum_{k=1}^{K} |c_k|^2 \left| c_k^{-1} r_k - s_k \right|^2. \tag{2.29}$$

This equation allows an interesting interpretation of the optimum receiver. First, the receive symbols r_k are multiplied by the inverse of the complex channel coefficient $c_k = a_k e^{j\varphi_k}$. This means that, by multiplying with c_k^{-1}, the channel phase shift φ_k is back rotated, and the receive symbol is divided by the channel amplitude a_k to adjust the symbols to their original size. We may regard this as an *equalizer*. Each properly equalized receive symbol will be compared with the possible transmit symbol s_k by means of the squared Euclidean distance. These individual decision variables for each index k must be summed up with weighting factors given by $|c_k|^2$, the squared channel amplitude. Without these weighting factors, the receiver would inflate the noise for the very unreliable receive symbols. If a deep fade occurs at the index k, the channel transmit power $|c_k|^2$ may be much less than the power of the noise. The receive symbol r_k is nearly absolutely unreliable and provides us with nearly no useful information about the most likely transmit vector $\hat{\mathbf{s}}$. It would thus be much better to ignore that very noisy receive symbol instead of amplifying it and using it like the more reliable ones. The factor $|c_k|^2$ just takes care of the weighting with the individual reliabilities.

As in Subsection 1.4.2, we may use another form of the maximum likelihood condition. Replacing the vector $\mathbf{s}$ by $\mathbf{Cs}$ in Equation (1.78), we obtain

$$\hat{\mathbf{s}} = \arg\max_{\mathbf{s}} \left(\Re \left\{ \mathbf{s}^\dagger \mathbf{C}^\dagger \mathbf{r} \right\} - \frac{1}{2} \|\mathbf{Cs}\|^2 \right). \tag{2.30}$$

There is one difference to the AWGN case: in the first term, before cross-correlating with all possible transmit vectors $\mathbf{s}$, the receive vector $\mathbf{r}$ will first be processed by multiplication with the matrix $\mathbf{C}^\dagger$. This operation performs a back rotation of the channel phase shift φ_k for each receive symbol r_k and a weighting with the channel amplitude a_k. The resulting vector

$$\mathbf{C}^\dagger \mathbf{r} = \begin{bmatrix} c_1^* r_1 \\ \vdots \\ c_K^* r_K \end{bmatrix}.$$

must be cross-correlated with all possible transmit vectors. The second term takes the different energies of the transmit vectors $\mathbf{Cs}$ into account, including the multiplicative fading channel. If all transmit symbols s_k have the same constant energy $E_S = |s_k|^2$ as it is the case for PSK signaling,

$$\|\mathbf{Cs}\|^2 = \sum_{k=1}^{K} |c_k|^2 |s_k|^2 = E_S \sum_{k=1}^{K} |c_k|^2$$

is the same for all transmit vectors $\mathbf{s}$ and can therefore be ignored for the decision.

2.4.2 Real-valued discrete-time fading channels

Even though complex notation is a common and familiar tool in communication theory, there are some items where it is more convenient to work with real-valued quantities. If Euclidean distances between vectors have to be considered – as it is the case in the derivation of estimators and in the evaluation of error probabilities – things often become simpler if one recalls that a K-dimensional complex vector space has equivalent distances

as a $2K$-dimensional real vector space. We have already made use of this fact in Subsection 1.4.3, where pairwise error probabilities for the AWGN channel were derived. For a discrete fading channel, things become slightly more involved because of the multiplication of the complex transmit symbols s_k by the complex fading coefficients c_k. In the corresponding two-dimensional real vector space, this corresponds to a multiplication by a rotation matrix together with an attenuation factor. Surely, one prefers the simpler complex multiplication by $c_k = a_k e^{j\varphi_k}$, where a_k and φ_k are the amplitude and the phase of the channel coefficient. At the receiver, the phase will be back rotated by means of a complex multiplication with $e^{j\varphi_k}$ corresponding to multiplication by the inverse rotation matrix in the real vector space. Obviously, no information is lost by this back rotation, and we still have a set of sufficient statistics. We may thus work with a discrete channel model that includes the back rotation and where the fading channel is described by a multiplicative real fading amplitude.

To proceed as described above, we rewrite Equation (2.27) as

$$\mathbf{r} = \mathbf{C}\mathbf{s} + \mathbf{n}_c.$$

Here $\mathbf{C}$ is the diagonal matrix of complex fading amplitudes $c_k = a_k e^{j\varphi_k}$ and $\mathbf{n}_c$ is complex AWGN. We may write

$$\mathbf{C} = \mathbf{D}\mathbf{A}$$

with

$$\mathbf{A} = \mathrm{diag}(a_1, \ldots, a_K)$$

is the diagonal matrix of real fading amplitudes and

$$\mathbf{D} = \mathrm{diag}(e^{j\varphi_1}, \ldots, e^{j\varphi_K})$$

is the diagonal matrix of phase rotations. We note that $\mathbf{D}$ is a unitary matrix, that is, $\mathbf{D}^{-1} = \mathbf{D}^{\dagger}$. The discrete channel can be written as

$$\mathbf{r} = \mathbf{D}\mathbf{A}\mathbf{s} + \mathbf{n}_c.$$

We apply the back rotation of the phase and get

$$\mathbf{D}^{\dagger}\mathbf{r} = \mathbf{A}\mathbf{s} + \mathbf{n}_c.$$

Note that a phase rotation does not change the statistical properties of the Gaussian white noise, so that we can write $\mathbf{n}_c$ instead of $\mathbf{D}^{\dagger}\mathbf{n}_c$. We now decompose the complex vectors into their real and imaginary parts as

$$\mathbf{s} = \mathbf{x}_1 + j\mathbf{x}_2,$$

$$\mathbf{D}^{\dagger}\mathbf{r} = \mathbf{y}_1 + j\mathbf{y}_2$$

and

$$\mathbf{n}_c = \mathbf{n}_1 + j\mathbf{n}_2.$$

Then the complex discrete channel can be written as two real channels in K dimensions given by

$$\mathbf{y}_1 = \mathbf{A}\mathbf{x}_1 + \mathbf{n}_1$$

and

$$\mathbf{y}_2 = \mathbf{A}\mathbf{x}_2 + \mathbf{n}_2$$

corresponding to the inphase and the quadrature component, respectively. Depending on the situation, one may consider each K-dimensional component separately, as in the case of square QAM constellations and then drop the index. Or one may multiplex both together to a $2K$-dimensional vector, as in the case of PSK constellations. One must keep in mind that each multiplicative fading amplitude occurs twice because of the two components. In any case, we may write

$$\mathbf{y} = \mathbf{A}\mathbf{x} + \mathbf{n} \tag{2.31}$$

for the channel with an appropriately redefined matrix $\mathbf{A}$. We finally mention that Equation (2.30) has its equivalent in this real model as

$$\hat{\mathbf{x}} = \arg\max_{\mathbf{x}} \left(\mathbf{x} \cdot \mathbf{A}\mathbf{y} - \frac{1}{2} \|\mathbf{A}\mathbf{s}\|^2 \right).$$

2.4.3 Pairwise error probabilities for fading channels

In this subsection, we consider the case that the fading amplitude is even constant during the whole transmission of a complete transmit vector, that is, the channel of Equation (2.31) reduces to

$$\mathbf{y} = a\mathbf{x} + \mathbf{n}$$

with a constant real fading amplitude a. A special case is, of course, a symbol by symbol transmission where only one symbol is be considered. If that symbol is real, the vector $\mathbf{x}$ reduces to a scalar. If the symbol is complex, $\mathbf{x}$ is a two-dimensional vector.

Let the amplitude a be a random variable with pdf $p(a)$. For a fixed amplitude value a, we can apply the results of Subsection 1.4.3 with $\mathbf{x}$ replaced by $a\mathbf{x}$. Then Equation (1.83) leads to the conditioned pairwise error probability

$$P(\mathbf{x} \mapsto \hat{\mathbf{x}}|a) = Q\left(\frac{ad}{\sigma}\right) = \frac{1}{2}\mathrm{erfc}\left(\sqrt{\frac{a^2}{4N_0}\|\mathbf{x} - \hat{\mathbf{x}}\|^2}\right)$$

with $\sigma^2 = N_0/2$ and

$$d = \frac{1}{2}\|\mathbf{x} - \hat{\mathbf{x}}\|.$$

The overall pairwise error probability

$$P(\mathbf{x} \mapsto \hat{\mathbf{x}}) = \int_0^\infty P(\mathbf{x} \mapsto \hat{\mathbf{x}}|a)\, p(a)\, \mathrm{d}a$$

is obtained by averaging over the fading amplitude a.

We first consider the Rayleigh fading channel and insert the integral expression for $Q(x)$ to obtain

$$P(\mathbf{x} \mapsto \hat{\mathbf{x}}) = \int_0^\infty \mathrm{d}a\, 2a\mathrm{e}^{-a^2} \frac{1}{\sqrt{2\pi\sigma^2/d^2}} \int_a^\infty \mathrm{d}t \mathrm{e}^{-\frac{d^2 t^2}{2\sigma^2}}.$$

We change the order of integration resulting in

$$P(\mathbf{x} \mapsto \hat{\mathbf{x}}) = \frac{1}{\sqrt{2\pi\sigma^2/d^2}} \int_0^\infty \mathrm{d}t\, \mathrm{e}^{-\frac{d^2t^2}{2\sigma^2}} \int_0^t \mathrm{d}a\, 2a\mathrm{e}^{-a^2}.$$

The second integral is $1 - \mathrm{e}^{-t^2}$ so that

$$P(\mathbf{x} \mapsto \hat{\mathbf{x}}) = \frac{1}{\sqrt{2\pi\sigma^2/d^2}} \int_0^\infty \left(\mathrm{e}^{-\frac{d^2t^2}{2\sigma^2}} - \mathrm{e}^{-\frac{d^2+2\sigma^2}{2\sigma^2}t^2}\right) \mathrm{d}t,$$

which can be solved resulting in

$$P(\mathbf{x} \mapsto \hat{\mathbf{x}}) = \frac{1}{2}\left[1 - \sqrt{\frac{d^2/2\sigma^2}{1 + d^2/2\sigma^2}}\right]$$

or

$$P(\mathbf{x} \mapsto \hat{\mathbf{x}}) = \frac{1}{2}\left[1 - \sqrt{\frac{\frac{1}{4N_0}\|\mathbf{x} - \hat{\mathbf{x}}\|^2}{1 + \frac{1}{4N_0}\|\mathbf{x} - \hat{\mathbf{x}}\|^2}}\right].$$

For BPSK and QPSK transmission, each bit error corresponds to an error for one real symbol x, that is, $P_b = P(x \mapsto \hat{x})$ with $\hat{x} = -x$ and

$$\frac{1}{4N_0}\|x - \hat{x}\|^2 = \frac{E_b}{N_0}$$

holds. Thus,

$$P_b = \frac{1}{2}\left[1 - \sqrt{\frac{\frac{E_b}{N_0}}{1 + \frac{E_b}{N_0}}}\right].$$

To discuss the asymptotic behavior for large E_b/N_0 of this expression, we observe that $\sqrt{1+x} \approx 1 + x/2$ for small values of $x = N_0/E_b$ and find the approximation

$$P_b \approx \frac{1}{2}\frac{1}{1 + 2\frac{E_b}{N_0}} \approx \left(4\frac{E_b}{N_0}\right)^{-1}$$

for large SNRs. For other modulation schemes than BPSK or QPSK,

$$P(\mathbf{x} \mapsto \hat{\mathbf{x}}) \approx \frac{1}{2}\frac{1}{1 + \frac{1}{2N_0}\|\mathbf{x} - \hat{\mathbf{x}}\|^2} \approx \left(\frac{1}{N_0}\|\mathbf{x} - \hat{\mathbf{x}}\|^2\right)^{-1}$$

holds. There is always the proportionality

$$\frac{1}{4N_0}\|\mathbf{x} - \hat{\mathbf{x}}\|^2 \propto SNR \propto \frac{E_b}{N_0}.$$

As a consequence, the error probabilities always decrease asymptotically as SNR^{-1} or $(E_b/N_0)^{-1}$.

2.4.4 Diversity for fading channels

In a Rayleigh fading channel, the error probabilities P_{error} decrease asymptotically as slow as $P_{\text{error}} \propto SNR^{-1}$. To lower P_{error} by a factor of 10, the signal power must be increased by a factor of 10. This is related to the fact that, for an average receive signal power γ_m, the probability $P\left(A^2 < \gamma\right)$ that the signal power A^2 falls below a value γ is given by

$$P\left(A^2 < \gamma\right) = 1 - \mathrm{e}^{-\frac{\gamma}{\gamma_m}}$$

which decreases as

$$P\left(A^2 < \gamma\right) \approx \frac{\gamma}{\gamma_m} \propto SNR^{-1}$$

for high SNRs.

The errors occur during the deep fades, and thus the error probability is proportional to the probability of deep fades. A simple remedy against this is twofold (or L-fold) *diversity reception*: if two (or L) replicas of the same information reach the transmitter via two (or L) channels with statistically independent fading amplitudes, the probability that the whole received information is affected by a deep fade will be (asymptotically) decrease as SNR^{-2} (or SNR^{-L}). The same power law will then be expected for the probability of error. L is referred to as the *diversity degree* or the number of *diversity branches*. The following diversity techniques are commonly used:

- *Receive antenna diversity* can be implemented by using two (or L) receive antennas that are sufficiently separated in space. To guarantee statistical independence, the antenna separation Δx should be much larger than the wavelength λ. For a mobile receiver, $\Delta x \approx \lambda/2$ is often regarded as sufficient (without guarantee). For the base station receiver, this is certainly not sufficient.

- *Transmit antenna diversity* techniques were developed only a few years ago. Since then, these methods have evolved in a widespread area of research. We will discuss the basic concept later in a separate subsection.

- *Time diversity* reception can be implemented by transmitting the same information at two (or L) sufficiently separated time slots. To guarantee statistical independence, the time difference Δt should be much larger than the correlation time $t_{\text{corr}} = \nu_{\max}^{-1}$.

- *Frequency diversity* reception can be implemented by transmitting the same information at two (or L) sufficiently separated frequencies. To guarantee statistical independence, the frequency separation Δf should be much larger than $f_{\text{corr}} = \Delta\tau^{-1}$, that is, the correlation frequency (coherency bandwidth) of the channel.

It is obvious that L-fold time or frequency diversity increases the bandwidth requirement for a given data rate by a factor of L. Antenna diversity does not increase the required bandwidth, but increases the hardware expense. Furthermore, it increases the required space, which is a critical item for mobile reception.

The replicas of the information that have been received via several and (hopefully) statistical independent fading channels can be combined by different methods:

- *Selection diversity combining* simply takes the strongest of the L signals and ignores the rest. This method is quite crude, but it is easy to implement. It needs a selector, but only one receiver is required.

- *Equal gain combining* (EGC) needs L receivers. The receiver outputs are summed as they are (i.e. with *equal gain*), thereby ignoring the different reliabilities of the L signals.
- *Maximum ratio combining* (MRC) also needs L receivers. But in contrast to EGC, the receiver outputs are properly weighted by the fading amplitudes, which must be known at the receiver. The MRC is just a special case of the maximum likelihood receiver that has been derived in Subsection 2.4.1. The name *maximum ratio* stems from the fact that the maximum likelihood condition always minimizes the noise (i.e. *maximizes* the signal-to-noise *ratio*) (see Problem 3).

Let E_b be the total energy per data bit available at the receiver and let $E_S = \mathrm{E}\{|s_i|^2\}$ be the average energy per complex transmit symbol s_i. We assume M-ary modulation, so each symbol carries $\log_2(M)$ data bits. We normalize the average power gain of the channel to one, that is, $\mathrm{E}\left\{A^2\right\} = 1$. Thus, for L-fold diversity, the energy E_S is available L times at the receiver. Therefore, the total energy per data bit E_b and the symbol energy are related by

$$LE_S = \log_2(M)E_b. \tag{2.32}$$

As discussed in Section 1.5, for linear modulations schemes $SNR = E_S/N_0$ holds, that is,

$$SNR = \frac{\log_2(M)}{L}\frac{E_b}{N_0}. \tag{2.33}$$

Because the diversity degree L is a multiplicative factor between SNR and E_b/N_0, it is very important to distinguish between both quantities when speaking about *diversity gain*. A fair comparison of the power efficiency must be based on how much energy per bit, E_b, is necessary at the receiver to achieve a reliable reception. If the power has a fixed value and we transmit the same signal via L diversity branches, for example, L different frequencies, each of them must reduce the power by a factor of L to be compared with a system without diversity. This is also true for receive antenna diversity: L receive antennas have L times the area of one antenna. But this is an antenna gain, not a diversity gain. We must therefore compare, for example, a setup with L antenna dishes of $1\,\mathrm{m}^2$ with a setup with one dish of $L\,\mathrm{m}^2$. We state that there is no diversity gain in an AWGN channel. Consider for example, BPSK with transmit symbols $x_k = \pm\sqrt{E_S}$. For L-fold diversity, there are only two possible transmit sequences. The pairwise error probability then equals the bit error probability

$$P_b = P(\mathbf{x} \mapsto \hat{\mathbf{x}}) = \frac{1}{2}\mathrm{erfc}\left(\sqrt{\frac{1}{4N_0}\left\|\mathbf{x} - \hat{\mathbf{x}}\right\|^2}\right).$$

With $\mathbf{x} = -\hat{\mathbf{x}}$ and $\|\mathbf{x}\|^2 = LE_S$ we obtain

$$P_b = \frac{1}{2}\mathrm{erfc}\left(\sqrt{L \cdot SNR}\right)$$

for P_b as a function of the SNR but

$$P_b = \frac{1}{2}\mathrm{erfc}\left(\sqrt{\frac{E_b}{N_0}}\right)$$

for P_b as a function of E_b/N_0. Thus, for time or frequency diversity, we have wasted bandwidth by a factor of L without any gain in power efficiency.

2.4.5 The MRC receiver

We will now analyze the MRC receiver in some more detail. For L-fold diversity, L replicas of the same information reach the transmitter via L statistically independent fading amplitudes. In the simplest case, this information consists only of one complex PSK or QAM symbol, but in general, it may be any sequence of symbols, for example, of chips in the case of orthogonal modulation with Walsh vectors. The general case is already included in the treatment of Subsection 2.4.1. Here we will discuss the special case of repeating only one symbol in more detail.

Consider a single complex PSK or QAM symbol $s \equiv s_1$ and repeat it L times over different channels. The diversity receive vector can be described by Equation (2.26) by setting $s_1 = \cdots = s_L$ with K replaced by L. The maximum likelihood transmit symbol $\hat{s}$ is given by Equations (2.28) and (2.29), which simplifies to

$$\hat{s} = \arg\min_{s} \sum_{i=1}^{L} |c_i|^2 \left| c_i^{-1} r_i - s \right|^2,$$

that is, the receive symbols r_i are equalized, and next the squared Euclidean distances to the transmit symbol are summed up with the weights given by the powers of the fading amplitudes.

We may write Equation (2.27) in a simpler form as

$$\mathbf{r} = s\mathbf{c} + \mathbf{n}_c, \tag{2.34}$$

with the channel vector $\mathbf{c}$ given by

$$\mathbf{c} = (c_1, \ldots, c_L)^T$$

and complex AWGN $\mathbf{n}_c$. The vector $\mathbf{c}$ defines a (complex) one-dimensional transmission base, and sufficient statistics is given by calculating the scalar product $\mathbf{c}^\dagger \mathbf{r}$ at the receiver. The complex number $\mathbf{c}^\dagger \mathbf{r}$ is the output of the maximum ratio combiner, which, for each receive symbol r_i back rotates the phase φ_i, weights each with the individual channel amplitude $a_i = |c_i|$, and forms the sum of all these L signals.

Here we note that EGC cannot be optimal because at the receiver, the scalar product $\left(\mathrm{e}^{-j\varphi_1}, \ldots, \mathrm{e}^{-j\varphi_L}\right)\mathbf{r}$ is calculated, and this is not a set of sufficient statistics because $\left(\mathrm{e}^{j\varphi_1}, \ldots, \mathrm{e}^{j\varphi_L}\right)^T$ does not span the transmit space.

Minimizing the squared Euclidean distance yields

$$\hat{s} = \arg\min_{s} \|\mathbf{r} - s\mathbf{c}\|^2$$

or

$$\hat{s} = \arg\max_{s} \left(\Re\left\{ s^* \mathbf{c}^\dagger \mathbf{r} \right\} - \frac{1}{2} |s|^2 \, \|\mathbf{c}\|^2 \right), \tag{2.35}$$

which is a special case of Equation (2.30).

The block diagram for the MRC receiver is depicted in Figure 2.11. First, the combiner calculates the quantity

$$v = \mathbf{c}^\dagger \mathbf{r} = \sum_{k=1}^{L} c_k^* r_k = \sum_{k=1}^{L} a_k \mathrm{e}^{-j\varphi_k} r_k,$$

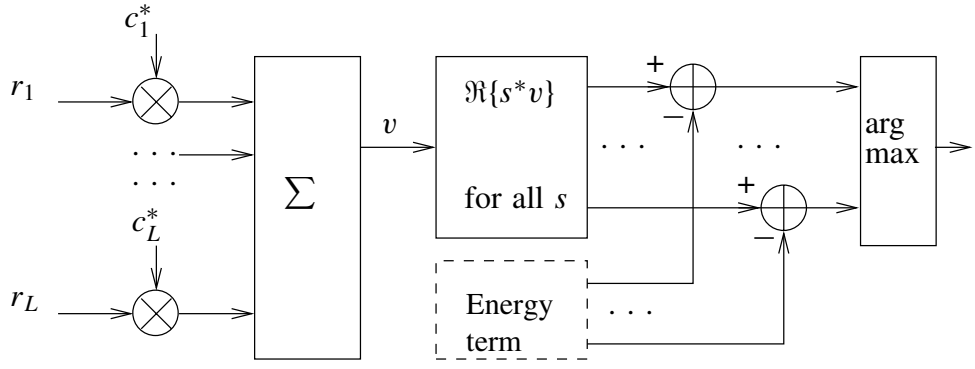

Figure 2.11 Block diagram for the MRC diversity receiver.

that is, it back rotates the phase for each receive symbol r_k and then sums them up (*combines* them) with a weight given by the channel amplitude $a_k = |c_k|$. The first term in Equation (2.35) is the correlation between the MRC output $v = \mathbf{c}^\dagger \mathbf{r}$ and the possible transmit symbols s. For general signal constellations, second (energy) term in Equation (2.35) has to be subtracted from the combiner output before the final decision. For PSK signaling, it is independent of s and can thus be ignored. For BPSK, the bit decision is given by the sign of $\Re\{v\}$. For QPSK, the two bit decisions are obtained from the signs of $\Re\{v\}$ and $\Im\{v\}$.

For the theoretical analysis, it is convenient to consider the transmission channel including the combiner. We define the composed real fading amplitude

$$a = \sqrt{\sum_{i=1}^{L} a_i^2}$$

and normalize the combiner output by

$$u = a^{-1}\mathbf{c}^\dagger \mathbf{r}.$$

We multiply Equation (2.34) by $a^{-1}\mathbf{c}^\dagger$ and obtain the one-dimensional scalar transmission model

$$u = as + n_c,$$

where $n_c = a^{-1}\mathbf{c}^\dagger \mathbf{n}_c$ can easily be proven to be one-dimensional discrete complex AWGN with variance $\sigma^2 = N_0$. A two-dimensional equivalent real-valued vector model

$$\mathbf{y} = a\mathbf{x} + \mathbf{n}, \tag{2.36}$$

can be obtained by defining real transmit and receive vectors

$$\mathbf{x} = \begin{bmatrix} \Re\{s\} \\ \Im\{s\} \end{bmatrix}, \quad \mathbf{y} = \begin{bmatrix} \Re\{u\} \\ \Im\{u\} \end{bmatrix}.$$

Here, $\mathbf{n}$ is two-dimensional real AWGN. Minimizing the squared Euclidean distance in the real vector space yields

$$\hat{\mathbf{x}} = \arg\min_{s} \|\mathbf{y} - a\mathbf{x}\|^2$$

or

$$\hat{\mathbf{x}} = \arg\max_{\mathbf{x}} \left(a\mathbf{y} \cdot \mathbf{x} - \frac{1}{2}|a^2 \, \|\mathbf{x}\|^2 \right). \tag{2.37}$$

The first term is the correlation (scalar product) of the combiner output $a\mathbf{y}$ and the transmit symbol vector $\mathbf{x}$, and the second is the energy term. For PSK signaling, this term is independent of $\mathbf{x}$ and can thus be ignored. In that case, the maximum likelihood transmit symbol vector $\mathbf{x}$ is the one with the smallest angle to the MRC output. For QPSK with Gray mapping, the two dimensions of $\mathbf{x}$ are independently modulated, and thus the signs of the components of $\mathbf{y}$ lead directly to bit decisions.

2.4.6 Error probabilities for fading channels with diversity

Consider again the frequency nonselective, slowly fading channel with the receive vector

$$\mathbf{r} = \mathbf{C}\mathbf{s} + \mathbf{n}$$

as discussed in Subsection 2.4.1. Assume that the diagonal matrix of complex fading amplitudes $\mathbf{C} = \text{diag}\,(c_1, \ldots, c_K)$ is fixed and known at the receiver. We ask for the conditional pairwise error probability $P(\mathbf{s} \mapsto \hat{\mathbf{s}}|\mathbf{C})$ that the receiver erroneously decides for $\hat{\mathbf{s}}$ instead of $\mathbf{s}$ for that given channel. Since $P(\mathbf{s} \mapsto \hat{\mathbf{s}}|\mathbf{C}) = P(\mathbf{C}\mathbf{s} \mapsto \mathbf{C}\hat{\mathbf{s}})$, we can apply the results of Subsection 1.4.3 by replacing $\mathbf{s}$ with $\mathbf{C}\mathbf{s}$ and $\hat{\mathbf{s}}$ with $\mathbf{C}\hat{\mathbf{s}}$ and get

$$P(\mathbf{s} \mapsto \hat{\mathbf{s}}|\mathbf{C}) = \frac{1}{2}\text{erfc}\left(\sqrt{\frac{1}{4N_0} \, \|\mathbf{C}\mathbf{s} - \mathbf{C}\hat{\mathbf{s}}\|^2} \right).$$

Let $\mathbf{s} = (s_1, \ldots, s_K)$ and $\hat{\mathbf{s}} = (\hat{s}_1, \ldots, \hat{s}_K)$ differ exactly in $L \leq K$ positions. Without losing generality we assume that these are the first ones. This leads to the expression

$$P(\mathbf{s} \mapsto \hat{\mathbf{s}}|\mathbf{C}) = \frac{1}{2}\text{erfc}\left(\sqrt{\frac{1}{4N_0} \sum_{i=1}^{L} |c_i|^2 \, |s_i - \hat{s}_i|^2} \right).$$

The pairwise error probability is the average $\text{E}_{\mathbf{C}}\{\cdot\}$ over all fading amplitudes, that is,

$$P(\mathbf{s} \mapsto \hat{\mathbf{s}}) = \text{E}_{\mathbf{C}}\left\{ \frac{1}{2}\text{erfc}\left(\sqrt{\frac{1}{4N_0} \sum_{i=1}^{L} |c_i|^2 \, |s_i - \hat{s}_i|^2} \right) \right\}. \tag{2.38}$$

For the following treatment, we use the polar representation

$$\frac{1}{2}\text{erfc}(x) = \frac{1}{\pi} \int_0^{\pi/2} \exp\left(-\frac{x^2}{\sin^2\theta} \right) \text{d}\theta$$

of the complementary error integral (see Subsection 1.4.3) and obtain the expression

$$P(\mathbf{s} \mapsto \hat{\mathbf{s}}) = \frac{1}{\pi} \int_0^{\pi/2} \text{E}_{\mathbf{C}}\left\{ \exp\left(-\frac{1}{4N_0 \sin^2\theta} \sum_{i=1}^{L} |c_i|^2 \, |s_i - \hat{s}_i|^2 \right) \right\} \text{d}\theta. \tag{2.39}$$

This method proposed by Simon and Alouini (2000); Simon and Divsalar (1998) is very flexible because the expectation of the exponential is just the moment generating function of the pdf of the power, which is usually known. The remaining finite integral over θ is easy to calculate by simple numerical methods. Let us assume that the fading amplitudes are statistically independent. Then the exponential factorizes as

$$\mathrm{E}_{\mathbf{C}}\left\{\exp\left(-\frac{1}{4N_0\sin^2\theta}\sum_{i=1}^{L}|c_i|^2\,|s_i-\hat{s}_i|^2\right)\right\}=\prod_{i=1}^{L}\mathrm{E}_{a_i}\left\{\exp\left(-\frac{a_i^2\,|s_i-\hat{s}_i|^2}{4N_0\sin^2\theta}\right)\right\},$$

where $\mathrm{E}_{a_i}\{\cdot\}$ is the expectation over the fading amplitude $a_i=|c_i|$. We note that with this expression, it will not cause additional problems if the L fading amplitudes have different average powers or even have different types of probability distribution. If they are identically distributed, the expression further simplifies to

$$\mathrm{E}_{\mathbf{C}}\left\{\exp\left(-\frac{1}{4N_0\sin^2\theta}\sum_{i=1}^{L}|c_i|^2\,|s_i-\hat{s}_i|^2\right)\right\}=\prod_{i=1}^{L}\mathrm{E}_{a}\left\{\exp\left(-\frac{a^2\Delta_i^2}{N_0\sin^2\theta}\right)\right\},$$

where $\Delta_i=\frac{1}{2}\,|s_i-\hat{s}_i|$ and $\mathrm{E}_a\{\cdot\}$ is the expectation over the fading amplitude $a=a_i$. For Rayleigh fading, the moment generating function of the squared amplitude can easily be calculated as

$$\mathrm{E}_a\left\{\mathrm{e}^{-xa^2}\right\}=\int_0^{\infty}2a\mathrm{e}^{-a^2}\mathrm{e}^{-xa^2}\,\mathrm{d}a$$

resulting in

$$\mathrm{E}_a\left\{\mathrm{e}^{-xa^2}\right\}=\frac{1}{1+x}.$$

With this expression, Equation (2.39) now simplifies to

$$P(\mathbf{s}\mapsto\hat{\mathbf{s}})=\frac{1}{\pi}\int_0^{\pi/2}\prod_{i=1}^{L}\frac{1}{1+\frac{\Delta_i^2}{N_0\sin^2\theta}}\,\mathrm{d}\theta. \tag{2.40}$$

We note that an upper bound can easily be obtained by upper bounding the integrand by its maximum at $\theta=\pi/2$, leading to

$$P(\mathbf{s}\mapsto\hat{\mathbf{s}})\le\frac{1}{2}\prod_{i=1}^{L}\frac{1}{1+\frac{\Delta_i^2}{N_0}}. \tag{2.41}$$

Obviously, this quantity decreases asymptotically as SNR^{-L}. We note that bounds of this type – but without the factor $1/2$ in front – are commonly obtained by Chernoff bound techniques (Jamali and Le-Ngoc 1994). A method described by Viterbi (Viterbi 1995) improved those bounds by a factor of two and yields (2.41).

A similar bound that is tighter for high SNRs but worse for low SNRs can be obtained by using the inequality

$$\frac{1}{1+\frac{1}{\sin^2\theta}\frac{\Delta_i^2}{N_0}}\le\sin^2\theta\left(\frac{\Delta_i^2}{N_0}\right)^{-1}$$

to upper bound the integrand. The integral can then be solved resulting in the asymptotically tight upper bound

$$P(\mathbf{s} \mapsto \hat{\mathbf{s}}) \leq \frac{1}{2}\frac{1}{4^L}\begin{pmatrix} 2L \\ L \end{pmatrix}\prod_{i=1}^{L}\frac{N_0}{\Delta_i^2}, \tag{2.42}$$

which again shows that the error probability decreases with the power L of the inverse SNR for L-fold repetition diversity.

Consider BPSK as an example. Here, $\Delta_i^2 = E_S$ for all values of i and, by Equation (2.32) with $M = 2$,

$$E_S = \frac{1}{L}E_b$$

holds. Thus, by Equation (2.40), the expression for the bit error rate $P_b = P(\mathbf{s} \mapsto \hat{\mathbf{s}})$ becomes

$$P_b = \frac{1}{\pi}\int_0^{\pi/2}\left(\frac{1}{1+\frac{1}{L}\frac{E_b}{N_0\sin^2\theta}}\right)^L \mathrm{d}\theta \tag{2.43}$$

which may be upper bounded by

$$P(\mathbf{s} \mapsto \hat{\mathbf{s}}) \leq \frac{1}{2}\left(\frac{1}{1+\frac{1}{L}\frac{E_b}{N_0}}\right)^L.$$

It is interesting to note that we can see from Equation (2.43) that in the limit that the diversity degrees approach infinity, we reach the performance of an AWGN channel. Using the formula

$$\lim_{n\to\infty}\left(1+\frac{1}{n}x\right)^n = \mathrm{e}^x$$

we obtain

$$\lim_{L\to\infty}\frac{1}{\pi}\int_0^{\pi/2}\left(\frac{1}{1+\frac{1}{L}\frac{E_b}{N_0\sin^2\theta}}\right)^L \mathrm{d}\theta = \frac{1}{\pi}\int_0^{\pi/2}\exp\left(-\frac{E_b}{N_0\sin^2\theta}\right)\mathrm{d}\theta.$$

By the polar representation of the error integral, the r.h.s. equals

$$P_b = \frac{1}{2}\mathrm{erfc}\left(\sqrt{\frac{E_b}{N_0}}\right),$$

which is the BER for BPSK in the AWGN channel. Figure 2.12 shows these curves for $L = 1, 2, 4, 8, 16, 32, 64$ compared to the AWGN limit.

For Ricean fading with Rice factor K, the characteristic function can be calculated as well, resulting in the expression for the error probability

$$P(\mathbf{s} \mapsto \hat{\mathbf{s}}) = \frac{1}{\pi}\int_0^{\pi/2}\prod_{i=1}^{L}R_K\left(\frac{\Delta_i^2}{N_0\sin^2\theta}\right)\mathrm{d}\theta \tag{2.44}$$

with the abbreviation

$$R_K(x) = \frac{1+K}{1+K+x}\exp\left(-\frac{Kx}{1+K+x}\right)$$

(see (Benedetto and Biglieri 1999; Jamali and Le-Ngoc 1994)).

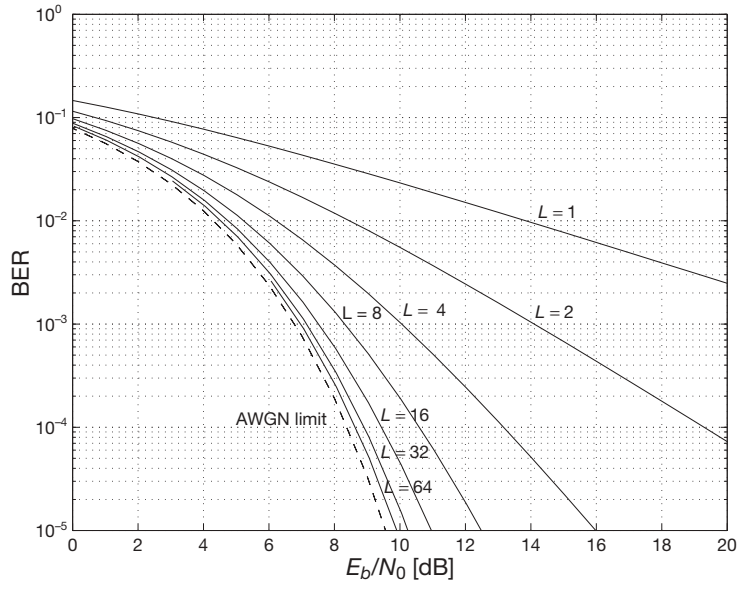

Figure 2.12 Error rates for BPSK with L-fold diversity for different values of L in a Rayleigh fading channel.

Some alternative expressions for error probabilities with diversity reception

The above method that utilizes the polar representation of the complementary Gaussian error integral is quite flexible because the fading coefficients may or may not have equal power. We will see later that it is also suited very well to investigate error probabilities for codes QAM. One drawback of this method is that it does not apply to differential modulation.

For the sake of completeness, we will now present some formulas that are valid for differential and coherent BPSK ($M = 2$) and QPSK ($M = 4$). These formulas can be found in (Hagenauer 1982; Hagenauer *et al.* 1990; Proakis 2001). We define the SNR

$$\gamma_S = E_S/N_0 = \log_2(M)E_b/N_0.$$

For coherent modulation, we define a parameter

$$\xi = \begin{cases} \sqrt{\frac{\gamma_s}{1+\gamma_s}}: & M = 2 \\ \sqrt{\frac{\gamma_s}{2+\gamma_s}}: & M = 4 \end{cases}.$$

Note that

$$\xi = \sqrt{\frac{E_b/N_0}{1 + E_b/N_0}}$$

for both cases. For differential modulation, we define

$$\xi = \begin{cases} \frac{\gamma_s R_1}{1+\gamma_s} : & M = 2 \\ \frac{\gamma_s R_1}{\sqrt{2(1+\gamma_s)^2 - \gamma_s^2 R_1^2}} : & M = 4 \end{cases},$$

where

$$R_1 = \mathcal{R}_c(T_S)$$

is the value of the time autocorrelation $\mathcal{R}_c(t)$ of the channel, taken at the symbol duration $t = T_S$. For the Jakes Doppler spectrum, we obtain from Equation (2.8)

$$\mathcal{R}_c(T_S) = \mathrm{J}_0\left(2\pi \nu_{\max} T_S\right),$$

which is obviously a function of the product $\nu_{\max} T_S$. As discussed in Subsection 2.2.1, for $\nu_{\max} T_S \ll 1$, we can approximate $\mathcal{R}_c(T_S)$ by the second order of the Taylor series as

$$\mathcal{R}_c(T_S) \approx 1 - \left(\pi \nu_{\max} T_S\right)^2.$$

The bit error probabilities P_L for L-fold diversity can then be expressed by either of the three following equivalent expressions:

$$P_L = \frac{1}{2}\left[1 - \xi \sum_{k=0}^{L-1} \binom{2k}{k} \left(\frac{1-\xi^2}{4}\right)^k\right]$$

$$P_L = \left(\frac{1-\xi}{2}\right)^L \sum_{k=0}^{L-1} \binom{L-1+k}{k} \left(\frac{1+\xi}{2}\right)^k$$

$$P_L = \left(\frac{1-\xi}{2}\right)^{2L-1} \sum_{k=0}^{L-1} \binom{2L-1}{k} \left(\frac{1+\xi}{1-\xi}\right)^k$$

We note that – as expected – these expressions are identical for coherent BPSK and QPSK if they are written as functions of E_b/N_0. DBPSK (differential BPSK) and DQPSK are numerically very close together.

2.4.7 Transmit antenna diversity

In many wireless communications scenarios, the practical boundary conditions at the transmitter and at the receiver are asymmetric. Consider as an example the situation of mobile radio. The mobile unit must be as small as possible and it is practically not feasible to apply receive antenna diversity and mount two antennas with a distance larger than half the wavelength. At the base station site, this is obviously not a problem. Transmit antenna diversity is thus very desirable because multiple antennas at the base station can then be used for the uplink and for the downlink as well. However, if one transmits signals from two or more antennas via the same physical medium, the signals will interfere and the receiver will be faced with the difficult task of disentangling the information from the superposition of signals. It is apparent that this cannot be done without loss in any case. Only a few years

ago, Alamouti (Alamouti 1998) found a quite simple setup for two antennas for which it is possible to disentangle the information without loss. The scheme can even be proven to be in some sense equivalent to a setup with two receive antennas. For the geometrical interpretation of this fact and the situation for more than two antennas, we refer to the discussion in (Schulze 2003a).

The Alamouti scheme

This scheme uses two transmit antennas to transmit a pair of two complex symbols (s_1, s_2) during two time slots. We assume that for both antennas the channel can be described by the discrete-time fading model with complex fading coefficients c_1 and c_2, respectively. We assume that the time variance of the channel is slow enough so that we can assume that these coefficients do not change from one time slot to the other.

The pair of complex transmit symbols (s_1, s_2) is then processed in the following way: at time slot 1, the symbol s_1 is transmitted from antenna 1 and s_2 is transmitted from antenna 2. The received signal (without noise) at time slot 1 is then given by $c_1 s_1 + c_2 s_2$. At time slot 2, the symbol s_2^* is transmitted from antenna 1 and $-s_1^*$ is transmitted from antenna 2. The received signal at time slot 2 is then given by $-c_2 s_1^* + c_1 s_2^*$. It is convenient for the analysis to take the complex conjugate of the received symbol in the second time slot before any other further processing at the receiver. We can therefore say that, at time slot 2, s_1 and s_2 have been transmitted over channel branches with fading coefficients $-c_2^*$ and c_1^*, respectively. The received symbols with additive white Gaussian noise at time slots 1 and 2 are given by

$$r_1 = c_1 s_1 + c_2 s_2 + n_{c1}$$

and

$$r_2 = -c_2^* s_1 + c_1^* s_2 + n_{c2},$$

respectively, where n_{c1} and n_{c2} are the independent complex Gaussian noise components with variance $\sigma^2 = N_0/2$ in each real dimension. We can write this in vector notation as

$$\mathbf{r} = \mathbf{C}\mathbf{s} + \mathbf{n}_c \tag{2.45}$$

with the vectors $\mathbf{s} = (s_1, s_2)^T$, $\mathbf{r} = (r_1, r_2)^T$, $\mathbf{n} = (n_1, n_2)^T$ and the *channel matrix*

$$\mathbf{C} = \begin{bmatrix} c_1 & c_2 \\ -c_2^* & c_1^* \end{bmatrix}. \tag{2.46}$$

We observe that the channel matrix has the property

$$\mathbf{C}^\dagger \mathbf{C} = \mathbf{C}\mathbf{C}^\dagger = \left(|c_1|^2 + |c_2|^2\right) \mathbf{I}_2, \tag{2.47}$$

where $\mathbf{I}_2$ is the 2×2 identity matrix. Equation (2.47) means that the channel matrix can be written as

$$\mathbf{C} = \sqrt{|c_1|^2 + |c_2|^2}\, \mathbf{U},$$

where $\mathbf{U}$ is a unitary matrix, that is, a matrix with the property $\mathbf{U}^\dagger \mathbf{U} = \mathbf{U}\mathbf{U}^\dagger = \mathbf{I}_2$. Unitary matrices (like orthogonal matrices for real vector spaces) are invertible matrices that leave

Euclidean distances invariant (see e.g. (Horn and Johnson 1985)). They can be visualized as rotations (possibly combined with a reflection) in an Euclidean space. This means that the transmission channel given by Equation (2.45) can be separated into three parts:

1. A rotation of the vector $\mathbf{s}$ in two complex (= four real) dimensions.
2. An attenuation by the composed fading amplitude $\sqrt{|c_1|^2 + |c_2|^2}$.
3. An AWGN channel.

Keeping in mind that multiplicative fading is just a phase rotation together with an attenuation by a real fading amplitude, we can now interpret this transmission according to Equation (2.45) with a matrix given by Equation (2.46) as a generalization of the familiar multiplicative fading from one to two complex dimensions, or, if this is easier to visualize, from two to four real dimensions. The two-dimensional rotation by the channel phase is replaced by a four-dimensional rotation, and the (real-valued) channel fading amplitude has to be replaced by the composed fading amplitude

$$a = \sqrt{|c_1|^2 + |c_2|^2}.$$

This geometrical view shows that the receiver must back rotate the receive signal $\mathbf{r}$, and then estimate the transmit vector $\mathbf{s}$ in the familiar way as known for the AWGN channel, thereby taking into account the amplitude factor a.

For the formal derivation of the diversity combiner, we proceed as in Subsection 2.4.1. The channel given by Equation (2.45) looks formally the same as the channel considered there, only the matrix $\mathbf{C}$ has a different structure. The maximum likelihood transmit vector $\hat{\mathbf{s}}$ is the one that minimizes the squared Euclidean distance, that is,

$$\hat{\mathbf{s}} = \arg\min_{\mathbf{s}} \|\mathbf{r} - \mathbf{C}\mathbf{s}\|^2 .$$

Equivalently, we may write

$$\hat{\mathbf{s}} = \arg\max_{\mathbf{s}} \left(\Re\left\{\mathbf{s}^\dagger \mathbf{C}^\dagger \mathbf{r}\right\} - \frac{1}{2} \|\mathbf{C}\mathbf{s}\|^2 \right).$$

Using Equation (2.47), we can evaluate the energy term and obtain the expression

$$\hat{\mathbf{s}} = \arg\max_{\mathbf{s}} \left(\Re\left\{\mathbf{s}^\dagger \mathbf{C}^\dagger \mathbf{r}\right\} - \frac{1}{2} \left(|c_1|^2 + |c_2|^2\right) \|\mathbf{s}\|^2 \right).$$

We note that the energy term can be discarded if all signal vectors $\mathbf{s}$ have the same energy. This is obviously the case if the (two-dimensional) symbols s_i have always equal energy as for PSK signaling, but this is not necessary. It remains true if the symbol energy differs, but all vectors of a four-dimensional signal constellation lie on a four-dimensional sphere.

The diversity combiner processes the receive vector $\mathbf{r}$ to the vector

$$\mathbf{C}^\dagger \mathbf{r} = \begin{bmatrix} c_1^* r_1 - c_2 r_2 \\ c_2^* r_1 + c_1 r_2 \end{bmatrix}$$

and correlates it with all possible transmit vectors, thereby – if necessary – taking into account their different energies. We note that for QPSK with Gray mapping, the signs of the real and imaginary parts of $\mathbf{C}^\dagger\mathbf{r}$ provide us directly with the bit decisions.

The strong formal similarity to two-antenna receive antenna diversity becomes evident in the equivalent real-valued model. We multiply Equation (2.45) by the back-rotation matrix $\mathbf{U}^\dagger = |\mathbf{c}|^{-1}\mathbf{C}^\dagger$ and obtain

$$\mathbf{U}^\dagger\mathbf{r} = a\mathbf{s} + \mathbf{n}_c,$$

where we made use of the fact that $\mathbf{U}^\dagger\mathbf{n}_c$ has the same statistical properties as $\mathbf{n}_c$. We define the four-dimensional real transmit and receive vectors

$$\mathbf{x} = \begin{bmatrix} \Re\{\mathbf{s}\} \\ \Im\{\mathbf{s}\} \end{bmatrix}, \quad \mathbf{y} = \begin{bmatrix} \Re\left\{\mathbf{U}^\dagger\mathbf{r}\right\} \\ \Im\left\{\mathbf{U}^\dagger\mathbf{r}\right\} \end{bmatrix}$$

and obtain the real-valued time-discrete vector model

$$\mathbf{y} = a\mathbf{x} + \mathbf{n}, \tag{2.48}$$

where $\mathbf{n}$ is four-dimensional real AWGN. This is formally the same as the real-valued model for the MRC combiner given by Equation (2.36). The only difference is the extension from two to four dimensions. As for the MRC combiner, minimizing the squared Euclidean distance in the real vector space yields

$$\hat{\mathbf{x}} = \arg\min_s \|\mathbf{y} - a\mathbf{x}\|^2$$

or

$$\hat{\mathbf{x}} = \arg\max_{\mathbf{x}} \left(a\mathbf{y}\cdot\mathbf{x} - \frac{1}{2}|a^2\,\|\mathbf{x}\|^2 \right).$$

The first term is the correlation (scalar product) of the combiner output $a\mathbf{y}$ and the transmit symbol vector $\mathbf{x}$, and the second is the energy term. For PSK signaling, this term is independent of $\mathbf{x}$ and can thus be ignored. In that case, the maximum likelihood transmit symbol vector $\mathbf{x}$ is the one with the smallest angle to the MRC output. For QPSK with Gray mapping, the two dimensions of $\mathbf{x}$ are independently modulated, and thus the signs of the components of $\mathbf{y}$ lead directly to bit decisions.

The conditional pairwise error probability given a fixed channel matrix $\mathbf{C}$ will be obtained similar to that of conventional diversity discussed in Subsection 2.4.6 as

$$P(\mathbf{s} \mapsto \hat{\mathbf{s}}|\mathbf{C}) = \frac{1}{2}\mathrm{erfc}\left(\sqrt{\frac{1}{4N_0}\,\|\mathbf{C}\mathbf{s} - \mathbf{C}\hat{\mathbf{s}}\|^2}\right).$$

In Subsection 2.4.6, the matrix $\mathbf{C}$ is diagonal, but here it has the property given by Equations (2.47). Thus the squared Euclidean distance can be simplified according to $\|\mathbf{C}\mathbf{s} - \mathbf{C}\hat{\mathbf{s}}\|^2 = \left(|c_1|^2 + |c_2|^2\right)\|\mathbf{s} - \hat{\mathbf{s}}\|^2$ and we find the expression for the pairwise error probability

$$P(\mathbf{s} \mapsto \hat{\mathbf{s}}) = \mathrm{E}_{\mathbf{C}}\left\{\frac{1}{2}\mathrm{erfc}\left(\sqrt{\frac{\|\mathbf{s} - \hat{\mathbf{s}}\|^2}{4N_0}\left(|c_1|^2 + |c_2|^2\right)}\right)\right\},$$

where $\mathrm{E}_{\mathbf{C}}$ means averaging over the channel. This equation is a special case of Equation (2.38), and it can be analyzed using the same methods.

Now let E_b be the total energy per data bit available at the receiver and E_S the energy per complex transmit symbol s_1 or s_2. We assume M-ary modulation, so each of them carries $\log_2(M)$ data bits. Both symbols are assumed to be of equal (average) energy, which means that $E_S = \mathrm{E}\{|s_1|^2\} = \mathrm{E}\{|s_2|^2\} = \mathrm{E}\{\|\mathbf{s}\|^2/2\}$. We normalize the average power gain for each antenna channel coefficient to one, that is, $\mathrm{E}\left\{|c_1|^2\right\} = \mathrm{E}\left\{|c_2|^2\right\} = 1$. Then, for each time slot, the total energy $2E_S$ is transmitted at both antennas together and the same (average) energy is available at each of the receive antenna. Therefore, the total energy available at the receiving site for that time slot is

$$2E_S = \log_2(M)E_b.$$

For only one transmit antenna, $SNR = E_S/N_0$ is the SNR at the receive antenna for linear modulation. For two transmit antennas, we have $SNR = 2E_S/N_0$. For uncoded BPSK or QPSK transmission, the value of each data bit affects only one real dimension. The event of an erroneous bit decision corresponds to the squared Euclidean distance

$$\|\mathbf{s} - \hat{\mathbf{s}}\|^2 = 4E_S/\log_2(M) = 2E_b,$$

which means that both BPSK ($M = 2$) and QPSK ($M = 4$) have the bit error probability

$$P_b = \mathrm{E}_{\mathbf{C}}\left\{\frac{1}{2}\mathrm{erfc}\left(\sqrt{\frac{E_b}{2N_0}\left(|c_1|^2 + |c_2|^2\right)}\right)\right\}$$

as a function of E_b/N_0. This is exactly the same as for twofold receive antenna diversity, which is a special case of the results in Subsection 2.4.6 and we can apply the formulas given there for independent Rayleigh or Ricean fading.

We note that Alamouti's twofold transmit antenna diversity has the same performance as the twofold receive antenna diversity only if we write P_b as a function of E_b/N_0 because $SNR = \log_2 M \cdot E_b/N_0$ holds for the first case and $SNR = \frac{1}{2}\log_2 M \cdot E_b/N_0$ holds for the latter.

2.5 Bibliographical Notes

The classical textbook about mobile radio channels is (Jakes 1975). However, fading channels are treated in many modern textbooks about digital communication techniques (see e.g. (Benedetto and Biglieri 1999; Kammeyer 2004; Proakis 2001)). We also recommend the introductory chapter of (Jamali and Le-Ngoc 1994).

The system theory of WSSUS processes goes back to the classical paper of (Bello 1963). The practical simulation method described in this chapter has been developed by one of the authors (Schulze 1988) and has later been refined and extended by Hoeher (1992). We would like to point out that the line of thought for this model was mainly inspired by the way physicists looked at statistical mechanics (see e.g. (Hill 1956; Landau and Lifshitz 1958)). All measurements are time averages, while the statistical theory deals with statistical (so-called *ensemble*) averages. This replacement (the so-called *ergodic hypothesis*) is mathematically nontrivial, but is usually heuristically justified. Systems in statistical physics that are too complex to be studied analytically are often investigated by the so-called *Monte-Carlo* Simulations. The initial conditions (locations and velocities) of

the particles (e.g. molecules) are generated as (pseudo) random variables by a computer, and the dynamics of the system has to be calculated, for example, by the numerical solution of differential equations. From these solutions, time averages of physical quantities are calculated. For a mobile radio system, we generate phases, Doppler shifts and delay (*as initial conditions* of the system) and calculate the system dynamics from these quantities. Finally, time averages, for example, for the bit error rate are calculated.

2.6 Problems

1. Let $z(t) = x(t) + jy(t)$ be a stochastic process with the property

$$\mathrm{E}\{z(t+\tau)z(t)\} = 0.$$

Show the properties

$$\mathrm{E}\{x(t+\tau)x(t)\} = \mathrm{E}\{y(t+\tau)y(t)\}$$

and

$$\mathrm{E}\{x(t+\tau)y(t)\} = -\mathrm{E}\{y(t+\tau)x(t)\}.$$

2. Show that for the Jakes Doppler spectrum $\mathcal{S}_c(\nu)$, the second moment is given by

$$\mu_2\{\mathcal{S}_c(\nu)\} = \frac{\nu_{\max}^2}{2}.$$

3. An L-branch diversity channel is given by the receive signal vector

$$\mathbf{r} = s\mathbf{c} + \mathbf{n},$$

with the channel vector $\mathbf{c}$ given by

$$\mathbf{c} = (c_1, \ldots, c_L)^T,$$

where s is the transmit symbol and $\mathbf{n}$ is L-dimensional (not necessarily Gaussian) complex white noise. A linear combiner is given by the operation $u = \mathbf{v}^\dagger\mathbf{r}$ with a given vector $\mathbf{v}$. Show that the SNR for the combiner output is maximized for $\mathbf{v} = \mathbf{c}$.

3

Channel Coding

3.1 General Principles

3.1.1 The concept of channel coding

Channel coding is a common strategy to make digital transmission more reliable, or, equivalently, to achieve the same required reliability for a given data rate at a lower power level at the receiver. This gain in power efficiency is called *coding gain*. For mobile communication systems, channel coding is often indispensable. As discussed in the preceding chapter, the bit error rate in a Rayleigh fading channel decreases as $P_b \sim (E_b/N_0)^{-1}$, which would require an unacceptable high transmit power to achieve a sufficiently low bit error rate. We have seen that one possible solution is diversity. We will see in the following sections that channel coding can achieve the same gain as diversity with less redundancy.

This chapter gives a brief but self-contained overview over the channel coding techniques that are commonly applied in OFDM and CDMA systems. For a more detailed discussion, we refer to standard text books cited in the Bibliographical Notes.

Figure 3.1 shows the classical channel coding setup for a digital transmission system. The channel encoder adds redundancy to digital data b_i from a data source. For simplicity, we will often speak of data bits b_i and channel encoder output bits c_i, keeping in mind that other data symbol alphabets than binary ones are possible and the same discussion applies to that case. We briefly review some basic concepts and definitions.

- The output of the encoder is called a *code word*. The set of all possible code words is the *code*. The encoder itself is a mapping rule from the set of possible data words into the code. We remark that a code (which is a set) may have many different encoders (i.e. different mappings with that same set as the image).

- *Block codes*: If the channel encoder always takes a data block $\mathbf{b} = (b_1, \ldots, b_K)^T$ of a certain length K and encodes it to a code word $\mathbf{c} = (c_1, \ldots, c_N)^T$ of a certain length N, we speak of an (N, K) *block code*. For other codes than block codes, for example, convolutional codes, it is often convenient to work with code words of finite length, but it is not necessary, and the length is not determined by the code.

Theory and Applications of OFDM and CDMA Henrik Schulze and Christian Lüders

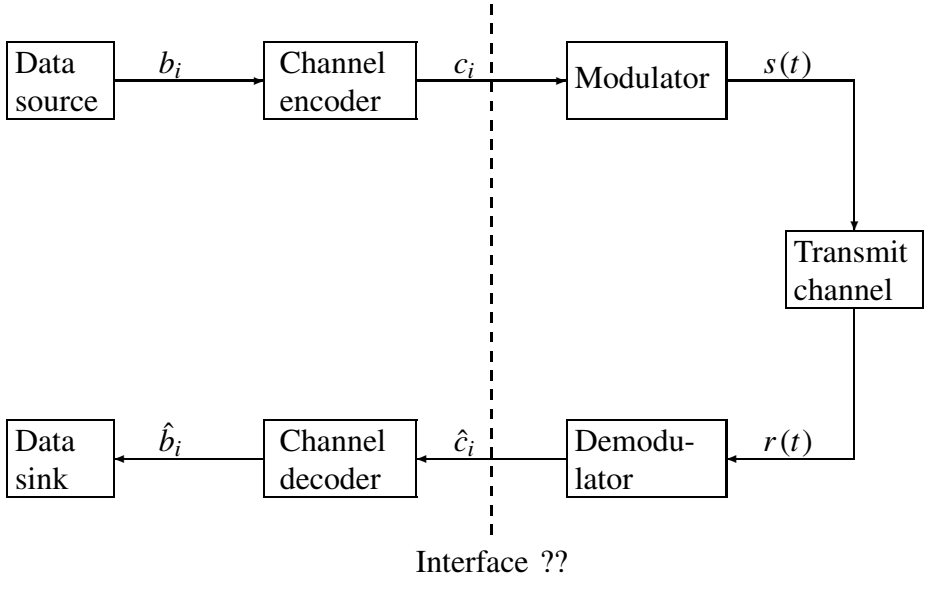

Figure 3.1 Block diagram for a digital transmission setup with channel coding.

- If the encoder maps $\mathbf{b} = (b_1, \ldots, b_K)^T$ to the code word $\mathbf{c} = (c_1, \ldots, c_N)^T$, the ratio $R_c = K/N$ is called the *code rate*.

- If two code words differ in d positions, then d is called the *Hamming distance* between the two code words. The minimum Hamming distance between any two code words is called the *Hamming distance of the code* and is usually denoted by d_H. For an (N, K) block code, we write the triple (N, K, d_H) to characterize the code.

- If the vector sum of any two code words is always a code word, the code is called *linear*.

- The Hamming distance of a linear code equals the minimum number of nonzero elements in a code word, which is called the *weight* of the code. A code can correct up to t errors if $2t + 1 \leq d_H$ holds.

- An encoder is called *systematic* if the data symbols are a subset of the code word. Obviously, it is convenient but not necessary that these systematic (i.e. data) bits (or symbols) are positioned at the beginning of the code word. In that case the encoder maps $\mathbf{b} = (b_1, \ldots, b_K)^T$ to the code word $\mathbf{c} = (c_1, \ldots, c_N)^T$ and $b_i = c_i$ for $i = 1, \ldots, K$. The nonsystematic symbols of the code word are called *parity check* (PC) *symbols.*

The channel decoder outputs c_i are the inputs of the modulator. Depending on these data, the modulator transmits one out of a set of possible signals $s(t)$. For binary codes, there are 2^K code words and thus there are 2^K possible signals $s(t)$. For a linear modulation

scheme, such a signal can be written as

$$s(t) = \sum_{i=1}^{L} s_i g_i(t)$$

with an orthonormal transmit base $\{g_i(t)\}_{i=1}^{L}$. Each possible signal can then uniquely be characterized by the corresponding transmit symbol vector $\mathbf{s} = (s_1, \ldots, s_L)^T$. Generally, there is a one-to-one correspondence between the code word vectors $\mathbf{c} = (c_1, \ldots, c_N)^T$ and the transmit symbol vector $\mathbf{s} = (s_1, \ldots, s_L)^T$. Because each code word $\mathbf{c}$ is uniquely determined by the corresponding data word $\mathbf{b}$, the mapping $\mathbf{b} \mapsto \mathbf{c}$ is uniquely defined and one may regard the channel encoder and the modulator as one single device that corresponds to the mapping $\mathbf{b} \mapsto \mathbf{s}$. This natural, but modern concept is called *coded modulation* and it has the advantage that it is quite natural to look for a joint optimization of channel coding and modulation (see e.g. (Biglieri *et al.* 1991; Jamali and Le-Ngoc 1994; Ungerboeck 1982)).

The more traditional concept as depicted in Figure 3.1 keeps both parts separated, and the modulator is one of the classical concatenation schemes discussed in Section 1.4. We may have a simple M-ary PSK or QAM symbol mapping for the s_i. Then, a subset of $m = \log_2(M)$ bits of one code word will be mapped on each symbol s_i. Or, alternatively, $m = \log_2(M)$ bits taken from m different code words will be mapped on each symbol s_i. The latter turns out to be a better choice for fading channels to avoid two bits of the same code word being affected by the same fading amplitude. We note that for M-ary signal constellations and a code rate R_c, only $R_c \log_2(M)$ useful bits are transmitted per complex symbol s_i. Thus, the energy E_b per useful bit is related to the average symbol energy $E_S = \mathrm{E}\left\{|s_k|^2\right\}$ by the equation

$$E_S = R_c \log_2(M) \cdot E_b. \tag{3.1}$$

Following Figure 3.1, the modulated signal is corrupted by the noisy transmission channel. Thus, some of the demodulator output bits $\hat{c}_i$ will be erroneously decided from the received signal $r(t)$. The channel decoder then uses the redundancy of the code to correct the errors and delivers (hopefully) correct data $\hat{b}_i$ identical to the source data b_i.

The crucial point of this traditional conception of correcting bit errors is the interface between CoDec (Coder/Decoder) and the MoDem (Modulator/Demodulator). We have seen that there is no fundamental reason to distinguish between these blocks at the transmitter. And, as we know from the detection theory as discussed in Section 1.3, the MLSE will find the most probable transmit vector $\hat{\mathbf{s}}$ that corresponds uniquely to a data vector $\hat{\mathbf{b}}$. The only reason to separate demodulator and decoder is a practical one: often, especially for long block codes, the MLSE requires quite an exhaustive search that cannot be implemented. But there are often algebraic decoding techniques for such codes that require binary inputs[1]. There may be good reasons to proceed this way but one should always keep in mind that any hard bit decision before the decoder causes loss of information. For convolutional codes, the MLSE can be easily implemented by the Viterbi decoder (see the following text). Hard decisions would cause a needless loss of approximately 2 dB in performance for convolutional codes.

The following example shows how the same transmission setup can be interpreted according to different points of view.

[1]Or, for nonbinary codes, discrete valued inputs are taken from some other finite signal alphabet.

Example 6 (Walsh–Hadamard codes) *Consider an encoder map* $\mathbf{b} \mapsto \mathbf{c}$ *for a linear* (8, 3, 4) *block code given by*

$$\begin{bmatrix} 0 & 1 & 0 & 1 & 0 & 1 & 0 & 1 \\ 0 & 0 & 1 & 1 & 0 & 0 & 1 & 1 \\ 0 & 0 & 0 & 0 & 1 & 1 & 1 & 1 \end{bmatrix} \mapsto \begin{bmatrix} 0 & 0 & 0 & 0 & 0 & 0 & 0 & 0 \\ 0 & 1 & 0 & 1 & 0 & 1 & 0 & 1 \\ 0 & 0 & 1 & 1 & 0 & 0 & 1 & 1 \\ 0 & 1 & 1 & 0 & 0 & 1 & 1 & 0 \\ 0 & 0 & 0 & 0 & 1 & 1 & 1 & 1 \\ 0 & 1 & 0 & 1 & 1 & 0 & 1 & 0 \\ 0 & 0 & 1 & 1 & 1 & 1 & 0 & 0 \\ 0 & 1 & 1 & 0 & 1 & 0 & 0 & 1 \end{bmatrix},$$

where the eight possible data words $\mathbf{b}$ *are the columns of the left matrix, and the corresponding code words* $\mathbf{c}$ *are the columns of the right matrix. One can easily verify that this code is linear (see Proposition 3.1.1) and that the Hamming distance is given by* $d_H = 4$. *Thus, it can correct one bit error. We now use a BPSK modulator with the symbol mapping* $c_i \mapsto s_i = (-1)^{c_i}$. *The composed mapping* $\mathbf{b} \mapsto \mathbf{s}$ *is then given by*

$$\begin{bmatrix} 0 & 1 & 0 & 1 & 0 & 1 & 0 & 1 \\ 0 & 0 & 1 & 1 & 0 & 0 & 1 & 1 \\ 0 & 0 & 0 & 0 & 1 & 1 & 1 & 1 \end{bmatrix} \mapsto \begin{bmatrix} 1 & 1 & 1 & 1 & 1 & 1 & 1 & 1 \\ 1 & -1 & 1 & -1 & 1 & -1 & 1 & -1 \\ 1 & 1 & -1 & -1 & 1 & 1 & -1 & -1 \\ 1 & -1 & -1 & 1 & 1 & -1 & -1 & 1 \\ 1 & 1 & 1 & 1 & -1 & -1 & -1 & -1 \\ 1 & -1 & 1 & -1 & -1 & 1 & -1 & 1 \\ 1 & 1 & -1 & -1 & -1 & -1 & 1 & 1 \\ 1 & -1 & -1 & 1 & -1 & 1 & 1 & -1 \end{bmatrix}.$$

The resulting matrix is the Hadamard matrix for $M = 8$, *and it is obvious that this scheme is nothing but orthogonal Walsh modulation as discussed in Subsection 1.1.4. The columns of the matrix just represent the signs of the Walsh functions of Figure 1.7. These codes corresponding to Hadamard matrices are called* Walsh–Hadamard (WH) *codes. The example here is the WH(8, 3, 4) code.*

We now consider as an example detector outputs given by the receive vector $\mathbf{r} = (1.5, 1.2, 0.9, 0.4, 0.8, -0.2, 1.2, -0.3)^T$. *The hard decision BPSK demodulator produces the output* $\hat{\mathbf{c}} = (0, 0, 0, 0, 0, 1, 0, 1)^T$. *This vector differs in two positions from the first and in two positions from the second code word. Thus, (at least) two errors have occurred that cannot be corrected. However, the MLSE for orthogonal Walsh modulation calculates the eight scalar products* $\mathbf{r} \cdot \mathbf{s}$ *that are the elements of the row vector* (5.4, 3.2, 1.2, 1.2, −0.6, 2.6, 1.6, 0.2) *and decides in favor of the first vector of the Hadamard matrix with the maximal scalar product* $\mathbf{r} \cdot \mathbf{s} = 5.4$.

This example shows that there is often an ambiguity in what we call channel coding and what we call modulation. For example, we may regard any linear modulation scheme as a code. The symbol mapper is an encoder that produces real or complex outputs. Here, we prefer real symbols, that is, we identify the complex plane with the two-dimensional (real) space. An M-PSK or M-QAM symbol is a code word of length $N = 2$ with M code words labeled by $K = \log_2 M$ data bit. This is a (N, K) block code. The alphabet of the

coded symbols is a finite set of real numbers. For 8-PSK, for example, this is given by $\{0, \pm\frac{1}{2}\sqrt{2}, \pm 1\}$.

A code word is given by a vector

$$\mathbf{x} = (x_1, \ldots, x_N)^T$$

of real-valued modulation symbols. To interpret the orthogonal Walsh modulation of Subsection 1.1.4 as channel coding, we set $N = M$, and the vectors $\mathbf{x}$ are the columns of the $M \times M$ Hadamard matrix. The transmit signal is given by

$$s(t) = \sum_{m=1}^{M} x_m g_m(t).$$

Note that now the base pulses $g_m(t)$ of this linear modulation correspond to what has been called *chip pulses* in that subsection.

As discussed in Subsection 2.4.1, we may consider the real-valued fading channel with AWGN disturbance given by

$$y_i = a_i x_i + n_i$$

with real-valued receive symbols y_i, fading amplitudes a_i, transmit symbols x_i and noise samples n_i with variance $\sigma^2 = N_0/2$ in each dimension. Using vector notation, we may write

$$\mathbf{y} = \mathbf{A}\mathbf{x} + \mathbf{n}.$$

The MLSE receiver calculates the most probable transmit vector $\mathbf{x}$ from the receive vector $\mathbf{y}$. Because the input of the MLSE, that is, the components y_i of the receive vector, are real numbers, the MLSE is called a *soft decision* receiver, in contrast to a *hard decision* receiver, where (*hard*) bit decisions are taken from the y_i and these bits are passed to the decoder (see Figure 3.1). However, the output of the MLSE receiver is the bit sequence that labels the most likely transmit vector. Thus, the MLSE is a *hard output* receiver. Receivers with soft output (i.e. with reliability information about the decisions) are desirable for *concatenated coding* schemes as described in Subsection 3.1.4. A receiver with soft inputs and soft outputs is called a *SISO*(*soft-in, soft-out*) receiver.

3.1.2 Error probabilities

In this subsection, we discuss error rates for binary codes with antipodal signaling, that is, BPSK. The same formulas apply for QPSK, which can be separated into antipodal signaling for both the in-phase and quadrature component.

Error probabilities for the MLSE receiver and the AWGN channel

For the MLSE receiver, general expressions for the pairwise error probabilities in the AWGN channel were derived in Subsection 1.4.3. The probability that the receiver erroneously decides for the transmit vector $\mathbf{s}$ instead of the transmitted vector $\hat{\mathbf{s}}$ is given by Equation (1.84), that is, the expression

$$P(\mathbf{s} \mapsto \hat{\mathbf{s}}) = \frac{1}{2}\mathrm{erfc}\left(\sqrt{\frac{1}{4N_0}\|\mathbf{s} - \hat{\mathbf{s}}\|^2}\right).$$

For BPSK transmission, we have $\mathbf{s} = (s_1, \ldots, s_L)^T$ with $s_i = \pm\sqrt{E_S}$, where E_S is the symbol energy. We assume a binary code with rate R_c and Hamming distance d_H. Assume that $\mathbf{s}$ corresponds to a code word $\mathbf{c}$ and the receiver decides for a code word $\hat{\mathbf{c}}$ corresponding to the signal vector $\hat{\mathbf{s}}$, and the code words $\mathbf{c}$ and $\hat{\mathbf{c}}$ have the Hamming distance d. Then,

$$\|\mathbf{s} - \hat{\mathbf{s}}\|^2 = 4dE_S.$$

For each transmitted symbol, only R_c useful bits are transmitted. Thus, $E_S = R_c E_b$, and the error event probability P_d for an erroneous decision corresponding to a Hamming distance d is given by

$$P_d = \frac{1}{2}\text{erfc}\left(\sqrt{dR_c\frac{E_b}{N_0}}\right). \tag{3.2}$$

For high values of E_b/N_0, the total error probability is dominated by the most probable error event corresponding to $d = d_H$. Asymptotically, the number of such events (that leads to a factor in front of the complementary error function) can be ignored and we may say that we obtain an *asymptotic coding gain* of

$$G_a = 10\,\log_{10}(d_H R_c)\,\text{dB}$$

compared to uncoded BPSK. We note that the expression (3.2) for P_d – written as a function of E_b/N_0 – also holds for QPSK with Gray mapping and the coding gain is also the same. For higher level modulation schemes, the analysis is more complicated because the Euclidean distances between the symbols are different.

Error probabilities for the MLSE receiver and the Rayleigh fading channel

We assume a discrete-time fading channel with receive symbols given by

$$r_i = a_i s_i + n_i,\ i = 1, \ldots, N$$

with discrete AWGN n_i and real fading amplitudes a_i, that is, the phase has already been back rotated. We consider BPSK transmission with $s_i = \pm\sqrt{E_S}$ and a binary code of rate R_c and Hamming distance d_H. Assume that $\mathbf{s}$ corresponds to a code word $\mathbf{c}$ of length N and the receiver decides for a code word $\hat{\mathbf{c}}$ corresponding to the signal vector $\hat{\mathbf{s}}$, and the code words $\mathbf{c}$ and $\hat{\mathbf{c}}$ have the Hamming distance d. We ask for the probability P_d that the code word $\mathbf{c}$ has been transmitted and the receiver erroneously decides for another code word $\hat{\mathbf{c}}$. To keep the notation simple, we assume a renumbering of the indices in such a way that the different positions are those with $i = 1, \ldots, d$ and write $\mathbf{s} = (s_1, \ldots, s_d)^T$ for the symbol vector corresponding to the first d positions of $\mathbf{c}$ and $\hat{\mathbf{s}} = (\hat{s}_1, \ldots, \hat{s}_d)^T$ for the symbol vector corresponding to the first d positions of $\hat{\mathbf{c}}$. The last $N - d$ symbols are irrelevant for the decision. This is just the same as the problem of d-fold diversity that was treated in Subsection 2.4.6. We can apply Equation (2.38) with $|s_i - \hat{s}_i|^2 = 4E_S$ and obtain the expression

$$P_d = \text{E}_{a_i}\left\{\frac{1}{2}\text{erfc}\left(\sqrt{\frac{E_S}{N_0}\sum_{i=1}^{d}|a_i|^2}\right)\right\}, \tag{3.3}$$

where $\mathrm{E}_{a_i}\{\cdot\}$ is the average over all fading amplitudes. For a Rayleigh channel with identically distributed and independent fading amplitudes of average power one, the average can be easily performed as shown in Subsection 2.4.5 resulting in

$$P_d = \frac{1}{\pi}\int_0^{\pi/2}\left(\frac{1}{1+R_c\frac{E_b}{N_0\sin^2\theta}}\right)^d \mathrm{d}\theta, \tag{3.4}$$

where we have used $E_S = R_c E_b$. As an alternative to this polar representation expression, the formulas given at the end of Subsection 2.4.6 can be applied. We thus have seen that the Hamming distance can be interpreted as diversity that is provided by the code. Using Equation (2.42), P_d can be tightly upper bounded by

$$P_d \leq \frac{1}{2}\frac{1}{4^L}\binom{2d}{d}\left(R_c\frac{E_b}{N_0}\right)^{-d}.$$

Thus, for a code with Hamming distance d_H, the error rates asymptotically decay as SNR^{-d_H} in an independently fading Rayleigh channel. These expressions for P_d – written as a function of E_b/N_0 – also hold for QPSK if the two bits corresponding to a QPSK symbol s_i belong to different code words. Otherwise, two bits of the same code word will be affected by the same fading amplitude, which would result in a loss of diversity.

Residual bit error rates for hard decision decoding of block codes

We consider an (N, K, d_H) binary block code with hard decision error correction capability of t bit errors. For an odd Hamming distance d_H, we have $d_H = 2t+1$, and for even d_H, we have $d_H = 2t+2$. Let p be the channel bit error probability and assume that $i \geq t+1$ channel bit errors occurs inside the code word. The probability for a certain error pattern with i bit errors is given by

$$p^i(1-p)^{N-i}.$$

There are $\binom{N}{i}$ such possible patterns for a code word of length N. Thus, the block error probability, that is, the probability for a wrong decoding decision for the code word is given by

$$P_{\mathrm{Block}} = \sum_{i=t+1}^{N}\binom{N}{i}p^i(1-p)^{N-i}. \tag{3.5}$$

Often, one is interested not only in the block error probability, but in the bit error probability. If the error correction capability is t, the decoder may change at most t bits inside the code word when trying to correct the error. If $i > t$ errors have occurred, this will result in a wrong decision and the decoder will erroneously change at most t additional bits, resulting in at most $i+t$ errors. Thus, if we consider only error events corresponding to exactly i errors ($i > t$), the bit error probability for such an event is bounded by

$$\frac{t+i}{N}\binom{N}{i}p^i(1-p)^{N-i}.$$

Keeping in mind that not more than N errors may occur, the bound can be slightly improved if we replace $t+i$ in the numerator by $\min(t+i, N)$. Summing up over all possible

numbers of errors, we get the bound for the bit error probability

$$P_b \leq \sum_{i=t+1}^{N} \frac{\min(t+i, N)}{N} \binom{N}{i} p^i (1-p)^{N-i}. \tag{3.6}$$

Although it is more popular to talk about bit error probabilities rather than block error probabilities, one should keep in mind that the block error probability is often more relevant for an application than the bit error probability. For the application, the average time between two error events is often the most relevant figure. In case of a decoding error, at least d_H bit errors occur at the same time. The error event corresponding to d_H errors is the most probable one, and it is dominant if the channel is not too bad. Looking only at P_b without knowledge of the code may give rise to wrong interpretations. A residual bit error rate of $P_b = 10^{-6}$ for a rate of 10 kbit/s does not mean that in average one bit error occurs every 100 seconds, but approximately d_H errors occur every 100 d_H seconds. For large values of d_H, this makes a great difference for the application.

3.1.3 Some simple linear binary block codes

In this subsection, we will present some facts about linear binary block codes and give some examples. We will not go into further details and refer to the text books about channel coding cited in the Bibliographical Notes.

Let $\mathcal{C}$ be a linear binary (N, K) block code. We write all the $M = 2^K$ code words of length N as binary columns $\mathbf{c}_m \in \mathcal{C}$, $m = 1, \ldots, M$ and join them together to a matrix

$$\mathbf{C} = [\mathbf{c}_1, \ldots, \mathbf{c}_M].$$

There are M bit tuples of length K. We write them as column vectors $\mathbf{b}_m$, $m = 1, \ldots, M$ with the LSB (Least Significant Bit) in the upper position. We join them together to a binary tuple matrix

$$\mathbf{B} = [\mathbf{b}_1, \ldots, \mathbf{b}_M].$$

For $M = 8$, for example, this matrix is given by

$$\mathbf{B} = \begin{pmatrix} 0 & 1 & 0 & 1 & 0 & 1 & 0 & 1 \\ 0 & 0 & 1 & 1 & 0 & 0 & 1 & 1 \\ 0 & 0 & 0 & 0 & 1 & 1 & 1 & 1 \end{pmatrix}.$$

We write $\mathcal{B}$ for the set of all these binary vectors. The encoder can then be written as a linear mapping

$$\mathbf{G} : \mathcal{B} \to C, \ \mathbf{b}_m \mapsto \mathbf{c}_m = \mathbf{G}\mathbf{b}_m$$

between the vector spaces $\mathcal{B}$ and $\mathcal{C}$. $\mathbf{G}$ is called the *generator matrix*. Using matrix notation, we may also write

$$\mathbf{C} = \mathbf{G}\mathbf{B}.$$

From linear algebra we know that $\mathbf{G}$ is given by an $N \times K$ matrix, with K columns given by the images of the K canonical base vectors, that is, those vectors in $\mathbf{B}$ with only one 1 and all other entries equal to 0. From the structure of $\mathbf{B}$, we see that these are the vectors $\mathbf{c}_m$ with $m = 2^k + 1$, $k = 0, 1, \ldots, K-1$, that is,

$$\mathbf{G} = [\mathbf{c}_2, \mathbf{c}_3, \mathbf{c}_5, \mathbf{c}_9, \ldots, \mathbf{c}_{M/2+1}].$$

The dual code $\mathcal{C}^{\perp}$ is just the orthogonal complement of $\mathcal{C}$ in the N-dimensional vector space over the binary numbers. Its $(N-K)\times N$ generator matrix $\mathbf{H}$ is related to $\mathbf{G}$ by

$$\mathbf{H}^T\mathbf{G}=0.$$

Because $\mathbf{H}^T\mathbf{c}=0$ for each $\mathbf{c}\in\mathcal{C}$, $\mathbf{H}$ is called the *parity check matrix* of the code $\mathcal{C}$.

Repetition (RP) codes

A very naive idea for coding is a simple repetition of the bits. An RP$(N, 1, N)$ code has $d_H=N$ and $R_c=1/N$ and, thus, the coding gain is zero. Obviously, RP coding is just another word for diversity, and, in a fading channel, it has a diversity gain if the fading amplitudes of the received coded symbols are sufficiently independent. The generator matrix of this code is the all-one column vector of length N.

Single parity check (SPC) codes

The matrix of code words $\mathbf{C}$ for the SPC$(K+1, K, 2)$ code is obtained from the binary tuple matrix $\mathbf{B}$ by appending one row in such a way that the (modulo 2) sum over each column equals zero, that is, all code words must have even parity. For the SPC(4, 3, 2) code, for example, we have

$$\mathbf{C}=\begin{bmatrix}0&1&0&1&0&1&0&1\\0&0&1&1&0&0&1&1\\0&0&0&0&1&1&1&1\\0&1&1&0&1&0&0&1\end{bmatrix}$$

and

$$\mathbf{G}=\begin{bmatrix}1&0&0\\0&1&0\\0&0&1\\1&1&1\end{bmatrix}.$$

An SPC$(K+1, K, 2)$ code has Hamming distance $d_H=2$ and rate $R_c=K/(K+1)$. The most popular application for SPC (single parity check) codes is error detection by checking the parity. Obviously, the detection is not very reliable because only one error can be detected, not two. It is generally believed that SPC codes can only detect errors, but cannot correct them. This is only the case for hard decision. When using an MLSE receiver, SPC codes have an asymptotic coding gain of

$$G_a=10\log_{10}\frac{2K}{K+1}\,\text{dB},$$

which approximately approaches a 3 dB gain for high values of N.

Walsh–Hadamard (WH) codes

As already discussed in the example in the last subsection, Walsh–Hadamard codes will be obtained from the Hadamard matrices by replacing each $+1$ by a 0 and -1 by a 1. The code words of the WH$(M, \log_2 M, M/2)$ code of length $M=2^K$ and Hamming distance $M/2$

are the columns of the resulting $M \times M$ matrix. Transmitting these code words with BPSK modulation brings us back to orthogonal signaling with Walsh functions. The asymptotic coding gain

$$G_a = 10 \log_{10} \frac{K}{2} \text{ dB}$$

has already been obtained in Subsection 1.4.3, where the pairwise error probabilities of orthogonal modulation has been derived.

Proposition 3.1.1 *The WH codes are linear codes.*

Proof. The proof is by induction over K, where $M = 2^K$. The statement is trivially true for $K = 0$, that is, $M = 1$. We will show that if it is true for any $M/2$, it is true for M. Let $\mathbf{C} = [\mathbf{c}_1, \ldots, \mathbf{c}_M]$ be the $M \times M$ matrix obtained from the $M \times M$ Hadamard matrix as described above. The column vectors are the code words. Then, by construction of the Hadamard matrices, the code words $\mathbf{c}_m$ are exactly those vectors that have either the structure

$$\mathbf{c}_m = \begin{bmatrix} \mathbf{c}' \\ \mathbf{c}' \end{bmatrix} \text{ for } m \in \{1, \ldots, M/2\}$$

or

$$\mathbf{c}_m = \begin{bmatrix} \mathbf{c}' \\ \mathbf{c}' \oplus 1 \end{bmatrix} \text{ for } m \in \{M/2 + 1, \ldots, M\},$$

where $\mathbf{c}'$ is a code word of the WH$(M/2, \log_2 M - 1, M/4)$ code, which, by assumption, has already been proven to be a linear code. From the above decomposition it can easily be seen that the sum of any such vectors has again this structure and thus is a code word of WH$(M, \log_2 M, M/2)$.

From the recursive construction of the Hadamard matrices, we observe that the column $\mathbf{c}_{M/2+1}$ equals the last row of $\mathbf{B}$ (the MSB (Most Significant Bit) row), the column $\mathbf{c}_{M/4+1}$ equals the second last row of $\mathbf{B}$, and so on. Thus, we find that for the WH code, the interesting property

$$\mathbf{G} = \mathbf{B}^T$$

holds, and the matrix of code words is given by

$$\mathbf{C} = \mathbf{B}^T \mathbf{B}.$$

Since $\mathbf{B}$ has the canonical base as column numbers $m = 2^k + 1$, $k = 0, 1, \ldots, K - 1$, the generator matrix $\mathbf{G}$ provides a systematic encoder with the systematic bit number $k + 1$ at the position $m = 2^k + 1$, $k = 0, 1, \ldots, K - 1$ in the code word. For $M = 8$, for example, the three systematic bit can be found in the positions 2, 3 and 5 of the code word.

Simplex (SPL) codes

An SPL$(M - 1, \log_2 M, M/2)$ is obtained by omitting the first bit of every WH $(M, \log_2 M, M/2)$ code word. This can be done without any loss in performance because this bit is always zero. Because of the higher code rate, the performance is even better,

especially for small values of M. For $M = 8$, the matrix of code words is given by

$$\mathbf{C} = \begin{bmatrix} 0 & 1 & 0 & 1 & 0 & 1 & 0 & 1 \\ 0 & 0 & 1 & 1 & 0 & 0 & 1 & 1 \\ 0 & 1 & 1 & 0 & 0 & 1 & 1 & 0 \\ 0 & 0 & 0 & 0 & 1 & 1 & 1 & 1 \\ 0 & 1 & 0 & 1 & 1 & 0 & 1 & 0 \\ 0 & 0 & 1 & 1 & 1 & 1 & 0 & 0 \\ 0 & 1 & 1 & 0 & 1 & 0 & 0 & 1 \end{bmatrix},$$

and the generator matrix is

$$\mathbf{G} = \begin{bmatrix} 1 & 0 & 0 \\ 0 & 1 & 0 \\ 1 & 1 & 0 \\ 0 & 0 & 1 \\ 1 & 0 & 1 \\ 0 & 1 & 1 \\ 1 & 1 & 1 \end{bmatrix}.$$

Hamming codes

Hamming codes are the dual codes of simplex codes. A $(2^K - 1, 2^K - 1 - K, 3)$ Hamming code can correct one error. Hamming codes are simple and weak codes, but they are popular to explain the concepts of algebraic coding. We do not discuss them further because they are exhaustively treated in most text books.

3.1.4 Concatenated coding

If an application requires very low bit error rates, concatenated coding is often the most efficient method to reach this goal. In such a setup, two codes are combined to a stronger overall concatenated code (see Figure 3.2). At the transmitter, the source data will first be encoded by the *outer code*. The code words of this code will then serve as the input data for the *inner code*[2]. Between the two encoders, the order of the symbols inside the stream of code words may be changed by a device that is called *interleaver*. Interleaver structures will be discussed later in Subsection 4.4.2. The code words of the inner code are transmitted over the channel and then decoded by the inner decoder. The inner decoder has to be matched to the channel. At its output, the error rate will be low, but the errors are not uniformly distributed. The inner decoder will typically produce error bursts, that is, connected sequences of unreliable symbols between long sequences of reliable symbols. For block codes, a burst error corresponds to an erroneously decided code word. For convolutional codes, an error burst corresponds to the sequence of states in the trellis, where the correct path and the maximum likelihood path are different (see Subsection 3.2.2). The deinterleaver inverts the interleaver. The interleaving scheme breaks up the error bursts and has to be matched to the error correction capabilities of the outer code, that is, to its Hamming distance and code word length. For a properly designed concatenated coding scheme, the output of the outer decoder will be nearly error free. Thus, one can

[2]The naming *inner* and *outer* code stems from the fact that the inner code is closer to the channel than the outer code.

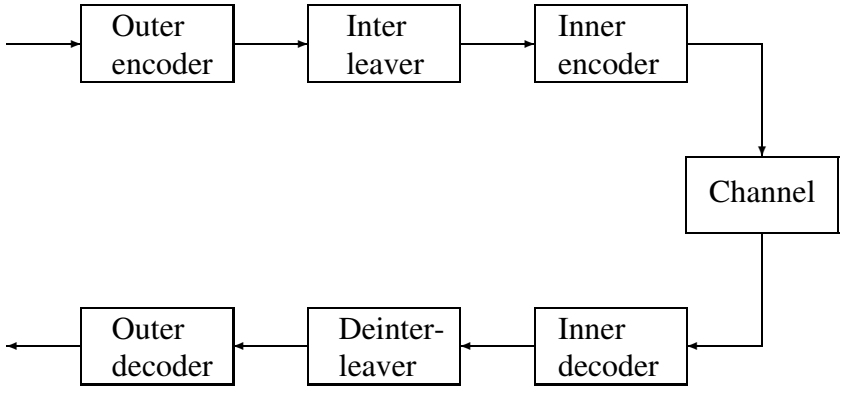

Figure 3.2 Block diagram for a concatenated coding setup.

visualize the inner decoder as a device that is suited for coarsely cleaning up the errors that are produced by a severely corrupted transmission channel. The outer decoder will then clean up the residual errors left by the outer decoder.

We note that in some cases the inner decoder may pass soft decision values rather than hard decision bits to the outer decoder. This is, for example, an important item for a concatenated coding scheme with two convolutional codes. Turbo codes are a setup of two parallel concatenated codes (see Subsection 3.2.5). The classical concatenation described above is sometimes called *serial* concatenation to distinguish from such setups. For serially concatenated convolutional codes, we refer to (Benedetto and Biglieri 1999).

If we regard QAM or PSK modulation as (nonbinary) coding schemes (see the discussion at the end of Subsection 3.1.1), QAM or PSK with additional (convolutional) coding is a concatenated coding scheme. The outer QAM or PSK decoder will typically pass *soft bits* to the outer (convolutional) decoder. The optimal soft bits are the LLRs (log-likelihood ratios) calculated by the MAP receiver (see Subsection 3.1.5).

Probably the most popular concatenated coding scheme is an inner convolutional code with an outer Reed–Solomon (RS) code. Both types of codes are discussed in the following sections. Convolutional codes with soft decision decoding are well suited for channels that are severely corrupted by a high noise level and/or by multipath fading. MLSE can be easily implemented by the Viterbi decoder. However, because of their typically quite low Hamming distance, the BER curves show a poor decay. Thus, a high SNR is needed if very low BERs are required. The convolutional decoder produces bursts of erroneously decided bits. RS codes can be designed as strong codes with high Hamming distances. They are based on byte arithmetics rather than bit arithmetics, that is, they correct byte errors rather than bit errors. The decoder works with hard decision input bytes. The favorable input for the decoder is a data stream with bit errors that are grouped together into bytes, but the byte error structure should not be bursty. Thus, a convolutional decoder together with a byte interleaving produces the favorite input for the RS decoder.

Deep space communication was one of the first applications of such a scheme with a convolutional code and an RS code (see (McEliece and Swanson 2001)). Because of the power limitation, the physical channel is a very noisy AWGN channel that makes

convolutional codes the best choice. If, for example, data compressed pictures have to be transmitted, the bit error rate has to be very low. Therefore an outer RS will give a considerable gain (see (McEliece and Swanson 2001)). For this application, the outer codes give an additional coding gain of 2.5 dB at BER $= 10^{-6}$ or a gain in data rate of 78%.

Another concatenated coding scheme with a convolutional code and an RS code is applied in the DVB-T system, which will be described in Subsection 4.6.2. DVB-T is an OFDM system with QAM modulation. Because QAM with convolutional coding can already be interpreted as code concatenation, we have a twofold concatenation in this system. The outer RS code has been chosen because the goal has been to reach the extremely low residual bit error rate 10^{-11} in the video data stream. This cannot be reached with convolutional codes at a reasonable effort, especially in a fading channel.

We note that in a concatenated decoding setup as depicted in Figure 3.2, the decoding will be done stepwise and the two decoders are separate devices. This is in general suboptimal compared to a MLSE or MAP receiver for the complete concatenated code. Improvements can be obtained if the decoders can help each other by means of iterative decoding. Turbo codes may be the most famous application (see Subsection 3.2.5). The idea of iterative decoding had been applied earlier in deep space communications (Hagenauer *et al.* 2001). Another application is multistage coding, which is implemented in the OFDM system DRM (Digital Radio Mondiale). The iterative decoding of a convolutionally coded QAM system with OFDM will be discussed in Subsection 4.5.2.

3.1.5 Log-likelihood ratios and the MAP receiver

Until now, we have discussed only the maximum likelihood sequence estimator at the receiver. For a channel with additive white Gaussian noise, and a given receive signal vector $\mathbf{r}$, this receiver estimates the most probable transmit signal vector $\hat{\mathbf{s}}$ out of a finite set of possible transmit vectors. This most probable transmit vector is the one for which the squared Euclidean distance $\|\mathbf{r} - \hat{\mathbf{s}}\|^2$ is minimized, or, for transmit vectors of equal energy, the correlation given by $\Re\{\mathbf{r} \cdot \hat{\mathbf{s}}\}$ is maximized. The MLSE estimates transmit vectors (*sequences*), not bits. Since there is a one-to-one correspondence to the bit sequences $\mathbf{b}$, we get an estimate for each bit. Thus, MLSE does not provide us directly with an estimate for the most probable value of a bit. Both may sometimes be different [3] (see Problem 2).

In this subsection, we introduce a receiver that gives an estimate for the bit together with a reliability information of the decision. It does not need the assumption of Gaussian statistics, and is able to provide a reliability measure for each decision, even for single bit decisions. Furthermore, we can incorporate *a priori* probabilities of the bits. This is of high value for any kind of iterative decoding algorithms, as applied in the turbo decoding and multistage decoding. The basic tool is the log-likelihood ratio, which is defined by

Definition 3.1.2 (Log-likelihood ratio) *Let $P(A)$ be the probability of an event A. Then the LLR of this event is defined as*

$$L(A) = \log \frac{P(A)}{1 - P(A)}. \tag{3.7}$$

We add the following remarks.

[3] Even though in practice, for reasonably high SNRs, both will be the same with extremely high probability.

- The LLR is the ratio between the probability that something is true and that it is not true, viewed on a logarithmic scale. This is extremely useful if the probabilities are very high or very small. This is quite similar to the familiar decibel calculus for signal power levels. Even though the logarithm in Equation (3.7) is usually understood as a natural logarithm, one can in principle also use $10\log_{10}$ there and then, for example, regard the probability $P(A) = 0.999$ as an LLR of approximately 30 dB or the probability $P(A) = 0.001$ as an LLR of approximately -30 dB.

- One easily finds that the probability can be expressed by the LLR as

$$P(A) = \frac{\mathrm{e}^{\frac{1}{2}L(A)}}{\mathrm{e}^{\frac{1}{2}L(A)} + \mathrm{e}^{-\frac{1}{2}L(A)}}. \tag{3.8}$$

- The LLR of the complementary event $\bar{A}$ is given by

$$L(\bar{A}) = -L(A).$$

Soft bits

We often deal with the probability that a random bit takes the value 0 or 1. We will therefore derive some simple properties of the corresponding random LLRs. To do this, it is very convenient to replace bits by signs, that is, write $+1$ for the bit value 0 and -1 for the bit value 1. This can be interpreted as antipodal (BPSK) signaling with energy 1 given by the mapping

$$s = (-1)^b = 1 - 2b$$

between the bit b and the sign (BPSK symbol) s. In the following text, we will speak of bits and their corresponding signs synonymously. To avoid confusion, we will (at this place) carefully distinguish, in our notation, between random variables (written as capital letters) and their values. That is, we deal with a random variable S, which is a random sign that takes values $s \in \{+1, -1\}$. The LLR for the event $S = s$ is then given by

$$L(S = s) = \log \frac{P(S = s)}{P(S = -s)}.$$

From $L(S = s) = -L(S = -s)$, we easily see that $L(S = s) = sL(S = +1)$. If no confusion may arise, we simply write

$$L = L(S = +1) \tag{3.9}$$

We call this the L-value of the random bit S. We note that

$$L(S = s) = sL. \tag{3.10}$$

The L-value of a random bit S (written as a sign) has a very natural interpretation as a *soft* bit. The sign of L says which of the two possible events $S = +1$ or $S = -1$ is more probable, that is, the sign gives a *hard* bit decision. The absolute value of L is a logarithmic measure for the reliability of this decision. For those who like to express everything in decibels, we can write $10\log_{10}$ for the logarithm in the definition of the LLR. Then, for example, an LLR value of $+30$ dB means that the random bit equals zero with

a probability 0.999 (approximately), and an LLR value of −30 dB means that the random bit equals one with a probability 0.999 (approximately).

Using Equation (3.8), the probability for the random bit can be expressed by the LLR as

$$P(S=s)=\frac{\mathrm{e}^{\frac{1}{2}sL}}{\mathrm{e}^{\frac{1}{2}L}+\mathrm{e}^{-\frac{1}{2}L}}. \tag{3.11}$$

We note that

$$P(S=s)=C\,\mathrm{e}^{\frac{1}{2}sL},$$

where the constant $C=\left(\mathrm{e}^{\frac{1}{2}L}+\mathrm{e}^{-\frac{1}{2}L}\right)^{-1}$ does not depend on the value of s. Using the definition of the LLR, we find

$$L(S=s)=\log\left(\frac{P(S=s)}{\sqrt{P(S=-s)P(S=s)}}\right)^2$$

and

$$P(S=s)=\sqrt{P(S=+1)P(S=-1)}\,\mathrm{e}^{\frac{1}{2}sL}, \tag{3.12}$$

which is an alternative representation with the constant C expressed by the probabilities.

Sequences of random signs

Now consider a vector $\mathbf{S}=(S_1,\ldots,S_K)^T$ of statistically independent random signs. Then, the probability for the event that $\mathbf{S}$ takes a certain value $\mathbf{s}=(s_1,\ldots,s_K)^T$ factorizes into the probabilities of the single signs, that is,

$$P(\mathbf{S}=\mathbf{s})=\prod_{i=1}^{K}P(S_i=s_i).$$

Using Equation (3.12), we may write this as

$$P(\mathbf{S}=\mathbf{s})=\prod_{i=1}^{K}\sqrt{P(S_i=+1)P(S_i=-1)}\,\mathrm{e}^{\frac{1}{2}s_iL_i},$$

where $L_i=\log(P(S_i=+1)/P(S_i=-1))$. This takes the more compact form

$$P(\mathbf{S}=\mathbf{s})=C\,\exp\left(\frac{1}{2}\sum_{i=1}^{K}s_iL_i\right)=C\,\exp\left(\frac{1}{2}\mathbf{s}\cdot\mathbf{L}\right),$$

where we have defined a log-likelihood vector $\mathbf{L}=(L_1,\ldots,L_K)$. The constant C is now given by

$$C=\prod_{i=1}^{K}\sqrt{P(S_i=+1)P(S_i=-1)}.$$

We see that as in the case of the MLSE estimator for the AWGN channel, we find the most probable sequence (which is here directly a bit sequence) by maximizing a correlation that is given by the scalar product $\mathbf{s}\cdot\mathbf{L}$. Here we have derived the general case, and the LLR expressions must be evaluated for any special statistics.

Products of random signs

Consider a random sign S. The expectation value of S is given by

$$\mathrm{E}\{S\} = (+1) \cdot \Pr(S = +1) + (-1) \cdot \Pr(S = -1).$$

Using Equation (3.11), we easily obtain

$$\mathrm{E}\{S\} = \tanh\left(\frac{1}{2}L\right),$$

where again we have used the shorthand notation $L = L(S = +1)$. Now let S_1 and S_2 be two independent random signs and define $S = S_1 \cdot S_2$ and write $L_1,\ L_2,\ L$ for the corresponding LLRs for the positive sign. From

$$\mathrm{E}\{S\} = \mathrm{E}\{S_1\}\,\mathrm{E}\{S_2\},$$

we conclude

$$\tanh\left(\frac{1}{2}L\right) = \tanh\left(\frac{1}{2}L_1\right)\tanh\left(\frac{1}{2}L_2\right)$$

or

$$L = 2\,\mathrm{artanh}\left(\tanh\left(\frac{1}{2}L_1\right)\tanh\left(\frac{1}{2}L_2\right)\right). \tag{3.13}$$

Using the relations

$$2\,\mathrm{artanh}\,(x) = \log\frac{1+x}{1-x}$$

and

$$\tanh(x) = \frac{\mathrm{e}^x - 1}{\mathrm{e}^x + 1},$$

one can show that this equals

$$L = \log\frac{1 + \mathrm{e}^{L_1}\mathrm{e}^{L_2}}{\mathrm{e}^{L_1} + \mathrm{e}^{L_2}}.$$

This can be approximated as

$$L \approx \mathrm{sign}\,(L_1)\,\mathrm{sign}\,(L_2)\,\min\left(|L_1|, |L_2|\right)$$

(see Problem 3). We can interpret this expression as follows: multiplication of random signs corresponds to the modulo 2 addition of the corresponding random bits. Thus, the modulo 2 addition of two random bits can (approximately) be realized as follows: the hard decision value of the result is obtained as modulo 2 addition of the hard decision values of the two bits. Its reliability given by $|L|$ equals the reliability of the least reliable of the two bits, similar to the saying that a chain is as strong as its weakest link. This becomes especially obvious if we generalize the approximation to the modulo 2 addition of more than two random bits and write

$$L \approx \prod_{i=1}^{K} \mathrm{sign}\,(L_i) \cdot \min\left(|L_1|, \ldots, |L_K|\right). \tag{3.14}$$

LLRs for BPSK and additive white Gaussian noise

Until now, no assumption has been made about the special statistics. It is instructive to exploit the concept of LLRs for the special case of antipodal transmission in an additive white Gaussian noise channel. In the context of channel coding, it is often convenient to deal with quantities that have no physical dimension. We rewrite BPSK transmission in an AWGN channel as

$$y_i = x_i + n_i,$$

where $x_i \in \{\pm 1\}$ and n_i is real and normalized discrete AWGN with variance

$$\sigma^2 = \frac{N_0}{2E_b}.$$

The transmit symbols x_i and the receive symbols y_i are regarded as random variables[4]. According to Bayes' law, the probability $P(x_i|y_i)$ that x_i has been transmitted under the condition that y_i has been received is given by

$$P(x_i|y_i) = \frac{p(y_i|x_i)P(x_i)}{p(y_i)}.$$

Here $P(x_i)$ is the *a priori* probability that x_i was transmitted, $p(y_i)$ is the probability density for the receive symbol y_i and $p(y_i|x_i)$ is the probability density for the receive symbol y_i under the condition that x_i was transmitted. This is just the Gaussian probability density with mean x_i and variance σ^2, that is,

$$p(y_i|x_i = \pm 1) = \frac{1}{\sqrt{2\pi\sigma^2}} \exp\left(-\frac{1}{2\sigma^2}|y_i \mp 1|^2\right).$$

We write

$$L_i = \log \frac{P(x_i = +1|y_i)}{P(x_i = -1|y_i)}$$

and get

$$L_i = \log \frac{\exp\left(-\frac{1}{2\sigma^2}|y_i - 1|^2\right) P(x_i = +1)}{\exp\left(-\frac{1}{2\sigma^2}|y_i + 1|^2\right) P(x_i = -1)},$$

which can eventually be written as

$$L_i = L_i^c + L_i^a, \tag{3.15}$$

where

$$L_i^c = \log \frac{p(y_i|x_i = +1)}{P(y_i|x_i = -1)} = \frac{2}{\sigma^2} y_i$$

is the *channel* LLR obtained from the symbol transmitted over the channel, and

$$L_i^a = \log \frac{P(x_i = +1)}{P(x_i = -1)} \tag{3.16}$$

is the *a priori* LLR corresponding to the *a priori* probability of the bit.

[4]Here we fall back into the lax usage of notation that is common in engineering not to distinguish between random variables and their values.

For a multiplicative fading channel given by

$$y_i = a_i x_i + n_i,$$

where a_i is a real fading amplitude, one easily sees that the channel LLR turns out to be

$$L_i^c = \frac{2}{\sigma^2} a_i y_i, \tag{3.17}$$

that is, the receive symbol must be weighted by the fading amplitude. We note that a one bit hard BPSK decision will be based on the sign of

$$L_i = \frac{2}{\sigma^2}\left(a_i y_i + \frac{\sigma^2}{2} L_i^a\right).$$

A positive sign corresponds to a 0, a negative to 1. The second term corresponds to a shift of the decision threshold that is proportional to the *a priori* LLR and to the noise.

The conditional probability for the BPSK symbol x_i under the condition that y_i was received is given by

$$P(x_i|y_i) = \sqrt{P(x_i = +1|y_i)P(x_i = -1|y_i)}\, \mathrm{e}^{\frac{1}{2}x_i L_i}.$$

For uncoded transmission, the transmit symbols are statistically independent, and thus the conditional probability $P(\mathbf{x}|\mathbf{y})$ for the whole BPSK vector $\mathbf{x} = (x_1, \ldots, x_K)^T$ given that $\mathbf{y}$ was received factorizes to

$$P(\mathbf{x}|\mathbf{y}) = \prod_{i=1}^{K} P(x_i|y_i) = \prod_{i=1}^{K} \sqrt{P(x_i = +1|y_i)P(x_i = -1|y_i)}\, \mathrm{e}^{\frac{1}{2}x_i L_i}.$$

General signal constellation and coded transmission

We consider a set $\mathcal{C}$ of $M = 2^K$ real transmit signal vectors $\mathbf{x} = (x_1, \ldots, x_N)^T$ labeled by bit tuples of length K written as binary vectors $\mathbf{b} = (b_1, \ldots, b_K)^T$. We write $\mathcal{B}$ for the set of these tuples. As discussed at the end of Subsection 3.1.1, the mapping

$$X : \mathcal{B} \to \mathcal{C}, \quad \mathbf{b} \mapsto \mathbf{x}$$

can be interpreted as a joint channel encoder and symbol mapper. When using LLR values, it is convenient to replace a binary vector $\mathbf{b}$ by its equivalent sign vector $\mathbf{u} = (u_1, \ldots, u_K)^T$ defined by $u_k = (-1)^{b_k}$. The set of these vectors will be denoted by $\mathcal{U}$.

First, we ask for the conditional probability $P(\mathbf{x}|\mathbf{y})$ for a transmitted signal vector $\mathbf{x}$ given that the vector $\mathbf{y}$ has been received. According to Bayes' law, we have

$$P(\mathbf{x}|\mathbf{y}) = \frac{p(\mathbf{y}|\mathbf{x})P(\mathbf{x})}{p(\mathbf{y})}.$$

Here, $P(\mathbf{x})$ is the *a priori* probability that $\mathbf{x}$ was transmitted, $p(\mathbf{y})$ is the probability density function for the receive symbol vector $\mathbf{y}$ and $p(\mathbf{y}|\mathbf{x})$ is the probability density function for the receive symbol $\mathbf{y}$ under the condition that $\mathbf{x}$ has been transmitted. We have fallen back into the loose notation for random variables, that is, we use $\mathbf{x}$ for the random variable and

for the value of the random variable as well. We may replace $P(\mathbf{x})$ by $P(\mathbf{b})$, which is the *a priori* probability for the bit tuple $\mathbf{b}$ that corresponds to $\mathbf{x}$ or by the *a priori* probability $P(\mathbf{u})$ of the sign vector $\mathbf{u}$. Assuming that the *a priori* probabilities of the bits are statistically independent and that $p(\mathbf{y}|\mathbf{x})$ factorizes as well because of statistical independence, we may write

$$P(\mathbf{x}|\mathbf{y}) = \frac{1}{p(\mathbf{y})} \prod_{i=1}^{N} p(y_i|x_i) \prod_{k=1}^{K} p(u_k).$$

To find the most probable transmit vector for a general signal constellation, this expression must be maximized.

For the special case of a binary code with antipodal signaling with $x_i \in \{\pm 1\}$, we define

$$L_i^c = \log \frac{p(y_i|x_i = +1)}{P(y_i|x_i = -1)}, \quad L_k^a = \log \frac{P(u_k = +1)}{P(u_k = -1)}.$$

It is convenient to define channel and *a priori* LLR vectors as $\mathbf{L}^c = (L_1^c, \ldots, L_K^c)$ and $\mathbf{L}^a = (L_1^a, \ldots, L_N^a)$. The channel LLR vector can be written as

$$\mathbf{L}^c = \frac{2}{\sigma^2}\mathbf{A}\mathbf{y}$$

with the diagonal matrix of fading amplitudes $\mathbf{A} = \mathrm{diag}(a_1, \ldots, a_K)$. The conditional probability that a certain sequence has been transmitted is then given by

$$P(\mathbf{x}|\mathbf{y}) = C \exp\left(\frac{1}{\sigma^2}\mu(\mathbf{x})\right) \tag{3.18}$$

with a constant C that does not depend on the transmitted sequence and a *metric* defined by

$$\mu(\mathbf{x}) = \frac{\sigma^2}{2}\left(\mathbf{x} \cdot \mathbf{L}^c + \mathbf{u} \cdot \mathbf{L}^a\right). \tag{3.19}$$

To find the most probable sequence $\mathbf{x}$, this correlation metric $\mu(\mathbf{x})$ has to be maximized. We have chosen this normalization, because in the case of BPSK without *a priori* information, Equation (3.17) yields $\mu(\mathbf{x}) = \mathbf{A}\mathbf{y} \cdot \mathbf{x}$, which does not depend on σ.

For the special case of a systematic code, the vector $\mathbf{x}$ consists of a systematic part $\mathbf{x}_s = \mathbf{u}$ and a parity check part $\mathbf{x}_p$. In that case, the correlation metric becomes

$$\mu(\mathbf{x}) = \mathbf{x}_s \cdot \left(\mathbf{L}^a + \mathbf{L}_s^c\right) + \mathbf{x}_p \cdot \mathbf{L}_p^c. \tag{3.20}$$

Thus, the channel LLR can be split up to a part $\mathbf{L}_s^c$ corresponding to the systematic symbol vector and a part $\mathbf{L}_p^c$ corresponding to the parity check symbol vector. The *a priori* LLR will be added to the channel LLR for the systematic part.

For an arbitrary signal constellation and a (real-valued) discrete fading channel with AWGN of variance σ^2, we have

$$P(\mathbf{x}|\mathbf{y}) = C_1 \exp\left(\frac{1}{2\sigma^2}\|\mathbf{y} - \mathbf{A}\mathbf{x}\|^2\right) \cdot \exp\left(\frac{1}{2}\mathbf{u} \cdot \mathbf{L}^a\right),$$

which can be written as

$$P(\mathbf{x}|\mathbf{y}) = C_2 \exp\left(\frac{1}{\sigma^2}\left(\mathbf{x} \cdot \mathbf{A}\mathbf{y} - \frac{1}{2}\|\mathbf{A}\mathbf{x}\|^2\right)\right) \cdot \exp\left(\frac{1}{2}\mathbf{u} \cdot \mathbf{L}^a\right),$$

with properly defined constant C_1 and C_2. This can be written as Equation (3.18) with the metric expression of Equation (3.19) replaced by

$$\mu(\mathbf{x}) = \frac{\sigma^2}{2}\left(\mathbf{x}\cdot\mathbf{L}^c + \mathbf{u}\cdot\mathbf{L}^a\right) - \frac{1}{2}\left\|\mathbf{A}\mathbf{x}\right\|^2, \tag{3.21}$$

that is, an energy term must be taken into account.

The bitwise MAP receiver

We now want to analyze decisions about single bits instead of whole sequences. We ask for the probability $P(b_k = 0|\mathbf{y})$ that the kth bit b_k in the tuple $\mathbf{b}$ has the value zero under the condition that the vector $\mathbf{y}$ was received. The corresponding LLR is given by

$$L(b_k = 0|\mathbf{y}) = \log\frac{P(b_k = 0|\mathbf{y})}{P(b_k = 1|\mathbf{y})}.$$

We write $\mathcal{B}_k^{(0)}$ for the set of those vectors $\mathbf{b} \in \mathcal{B}$ for which $b_k = 0$ and $\mathcal{B}_k^{(1)}$ for the set of those for which $b_k = 1$. Then,

$$P(b_k = 0|\mathbf{y}) = \sum_{\mathbf{b}\in\mathcal{B}_k^{(0)}} P(\mathbf{b}|\mathbf{y})$$

and

$$P(b_k = 1|\mathbf{y}) = \sum_{\mathbf{b}\in\mathcal{B}_k^{(1)}} P(\mathbf{b}|\mathbf{y})$$

hold and the LLR can be written as

$$L(b_k = 0|\mathbf{y}) = \log\left(\frac{\sum_{\mathbf{b}\in\mathcal{B}_k^{(0)}} P(\mathbf{b}|\mathbf{y})}{\sum_{\mathbf{b}\in\mathcal{B}_k^{(1)}} P(\mathbf{b}|\mathbf{y})}\right). \tag{3.22}$$

Applying Bayes' law for $P(\mathbf{b}|\mathbf{y})$, we get

$$L(b_k = 0|\mathbf{y}) = \log\left(\frac{\sum_{\mathbf{b}\in\mathcal{B}_k^{(0)}} p(\mathbf{y}|\mathbf{b})P(\mathbf{b})}{\sum_{\mathbf{b}\in\mathcal{B}_k^{(1)}} p(\mathbf{y}|\mathbf{b})P(\mathbf{b})}\right), \tag{3.23}$$

where $P(\mathbf{b})$ is the *a priori* probability of vector $\mathbf{b}$, and $p(\mathbf{y}|\mathbf{b})$ is the conditional probability density for the receive vector $\mathbf{y}$ given that the signal vector $\mathbf{x}$ corresponding to $\mathbf{b}$ was transmitted. If $L(b_k = 0|\mathbf{y}) > 0$, the receiver decides for $b_k = 0$ and otherwise for $b_k = 1$. Furthermore, this receiver provides information about the reliability of the decision, which is given by the absolute value of $L(b_k = 0|\mathbf{y})$. We call such a receiver a *(bitwise) maximum a posteriori probability* (MAP) receiver. As we have already seen above, we may write

$$p(\mathbf{y}|\mathbf{b})P(\mathbf{b}) = C\ \exp\left(\frac{1}{\sigma^2}\mu\left(\mathbf{x}\right)\right) \tag{3.24}$$

with a metric $\mu(\mathbf{x})$ that depends on the code and the signal constellation. The constant C is the same in numerator and denominator.

The SISO decoder for systematic codes

For the special case of a binary systematic code, the metric $\mu(\mathbf{x})$ is given by Equation (3.20). We insert that expression into Equation (3.23) and get the LLR expression

$$L(b_k = 0|\mathbf{y}) = \log\left(\frac{\sum_{\mathbf{b}\in\mathcal{B}_k^{(0)}} \exp\left(\frac{1}{2}\left(\mathbf{x}_s \cdot \left(\mathbf{L}^a + \mathbf{L}_s^c\right) + \mathbf{x}_p \cdot \mathbf{L}_p^c\right)\right)}{\sum_{\mathbf{b}\in\mathcal{B}_k^{(1)}} \exp\left(\frac{1}{2}\left(\mathbf{x}_s \cdot \left(\mathbf{L}^a + \mathbf{L}_s^c\right) + \mathbf{x}_p \cdot \mathbf{L}_p^c\right)\right)}\right) \tag{3.25}$$

for the MAP receiver. Here, the sum has to be understood in such a way that, for each binary vector $\mathbf{b}$, there are uniquely determined corresponding vectors $\mathbf{x}_s$ and $\mathbf{x}_p$. We may now split up this equation into three terms that have an intuitively obvious interpretation. To do this, we keep the index k fixed and split up the exponents in the numerator and the denominator as

$$\mathbf{x}_s \cdot \left(\mathbf{L}^a + \mathbf{L}_s^c\right) + \mathbf{x}_p \cdot \mathbf{L}_p^c = x_{sk}(L_k^a + L_{sk}^c) + \sum_{i\neq k} x_{si}(L_i^a + L_{si}^c) + \mathbf{x}_p \cdot \mathbf{L}_p^c.$$

In the numerator, the first term is constantly $+(L_k^a + L_{sk}^c)$, and in the denominator, it is constantly $-(L_k^a + L_{sk}^c)$. We can thus extract this term from the sum. $L_k = L(b_k = 0|\mathbf{y})$ in Equation (3.25) can then be written as

$$L_k = L_k^a + L_{sk}^c + L_k^e \tag{3.26}$$

with the *extrinsic* LLR defined by

$$L_k^e = \log\left(\frac{\sum_{\mathbf{b}\in\mathcal{B}_k^{(0)}} \exp\left(\frac{1}{2}\left(\sum_{i\neq k} x_{si}(L_i^a + L_{si}^c) + \mathbf{x}_p \cdot \mathbf{L}_p^c\right)\right)}{\sum_{\mathbf{b}\in\mathcal{B}_k^{(1)}} \exp\left(\frac{1}{2}\left(\sum_{i\neq k} x_{si}(L_i^a + L_{si}^c) + \mathbf{x}_p \cdot \mathbf{L}_p^c\right)\right)}\right).$$

Comparing this with Equation (3.15) for uncoded transmission, we see that this extrinsic LLR corresponds to the additional information gain due to channel coding. It depends on all other received symbols – systematic symbols and parity check symbols – except the one corresponding to b_k. This LLR adds to the LLRs L_k^a and L_{sk}^c that already occur in case of uncoded transmission.

We now write Equation (3.26) in vector notation as

$$\mathbf{L} = \mathbf{L}^a + \mathbf{L}^c + \mathbf{L}^e$$

and interpret the MAP as a SISO receiver that has soft LLR vectors as input and output as depicted in Figure 3.3. The input vectors of the SISO are $\mathbf{L}^a$ and $\mathbf{L}^c$, where $\mathbf{L}^c$ consists of the two parts $\mathbf{L}_s^c$ and $\mathbf{L}_p^c$. The systematic MAP of Equation (3.25) has the two inputs $\mathbf{L}^a + \mathbf{L}_s^c$ and $\mathbf{L}_p^c$. The output vector is $\mathbf{L}$. The extrinsic LLR vector $\mathbf{L}^e$ of that vector is obtained from the output $\mathbf{L}$ by

$$\mathbf{L}^e = \mathbf{L} - \mathbf{L}^a - \mathbf{L}_s^c.$$

The SISO may be regarded as a device that calculates extrinsic LLR information due to the code. The total LLR is the sum of this extrinsic LLR and the (*a priori* and channel) LLR information already available before decoding.

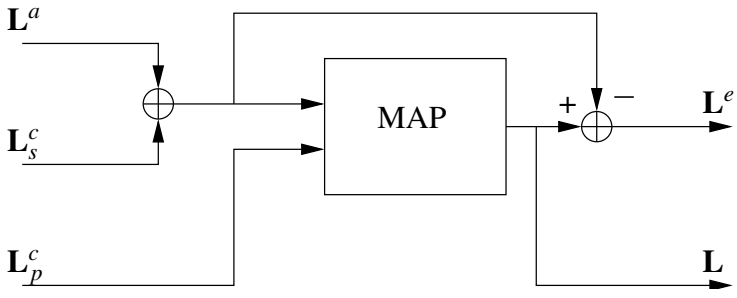

Figure 3.3 The soft-input/soft-output (SISO) decoder.

The maxlog MAP approximation

The expression (3.23) for the MAP receiver contains transcendental functions and thus it may sometimes be too costly to implement. The *maxlog* MAP approximation is often used in practice because it is quite accurate if the SNR is not extremely low. In that case, the sums in the numerator and denominator are dominated by their respective largest term and Equation (3.23) can be approximated by

$$L(b_k = 0|\mathbf{y}) \approx \max_{\mathbf{b}\in\mathcal{B}_k^{(0)}} \log\left(p(\mathbf{y}|\mathbf{b})P(\mathbf{b})\right) - \max_{\mathbf{b}\in\mathcal{B}_k^{(1)}} \log\left(p(\mathbf{y}|\mathbf{b})P(\mathbf{b})\right). \tag{3.27}$$

We note that the hard bit decisions obtained by this maxlog MAP receiver are always identical to those obtained from the MLSE receiver because the latter searches for $\max_{\mathbf{b}\in\mathcal{B}} \log\left(p(\mathbf{y}|\mathbf{b})P(\mathbf{b})\right)$ and decides for the corresponding sequence $\mathbf{b} = \hat{\mathbf{b}}$ and thus $L(b_k = 0|\mathbf{y})$ has always the same sign as the sign obtained from the MLSE.

If we insert Equation (3.24) for the argument of the logarithm, we can write this as

$$L(b_k = 0|\mathbf{y}) \approx \frac{1}{\sigma^2}\left(\max_{\mathbf{b}\in\mathcal{B}_k^{(0)}} \mu(\mathbf{x}) - \max_{\mathbf{b}\in\mathcal{B}_k^{(1)}} \mu(\mathbf{x})\right).$$

For a binary code with antipodal signaling, the metric is given by

$$\mu(\mathbf{x}) = \mathbf{A}\mathbf{y}\cdot\mathbf{x} + \frac{\sigma^2}{2}\mathbf{L}^a\mathbf{u}.$$

If no *a priori* information is available, both the input LLR $\mathbf{L}^c = \frac{1}{\sigma^2}\mathbf{A}\mathbf{y}\cdot\mathbf{x}$ and the output LLR $\mathbf{L}$ are linear in the SNR value σ^{-2}. This linear scale factor can be omitted without any loss and is only needed for the calculation of absolute probabilities. This is in contrast to the exact MAP, where the output is a nonlinear function in the SNR and even the hard decision value may depend on its value.

3.2 Convolutional Codes

3.2.1 General structure and encoder

In contrast to block codes, convolutional codes do not have a defined block structure. A continuously flowing data stream will be encoded into a continuously flowing code word.

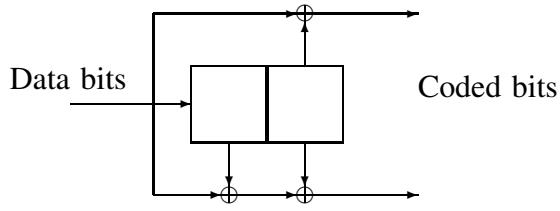

Figure 3.4 Block diagram for a simple convolutional encoder.

Even though it is reasonable for practical and theoretical reasons to work with finite sets of data and coded bits, the length of a code word is given by other requirements than the structure of the code. Convolutional encoders are linear and time-invariant systems given by the convolution of a binary data stream with generator sequences. They can be implemented by shift registers. Figure 3.4 shows a simple example of such an encoder with rate $R_c = 1/2$ and memory $m = 2$.

Given an input bit stream $\{b_i\}_{i=0}^{\infty}$, a convolutional encoder of code rate $R_c = 1/n$ produces n parallel data streams $\{c_{\nu,i}\}_{i=0}^{\infty}$, $\nu = 1, \ldots, n$ that may be multiplexed to one serial code word before transmission. It can be written as

$$c_{\nu,i} = \sum_{k=0}^{m} g_{\nu,k} b_{i-k},$$

where we have set $b_i = 0$ für $i < 0$. The sum has to be understood as *modulo* 2 sum. Here, $g_{\nu,k}$, $(\nu = 1, \ldots, n;\ k = 0, \ldots, m)$ are the generators that can also be written as generator polynomials

$$g_\nu(D) = \sum_{k=0}^{m} g_{\nu,k} D^k,$$

where D is a formal variable that can be interpreted as *delay*. In the example of Figure 3.4, we have

$$g_1(D) = 1 + D^2 \equiv (101) \equiv 5_{\text{oct}},$$
$$g_2(D) = 1 + D + D^2 \equiv (111) \equiv 7_{\text{oct}},$$

where we have introduced the binary vector notation and the octal notation for the generators.

It is often convenient to work with formal power series instead of sequences. This is similar to the formalism in signal processing, where we may switch to the frequency domain to replace convolutions by multiplications. We define the power series

$$b(D) = \sum_{k=0}^{\infty} b_k D^k$$

for the data word and

$$c_\nu(D) = \sum_{k=0}^{\infty} c_{\nu k} D^k,\ \nu = 1, \ldots, n$$

for the code word. Then the encoder can be described by

$$c_\nu(D) = b(D)g_\nu(D) \tag{3.28}$$

or, in vector notation, as

$$\mathbf{c}(D) = b(D)\mathbf{g}(D), \tag{3.29}$$

that is,

$$\begin{bmatrix} c_1(D) \\ \vdots \\ c_n(D) \end{bmatrix} = b(D) \begin{bmatrix} g_1(D) \\ \vdots \\ g_n(D) \end{bmatrix}.$$

Convolutional codes are linear codes. Thus, the Hamming distance of the code is the minimum weight. This is called the *free distance* and will be denoted by d_{free}.

Trellis diagrams

For any time instant i, one can characterize the encoding step by the actual state $\mathbf{s} = (s_1, \ldots, s_m)$, that is, the content of the shift register (s_1 is the most recent bit that has been shifted into the register) and the actual input bit b_i. This uniquely defines the next state $\mathbf{s}' = (b_i, s_1, \ldots, s_{m-1})$ and the encoded output bits $c_{1i}, c_{2i}, \ldots, c_{ni}$. For the code given by Figure 3.4, there are four possible states $(s_1 s_2) \in \{(00), (10), (01), (11)\}$ and eight possible transitions from one stage to the following, as depicted in Figure 3.5. For each transition, there is an input bit b_i and a pair of output bits (c_{1i}, c_{2i}) denoted by $b_i/c_{1i}c_{2i}$ at each transition line in the figure. Now consider a certain number of such transitions. They can

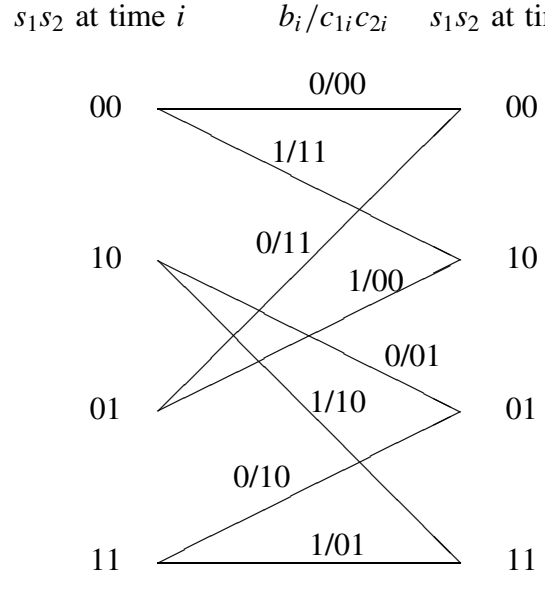

Figure 3.5 State transitions for the $(1 + D^2, 1 + D + D^2)$ convolutional code.

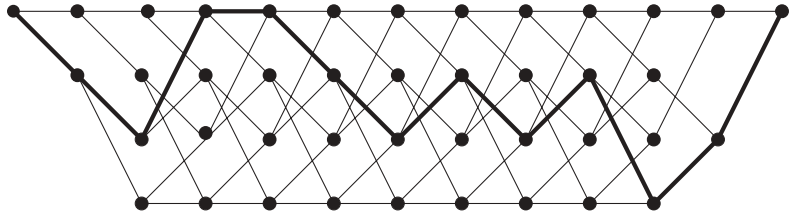

Figure 3.6 Trellis diagram for the $(1 + D^2, 1 + D + D^2)$ convolutional code.

be depicted by successively appending such transitions as shown in Figure 3.6. This is called a *trellis diagram*. Given a defined initial state of the shift register (usually the all-zero state), each code word is characterized by sequence of certain transitions. We call this a *path* in the trellis. In Figure 3.6, the path corresponding to the data word 1000 0111 0100 and the code word 11 01 11 00 00 11 10 01 10 00 01 11 is depicted by bold lines for the transitions in the trellis. In this example, the last $m = 2$ bits are zero and, as a consequence, the final state in the trellis is the all-zero state. It is common practice to start and to stop with the all-zero state because it helps the decoder. This can easily be achieved by appending m zeros – the so-called *tail bits* – to the useful bit stream.

State diagrams

One can also characterize the encoder by states and inputs and their corresponding transitions as depicted in part (a) of Figure 3.7 for the code under consideration. This is known as a *Mealy automat*. To evaluate the free distance of a code, it is convenient to cut open the automat diagram as depicted in part (b) of Figure 3.7. Each path (code word) that starts in the all-zero state and comes back to that state can be visualized by a sequence of states that starts at the all-zero state on the left and ends at the all-zero state on the right. We look at the coded bits in the labeling $b_i/c_{1i}c_{2i}$ and count the bits that have the value one. This is just the Hamming distance between the code word corresponding to that sequence and the all-zero code word. From the diagram, one can easily obtain the smallest distance d_{free} to the all-zero code word. For the code of our example, the minimum distance corresponds to the sequence of transitions $00 \rightarrow 10 \rightarrow 01 \rightarrow 00$ and turns out to be $d_{\text{free}} = 5$. The alternative sequence $00 \rightarrow 10 \rightarrow 11 \rightarrow 01 \rightarrow 00$ has the distance $d = 6$. All other sequences include loops that produce higher distances.

From the state diagram, we may also find the so-called *error coefficient* c_d. These error coefficients are multiplicative coefficients that relate the probability P_d of an error event of distance d to the corresponding bit error probability. To obtain c_d, we have to count all the nonzero data bits of all error paths of distance d to the all-zero code word. Using $P(A_1 \cup A_2) \leq P(A_1) + P(A_2)$, we obtain the union bound

$$P_b \leq \sum_{d=d_{\text{free}}}^{\infty} c_d P_d$$

for the bit error probability. The coefficients c_d for most relevant codes can be found in text books. The error event probability P_d, for example, for antipodal signaling is given

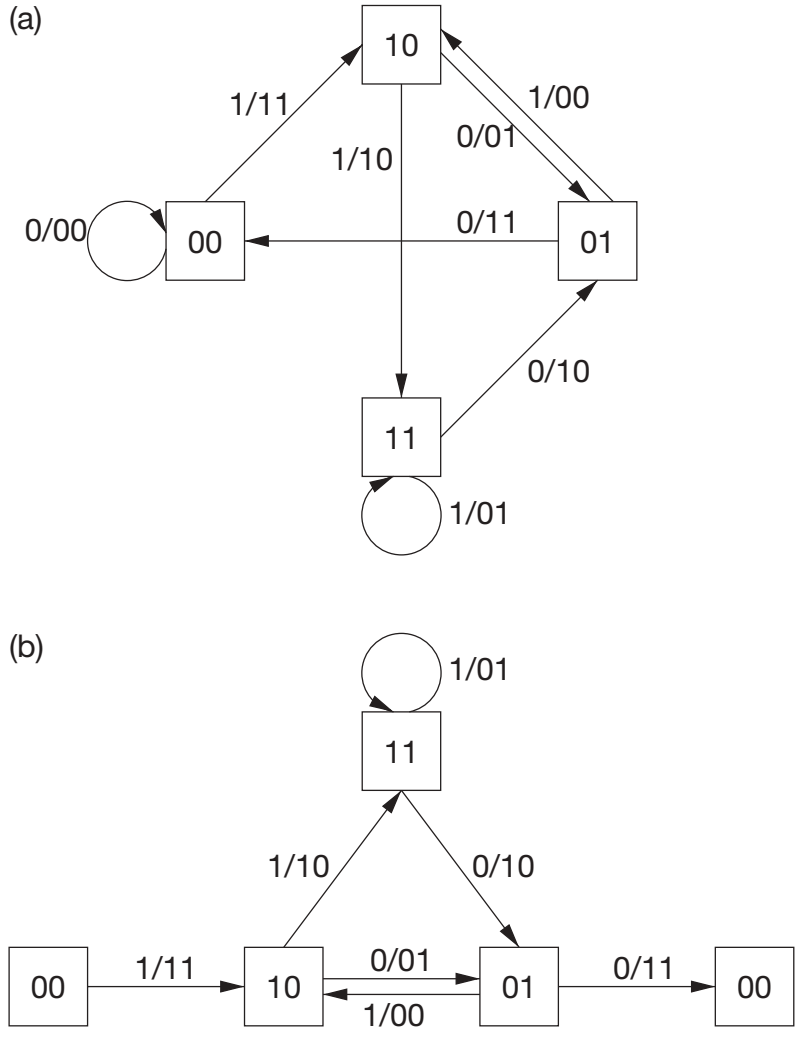

Figure 3.7 State diagram (Mealy automat) for the $(1 + D^2, 1 + D + D^2)$ convolutional code.

by Equation (3.2) for the AWGN channel and by Equation (3.4) for the Rayleigh fading channel.

Catastrophic codes

The state diagram also enables us to find a class of encoders called *catastrophic encoders* that must be excluded because they have the undesirable property of error propagation: if there is a closed loop in the state diagram where all the coded bits $c_{1i}c_{2i}$ are equal to zero, but at least one data bit b_i equals one, then there exists a path of infinite length with an infinite number of ones in the data, but with only a finite number of ones in the code word. As a

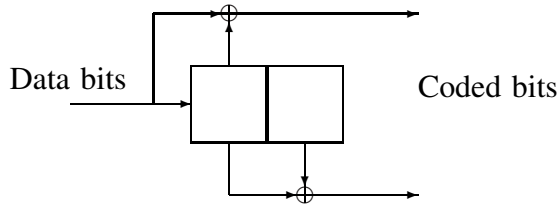

Figure 3.8 Example of a catastrophic convolutional encoder.

consequence, a finite number of channel bit errors may lead to an infinite number of errors in the data, which is certainly a very undesirable property. An example for a catastrophic encoder is the one characterized by the generators $(3,\ 6)_{\text{oct}} = (1 + D, D + D^2)$, which is depicted in Figure 3.8. Once in the state 11, the all-one input sequence will be encoded to the all-zero code word.

Punctured convolutional codes

Up to now, we have only considered convolutional codes of rate $R_c = 1/n$. There are two possibilities to obtain $R_c = k/n$ codes. The classical one is to use k parallel shift registers and combine their outputs. This, however, makes the implementation more complicated. A simpler and more flexible method called *puncturing* is usually preferred in practical communication systems. We explain it by means of the example of an $R_c = 1/2$ code that can be punctured to obtain an $R_c = 2/3$ code. The encoder produces two parallel encoded data streams $\{c_{1,i}\}_{i=0}^{\infty}$ and $\{c_{2,i}\}_{i=0}^{\infty}$. The first data stream will be left unchanged. From the other data stream every second bit will be discarded, that is, only the bits with even time index i will be multiplexed to the serial code word and then transmitted. Instead of the original code word

$$\left(\begin{array}{cccccccccc} c_{10} & c_{20} & c_{11} & c_{21} & c_{12} & c_{22} & c_{13} & c_{23} & c_{14} & \ldots \end{array} \right)$$

the punctured code word

$$\left(\begin{array}{cccccccccc} c_{10} & c_{20} & c_{11} & \bigcirc & c_{12} & c_{22} & c_{13} & \bigcirc & c_{14} & \ldots \end{array} \right)$$

will be transmitted. Here we have indicated the punctured bits by $\bigcirc$. At the receiver, the puncturing positions must be known. A soft decision (e.g. MLSE) receiver has metric values μ_{vi} as inputs that correspond to the encoded bits c_{vi}. The absolute value of μ_{vi} is an indicator for the reliability of the bit. Punctured bits can be regarded as bits with reliability zero. Thus, the receiver has to add dummy receive bits at the punctured positions of the code word and assign them the metric values $\mu_{vi} = 0$.

Recursive systematic convolutional encoders

Recursive systematic convolutional (RSC) encoders have become popular in the context of parallel concatenated codes and turbo decoding (see below). For every nonsystematic convolutional (NSC) $R_c = 1/n$ encoder, one can find an equivalent RSC encoder that

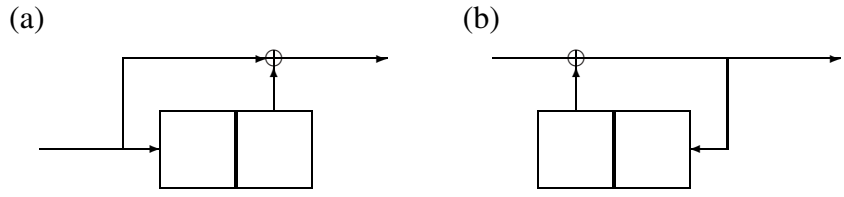

Figure 3.9 Inversion circuit for the generator polynomial $1 + D^2$.

produces the same code (i.e. the same set of code words) with a different relation between the data word and the code word. It can be constructed in such a way that the first of the n parallel encoded bit stream of the code word is systematic, that is, it is identical to the data word.

As an example, we consider the $R_c = 1/2$ convolutional code of Figure 3.4 that can be written in compact power series notation as

$$\begin{bmatrix} c_1(D) \\ c_2(D) \end{bmatrix} = b(D) \begin{bmatrix} 1 + D^2 \\ 1 + D + D^2 \end{bmatrix}.$$

The upper branch corresponding to the generator polynomial $g_1(D) = 1 + D^2$ of the shift register circuit depicted in part (a) of Figure 3.9 defines a one-to-one map from the set of all data words to itself. One can easily check that the inverse is given by the recursive shift register circuit depicted in part (b) of Figure 3.9. This can be described by the formal power series

$$g_1^{-1}(D) = \left(1 + D^2\right)^{-1} = 1 + D^2 + D^4 + D^6 + \cdots$$

This power series description of feedback shift registers is formally the same as the description of linear systems in digital signal processing[5], where the delay is usually denoted by $e^{-j\omega}$ instead of D. The shift register circuits of Figure 3.9 invert each other. Thus, $g_1^{-1}(D)$ is a one-to-one mapping between bit sequences. As a consequence, combining the convolutional encoder with that recursive shift register circuit as depicted in part (a) of Figure 3.10 leads to the same set of code words. This circuit is equivalent to the one depicted in part (b) of Figure 3.10. This RSC encoder with generator polynomials $(5,\ 7)_{\text{oct}}$ can formally be written as

$$\begin{bmatrix} c_1(D) \\ c_2(D) \end{bmatrix} = \tilde{b}(D) \begin{bmatrix} 1 \\ \frac{1+D+D^2}{1+D^2} \end{bmatrix},$$

where the bit sequences are related by $\tilde{b}(D) = (1 + D^2)\, b(D)$.

For a general $R_c = 1/n$ convolutional code, we have the NSC encoder given by the generator polynomial vector

$$\mathbf{g}(D) = \begin{bmatrix} g_1(D) \\ \vdots \\ g_n(D) \end{bmatrix}.$$

[5]In signal processing, we have an interpretation of ω as a (normalized) frequency, which has no meaning for convolutional codes. Furthermore, here all additions are modulo 2. However, all formal power series operations are the same.

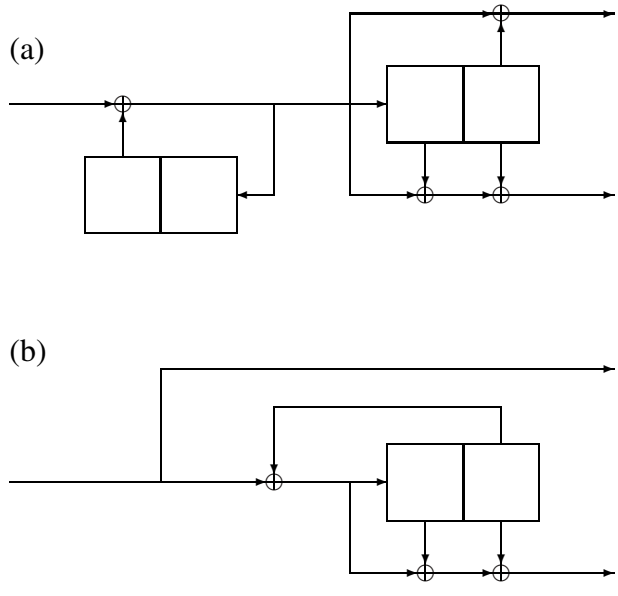

Figure 3.10 Recursive convolutional encoder.

The equivalent RSC encoder is given by the generator vector

$$\tilde{\mathbf{g}}(D) = \begin{bmatrix} 1 \\ g_2(D)/g_1(D) \\ \vdots \\ g_n(D)/g_1(D) \end{bmatrix}.$$

The bits sequence $b(D)$ encoded by $\mathbf{g}(D)$ results in the same code word as the bit sequence $\tilde{b}(D) = g_1(D)b(D)$ encoded by $\tilde{\mathbf{g}}(D) = g_1^{-1}(D)\mathbf{g}(D)$, that is,

$$\mathbf{c}(D) = b(D)\mathbf{g}(D) = \tilde{b}(D)\tilde{\mathbf{g}}(D).$$

An MLSE decoder will find the most likely code word that is uniquely related to a data word corresponding to an NSC encoder and another data word corresponding to an RSC encoder. As a consequence, one may use the same decoder for both and then relate the sequences as described above. But note that this is true only for a decoder that makes decisions about sequences. This is not true for a decoder that makes bitwise decisions like the MAP decoder.

3.2.2 MLSE for convolutional codes: the Viterbi algorithm

Let us consider a convolutional code with memory m and a finite sequence of K input data bits $\{b_k\}_{k=1}^{K}$. We denote the coded bits as c_i. We assume that the corresponding trellis starts and ends in the all-zero state. In our notation, the tail bits are included in $\{b_k\}_{k=1}^{K}$, that is, there are only $K - m$ bits that really carry information.

Although the following discussion is not restricted to that case, we first consider the concrete case of antipodal (BPSK) signaling, that is, transmit symbols $x_i = (-1)^{c_i} \in \{\pm 1\}$ written as a vector $\mathbf{x}$ and a real discrete AWGN channel given by

$$\mathbf{y} = \mathbf{x} + \mathbf{n},$$

where $\mathbf{y}$ is the vector of receive symbols and $\mathbf{n}$ is the real AWGN vector with components n_i of variance

$$\sigma^2 = \mathrm{E}\left\{n_i^2\right\} = \frac{N_0}{2E_S}.$$

Here, we have normalized the noise by the symbol energy E_S. We know from the discussion in Subsection 1.3.2 that, given a fixed receive vector $\mathbf{y}$, the most probable transmit sequence $\mathbf{x}$ for this case is the one that maximizes the *correlation metric* given by the scalar product

$$\mu(\mathbf{x}) = \mathbf{y} \cdot \mathbf{x}. \tag{3.30}$$

For an $R_c = 1/n$ convolutional code, the code word consists of nK encoded bits, and the metric can be written as a sum

$$\mu(\mathbf{x}) = \sum_{k=1}^{K} \mu_k \tag{3.31}$$

of metric increments

$$\mu_k = \mathbf{y}_k \cdot \mathbf{x}_k$$

corresponding to the K time steps $k = 1, \ldots, K$ of the trellis. Here $\mathbf{x}_k$ is the vector of the n symbols x_i that correspond to encoded bits for the time step number k where the bit b_k is encoded, and $\mathbf{y}_k$ is the vector of the corresponding receive vector.

The task now is to find the vector $\mathbf{x}$ that maximizes the metric given by Equation (3.31), thereby exploiting the special trellis structure of a convolutional code. We note that the following treatment is quite general and it is by no means restricted to the special case of the AWGN metric given by Equation (3.30). For instance, any metric that is given by expressions like Equations (3.19–3.21) can be written as Equation (3.31). Thus, *a priori* information about the bits also can be included in a straightforward manner by the expressions presented in Subsection 3.1.5, see also (Hagenauer 1995).

For a reasonable sequence length K, it is not possible to find the vector $\mathbf{x}$ by exhaustive search because this would require a computational effort that is proportional to 2^K. But, owing to the trellis structure of convolutional codes, this is not necessary. We consider two code words $\mathbf{x}$ and $\hat{\mathbf{x}}$ with corresponding paths merging at a certain time step k in a common state $\mathbf{s}_k$ (see Figure 3.11). Assume that for both paths the *accumulated metrics*, that is, the sum of all metric increments up to that time step

$$\Sigma_k = \sum_{i=1}^{k} \mu_i$$

for $\mathbf{x}$ and

$$\hat{\Sigma}_k = \sum_{i=1}^{k} \hat{\mu}_i$$

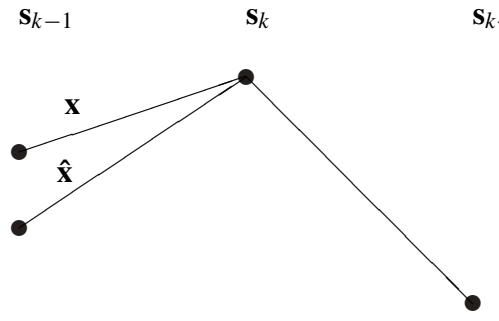

Figure 3.11 Transition where the paths $\mathbf{x}$ and $\hat{\mathbf{x}}$ merge.

for $\hat{\mathbf{x}}$ have been calculated. Because the two paths merge at time step k and will be identical for the whole future,

$$\mu(\hat{\mathbf{x}}) - \mu(\mathbf{x}) = \hat{\Sigma}_k - \Sigma_k$$

holds and we can already make a decision between both paths. Assume $\mu(\hat{\mathbf{x}}) - \mu(\mathbf{x}) > 0$. Then, $\hat{\mathbf{x}}$ is more likely than $\mathbf{x}$, and we can discard $\mathbf{x}$ from any further considerations. This fact allows us to sort out unlikely paths before the final decision and thus an effort that is exponentially growing with the time can be avoided.

The algorithm that does this is the Viterbi algorithm and it works as follows: starting from the initial state, the metric increments μ_k for all transitions between all the state $\mathbf{s}_{k-1}$ and $\mathbf{s}_k$ are calculated recursively and added up to the time accumulated metrics Σ_{k-1}. Then, for the two transitions with the same new state $\mathbf{s}_k$, the values of $\Sigma_{k-1} + \mu_k$ are compared. The larger value will serve as the new accumulated metric $\Sigma_k = \Sigma_{k-1} + \mu_k$, and the other one will be discarded. Furthermore, a pointer will be stored, which points from $\mathbf{s}_k$ to the preceding state corresponding to the larger metric value. Thus, going from the left to the right in the trellis diagram, for each time instant k and for all possible states, the algorithm executes the following steps:

1. Calculate the metric increments μ_k for all the $2 \cdot 2^m$ transitions between all the 2^m states $\mathbf{s}_{k-1}$ and all the 2^m states $\mathbf{s}_k$ and add them to the to the 2^m accumulated metric values Σ_{k-1} corresponding to the states $\mathbf{s}_{k-1}$.

2. For all states $\mathbf{s}_k$ compare the values of $\Sigma_{k-1} + \mu_k$ for the two transitions ending at $\mathbf{s}_k$ and select the one that is the maximum and then set $\Sigma_k = \Sigma_{k-1} + \mu_k$, which is the accumulated metric of that state.

3. Place a pointer to the state $\mathbf{s}_{k-1}$ that is the most likely preceding state for that transition.

Then, when all these calculations and assignments have been done, we start at the end of the trellis and trace back the pointers that indicate the most likely preceding states. This procedure finally leads us to the most likely path in the trellis.

3.2.3 The soft-output Viterbi algorithm (SOVA)

The soft-output Viterbi algorithm (SOVA) is a relatively simple modification of the Viterbi algorithm that allows to obtain an additional *soft* reliability information for the hard decision bits provided by the MLSE.

By construction, the Viterbi algorithm is a sequence estimator, not a bit estimator. Thus, it does not provide reliability information about the bits corresponding to the sequence. However, it can provide us with information about the reliability of the decision between two sequences. Let $\mathbf{x}$ and $\hat{\mathbf{x}}$ be two possible transmit sequences. Then, according to Equation (3.18), the conditional probability that this sequence has been transmitted given that $\mathbf{y}$ has been received is

$$P(\mathbf{x}|\mathbf{y}) = C \, \exp\left(\frac{1}{\sigma^2}\mu(\mathbf{x})\right)$$

for $\mathbf{x}$ and

$$P(\hat{\mathbf{x}}|\mathbf{y}) = C \, \exp\left(\frac{1}{\sigma^2}\mu(\hat{\mathbf{x}})\right)$$

for $\hat{\mathbf{x}}$. Now assume that $\hat{\mathbf{x}}$ is the maximum likelihood sequence obtained by the Viterbi algorithm. If one could be sure that one of the two sequences $\mathbf{x}$ or $\hat{\mathbf{x}}$ is the correct one (and not any other one), then $\Pr(\hat{\mathbf{x}}|\mathbf{y}) = 1 - \Pr(\mathbf{x}|\mathbf{y})$ and the LLR for a correct decision would be given by

$$L(\hat{\mathbf{x}}) = \log \frac{P(\hat{\mathbf{x}}|\mathbf{y})}{P(\mathbf{x}|\mathbf{y})} = \frac{1}{\sigma^2}\left(\mu(\hat{\mathbf{x}}) - \mu(\mathbf{x})\right), \tag{3.32}$$

that is, the metric difference is a measure for the reliability of the decision between the two sequences. We note that this LLR is conditioned by the event that one of both paths is the correct one.

We now consider a data bit $\hat{b}_k$ at a certain position in the bit stream corresponding to the ML sequence $\hat{\mathbf{x}}$ estimated by the Viterbi Algorithm[6]. The goal now is to gain information about the reliability of this bit by looking at the reliability of the decisions between $\hat{\mathbf{x}}$ and other sequences $\mathbf{x}^{(\beta)}$ whose paths merge with the ML path at some state $\mathbf{s}_k$. Any decision in favor of $\hat{\mathbf{x}}$ instead of the alternative sequence $\mathbf{x}^{(\beta)}$ with a bit $b_k^{(\beta)}$ is only relevant for that bit decision if $b_k^{(\beta)} \neq b_k$. Thus, we can restrict our consideration to the relevant sequences $\mathbf{x}^{(\beta)}$. Each of the relevant alternative paths labeled by the index β is the source of a possible erroneous decision in favor of $\hat{b}_k$ instead of $b_k^{(\beta)}$. We define a random error bit $e_k^{(\beta)}$ that takes the value $e_k^{(\beta)} = 1$ for an erroneous decision in favor of $\hat{b}_k$ instead of $b_k^{(\beta)}$ and $e_k^{(\beta)} = 0$ otherwise. We write $L_k^{(\beta)} = L\left(e_k^{(\beta)} = 0\right)$ for the L-values of the error bits. By construction, it is given by

$$L_k^{(\beta)} = \frac{1}{\sigma^2}\left(\mu(\hat{\mathbf{x}}) - \mu(\mathbf{x}^{\beta})\right).$$

Note that $L_k^{(\beta)} > 0$ holds because b_k belongs to the maximum likelihood path that is *per definitionem* more likely than any other.

It is important to note that all the corresponding probabilities are *conditional* probabilities because in any case it is assumed that one of the two sequences $\hat{\mathbf{x}}$ or $\mathbf{x}^{(\beta)}$ is the correct

[6]The same arguments apply if we consider a symbol $\hat{x}_i$ of the transmit sequence.

one. Furthermore, we only consider paths that merge directly with the ML path. Therefore, all paths that are discarded after comparing them with another path than the ML path are not considered. It is possible (but not very likely in most cases) that the correct path is among these discarded paths. This rare event has been excluded in our approximation. We further assume that the random error bits $e_k^{(\beta)}$ are statistically independent. All the random error bits $e_k^{(\beta)}$ together result in an error bit e_k that is assumed to be given by the modulo 2 sum

$$e_k = \sum_{\text{relevant } \beta} \oplus e_k^{(\beta)}.$$

We further write $L_k = L\,(e_k = 0)$ for the L-value of the resulting error bit. Using Equation (3.14), the L-value for this resulting error bit is approximately given by

$$L_k \approx \min_{\text{relevant } \beta} \left(L_k^{(\beta)} \right) = \min_{\text{relevant } \beta} \left(\frac{1}{\sigma^2} \left(\mu(\hat{\mathbf{x}}) - \mu(\mathbf{x}^{(\beta)}) \right) \right),$$

where we have used Equation (3.32). It is intuitively simple to understand that this is a reasonable reliability information about the bit b_k. We consider all the sequence decisions that are relevant for the decision of this bit. Then, according to the intuitively obvious rule that a chain is as strong as its weakest link, we assign the smallest of those sequence reliabilities as the bit reliability.

Now, in the Viterbi algorithm, the reliability information about the merging paths have to be stored for each state in addition to the accumulated metric and the pointer to the most likely preceding state. Then the reliability of the bits of the ML path will be calculated. First, they will all be initialized with $+\infty$, that is, practically speaking, with a very large number. Then, for each relevant decision between two paths, this value will be updated, that is, the old reliability will be replaced by the reliability of the path decision if the latter is smaller. To do this, every path corresponding to any sequence $\mathbf{x}^{(\beta)}$ that has been discarded in favor of the ML sequence $\hat{\mathbf{x}}$ has to be traced back to a point where both paths merge.

We finally note that the reliability information can be assigned to the transmit symbols $x_i \in \{\pm 1\}$ (i.e. the signs corresponding to the bits of the code word) as well as to the data bit itself.

3.2.4 MAP decoding for convolutional codes: the BCJR algorithm

To obtain LLR information about bits rather than about sequences, the bitwise MAP receiver of Equation (3.23) has to be applied instead of a MLSE. This equation cannot be applied directly because it would require an exhaustive search through all code words. For a convolutional code, the exhaustive search for the MLSE can be avoided in the Viterbi algorithm by making use of the trellis structure. For the MAP receiver, the exhaustive search can be avoided in the BCJR (Bahl, Cocke, Jelinek, Raviv) algorithm (Bahl *et al.* 1974). In contrast to the SOVA, it provides us with the exact LLR value for a bit, not just an approximate one. The price for this exact information is the higher complexity. The BCJR algorithm has been known for a long time, but it became very popular not before its widespread application in turbo decoding.

We consider a vector of data bits $\mathbf{b} = (b_1, \ldots, b_K)^T$ encoded to a code word $\mathbf{c}$ and transmitted with symbols $\mathbf{x}_k$. Given a receive symbol sequence $\mathbf{y} = (y_1, \ldots, y_N)^T$, we

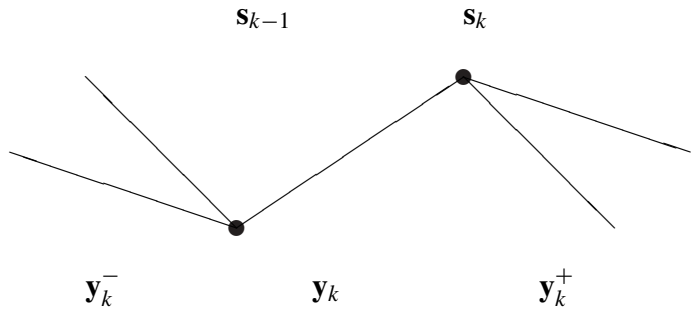

Figure 3.12 Transition.

want to calculate the LLR for a data bit b_k given as

$$L(b_k = 0|\mathbf{y}) = \log \frac{\sum_{\mathbf{b}\in\mathcal{B}_k^{(0)}} P(\mathbf{b}|\mathbf{y})}{\sum_{\mathbf{b}\in\mathcal{B}_k^{(1)}} P(\mathbf{b}|\mathbf{y})}. \tag{3.33}$$

Here, $\mathcal{B}_k^{(0)}$ is the set of those vectors $\mathbf{b} \in \mathcal{B}$ for which $b_k = 0$ and $\mathcal{B}_k^{(1)}$ is the set of those for which $b_k = 1$. We assume that the bit b_k is encoded during the transition between the states $\mathbf{s}_{k-1}$ and $\mathbf{s}_k$ of a trellis. For each time instant k, there are 2^m such transitions corresponding to $b_k = 0$ and 2^m transitions corresponding to $b_k = 1$. Each probability term $P(\mathbf{b}|\mathbf{y})$ in the numerator or denominator of Equation (3.33) can be written as the conditional probability $P(\mathbf{s}_k\mathbf{s}_{k-1}|\mathbf{y})$ for the transition between two states $\mathbf{s}_{k-1}$ and $\mathbf{s}_k$. Since the denominator in

$$P(\mathbf{s}_k\mathbf{s}_{k-1}|\mathbf{y}) = \frac{p(\mathbf{y}, \mathbf{s}_k\mathbf{s}_{k-1})}{p(\mathbf{y})}$$

cancels out in Equation (3.33), we can consider the joint probability density function $p(\mathbf{y}, \mathbf{s}_k\mathbf{s}_{k-1})$ instead of the conditional probability $P(\mathbf{s}_k\mathbf{s}_{k-1}|\mathbf{y})$. We now decompose the receive symbol vector into three parts: we write $\mathbf{y}_k^-$ for those receive symbols corresponding to time instants earlier than the transition between the states $\mathbf{s}_{k-1}$ and $\mathbf{s}_k$. We write $\mathbf{y}_k$ for those receives symbols corresponding to time instants at the transition between the states $\mathbf{s}_{k-1}$ and $\mathbf{s}_k$. And we write $\mathbf{y}_k^+$ for those receive symbols corresponding to time instants later than the transition between the states $\mathbf{s}_{k-1}$ and $\mathbf{s}_k$. Thus, the receive vector may be written as

$$\mathbf{y} = \begin{bmatrix} \mathbf{y}_k^- \\ \mathbf{y}_k \\ \mathbf{y}_k^+ \end{bmatrix}$$

(see Figure 3.12), and the probability density may be written as

$$p(\mathbf{y}, \mathbf{s}_k\mathbf{s}_{k-1}) = p(\mathbf{y}_k^+\mathbf{y}_k\mathbf{y}_k^-\mathbf{s}_k\mathbf{s}_{k-1}).$$

If no confusion arises, we dispense with the commas between vectors. Using the definition of conditional probability, we modify the right-hand side and get

$$p(\mathbf{y}, \mathbf{s}_k\mathbf{s}_{k-1}) = p(\mathbf{y}_k^+|\mathbf{y}_k\mathbf{y}_k^-\mathbf{s}_k\mathbf{s}_{k-1})p(\mathbf{y}_k\mathbf{y}_k^-\mathbf{s}_k\mathbf{s}_{k-1}),$$

and, in another step,

$$p(\mathbf{y}, \mathbf{s}_k\mathbf{s}_{k-1}) = p(\mathbf{y}_k^+|\mathbf{y}_k\mathbf{y}_k^-\mathbf{s}_k\mathbf{s}_{k-1})p(\mathbf{y}_k\mathbf{s}_k|\mathbf{y}_k^-\mathbf{s}_{k-1})p(\mathbf{y}_k^-\mathbf{s}_{k-1}).$$

We now make the assumptions

$$p(\mathbf{y}_k^+|\mathbf{y}_k\mathbf{y}_k^-\mathbf{s}_k\mathbf{s}_{k-1}) = p(\mathbf{y}_k^+|\mathbf{s}_k)$$

and

$$p(\mathbf{y}_k\mathbf{s}_k|\mathbf{y}_k^-\mathbf{s}_{k-1}) = p(\mathbf{y}_k\mathbf{s}_k|\mathbf{s}_{k-1}),$$

which are quite similar to the properties of a Markov chain. The first equation means that we assume that the random variable $\mathbf{y}_k^+$ corresponding to the receive symbols after state $\mathbf{s}_k$ depends on that state, but is independent of the earlier state $\mathbf{s}_{k-1}$ and any earlier receive symbols corresponding to $\mathbf{y}$ and $\mathbf{y}_k^-$. The second equation means that we assume that the random variable $\mathbf{y}_k$ corresponding to the receive symbols for the transition from the state $\mathbf{s}_{k-1}$ to $\mathbf{s}_k$ does not depend on earlier receive symbols corresponding to $\mathbf{y}_k^-$. For a given fixed receive sequence $\mathbf{y}$, we define

$$\alpha_{k-1}(\mathbf{s}_{k-1}) = p(\mathbf{y}_k^-\mathbf{s}_{k-1}), \quad \beta_k(\mathbf{s}_k) = p(\mathbf{y}_k^+|\mathbf{s}_k), \quad \gamma_k(\mathbf{s}_k|\mathbf{s}_{k-1}) = p(\mathbf{y}_k\mathbf{s}_k|\mathbf{s}_{k-1}) \tag{3.34}$$

and write

$$p(\mathbf{y}, \mathbf{s}_k\mathbf{s}_{k-1}) = \beta_k(\mathbf{s}_k)\gamma_k(\mathbf{s}_k|\mathbf{s}_{k-1})\alpha_{k-1}(\mathbf{s}_{k-1}).$$

The probability densities $\gamma_k(\mathbf{s}_k|\mathbf{s}_{k-1})$ for the transition from the state $\mathbf{s}_{k-1}$ to $\mathbf{s}_k$ can be obtained from the metric value μ_k calculated from $\mathbf{y}_k$. As shown in Section 3.1.5, for the AWGN channel with normalized noise variance σ^2 and bipolar transmission, we have simply

$$\gamma_k(\mathbf{s}_k|\mathbf{s}_{k-1}) = C \exp\left(\frac{1}{\sigma^2}\mathbf{x}_k \cdot \mathbf{y}_k\right) \cdot \Pr(\mathbf{x}_k),$$

where $\mathbf{x}_k$ is the transmit symbol and $P(\mathbf{x}_k)$ is the *a priori* probability corresponding to that transition. The α_k and β_k values have to be calculated using recursive relations. We state the following proposition.

Proposition 3.2.1 (Forward-backward recursions) *For α_k, β_k, γ_k as defined by Equation (3.34), the following two recursive relations*

$$\alpha_k(\mathbf{s}_k) = \sum_{\mathbf{s}_{k-1}} \gamma_k(\mathbf{s}_k|\mathbf{s}_{k-1})\alpha_{k-1}(\mathbf{s}_{k-1}) \tag{3.35}$$

and

$$\beta_{k-1}(\mathbf{s}_{k-1}) = \sum_{\mathbf{s}_k} \beta_k(\mathbf{s}_k)\gamma_k(\mathbf{s}_k|\mathbf{s}_{k-1}) \tag{3.36}$$

hold.

Proof. Forward recursion:

$$\begin{aligned}\alpha_k(\mathbf{s}_k) &= p(\mathbf{y}_{k+1}^-\mathbf{s}_k) = p(\mathbf{y}_k\mathbf{y}_k^-\mathbf{s}_k)\\ &= \textstyle\sum_{\mathbf{s}_{k-1}} p(\mathbf{y}_k\mathbf{y}_k^-\mathbf{s}_k\mathbf{s}_{k-1})\\ &= \textstyle\sum_{\mathbf{s}_{k-1}} p(\mathbf{y}_k\mathbf{s}_k|\mathbf{y}_k^-\mathbf{s}_{k-1})p(\mathbf{y}_k^-\mathbf{s}_{k-1})\end{aligned}$$

Using the Markov property $p(\mathbf{y}_k\mathbf{s}_k|\mathbf{y}_k^-\mathbf{s}_{k-1}) = p(\mathbf{y}_k\mathbf{s}_k|\mathbf{s}_{k-1})$, we obtain Equation (3.35).

Backward recursion:

$$\begin{aligned}\beta_{k-1}(\mathbf{s}_{k-1}) &= p(\mathbf{y}_{k-1}^{+}|\mathbf{s}_{k-1}) = p(\mathbf{y}_{k}^{+}\mathbf{y}_k|\mathbf{s}_{k-1}) = p(\mathbf{y}_{k}^{+}\mathbf{y}_k\mathbf{s}_{k-1})/\Pr(\mathbf{s}_{k-1}) \\ &= \textstyle\sum_{\mathbf{s}_k} p(\mathbf{y}_{k}^{+}\mathbf{y}_k\mathbf{s}_k\mathbf{s}_{k-1})/\Pr(\mathbf{s}_{k-1}) \\ &= \textstyle\sum_{\mathbf{s}_k} p(\mathbf{y}_{k}^{+}|\mathbf{y}_k\mathbf{s}_k\mathbf{s}_{k-1})p(\mathbf{y}_k\mathbf{s}_k\mathbf{s}_{k-1})/\Pr(\mathbf{s}_{k-1}).\end{aligned}$$

Using $p(\mathbf{y}_k\mathbf{s}_k\mathbf{s}_{k-1})/\Pr(\mathbf{s}_{k-1}) = p(\mathbf{y}_k\mathbf{s}_k|\mathbf{s}_{k-1})$ and the Markov property $p(\mathbf{y}_k^{+}|\mathbf{y}_k\mathbf{s}_k\mathbf{s}_{k-1}) = p(\mathbf{y}_k^{+}|\mathbf{s}_k)$, we obtain Equation (3.36).

The BCJR algorithm now proceeds as follows: initialize the initial and the final state of the trellis as $\alpha_0 = 1$ and $\beta_K = 1$ and calculate the α_k values according to the forward recursion of Equation (3.35) from the left to the right in the trellis and then calculate the β_k according to the backward recursion Equation (3.36) from the right to the left in the trellis. Then the LLRs for each transition can be calculated as

$$L(b_k = 0|\mathbf{y}) = \log \frac{\sum_{\mathbf{b}\in\mathcal{B}_k^{(0)}} p(\mathbf{y}, \mathbf{s}_k\mathbf{s}_{k-1})}{\sum_{\mathbf{b}\in\mathcal{B}_k^{(1)}} p(\mathbf{y}, \mathbf{s}_k\mathbf{s}_{k-1})}$$

that is,

$$L(b_k = 0|\mathbf{y}) = \log \frac{\sum_{\mathbf{b}\in\mathcal{B}_k^{(0)}} \alpha_{k-1}(\mathbf{s}_{k-1})\gamma_k(\mathbf{s}_k|\mathbf{s}_{k-1})\beta_k(\mathbf{s}_k)}{\sum_{\mathbf{b}\in\mathcal{B}_k^{(1)}} \alpha_{k-1}(\mathbf{s}_{k-1})\gamma_k(\mathbf{s}_k|\mathbf{s}_{k-1})\beta_k(\mathbf{s}_k)}.$$

In this notation, we understand the sum over all $\mathbf{b} \in \mathcal{B}_k^{(0)}$ as the sum over all transitions from $\mathbf{s}_{k-1}$ to $\mathbf{s}_k$ with $b_k = 0$ and sum over all $\mathbf{b} \in \mathcal{B}_k^{(1)}$ as the sum over all transitions from $\mathbf{s}_{k-1}$ to $\mathbf{s}_k$ with $b_k = 1$.

3.2.5 Parallel concatenated convolutional codes and turbo decoding

During the last decade, great success has been achieved in closely approaching the theoretical limit of channel coding. The codes that have been used for that are often called *turbo codes*. More precisely, one should carefully distinguish between the code and the decoding method. The first turbo code was a parallel concatenated convolutional code (PCCC). Parallel concatenation can be done with block codes as well. Also serial concatenation is possible. The novel decoding method that has been applied to all theses codes deserves the name *turbo decoder* because there is an iterative exchange of extrinsic and *a priori* information between the decoders of the component codes.

To explain the method, we consider the classical scheme with a parallel concatenation of two RSC codes of rate $R_c = 1/2$ as depicted in Figure 3.13. The data bit stream is encoded in parallel by two RSC encoders (that may be identical). The common systematic part $\mathbf{x}_s$ of both codes will be transmitted only once. Thus, the output code word consists of three parallel vectors: the systematic symbol vector $\mathbf{x}_s$ and the two nonsystematic PC symbol vectors $\mathbf{x}_{p1}$ and $\mathbf{x}_{p2}$. The input for the second RSC parity check encoder (RSC-PC2) is interleaved by a pseudo-random permutation Π before encoding. The resulting $R_c = 1/3$ code word may be punctured in the nonsystematic symbols to achieve higher code rates. Lower code rates can be achieved by additional RSC-PCs, together with interleavers. This setup may be regarded as well as a parallel concatenation of the first RSC code of rate $R_c = 1/2$ with an $R_c = 1$ recursive nonsystematic code that produces $\mathbf{x}_{p2}$. However, here

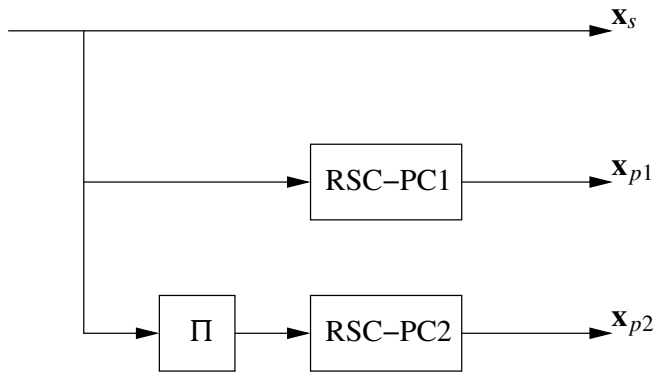

Figure 3.13 PCCC encoder.

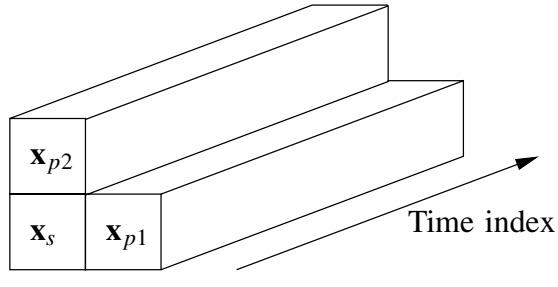

Figure 3.14 PCCC code word.

we prefer the point of view of two equal rate RSC codes with a common systematic symbol stream.

The code word consisting of three parallel symbol streams can be visualized as depicted in Figure 3.14. The vector $\mathbf{x}_{p1}$ can be regarded as a horizontal parity check, the vector $\mathbf{x}_{p2}$ as a vertical parity check. The time index is the third dimension. At the decoder, the corresponding receive vectors are denoted by $\mathbf{y}_s$, $\mathbf{y}_{p1}$ and $\mathbf{y}_{p2}$. With a diagonal matrix of fading amplitudes $\mathbf{A}$, the channel LLRs are

$$\mathbf{L}_s^c = \frac{2}{\sigma^2}\mathbf{A}\mathbf{y}_s, \quad \mathbf{L}_{p1}^c = \frac{2}{\sigma^2}\mathbf{A}\mathbf{y}_{p1}, \quad \mathbf{L}_{p2}^c = \frac{2}{\sigma^2}\mathbf{A}\mathbf{y}_{p2},$$

where σ^{-2} is the channel SNR. We write $\mathbf{L}_1^c = \left(\mathbf{L}_s^c, \mathbf{L}_{p1}^c\right)$ and $\mathbf{L}_2^c = \left(\mathbf{L}_s^c, \mathbf{L}_{p2}^c\right)$ for the respective channel LLRs. In the decoding process, independent extrinsic information $\mathbf{L}_1^e$ and $\mathbf{L}_2^e$ about the systematic part can be obtained from the horizontal and from the vertical decoding, respectively. Thus, the horizontal extrinsic information can be used as *a priori* information for vertical decoding and vice versa.

The turbo decoder setup is depicted in Figure 3.15. It consists of two SISO decoders, SISO1 and SISO2, for the decoding of RSC1 and RSC2, as depicted in Figure 3.3. To

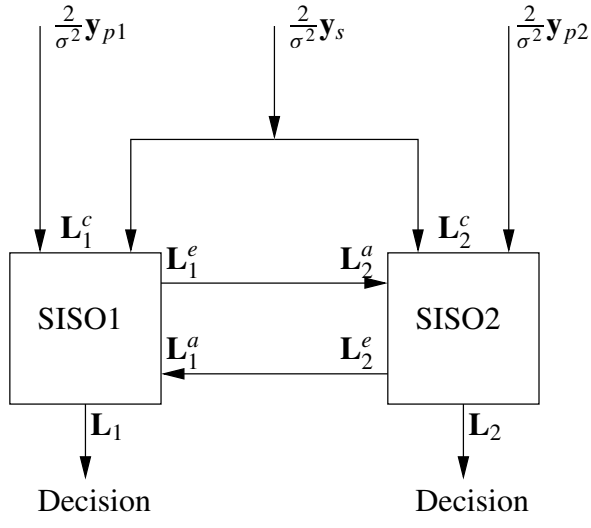

Figure 3.15 Turbo decoder.

simplify the figure, the necessary de−interleaver Π^{-1} at the input for $\mathbf{L}_s^c$ and $\mathbf{L}_2^a$ and the interleaver Π at the output for $\mathbf{L}_2^e$ and $\mathbf{L}_2$ of RSC2 are included inside the SISO2. The MAP decoder for convolutional codes will be implemented by the BCJR algorithm. In the iterative decoding process, the extrinsic output of one SISO decoder serves as the *a priori* input for the other. At all decoding steps, the channel LLR values are available at both SISOs. In the first decoding step, only the channel information, but no *a priori* LLR value is available at SISO1. Then SISO1 calculates the extrinsic LLR value $\mathbf{L}_1^e$ from the horizontal decoding. This serves as the *a priori* input LLR value $\mathbf{L}_2^a$ for SISO2. The extrinsic output $\mathbf{L}_2^e$ then serves as the *a priori* input for SISO1 in the second iteration. These iterative steps will be repeated until a break, and then a final decision can be obtained from the SISO total LLR output value $\mathbf{L}_2$ (or $\mathbf{L}_1$).

We note that the *a priori* input is not really an independent information at the second iteration step or later. This is because all the information of the code has already been used to obtain it. However, the dependencies are small enough so that the information can be successfully used to improve the reliability of the decision by further iterations. On the other hand, it is essential that there will be no feedback of LLR information from the output to the input. Such a feedback would be accumulated at the inputs and finally dominate the decision. Therefore, the extrinsic LLR must be used, where the SISO inputs have been subtracted from the LLR.

We add the following remarks:

- In the ideal case, the SISO is implemented by a BCJR MAP receiver. In practice, the maxlog MAP approximation may be used, which results only in a small loss in performance. This loss is due to the fact that the reliability of the very unreliable symbols is slightly overestimated. The SOVA may also be used, but the performance loss is higher.

- The exact MAP needs the knowledge of the SNR value σ^{-2}, which is normally not available. Thus, a rough estimate must be used. Using the maxlog MAP or SOVA, the SNR is not needed. This is due to the fact that in the first decoding step no *a priori* LLR is used, and, as a consequence, the SNR appears only as a common linear scale factor in all further calculated LLR outputs.

3.3 Reed–Solomon Codes

Reed–Solomon (RS) codes may be regarded as the most important block codes because of their extremely high relevance for many practical applications. These include deep space communications, digital storage media and, last but not least, the digital video broadcasting system (DVB). However, these most useful codes are based on quite sophisticated theoretical concepts that seem to be much closer to mathematics than to electrical engineering. The theory of RS codes can be found in many text books (Blahut 1983; Bossert 1999; Clark and Cain 1988; Lin and Costello 1983; Wicker 1995). In this section about RS codes, we restrict ourselves to some important facts that are necessary to understand the coding scheme of the DVB-T system discussed in Subsection 4.6.2. We will first discuss the basic properties of RS codes as far as they are important for the practical application. Then, we will give a short introduction to the theoretical background. For a deeper understanding of that background, we refer to the text books cited above.

3.3.1 Basic properties

Reed–Solomon codes are based on *byte arithmetics*[7] rather than on bit arithmetics. Thus, RS codes correct *byte errors* instead of bit errors. As a consequence, RS codes are favorable for channels with bursts of bit errors as long as these bursts do not affect too many subsequent bytes. This can be avoided by a proper interleaving scheme. Such bursty channels occur in digital recording. As another example, for a concatenated coding scheme with an inner convolutional code, the Viterbi decoder produces burst errors. An inner convolutional code concatenated with an outer RS code is therefore a favorable setup. It is used in deep space communications and for DVB-T.

Let $N = 2^m - 1$ with an integer number m. For the practically most important RS codes, we have $m = 8$ and $N = 255$. In that case, the symbols of the code word are bytes. For simplicity, in the following text, we will therefore speak of bytes for those symbols. For an RS(N, K, D) code, K data bytes are encoded to a code word of N bytes. The Hamming distance is given by $D = N - K + 1$ bytes. For odd values of D, the code can correct up to t byte errors with $D = 2t + 1$. For even values of D, the code can correct up to t byte errors with $D = 2t + 2$. RS codes are linear codes. For a linear code, any nonsystematic encoder can be transformed into a linear encoder by a linear transform. Figure 3.16 shows the structure of a systematic RS code word with an odd Hamming distance and an even number $N - K = D - 1 = 2t$ of redundancy bytes called *parity check* (PC) *bytes*. In that example, the parity check bytes are placed at the end of the code word. Other choices are possible. RS codes based on byte arithmetics have always the code word length $N = 2^8 - 1 = 255$.

[7] RS codes can be constructed for more general arithmetic structures, but only those based on byte arithmetics are of practical relevance.

Figure 3.16 A systematic RS code word.

Table 3.1 Some RS code parameters	
RS(255, 253, 3)	$t = 1$
RS(255, 251, 5)	$t = 2$
RS(255, 249, 7)	$t = 3$
...	
RS(255, 239, 17)	$t = 8$
...	

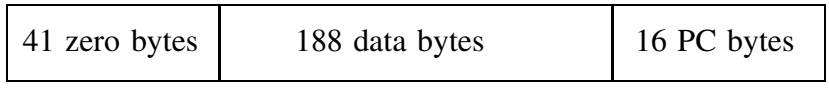

Figure 3.17 A shortened RS code word.

They can be constructed for any value of $D \leq N$. Table 3.1 shows some examples for odd values of D.

Shortened RS codes

In practice, the fixed code word length $N = 255$ is an undesirable restriction. One can get more flexibility by using a simple trick. For an RS(N, K, D) code with $N = 255$, we want to encode only $K_1 < K$ data byte and set the first $K - K_1$ bytes of the data word to zero. We then encode the K bytes (including the zeros) with the RS(N, K, D) systematic encoder to obtain a code word of length N whose first $K - K_1$ code words are equal to zero. These bytes contain no information and need not to be transmitted. By this method we have obtained a *shortened* RS(N_1, K_1, D) code word with $N_1 = N - (K - K_1)$. Figure 3.17 shows the code word of a shortened RS(204, 188, 17) code obtained from an RS(255, 239, 17) code. Before decoding, at the receiver, the $K - K_1$ zero bytes must be appended at the beginning of the code word and a RS(255, 239, 17) decoder will be used. This shortened RS code is used as the outer code for the DVB-T system.

Decoding failure

It may happen that the decoder detects errors that cannot be corrected. In the case of decoding failure, an error flag can be set to indicate that the data are in error. The application may then take benefit from this information.

Erasure decoding

If it is known that some received bytes are very unreliable (e.g. from an inner decoder that provides such reliability information), the decoder can make use of this fact in the decoding procedure. These bytes are called *erasures.*

3.3.2 Galois field arithmetics

Reed–Solomon codes are based on the arithmetics of *finite fields* that are usually called *Galois fields*. The mathematical concept of a *field* stands for a system of numbers, where addition and multiplication and the corresponding inverses are defined and which is commutative. The existence of an (multiplicative) inverse is crucial: for any field element a, there must exist a field element a^{-1} with the property $a^{-1}a = 1$. The rational numbers and the real numbers with their familiar arithmetics are fields. The integer numbers are not, because the (multiplicative) inverse of an integer is not an integer (except for the one).

A *Galois field* $GF(q)$ is a field with a finite number q of elements. One can very easily construct a Galois field $GF(q)$ with $q = p$, where p is a prime number. The $GF(p)$ arithmetics is then given by taking the remainder modulo p. For example, $GF(7)$ with the elements 0, 1, 2, 3, 4, 5, 6 is defined by the addition table

+	1	2	3	4	5	6
1	2	3	4	5	6	0
2	3	4	5	6	0	1
3	4	5	6	0	1	2
4	5	6	0	1	2	3
5	6	0	1	2	3	4
6	0	1	2	3	4	5

and the multiplication table

1	2	3	4	5	6
2	4	6	1	3	5
3	6	2	5	1	4
4	1	5	2	6	3
5	3	1	6	4	2
6	5	4	3	2	1

Note that every field element must occur exactly once in each column or row of the multiplication table to ensure the existence of a multiplicative inverse.

A Galois field has at least one *primitive element* α with the property that any nonzero field element can be uniquely written as a power of α. By using the multiplication table of $GF(7)$, we easily see that $\alpha = 5$ is such a primitive element and the nonzero field elements can be written as powers of α in the following way

$$\alpha^0 = 1,\ \alpha^1 = 5,\ \alpha^2 = 4,\ \alpha^3 = 6,\ \alpha^4 = 2,\ \alpha^5 = 3.$$

We note that since $\alpha^6 = \alpha^0 = 1$, negative powers of α like $\alpha^{-2} = \alpha^4$ are defined as well. We can easily visualize the multiplicative structure of $GF(7)$ as depicted in Figure 3.18. Each nonzero element is represented by the edge of a hexagon or the corresponding angle. α^0 has the angle zero, α^1 has the angle $\pi/3$, α^2 has the angle $2\pi/3$, and so on. Obviously,

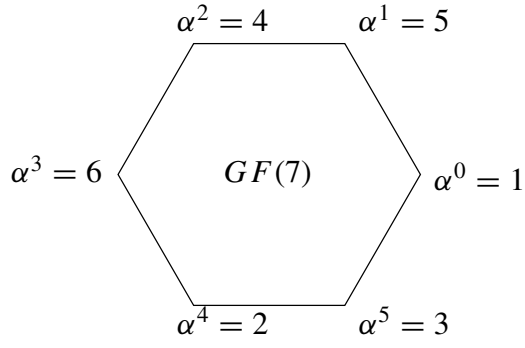

Figure 3.18 $GF(7)$.

the multiplication of field elements is represented by the addition of the corresponding angles. This is the same multiplicative group structure as if we would identify α with the complex phasor $\exp(j2\pi/N)$ with $N = q - 1$. This structure leads directly to a very natural definition of the discrete Fourier transform (DFT) for Galois fields (see below).

The primitive of $GF(q)$ element has the property $\alpha^N = 1$ and thus $\alpha^{iN} = 1$ for $i = 0, 1, \ldots, N - 1$. It follows that each element α^i of $GF(q)$ is a root of the polynomial $x^N - 1$, and we may write

$$x^N - 1 = \prod_{i=0}^{N-1} \left(x - \alpha^i\right).$$

Similarly,

$$x^N - 1 = \prod_{i=0}^{N-1} \left(x - \alpha^{-i}\right)$$

holds.

The prime number Galois fields $GF(p)$ are of some tutorial value. Of practical relevance are the *extension fields* $GF(2^m)$, where m is a positive integer. We state that a Galois field $GF(q)$ exists for every $q = p^m$, where p is prime[8]. Almost all practically relevant RS codes are based on $GF(2^8)$ because the field element can be represented as bytes. We will use the smaller field $GF(2^3)$ to explain the arithmetics of the extension fields.

The elements of an extension field $GF(p^m)$ can be represented as polynomials of degree $m - 1$ over $GF(p)$. Without going into mathematical details, we state that the primitive element α is defined as the root of a primitive polynomial. The arithmetic is then *modulo* that polynomial. Note that addition and subtraction is the same in $GF(2^m)$.

We explain the arithmetic for the example $GF(2^3)$. The primitive polynomial is given by $p(x) = x^3 + x + 1$. The primitive element α is the root of that polynomial, that is, we can set

$$\alpha^3 + \alpha + 1 \equiv 0.$$

We then write down all powers of alpha and reduce them to modulo $\alpha^3 + \alpha + 1$. For example, we may identify $\alpha^3 \equiv \alpha + 1$. Each element is thus given by a polynomial of

[8]For a proof, we refer to the text books mentioned above.

Table 3.2 Representation of $GF(2^3)$

dec	bin	poly	α^i
0	000	0	$*$
1	001	1	α^0
2	010	α	α^1
3	011	$\alpha+1$	α^3
4	100	α^2	α^2
5	101	α^2+1	α^6
6	110	$\alpha^2+\alpha$	α^4
7	111	$\alpha^2+\alpha+1$	α^5

degree 2 over the dual number system $GF(2)$ and can therefore be represented by a bit triple or a decimal number. Table 3.2 shows the equivalent representations of the elements of $GF(2^3)$. We note that for a Galois field $GF(2^m)$, the decimal representation of the primitive element is always given by the number 2.

The addition is simply defined as the addition of polynomials, which is equivalent to the vector addition of the bit tuples. Multiplication is defined as the multiplication of polynomials and reduction modulo $\alpha^3+\alpha+1$. The addition table is then given by

$+$	1	2	3	4	5	6	7
1	0	3	2	5	4	7	6
2	3	0	1	6	7	4	5
3	2	1	0	7	6	5	4
4	5	6	7	0	1	2	3
5	4	7	6	1	0	3	2
6	7	4	5	2	3	0	1
7	6	5	4	3	2	1	0

and the multiplication table by

1	2	3	4	5	6	7
2	4	6	3	1	7	5
3	6	5	7	4	1	2
4	3	7	6	2	5	1
5	1	4	2	7	3	6
6	7	1	5	3	2	4
7	5	2	1	6	4	3

We can visualize the multiplicative structure of $GF(8)$ as depicted in Figure 3.19. This will lead us directly to the discrete Fourier transform that will be defined in the following subsection.

3.3.3 Construction of Reed–Solomon codes

From the communications engineering point of view, the most natural way to introduce Reed–Solomon codes is via the DFT and general properties of polynomials.

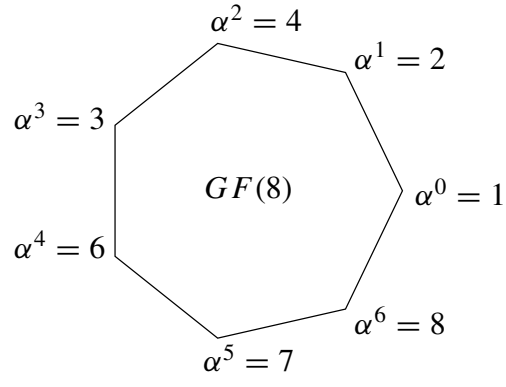

Figure 3.19 $GF(8)$.

The discrete Fourier transforms for Galois fields

Let

$$A = (A_0, A_1, \ldots, A_{N-1})^T$$

be a vector of length $N = q - 1$ with elements $A_i \in GF(q)$. We define the vector

$$a = (a_0, a_1, \ldots, a_{N-1})^T$$

of the DFT by the operation

$$a_j = \sum_{i=0}^{N-1} A_i \alpha^{ij}.$$

We note that the Fourier transform can be described by the multiplication of the vector A by the DFT matrix

$$\mathbf{F} = \begin{pmatrix} 1 & 1 & 1 & \cdots & 1 \\ 1 & \alpha & \alpha^2 & \cdots & \alpha^{N-1} \\ 1 & \alpha^2 & \alpha^4 & \cdots & \alpha^{2N-2} \\ \vdots & \vdots & \vdots & \ddots & \vdots \\ 1 & \alpha^{N-1} & \alpha^{2N-2} & \cdots & \alpha^{(N-1)(N-1)} \end{pmatrix}.$$

As mentioned above, the primitive element α of $GF(q)$ has the same multiplicative properties as $\exp(j2\pi/N)$ with $N = q - 1$. Thus, this is the natural definition of the DFT for Galois fields. We say that A is the *frequency domain vector* and a is the *time domain vector*. The *inverse discrete Fourier transform* (IDFT) in $GF(2^m)$ is given by

$$A_i = \sum_{j=0}^{N-1} a_j \alpha^{-ij}.$$

The proof is the same as for complex numbers, but we must use the fact that

$$\sum_{j=0}^{N-1} \alpha^0 = 1$$

in $GF(2^m)$. For other Galois fields, a normalization factor would occur for the inverse transform.

Any vector can be represented by a formal polynomial. For the frequency domain vector, we may write this formal polynomial as

$$A(x) = A_0 + A_1 x + \cdots + A_{N-1} x^{N-1}.$$

We note that x is only a dummy variable. We add two polynomials $A(x)$ and $B(x)$ by adding their coefficients. If we multiply two polynomials $A(x)$ and $B(x)$ and take the remainder modulo $x^N - 1$, the result is the polynomial that corresponds to the cyclic convolution of the vectors A and B. We write

$$A(x)B(x) \equiv A * B(x) \mod(x^N - 1).$$

The DFT can now simply be defined by

$$a_j = A(\alpha^j),$$

that is, the ith component a_j of the time domain vector a can be obtained by evaluating the frequency domain polynomial $A(x)$ for $x = \alpha^j$. We write the polynomial corresponding to the time domain vector a as

$$a(y) = a_0 + a_1 y + \cdots + a_{N-1} y^{N-1}.$$

Here, y is again a formal variable[9]. The IDFT is then given by

$$A_i = a(\alpha^{-i}).$$

As for the usual DFT, cyclic convolution in the time domain corresponds to elementwise multiplication in the frequency domain and vice versa. We may write this as

$$A * B \longleftrightarrow a \circ b$$
$$A \circ B \longleftrightarrow a * b$$

in $GF(2^m)$. Here we have written $a \circ b$ and $A \circ B$ for the *Hadamard* product, that is, the componentwise multiplication of vectors. We may define it formally as

$$A \circ B(x) = A_0 B_0 + A_1 B_1 x + \cdots + A_{N-1} B_{N-1} x^{N-1}.$$

[9]We may call it x as well.

Frequency domain encoding

We are now ready to define Reed–Solomon in the frequency domain. As an example, we start with the construction of the RS(7, 5, 3) code over $GF(8)$. We want to encode $K = 5$ useful data symbols A_i, $i = 0, 1, 2, 3, 4$ to a code word of length $N = 7$. The polynomial

$$A(x) = A_0 + A_1 x + A_2 x^2 + A_3 x^3 + A_4 x^4$$

of degree 4 cannot have more than four zeros. Thus, $a_j = A(\alpha^j)$ cannot be zero for more than four values of j. Then the time domain vector

$$a = (a_0, a_1, a_2, a_3, a_4, a_5, a_6)^T$$

has at least three nonzero components, that is, the *weight* of the vector is at least 3. The vector a is the RS code word. The Hamming distance of that code is then given by (at least) $D = 3$. Figure 3.20 shows this frequency domain encoding. The useful data are given by the data word (2, 7, 4, 3, 6) in decimal notation, where each symbol represents a bit triple according to Table 3.2. The code word in the frequency domain is given by

$$A = (2, 7, 4, 3, 6, 0, 0)^T.$$

Redundancy has been introduced by setting two frequencies equal to zero. This guarantees a minimum weight of three for the time domain code word, which is given by

$$a = (4, 6, 5, 1, 2, 3, 5)^T.$$

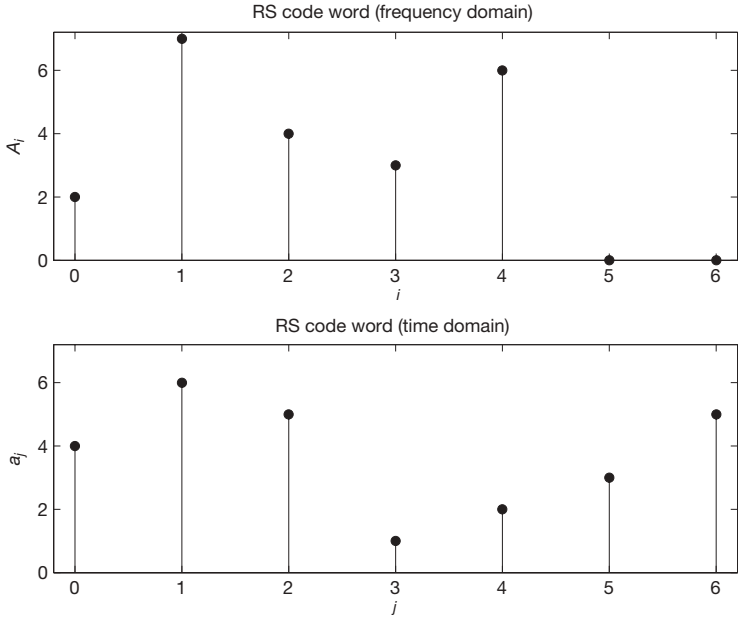

Figure 3.20 The RS(7, 5, 3) code word in the frequency domain.

A general RS(N, K, D) code over $GF(q)$ with $N = q - 1$ can be constructed in the following way. We consider polynomials

$$A(x) = A_0 + A_1 x + \cdots + A_{K-1} x^{K-1}$$

with K useful data symbols, that is, the last $N - K$ components A_i of the frequency domain vector A will be set equal to zero. We perform a DFT of length N. Since $A(x)$ has at most $K - 1$ zeros, $a_j = A(\alpha^j)$ can have at most $K - 1$ zeros. In other words, there are at least $D = N - K + 1$ nonzero components in the time domain code word

$$a = (a_0, a_1, \ldots, a_{N-1})^T.$$

Encoder and parity check

The encoder can be described by the matrix operation

$$\begin{pmatrix} a_0 \\ a_1 \\ a_2 \\ \vdots \\ a_{N-1} \end{pmatrix} = \begin{pmatrix} 1 & 1 & 1 & \cdots & 1 \\ 1 & \alpha & \alpha^2 & \cdots & \alpha^{K-1} \\ 1 & \alpha^2 & \alpha^4 & \cdots & \alpha^{2K-2} \\ \vdots & \vdots & \vdots & \ddots & \vdots \\ 1 & \alpha^{N-1} & \alpha^{2N-2} & \cdots & \alpha^{(K-1)(N-1)} \end{pmatrix} \begin{pmatrix} A_0 \\ A_1 \\ A_2 \\ \vdots \\ A_{K-1} \end{pmatrix},$$

that is, the generator matrix is the matrix of the first K columns of the DFT matrix. The condition that the last $N - K$ components A_i of the frequency domain vector A are equal to zero can be written as

$$\begin{pmatrix} 1 & \alpha^{-K} & \alpha^{-2K} & \cdots & \alpha^{-(N-1)K} \\ 1 & \alpha^{-(K+1)} & \alpha^{-2(K+1)} & \cdots & \alpha^{-(N-1)(K+1)} \\ \vdots & \vdots & \vdots & \ddots & \vdots \\ 1 & \alpha^{-(N-1)} & \alpha^{-2(N-1)} & \cdots & \alpha^{-(N-1)(N-K-1)} \end{pmatrix} \begin{pmatrix} a_0 \\ a_1 \\ a_2 \\ \vdots \\ a_{N-1} \end{pmatrix} = 0,$$

that is, the parity check matrix is the matrix of the last $N - K$ rows of the IDFT matrix.

The condition $A_i = a(\alpha^{-i}) = 0$ for $i = K, \ldots, N - 1$ means that the polynomial $a(x)$ has zeros for $x = \alpha^{-K}, \ldots, \alpha^{-(N-1)}$. We may thus factorize $a(x)$ as

$$a(x) = q(x) \prod_{i=K}^{N-1} \left(x - \alpha^{-i}\right)$$

with some quotient polynomial $q(x)$. We define the *generator polynomial*

$$g(x) = \prod_{i=K}^{N-1} \left(x - \alpha^{-i}\right).$$

The code (i.e. the set of code words) can thus equivalently be defined as those polynomials $a(x)$ that can be written as $a(x) = q(x)g(x)$.

We define the parity check polynomial

$$h(x) = \prod_{i=0}^{K-1} \left(x - \alpha^{-i}\right).$$

Obviously,

$$g(x)h(x) \equiv 0 \mod(x^N - 1)$$

and the code words $a(x)$ must fulfill the *parity check condition*

$$a(x)h(x) \equiv 0 \mod(x^N - 1).$$

3.3.4 Decoding of Reed–Solomon codes

Consider an RS(N, K, D) code with odd Hamming distance $D = 2t + 1$. We assume that a code word a has been transmitted, but another vector $r = (r_0, \ldots, r_{N-1})^T$ with elements $r_j \in GF(q)$ has been received. We write

$$r = a + e,$$

where $e = (e_0, \ldots, e_{N-1})^T$ with elements $e_j \in GF(q)$ has is the *error vector*. We write $E = (E_1, \ldots, E_{N-1})^T$ for the error in the frequency domain and $E(x)$ for the corresponding polynomial. We multiply the above equation by the parity check matrix. The result is the *syndrome vector*

$$\begin{pmatrix} S_1 \\ S_2 \\ S_3 \\ \vdots \\ S_{2t} \end{pmatrix} = \begin{pmatrix} 1 & \alpha^{-K} & \alpha^{-2K} & \cdots & \alpha^{-(N-1)K} \\ 1 & \alpha^{-(K+1)} & \alpha^{-2(K+1)} & \cdots & \alpha^{-(N-1)(K+1)} \\ \vdots & \vdots & \vdots & \ddots & \vdots \\ 1 & \alpha^{-(N-1)} & \alpha^{-2(N-1)} & \cdots & \alpha^{-(N-1)(N-K-1)} \end{pmatrix} \begin{pmatrix} e_0 \\ e_1 \\ e_2 \\ \vdots \\ e_{N-1} \end{pmatrix}.$$

If the syndrome is not equal to zero, then an error has occurred. We note that the syndrome is the vector of the last $N - K = 2t$ components of E, that is, $S_1 = E_K$, $S_2 = E_{K+1}$, $S_{2t} = E_{N-1}$. The task now is to calculate the error vector from the syndrome.

Error locations

First, we must find the error positions, that is, the set of indices

$$\sigma = \{j \,|\, e_j = E(\alpha^j) \neq 0\}$$

corresponding to the nonzero elements of the error vector. The complement of σ is given by

$$\rho = \{j \,|\, e_j = E(\alpha^j) = 0\}.$$

We define the *error location polynomial*

$$C(x) = \prod_{j \in \sigma} (x - \alpha^j)$$

and the polynomial of error-free positions

$$D(x) = \prod_{j \in \rho} (x - \alpha^j).$$

By construction,

$$C(x)D(x) \equiv 0 \mod(x^N - 1)$$

holds. Since ρ corresponds to the zeros of $E(x)$, it can be factorized as $E(x) = T(x)D(x)$ with some polynomial $T(x)$. It follows that

$$C(x)E(x) \equiv 0 \mod(x^N - 1).$$

Assume that exactly t errors have occurred. The zeros of $C(x)$ are then given by α^{j_l}, $l = 1, \ldots, t$. We write

$$X_l = \alpha^{-j_l}$$

for their inverses. The error positions are given by

$$j_l = -\log_\alpha X_l.$$

We now renormalize the error location polynomial in such a way that the first coefficient equals one, that is, we define

$$\Lambda(x) = \prod_{l=1}^{t}(1 - \alpha^{-j_l}x) = \prod_{l=1}^{t}(1 - X_l x) = \Lambda_0 + \Lambda_1 x + \Lambda_2 x^2 + \cdots + \Lambda_t x^t$$

with $\Lambda_0 = 1$. Obviously, $C(x)$ and $\Lambda(x)$ have the same zeros and

$$\Lambda(x)E(x) \equiv 0 \mod(x^N - 1)$$

holds, which means $\Lambda * E = 0$ for the cyclic convolution of the vectors. We may write this componentwise as

$$\sum_{i+j=k \,(\mathrm{mod}\, N)} E_i \Lambda_j = 0 \quad \forall k \in \{0, 1, 2, \ldots, N-1\}.$$

We write down the last t of these N linear equations and obtain

$$\begin{array}{cccccccc}
S_1\Lambda_t + & S_2\Lambda_{t-1} + & \ldots & +S_t\Lambda_1 & +S_t\Lambda_0 & = & 0 \\
S_2\Lambda_t + & S_3\Lambda_{t-1} + & \ldots & +S_{t+1}\Lambda_1 & +S_{t+2}\Lambda_0 & = & 0 \\
\vdots & \vdots & \vdots & \vdots & \vdots & \vdots & \vdots \\
S_t\Lambda_t + & S_{t+1}\Lambda_{t-1} + & \ldots & +S_{2t-1}\Lambda_1 & +S_{2t}\Lambda_0 & = & 0
\end{array}.$$

From $\Lambda_0 = 1$, we obtain

$$\begin{pmatrix} S_1 & S_2 & S_3 & \cdots & S_t \\ S_2 & S_3 & S_5 & \cdots & S_{t+1} \\ S_3 & S_4 & S_5 & \cdots & S_{t+2} \\ \vdots & \vdots & \vdots & \ddots & \vdots \\ S_t & S_{t+1} & S_{t+2} & \cdots & S_{2t-1} \end{pmatrix} \begin{pmatrix} \Lambda_t \\ \Lambda_{t-1} \\ \Lambda_{t-2} \\ \vdots \\ \Lambda_1 \end{pmatrix} = - \begin{pmatrix} S_{t+1} \\ S_{t+2} \\ S_{t+3} \\ \vdots \\ S_{2t} \end{pmatrix}.$$

This system of linear equations can be solved by matrix inversion. If less than t errors have occurred, the matrix will be singular. In that case, the polynomial $\Lambda(x)$ will be of degree $t - 1$ or less. Thus, we delete the first row and first column of the matrix and proceed this way until the remaining matrix is nonsingular. If the last equation $S_{2t-1}\Lambda_1 = -S_{2t}$ is still singular (i.e. $S_{2t-1} = 0$, but the syndrome is not equal to zero), then a decoding failure has occurred.

Once the coefficients of polynomial $\Lambda(x)$ have been found, we have to find the zeros X_l^{-1} of the polynomial. This will be simply done by evaluating the polynomial for all the N nonzero elements of $GF(q)$. This procedure is called *Chien search.* If less zeros than the degree of $\Lambda(x)$ or multiple zeros are found, then a decoding failure has occurred.

Error values

We are now ready to determine the values of the nonzero components of e. For simplicity, we consider the case that t errors have occurred. The treatment of less errors is similar. In the sum

$$E_i = \sum_{j=0}^{N-1} \alpha^{-ij} e_j$$

only those coefficients with $j \in \sigma$ occur, that is,

$$E_i = \sum_{l=1}^{t} \alpha^{-ij_l} e_{j_l} = \sum_{l=1}^{t} X_l^i e_{j_l}.$$

The syndrome coefficients $S_1 = E_K$, $S_2 = E_{K+1}$, $S_{2t} = E_{N-1}$ are known. We thus have $2t$ equations with t unknowns. We take only the first t of them, which leads to the system of linear equations given by

$$\begin{pmatrix} S_1 \\ S_2 \\ S_3 \\ \vdots \\ S_t \end{pmatrix} = \begin{pmatrix} X_1^K & X_2^K & X_3^K & \cdots & X_l^K \\ X_1^{K+1} & X_2^{K+1} & X_3^{K+1} & \cdots & X_l^{K+1} \\ X_1^{K+2} & X_2^{K+2} & X_3^{K+2} & \cdots & X_l^{K+2} \\ \vdots & \vdots & \vdots & \ddots & \vdots \\ X_1^{K+t-1} & X_2^{K+t-1} & X_3^{K+t-1} & \cdots & X_l^{K+t-1} \end{pmatrix} \begin{pmatrix} e_{j_1} \\ e_{j_2} \\ e_{j_3} \\ \vdots \\ e_{j_t} \end{pmatrix}.$$

The Vandermonde matrix is nonsingular and can thus be inverted, which provides us with the error vector e. The corrected code word will then be obtained as $a = r - e$.

3.4 Bibliographical Notes

For a more detailed treatment of channel coding, we refer to the text books (Blahut 1983; Bossert 1999; Clark and Cain 1988; Lin and Costello 1983; Wicker 1995). A delightful introduction into the conceptional ideas of channel coding can be found in the paper (Massey 1984). For a conceptional understanding of concatenated coding, we refer to the classical paper (Forney 1966). For a conceptional understanding of convolutional codes, we refer to (Forney 1970). It is interesting to note that this paper already described RSC encoders before they fell into oblivion for more than 30 years until turbo codes were discovered. The Viterbi algorithm, which is the MLSE for convolutional codes, has been developed by Viterbi (1967), even though the author did not point out that it is really the *optimum* MLSE receiver (note the word *asymptotically optimum* in the title of that paper). The conceptual understanding of the Viterbi algorithm as a MLSE receiver has been established by Forney (1973). Punctured convolutional codes can be found in classical text books (see e.g. (Clark and Cain

1988)). For their application, see (Hagenauer 1988). The concept of log-likelihood ratios is well established in probability theory. However, their usefulness for channel coding and their intuitively amazing visualization has been established in great parts by Hagenauer and coworkers (Hagenauer 1988, 1995; Hagenauer and Hoeher 1989; Hagenauer *et al.* 1996). It is interesting to note that the concept of soft-output decoding introduced as BCJR algorithm (Bahl *et al.* 1974) is nearly as old as the Viterbi algorithm, but seemingly it was too early for an application at that time. A much more popular soft-output decoder was established 25 years later (Hagenauer and Hoeher 1989) as the SOVA. The first turbo code simulations were done with the SOVA, but the BCJR algorithm turned out to be more efficient for that application. Turbo codes were introduced a decade ago (Berrou *et al.* 1993), a great step to their conceptional understanding is the paper (Hagenauer *et al.* 1996). RS codes have been developed by Reed and Solomon (1960). They are treated extensively in the text books cited above. Trellis coded modulation goes back to (Ungerboeck 1982). It is treated in the text books cited above (see also (Biglieri *et al.* 1991)). An interesting overview about their applications can be found in (Wicker and Bhargava 2001). Very enlightening and recommendable overviews about the application of channel coding for deep space communication can be found in (Massey 1992) and (McEliece and Swanson 2001). A concatenated coding scheme with an inner convolutional code and an outer RS code has been standardized for deep space communications (CCSDS 1987). Improvements for the corresponding decoder by using iterative decoding with reliability information are described in (Hagenauer *et al.* 2001).

3.5 Problems

1. Prove the identity

$$\log\left(\mathrm{e}^{x}+\mathrm{e}^{y}\right)=\max\left(x,\,y\right)+\log\left(1+\mathrm{e}^{-|x-y|}\right).$$

2. Consider a transmission setup with four possible signals given by the columns of the matrix

$$\mathbf{X}=\begin{pmatrix}1 & 1 & -1 & -1\\ 1 & -1 & 1 & -1\\ 1 & -1 & -1 & 1\end{pmatrix},$$

   which is an SPC(3, 2, 2) code with BPSK modulation. Find an example for which the ML receiver takes a different decision for the first bit than the MAP receiver.

3. Let $f(x,\,y)$ be a function of two real variables x and y defined by

$$f(x,\,y)=\log\left(\frac{1+\mathrm{e}^{x}\mathrm{e}^{y}}{\mathrm{e}^{x}+\mathrm{e}^{y}}\right).$$

   Show that

$$f(x,\,y)\approx\mathrm{sign}(x)\mathrm{sign}(y)\cdot\min(|x|\,,\,|y|)$$

   if either $|x|\ll|y|$ or $|x|\gg|y|$.

4

OFDM

4.1 General Principles

4.1.1 The concept of multicarrier transmission

Let us consider a digital transmission scheme with linear carrier modulation (e.g. M-PSK or M-QAM) and a symbol duration denoted by T_S. Let B be the occupied bandwidth. Typically, B is of the order of T_S^{-1}, for example, $B = (1+\alpha)T_S^{-1}$ for raised-cosine pulses with rolloff factor α. For a transmission channel with a delay spread τ_m, a reception free of intersymbol interference (ISI) is only possible if the condition

$$\tau_m \ll T_S$$

is fulfilled. As a consequence, the possible bit rate $R_b = \log_2(M)T_S^{-1}$ for a given single carrier modulation scheme is limited by the delay spread of the channel.

The simple idea of multicarrier transmission to overcome this limitation is to split the data stream into K substreams of lower data rate and to transmit these data substreams on adjacent *subcarriers*, as depicted in Figure 4.1 for $K = 8$. This can be regarded as a transmission parallel in the frequency domain, and it does not affect the total bandwidth that is needed. Each subcarrier has a bandwidth B/K, while the symbol duration T_S is increased by a factor of K, which allows for a K times higher data rate for a given delay spread. The factor K, however, cannot be increased arbitrarily, because too long symbol durations make the transmission too sensitive against the time incoherence of the channel that is related to the maximum Doppler frequency $\nu_{\max}$ (see the discussion in Section 2.2). There, we state that the condition

$$\nu_{\max} T_S \ll 1$$

must be fulfilled. Both conditions can only be valid simultaneously if the coherency factor $\kappa = \nu_{\max}\tau_m$ fulfills the condition $\kappa \ll 1$. For a given and sufficiently small factor κ, one should expect that there exists a symbol duration T_S that satisfies both requirements together to give the best possible transmission conditions for that channel. We may then choose this optimal symbol duration that is matched to the channel and parallelize the given data stream in an appropriate way.

Theory and Applications of OFDM and CDMA Henrik Schulze and Christian Lüders

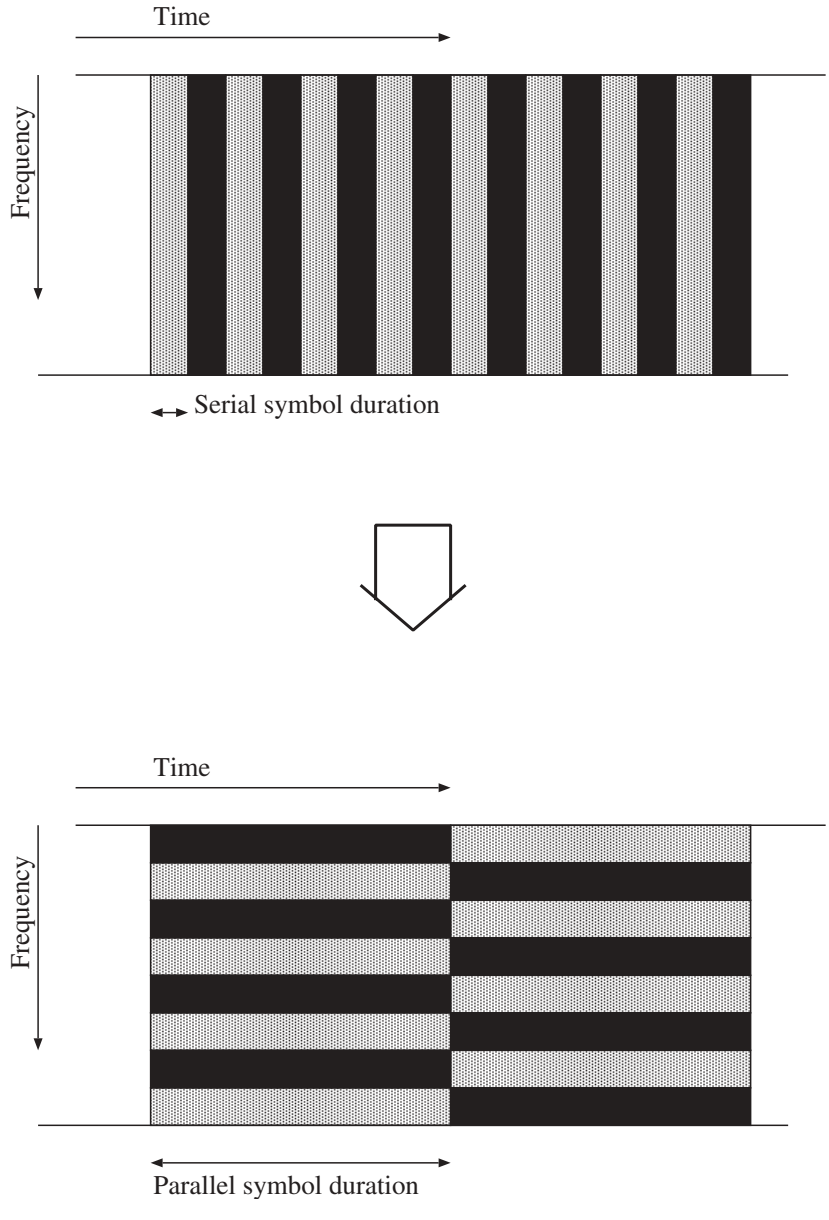

Figure 4.1 The multicarrier concept.

There are two possible ways to look at (and to implement) this idea of multicarrier transmission. Both are equivalent with respect to their transmission properties. Even though mathematically closely related, they differ slightly from the conceptual point of view. The first one emphasizes the multicarrier concept by having K individual carriers that are modulated independently. This concept is the favorite textbook point of view. The second

one is based on a filter bank of K adjacent bandpass filters that are excited by a parallel data stream, leading to a transmission parallel in frequency. This concept is usually implemented in practical systems.

The first concept keeps the subcarrier frequency fixed and considers the modulation in time direction for each subcarrier. The second one keeps a time slot of length T_S fixed and considers modulation in frequency direction for each time slot.

In the first setup, the data stream is split up into K parallel substreams, and each one is modulated on its own subcarrier at frequency f_k in the complex baseband, described by the complex harmonic wave $\exp(j2\pi f_k t)$. We denote the complex (e.g. PSK or QAM) modulation symbols by s_{kl}, where k is the frequency index and l is the time index. With a baseband transmission pulse $g(t)$, this setup can be visualized by Figure 4.2: The parallel data stream excites replicas of the same pulse-shaping filter $g(t)$, and the filtered signals are modulated on the different carriers and summed up before transmission. The complex baseband signal is then given by the expression

$$s(t) = \sum_k \mathrm{e}^{j2\pi f_k t} \sum_l s_{kl} g(t - lT_S), \tag{4.1}$$

where T_S is the parallel symbol duration. To keep the notation flexible, we do not specify the domain of the summation indices. If it is convenient, the time index l may run from zero or minus infinity to infinity. Since every real transmission starts and stops at some time instant, it is more realistic to let l run from 0 to $L-1$, where L is an integer. The frequency index may only run over a limited domain of, say, K different frequencies. From the mathematical point of view, we may choose $k = 0, 1, \ldots, K-1$. The engineer, however, would prefer to have f_0 in the middle, corresponding to DC in the complex baseband and to the center frequency f_c in the passband, with negative k for the lower sideband and positive k for the upper sideband. For reasons of symmetry, we may then choose the number of carriers to

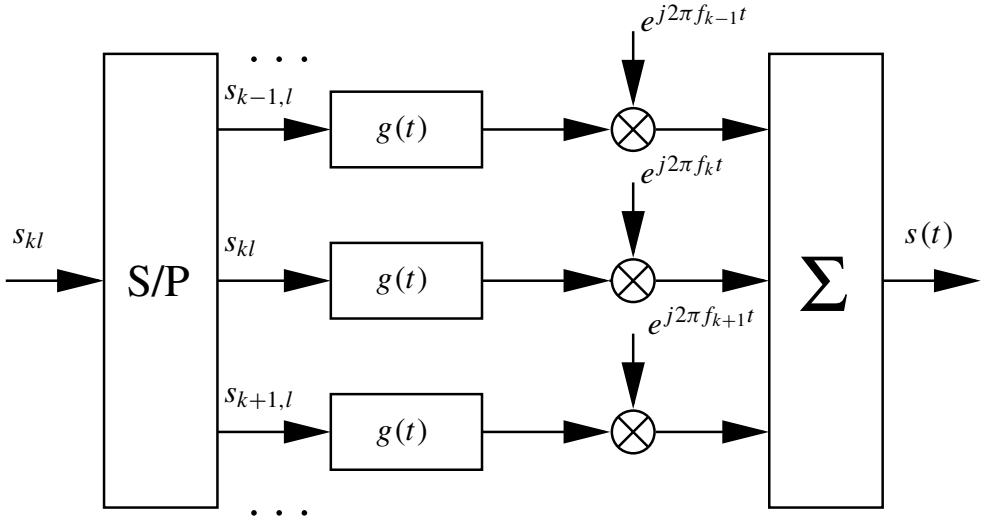

Figure 4.2 Block diagram for multicarrier transmission: Version 1.

be $K+1$, where K is an even integer, and let $k = 0, \pm 1, \pm 2, \ldots, \pm K/2$. The passband signal is then given by

$$\tilde{s}(t) = \Re\left\{\sqrt{2}\,\mathrm{e}^{j2\pi f_c t} s(t)\right\} = \Re\left\{\sqrt{2}\sum_k \mathrm{e}^{j2\pi(f_c+f_k)t}\sum_l s_{kl}\, g(t - lT_S)\right\}.$$

For reasons due to implementation, in practical systems, the DC component will sometimes be left empty, that is, only the subcarriers at $k = \pm 1, \pm 2, \ldots, \pm K/2$ are used.

In the second setup, we start with a base transmit pulse $g(t)$. We obtain frequency-shifted replicas of this pulse as

$$g_k(t) = \mathrm{e}^{j2\pi f_k t} g(t),$$

that is, if $g(t) = g_0(t)$ is located at the frequency $f = 0$, then $g_k(t)$ is located at $f = f_k$. In contrast to the first scheme, for each time instant l, the set of K (or $K+1$) modulation symbols is transmitted by using *different* pulse shapes $g_k(t)$: the parallel data stream excites a filter bank of K (or $K+1$) different bandpass filters. The filter outputs are then summed up before transmission. This setup is depicted in Figure 4.3. The transmit signal in the complex baseband representation is given by

$$s(t) = \sum_l \sum_k s_{kl}\, g_k(t - lT_S).$$

For the domain of the summation indices k and l, the same remarks apply as for the discussion of the first setup. We define

$$g_{kl}(t) = g_k(t - lT_S) = \mathrm{e}^{j2\pi f_k(t-lT_S)} g(t - lT_S)$$

to get the compact expression

$$s(t) = \sum_{kl} s_{kl}\, g_{kl}(t). \tag{4.2}$$

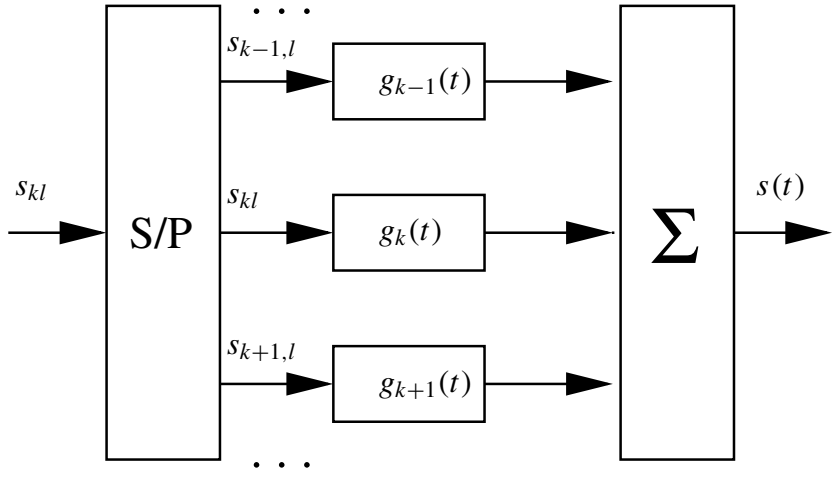

Figure 4.3 Block diagram for multicarrier transmission: Version 2.

It is obvious that we come back to the first setup if we replace the modulation symbols s_{kl} by $s_{kl}\mathrm{e}^{-j2\pi f_k l T_S}$ in Equation (4.1). Such a time-frequency-dependent phase rotation does not change the performance, so both methods can be regarded as equivalent. However, the second – the filter bank – point of view is closer to implementation, especially for the case of OFDM, where the filter bank is just an FFT, as it will be later. In the following discussion, we will refer to the second point of view.

4.1.2 OFDM as multicarrier transmission

So far, nothing has been said about the shape of the base transmission pulse $g(t)$. In Chapter 1, we have seen that it is very convenient to have an orthogonal transmit base. It therefore seems to be quite natural to choose the $g_{kl}(t)$ of Equation (4.2) in such a way that they are orthogonal in time and frequency, that is, we require

$$\langle g_{kl}, g_{k'l'} \rangle = \delta_{kk'}\delta_{ll'}. \tag{4.3}$$

Nonorthogonal bases (e.g. Gaussian) are possible and may have interesting properties, see for example, (Kammeyer *et al.* 1992). We will restrict ourselves on pulses with the property (4.3). As discussed in depth in Chapter 1, orthogonality ensures that the modulation symbol can be recovered from the transmit signal without ISI, that is, the detector $\mathcal{D}_{kl}$ for $g_{kl}(t)$ has just the modulation symbol s_{kl} as its output:

$$\mathcal{D}_{kl}[s] = \langle g_{kl}, s \rangle = s_{kl}.$$

In principle, there are two obvious approaches to satisfy the orthogonality condition for multicarrier transmission. We recall that two pulses are always orthogonal if they do not overlap either in time or in frequency domain, and that a pulse cannot be strictly band limited *and* time limited. Thus, we must decide on one of these two options.

The first approach is seemingly the most straightforward one to implement the idea of multicarrier modulation. We choose band-limited pulses that are orthogonal in time. In Subsection 1.1.2, we defined time-orthogonal Nyquist bases. The most important examples for a strictly band-limited Nyquist base are the (square root) raised-cosine pulses. The bandwidth B is related to the rolloff factor α by $BT_S = 1 + \alpha$. Let $g(t)$ be such a pulse that is concentrated in the frequency domain around $f = 0$, so that we may write $g(t) = g_0(t)$, that is, this is the pulse corresponding to the frequency index $k = 0$. The pulses $g_{0l}(t) = g_0(t - lT_S)$ with $l \in \{0, \pm 1, \pm 2, \ldots.\}$ are a Nyquist base, that is, they satisfy the orthogonality condition

$$\langle g_{0l}, g_{0l'} \rangle = \delta_{ll'}$$

in the time domain. With

$$f_k = k\frac{1+\alpha}{T_S},$$

we define

$$g_k(t) = \mathrm{e}^{j2\pi f_k t} g_0(t)$$

and

$$g_{kl}(t) = g_k(t - lT_S).$$

Since these pulses are strictly separated in frequency for different k, it is obvious that the condition (4.3) is fulfilled. This multicarrier modulation setup is depicted in Figure 4.4

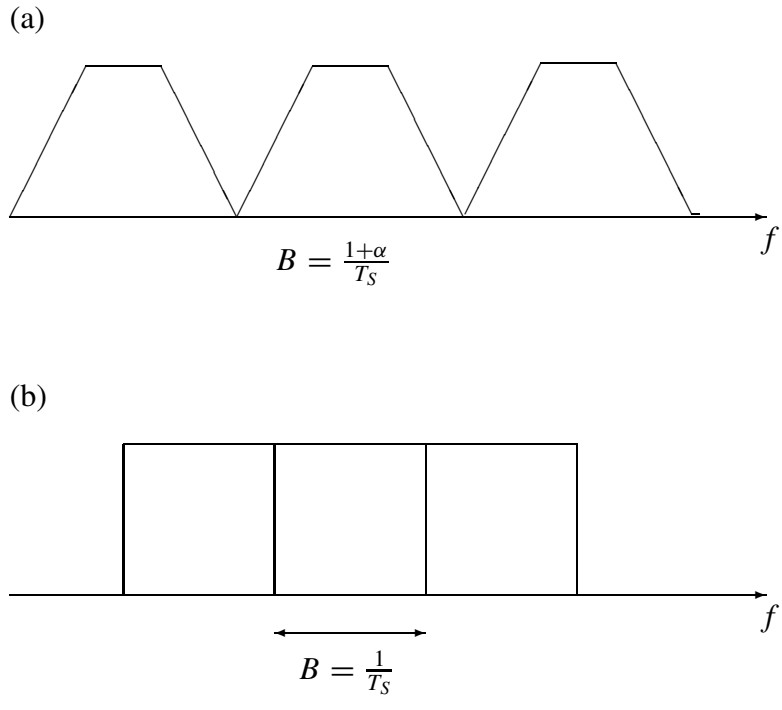

Figure 4.4 Multicarrier spectrum.

for $\alpha = 0.5$ and $\alpha = 0$. In this figure, we have replaced the raised-cosine spectrum by a trapezoidal one, which also corresponds to a Nyquist base. The case $\alpha = 0$ corresponding to an ideal rectangular spectral shape and sinc shaping in time domain and is spectrally most efficient, but not possible to be implemented in practice.

The second approach is to choose time-limited pulses that are orthogonal in frequency. In the example in Subsection 1.1.3, we have already seen that the time-limited complex exponentials of the Fourier series are such a base of time-limited orthogonal pulses. These are just the base pulses for OFDM transmission. However, there are more choices for time-limited orthogonal base pulses. We recall that the Nyquist base discussed in Subsection 1.1.3 fulfills just the condition that one base pulse and its periodically time-shifted replicas are orthogonal. Since the time and the frequency domain are mathematically equivalent, we may state the same orthogonality condition in the frequency domain. Doing this, we obtain strictly time-limited pulses $g_{kl}(t)$ that are orthogonal in frequency by the following construction: choose $g(t)$ to be a pulse that is strictly limited to the time interval[1] $[-T_S/2, T_S/2]$ of duration T_S in such a way that $|g(t)|^2$ has a raised-cosine shape with rolloff factor α. Let $G(f)$ be the pulse in the frequency domain. We define

$$f_k = k\frac{1+\alpha}{T_S}$$

[1]If this is more convenient, we may use the interval $[0, T_S]$ as well.

and the frequency-shifted pulse

$$g_k(t) = \mathrm{e}^{j2\pi f_k t} g(t)$$

written in the frequency domain as

$$G_k(f) = G(f - f_k).$$

From the discussion of the Nyquist pulses (with time and frequency domain interchanged), it follows immediately that

$$\langle G_k, G_{k'} \rangle = \langle g_k, g_{k'} \rangle = \delta_{kk'}.$$

We define

$$g_{kl}(t) = g_k(t - lT_S).$$

Using the fact that these pulses are strictly separated in time for different l, it can easily be verified that the condition (4.3) is fulfilled. This multicarrier modulation setup is depicted in Figure 4.5 for $\alpha = 0$. This corresponds to the Fourier bases discussed above. Note that there is always a spectral overlap of subcarriers, but the carriers can be separated due to their orthogonality.

In contrast to the method discussed earlier, $\alpha = 0$ is possible to be implemented with a reasonable accuracy in practical systems. Even though every orthogonal multicarrier pulse transmission as discussed above deserves to be called OFDM (*orthogonal frequency division*

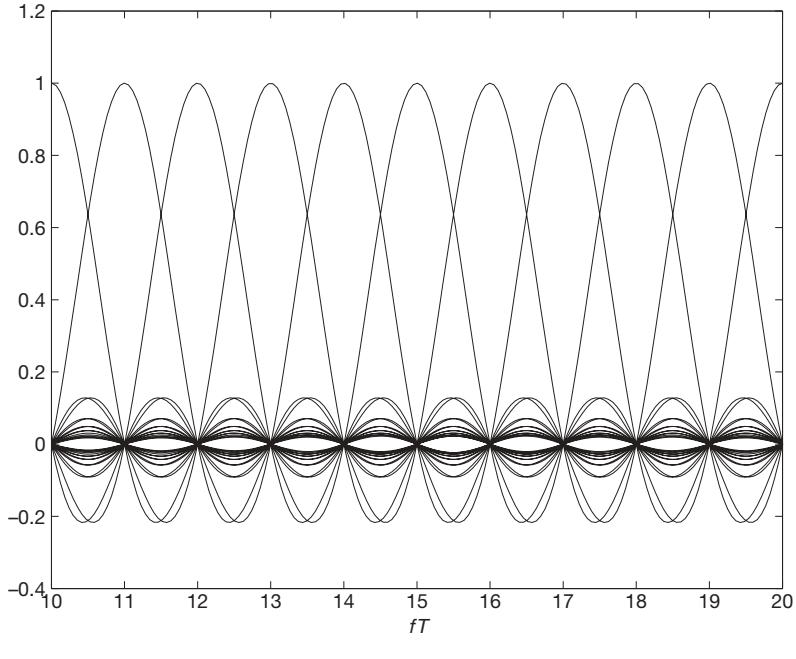

Figure 4.5 Orthogonal overlapping spectral shapes for OFDM.

multiplexing), it is indeed this case with $\alpha = 0$ which is the (narrow-sense) OFDM, because it is usually implemented. In that case, $g(t)$ is just a rectangle over an interval of length T_S, which we choose as $[0, T_S]$ for convenience. Then $f_k = k/T_S$, and the frequency-shifted pulses are just the Fourier base functions

$$g_k(t) = \sqrt{\frac{1}{T}} \exp\left(j2\pi \frac{k}{T} t\right) \Pi\left(\frac{t}{T} - \frac{1}{2}\right) \tag{4.4}$$

over the Fourier period of length $T = T_S$. OFDM transmission is therefore just a Fourier synthesis for every time interval, where the information is contained in the Fourier coefficients s_{kl}. For a receive signal $r(t)$, the detector outputs $\mathcal{D}_k[r] = \mathcal{D}_{g_k}[r]$ at frequency number k for $l = 0$ are just the results of the Fourier analysis given by

$$\mathcal{D}_k[r] = \langle g_k, r \rangle = \sqrt{\frac{1}{T}} \int_0^T \exp\left(-j2\pi \frac{k}{T} t\right) r(t)\, \mathrm{d}t, \tag{4.5}$$

which exactly recovers s_{k0} for the ideal transmission channel with $r(t) = s(t)$. For any general l, $\mathcal{D}_{kl}[r] = \langle g_{kl}, r \rangle$ is the Fourier analyzer output for the frequency number k at the time interval shifted by lT_S. We note that for this narrow-sense OFDM the two concepts of Figures 4.2 and 4.3 are equivalent because $f_k = 1/T = 1/T_S$ holds. This property will be lost when a guard interval is introduced (see Subsection 4.1.4).

The power density spectrum of an OFDM signal for $K + 1 = 97$ subcarriers is depicted in Figure 4.6. On the linear scale, it looks very similar to a rectangular spectrum. However, the linear scale is indeed a very flattering presentation of the OFDM spectrum. Note that

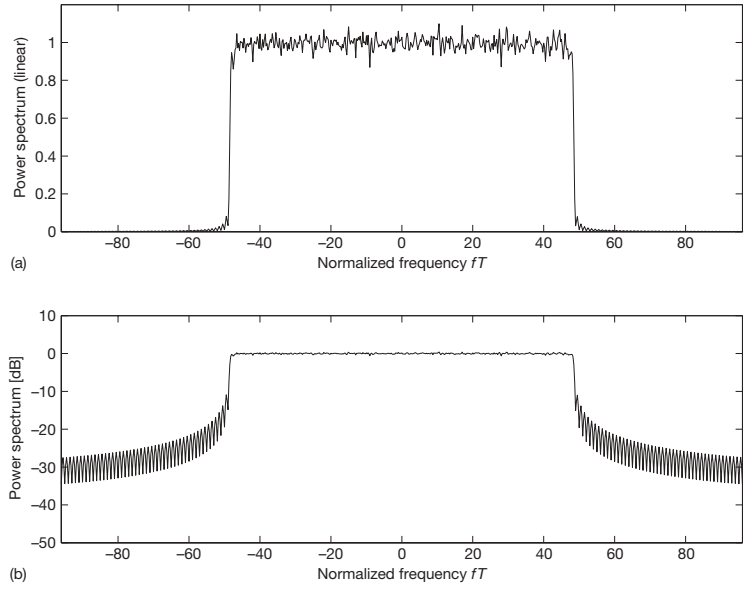

Figure 4.6 The power density spectrum of an OFDM signal on a linear scale (a) and on a logarithmic scale (b).

because of the rectangular pulse shape, at every subcarrier frequency $f_k = k/T$, the spectral shape is given by a sinc function. This can be seen very well at the edges of the spectrum. These edge effects are indeed a severe item and much care must be taken for them in practice. One usually reduces them by applying some filtering or smoothing (see Subsection 4.2.1). The relative size (compared to the bandwidth) of the edge effect region becomes smaller as the number of carriers K (or $K + 1$) increases. Therefore, the bandwidth needed to transmit K complex symbols in a time slot of length T grows linearly as $B \approx K/T + C$ with some constant C that is due to the edge effects. Thus, ideal narrow-sense OFDM in the limit $K \to \infty$ has the same spectral efficiency as the ideal sinc pulse shaping in time domain.

4.1.3 Implementation by FFT

The narrow-sense OFDM with the Fourier base is very simple to implement. If we consider one time interval (e.g. that for $l = 0$), the transmit signal is given by

$$s(t) = \frac{1}{\sqrt{T}} \sum_{k=-K/2}^{K/2} s_k \exp\left(j2\pi \frac{k}{T} t\right) \Pi\left(\frac{t}{T} - \frac{1}{2}\right).$$

This means that, for each time interval of length T, OFDM is just a Fourier synthesis for that period. The perfectly synchronized receiver just performs a Fourier analysis to recover the data symbols s_k from the signal:

$$s_k = \langle g_k, s \rangle = \frac{1}{\sqrt{T}} \int_0^T \exp\left(-j2\pi \frac{k}{T} t\right) s(t)\, \mathrm{d}t.$$

A Fourier analysis is preferably implemented by means of a fast Fourier transform (FFT), a synthesis by the inverse fast Fourier transform (IFFT), leading to a setup as depicted in Figure 4.7. The stream of digitally modulated symbols s_{kl} is divided into blocks of length K (or $K + 1$), discretely Fourier transformed by the IFFT, digital–analog converted and then transmitted. The FFT length N_{FFT} must be chosen to be significantly larger than K to ensure that the edge effects are neglectible at half the sampling frequency and to ensure that the shape of the reconstruction filter of the DAC (digital-to-analog converter) does not affect the significant part of the spectrum. Furthermore, the alias spectra must be suppressed. To give a concrete example, in the European DAB (Digital Audio Broadcasting) and in the DVB-T (Digital Video Broadcasting-Terrestrial) system (EN300401 2001a; EN300744 2001b; Hoeg and Lauterbach 2003), an FFT with $N_{\mathrm{FFT}} = 2048$ is used (among other FFT modes), and the number of modulated carriers is of the order $K \approx 1500$ and $K \approx 1700$, respectively. The $N_{\mathrm{FFT}} - K$ remaining spectral coefficients outside the transmission band are set to zero. At the receiver, the baseband signal will be analog-to-digital converted. Then, for each block of N_{FFT} samples, an FFT of that length is performed, and the K useful coefficients will be extracted from the N_{FFT} spectral coefficients.

This picture is very suggestive from a practical point of view and one feels easily inclined to believe that it should work, because every block on the transmit site has its corresponding inverse on the receive site, so all the data should be perfectly recovered if every block works perfectly. Without explaining anything about orthogonality, the picture is also suited to convince a practical engineer that the concept of OFDM should work.

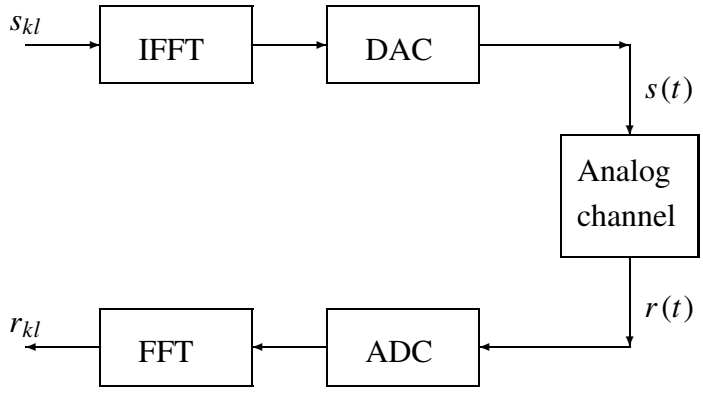

Figure 4.7 OFDM implementation by FFT.

However, the concept of orthogonality is only hidden in this picture under the cover of Fourier transform theory.

One should keep in mind that, for principal reasons, the block diagram of Figure 4.7 can never perfectly reflect the setup given by the theory. This is because the ideal OFDM signal is not strictly band limited due to the sinc shapes in the spectrum, while an analog signal can only be perfectly represented by its samples if it is strictly band limited. However, the problem of aliasing is a familiar one that occurs in many communications systems. For OFDM transmission, special care must be taken because of the poor spectral decay (see Subsection 4.2.1).

4.1.4 OFDM with guard interval

So far, we have always assumed perfect synchronization between transmitter and receiver. In a frequency-selective multipath fading channel, synchronization mismatches are typically of significant order, because every echo component of the signal is a poorly synchronized signal. As a consequence, the base pulses of the original OFDM signal and the delayed version of the signal are no longer orthogonal. This leads to severe intersymbol interference (ISI) in time and frequency as well because the detector output $\mathcal{D}_{kl}[s_\tau] = \langle g_{kl}, s_\tau \rangle$ at frequency number k and time slot l of the delayed signal $s_\tau(t) = s(t - \tau)$ with $0 < \tau < T$ has ISI contributions from pulses at all subcarrier frequencies at time slot l and $l - 1$. This property, which is a consequence of the loss of orthogonality due to the overlap of spectral components, would seemingly disqualify narrow-sense ODFM as a useful technique in a multipath channel. There is, however, a simple trick that modifies the transmit signal in such a way that the orthogonality is preserved in a certain manner in the presence of multipath signal components.

The idea is to introduce a *guard interval* (sometimes called *cyclic prefix*). By doing this, the symbol will be cyclically extended from the original harmonic wave of the Fourier period T by a guard interval of length Δ to become a harmonic of the same frequency and phase, but of duration $T_S = T + \Delta$. As depicted in Figure 4.8, this means that we copy a piece of length Δ from the end of the symbol and paste it in front of the signal. To express

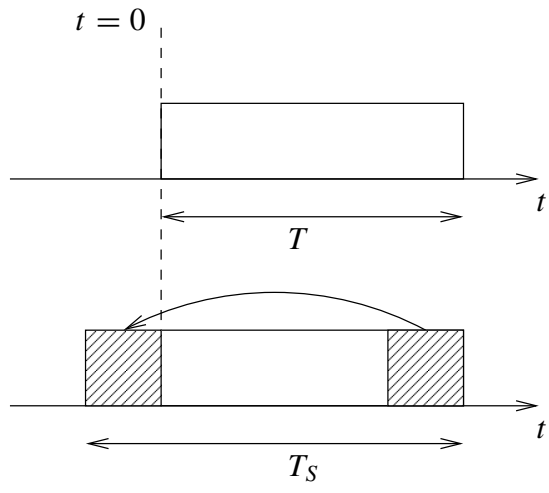

Figure 4.8 Introducing a guard interval.

this more formally, we replace the base pulse $g_k(t)$ as given by Equation (4.4) by a new base pulse defined by

$$g'_k(t) = \sqrt{\frac{1}{T_S}} \exp\left(j2\pi \frac{k}{T} t\right) \Pi\left(\frac{t+\Delta}{T_S} - \frac{1}{2}\right). \tag{4.6}$$

Note that the complex exponential remains exactly the same. The frequency is still $f_k = k/T$, and the phase is the same. Only the interval where the pulse does not vanish has been extended from $t \in [0, T)$ to $t \in [-\Delta, T)$. For convenience, we have chosen the factor in front in such a way that the energy of the pulse remains normalized to one. The transmit signal is then given by

$$s(t) = \sum_{kl} s_{kl} g'_{kl}(t) \tag{4.7}$$

with

$$g'_{kl}(t) = g'_k(t - lT_S). \tag{4.8}$$

We first note that these *transmit* pulses $g'_{kl}(t)$ by themselves are *not* pairwise orthogonal to each others. However, at the receiver, we work with a set of orthonormal *detector* pulses given by

$$g_{kl}(t) = g_k(t - lT_S),$$

where the $g_k(t)$ are still the Fourier base functions for the interval of length T as defined in Equation (4.4). This means that the *Fourier analysis* at the receiver works with the same analysis window of length T, but it will be performed once during the time period T_S instead of once during the time period T. As depicted in Figure 4.9, there is now a gap (or relaxation time) of length Δ between two adjacent analysis windows. We will see in the following text that it is just this gap together with the cyclically extended transmit pulse that allows a synchronization mismatch (and therefore, also echoes) of maximal duration

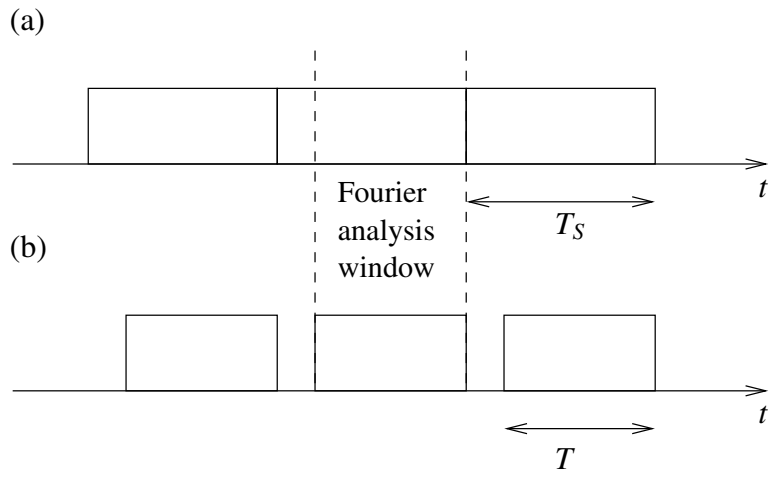

Figure 4.9 OFDM with guard interval: (a) Transmit pulses (b) Detector pulses.

$\tau = \Delta$, corresponding to a shift to the right of the signal in part (a) of Figure 4.9. The output of the detector for $g_{kl}(t)$, given that the pulse $g'_{k'l'}(t)$ has been transmitted, is

$$\left\langle g_{kl}, g'_{k'l'} \right\rangle = \sqrt{\frac{T}{T_S}}\, \delta_{kk'} \delta_{ll'}.$$

This means that the transmit base pulses $g_{kl}(t)$ and the detector base pulses $g'_{k'l'}(t)$ are orthogonal unless both the time and the frequency index are identical. Note that if they are identical the output does not take the value 1 but the smaller value $\sqrt{T/T_S}$. This can be understood as a waste of energy by transmitting a part of the symbol (i.e. the guard interval) that is not used for detection.

Now let $g'_{kl,\tau}(t) = g'_{kl}(t - \tau)$ with $0 < \tau < \Delta$ denote a base pulse delayed by τ. By writing down the corresponding integral, we easily see that

$$\left\langle g_{kl}, g'_{k'l',\tau} \right\rangle = \sqrt{\frac{T}{T_S}}\, \mathrm{e}^{-j2\pi f_k \tau}\, \delta_{kk'} \delta_{ll'}. \tag{4.9}$$

This means that – as long $\tau < \Delta$ holds – the orthogonality between the transmit and detect pulses for different indices is still preserved, and the detector output for the same index is only affected by a frequency-dependent phase factor. Now, let $s(t)$ be an OFDM signal given by Equation (4.7) and let $r(t) = s(t - \tau)$ with $0 < \tau < \Delta$ be the receive signal, which is just a delayed version of that signal. From the above equation and Equation (4.7), we obtain

$$\langle g_{kl}, r \rangle = \sqrt{\frac{T}{T_S}}\, \mathrm{e}^{-j2\pi f_k \tau}\, s_{kl},$$

that is, the transmit symbol s_{kl} is recovered without ISI, but only rotated by the phase factor. This phase factor cancels out for differential demodulation. For coherent demodulation, it must be determined by the channel estimation.

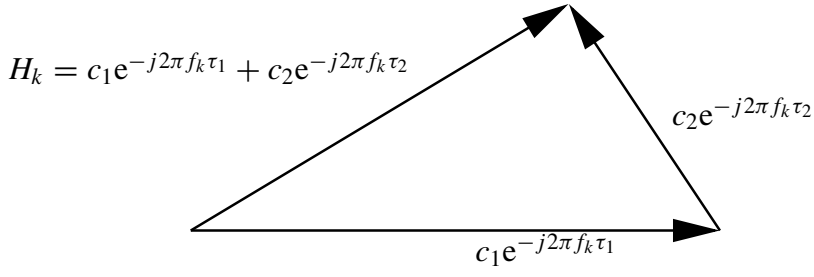

Figure 4.10 Signal plus echo.

If the received signal is the superposition of two delayed versions of the transmitted signal, that is, given by $r(t) = c_1 s(t - \tau_1) + c_2 s(t - \tau_2)$ with some complex constants c_1 and c_2, then s_{kl} will again be recovered without ISI if their delays do not exceed the guard interval. But they will be affected by a complex multiplicative factor $H_k = c_1 e^{-j2\pi f_k \tau_1} + c_2 e^{-j2\pi f_k \tau_2}$, which is the superposition of the phasors corresponding to the two echo paths (see Figure 4.10). The detector output is then given by

$$\mathcal{D}_{kl}[r] = \langle g_{kl}, r \rangle = \sqrt{\frac{T}{T_S}}\, H_k\, s_{kl}.$$

For a superposition of N such echo paths, we obtain the same expression with H_k given by

$$H_k = \sum_{n=1}^{N} c_n e^{-j2\pi f_k \tau_n}.$$

We now assume a time-variant channel given by a time-variant impulse response $h(\tau, t)$. We assume that $h(\tau, t) = 0$ for $\tau < 0$ and for $\tau > \Delta$. The corresponding time-variant transfer function $H(f, t)$ is then given by

$$H(f, t) = \int_0^{\Delta} e^{-j2\pi f \tau} h(\tau, t)\, d\tau.$$

The receive signal without noise is given by

$$r(t) = \int_0^{\Delta} h(\tau, t) s(t - \tau)\, d\tau.$$

We further assume that the channel is slowly time-variant so that it can be approximated to be time independent during the time slot number l, that is, $H(f, t) \approx H_l(f)$ and $h(\tau, t) \approx h_l(\tau)$ with

$$H_l(f) = \int_0^{\Delta} e^{-j2\pi f \tau} h_l(\tau)\, d\tau$$

during the OFDM symbol number l of length T_S. We now calculate the detector output for a base pulse transmitted over that channel, which is formally given by

$$\mathcal{D}_{kl}[h_{l'} * g'_{k'l'}] = \left\langle g_{kl}, h_{l'} * g'_{k'l'} \right\rangle.$$

This is the twofold integral

$$\mathcal{D}_{kl}[h_l * g'_{k'l'}] = \int_0^T \mathrm{d}t\, g^*_{kl}(t) \int_0^\Delta \mathrm{d}\tau\, h_{l'}(\tau) g'_{k'l'}(t-\tau)$$

with the first integral corresponding to the scalar product and the second one corresponding to the convolution. We change the order of integration and obtain

$$\mathcal{D}_{kl}[h_l * g'_{k'l'}] = \int_0^\Delta \mathrm{d}\tau\, h_{l'}(\tau) \int_0^T \mathrm{d}t\, g^*_{kl}(t) g'_{k'l'}(t-\tau).$$

The second integral is just $\langle g_{kl}, g'_{k'l',\tau}\rangle$. From Equation (4.9) we get

$$\mathcal{D}_{kl}[h_l * g'_{k'l'}] = \int_0^\Delta \mathrm{d}\tau\, h_{l'}(\tau) \sqrt{\frac{T}{T_S}}\, \mathrm{e}^{-j2\pi f_k \tau}\, \delta_{kk'}\delta_{ll'}$$

that is,

$$\mathcal{D}_{kl}[h_l * g'_{k'l'}] = \sqrt{\frac{T}{T_S}}\, H_l(f_k)\, \delta_{kk'}\delta_{ll'}.$$

The detector output at time l and frequency k for the noise-free receive signal $r(t)$ is then given by

$$\langle g_{kl}, r\rangle = \sqrt{\frac{T}{T_S}}\, H_l(f_k)\, s_{kl}. \tag{4.10}$$

We define $r_{kl} = \langle g_{kl}, r\rangle$ and $c_{kl} = H_l(f_k)$. Then, the OFDM transmission with guard interval in a noisy slowly fading channel can be described by the discrete channel model

$$r_{kl} = \sqrt{\frac{T}{T_S}}\, c_{kl} s_{kl} + n_{kl}, \tag{4.11}$$

where n_{kl} is discrete complex AWGN with variance $\sigma^2 = \mathrm{E}\left\{|n_{kl}|^2\right\} = N_0$. This is just the same as the discrete-time multiplicative fading channel that has been analyzed in Section 2.4, but with an additional second index for the frequency. The fading amplitude c_{kl} is typically modeled as Rayleigh or Ricean fading. We assume a channel transfer power normalized to one, that is, $\mathrm{E}\left\{|c_{kl}|^2\right\} = 1$. Note the factor $\sqrt{T/T_S}$, which means that there is an energy loss in performance because a part of the signal available at the receiver is not evaluated. All Euclidean distance in the expressions for error probabilities will be lowered by that factor, that is,

$$\frac{1}{2}\,\mathrm{erfc}\left(\sqrt{\frac{1}{N_0}\sum_{kl}|c_{kl}|^2\,|s_{kl}-\hat{s}_{kl}|^2}\right)$$

must be replaced by

$$\frac{1}{2}\,\mathrm{erfc}\left(\sqrt{\frac{1}{N_0}\frac{T}{T_S}\sum_{kl}|c_{kl}|^2\,|s_{kl}-\hat{s}_{kl}|^2}\right)$$

and thus all performance curves as functions of E_b/N_0 or E_S/N_0 have to be shifted by $10\log_{10}(T/T_S)$ decibels to the right. For the typical value $T/T_S = 0.8$, this loss is approximately 1 dB. Because the base pulses $g'_{kl}(t)$ are normalized according to $\left\|g'_{kl}\right\|^2 = 1$, we still have $E_S = \mathrm{E}\left\{|s_{kl}|^2\right\}$, and the SNR,

$$SNR = \frac{\mathrm{E}\left\{\left|\sqrt{\frac{T}{T_S}} s_{kl} c_{kl}\right|^2\right\}}{\mathrm{E}\left\{|n_{kl}|^2\right\}}$$

at the receiver is given by

$$SNR = \frac{T}{T_S} \cdot \frac{E_S}{N_0} = \frac{T}{T_S} \cdot R_c \log_2(M) \frac{E_b}{N_0} \tag{4.12}$$

for a modulation with $\log_2(M)$ bits per complex symbol and a code rate of R_c. This means that the performance curves *as a function of the SNR* will be left unchanged by the guard interval.

We summarize and add the following remarks:

- The time period of length T in Figure 4.9 that is used for the Fourier analysis at the detector will be called the *Fourier analysis window*. The spacing between two adjacent subcarriers is given by $\Delta f = f_k - f_{k-1} = T^{-1}$.
- $T_S = T + \Delta$ is the symbol period for each subcarrier. Thus, for each fixed index k, the symbol rate of the transmit symbols s_{kl} is given by T_S^{-1}.
- In contrast to OFDM without guard interval, the two concepts of Figures 4.2 and 4.3 are not equivalent because $f_k = 1/T \neq 1/T_S$. The FFT implementation of OFDM corresponds to that of Figure 4.3. To switch to the concept of Figure 4.2, we must multiply each modulation symbol s_{kl} by $\mathrm{e}^{-j2\pi klT/T_S}$. As there is no advantage in doing that, it is not implemented in any real system.
- The part of the signal transmitted during each time period T_S is called an *OFDM symbol*[2]. Each OFDM symbol corresponds to a number of K transmit symbols s_{kl}. Thus, the total symbol rate is given by $R_S = K\, T_S^{-1}$. Ignoring any other overhead (e.g. for synchronization), the useful bit rate is $R_b = K \cdot R_c \log_2(M) T_S^{-1}$, where we have assumed that M-PSK or M-QAM with code rate R_c is used for modulation and channel coding.
- The FFT length N is typically (but not necessarily) given by the smallest power of two that satisfies $K < N$. For example, the so-called *2k mode* of the DVB-T system has $K + 1 = 1705$, so $N = 2048$ is the smallest possible FFT length (which explains the name of the mode). However, one could also use an (I)FFT with $N = 4096$ for the Fourier analysis or synthesis. Such an oversampling may be useful for several purposes (see Subsection 4.2.1). Note that the FFT length is an implementation parameter for transmitter and receiver and it is not relevant for the description of the OFDM signal in the air.

[2]Here we have adopted the terminology used in the specification of the European DAB system.

4.2 Implementation and Signal Processing Aspects for OFDM

4.2.1 Spectral shaping for OFDM systems

In this subsection, we will discuss the implementation aspects that are related to the spectral properties of OFDM. We consider an OFDM system with subcarriers at frequency positions in the complex baseband given by $f_k = k/T$ with frequency index $k \in \{0, \pm 1, \pm 2, \ldots, \pm K/2\}$. As already discussed in Subsection 4.1.2, the subcarrier pulses in the frequency domain are shaped like sinc functions that superpose to a seemingly rectangular spectrum located between $-K/T$ and $+K/T$. However, as depicted in Figure 4.6, there is a severe out-of-band radiation outside this main lobe of the OFDM spectrum caused by the poor decay of the sinc function. That figure shows the spectrum of an OFDM signal without guard interval. The guard interval slightly modifies the spectral shape by introducing ripples into the main lobe and reducing the ripples in the side lobe. However, the statements about the poor decay remain valid. Figure 4.11 shows such an OFDM spectrum with $K = 96$. Here and in the following discussion, the guard interval length $\Delta = T/4$ has been chosen.

The number of subcarriers has a great influence on the decrease of the sidelobes. For a given main lobe bandwidth $B = K/T$, the spectrum of each individual subcarrier – including its side lobes – becomes narrower with increasing K. As a consequence,

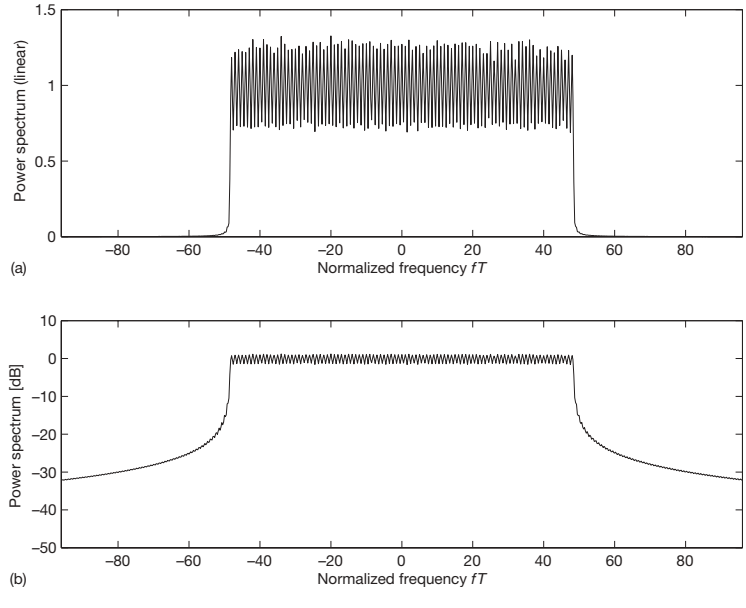

Figure 4.11 The power density spectrum of an OFDM signal with guard interval on a linear scale (a) and on a logarithmic scale (b).

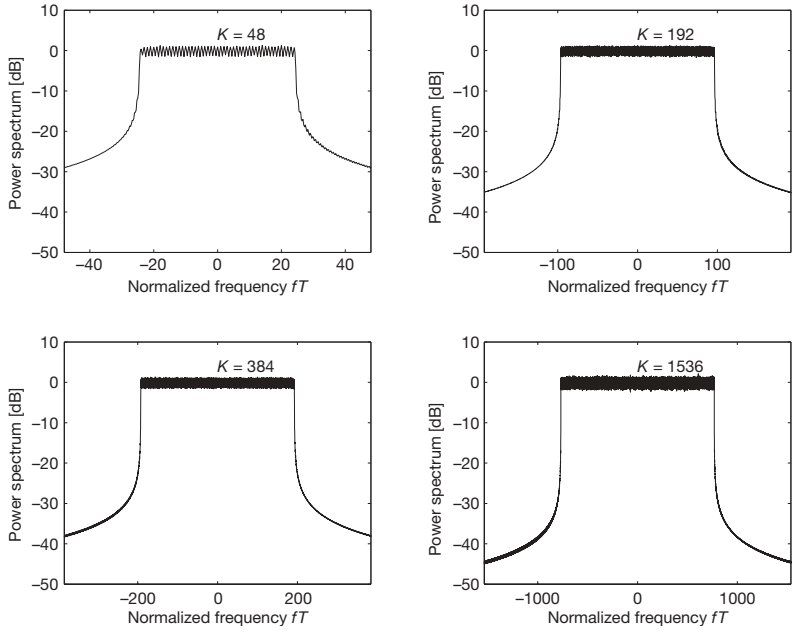

Figure 4.12 The power density spectra of an OFDM for $K = 48, 96, 384, 1536$.

the side lobes of the complete OFDM spectrum show a steeper decay and the spectrum comes closer to a rectangular shape. Figure 4.12 shows the OFDM spectra for $K = 48, 192, 384, 1536$. But, even for a high number of K, the decay may still not be sufficient to fulfill the network planning requirements. These are especially strict for broadcasting systems, where side lobe reduction in the order of -70 dB are mandatory. In that case, appropriate steps must be taken to reduce the out-of-band radiation.

We note that the spectra shown in the figures correspond to continuous OFDM signals[3].

Digital-to-analog conversion

In practice, discrete-time OFDM signals will be generated by an inverse discrete (fast) Fourier transform and then processed by a digital-to-analog converter (DAC). It is well known from signal processing theory that a discrete-time signal has a periodic spectrum from which the analog signal has to be reconstructed at the DAC by a low-pass filter (LPF) that suppresses these aliasing spectra beyond half the sampling frequency $f_s/2$. Figure 4.13(a) shows the periodic spectrum of a discrete OFDM signal with $K = 96$ and an FFT length $N = 128$, which is the lowest possible value for that number of subcarriers. The LPF must be flat inside the main lobe (i.e. for $|f| \leq 48/T$) and the side lobe must decay steeply enough so that the alias spectra at $|f| \geq 80/T$ will be suppressed. This analog filter is always a complexity item. It is a common practice to use oversampling

[3]The spectra shown above are computer simulations and not measurements of a continuous OFDM signal. However, the signal becomes quasi-continuous if the sampling rate is chosen to be high enough.

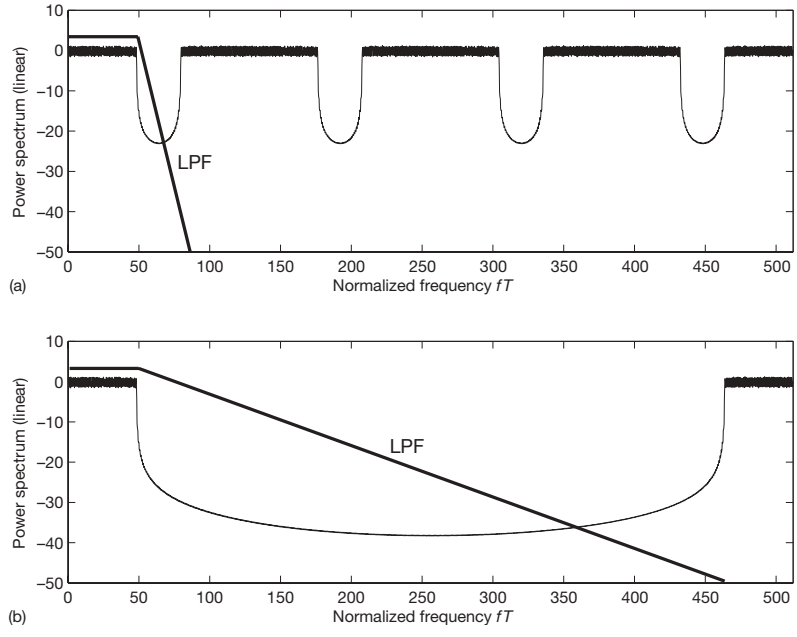

Figure 4.13 The periodic power density spectra of a discrete OFDM signal for $K = 96$ and FFT length $N = 128$ (a) and FFT length $N = 512$ (b).

to move complexity from the analog to the digital part of the system. Oversampling can be implemented by using a higher FFT length and padding zeros at the unused carrier positions[4]. Figure 4.13(b) shows the discrete spectrum for the same OFDM parameters with fourfold oversampling, that is, $N = 4 \cdot 128 = 512$ and $f_s/2 = 256/T$. Now the main lobe of the next alias spectrum starts at $|f| = 464/T$ and the requirements to the steepness of the LPF can be significantly reduced.

We finally note that since the signal is not strictly band limited, any filtering will always hurt the useful signal in some way because the sidelobes are a part of the signal, even though not the most significant.

Reduction of the out-of-band radiation

For a practical system, network planning aspects require a certain spectral mask that must not be exceeded by the implementation. Typically, this spectrum mask defined by the specification tells the maximal allowed out-of-band radiation at a given frequency. Figure 4.14 shows an example of such a spectrum mask similar to the one that is used for a wireless LAN system. The frequency is normalized with respect to the main lobe bandwidth $B = K/T$, that is, the main lobe is located between the normalized frequencies -0.5 and $+0.5$. We note that such a spectrum mask for a wireless LAN system is relatively loose compared, for example, to those for terrestrial broadcast systems like DAB and DVB-T.

[4]Alternatively, one may use the smallest possible FFT together with a commercially available oversampling circuit. This will be the typical implementation in a real system.

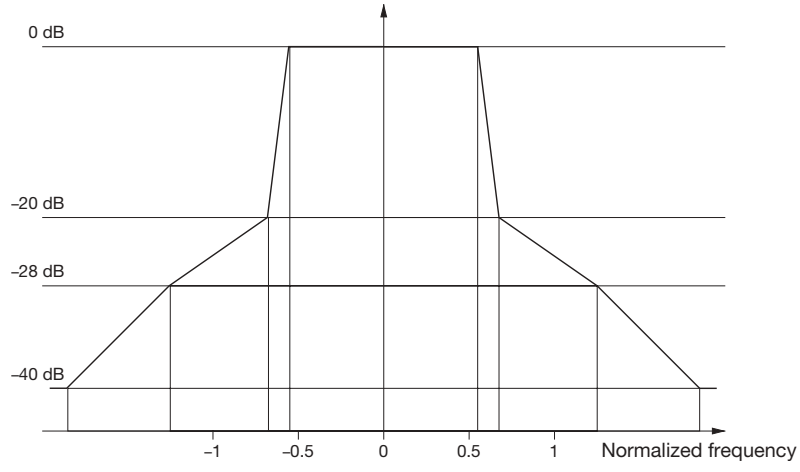

Figure 4.14 Example for the spectrum mask of an OFDM system as a function of the normalized bandwidth f/B.

To fulfill the requirements of a spectrum mask, it is often necessary to reduce the sidelobes. This can be implemented by – preferably digital – filtering.

As an example, we use a digital Butterworth filter to reduce the sidelobes of an OFDM signal with $K = 96$ and $N = 512$ (fourfold oversampling). To avoid significant attenuation or group delay distortion inside the main lobe, we choose a 3 dB filter bandwidth $f_{3\,\mathrm{dB}} = 64/T$. For this filter bandwidth, the amplitude is approximately flat and the phase is nearly linear within the main lobe. Figure 4.15 shows the OFDM spectrum filtered by a digital Butterworth filter of 5th and 10th order. As an example, let us assume that the spacing between two such OFDM signals inside a frequency band is $128/T$, that is, the lowest possible sampling frequency. Then, the main lobe of the next OFDM signal would begin at $(\pm)\, 80/T$. The out-of-band radiation at this frequency is reduced from -30 to -41 dB for the 5th order filter and to -52 dB for the 10th order filter.

One must keep in mind that any filtering will influence the signal. The rectangular pulse shape of each OFDM subcarrier will be smoothened and broadened by the convolution with the filter impulse response. The guard interval usually absorbs the resulting ISI, but this reduces the capability of the system to cope with physical echoes. Thus, the effective length of the guard interval will be reduced. Figure 4.16 shows the respective impulse responses of both filters that we have used. We recall that for $N = 512$, the guard interval is $N/4 = 128$ samples long. The filter impulse responses reduce the effective guard interval length by 10–20%.

Instead of low-pass filtering, one may also form the spectral shape by smoothing the shape of the rectangular subcarrier pulse. This can be done as described in the following text. We first cyclically extend the OFDM symbol *at the end* by δ to obtain a harmonic wave of symbol length $T_S + \delta$. We then choose a smoothing window that is equal to one for $-\Delta + \delta < t < T$ and decreases smoothly to zero outside that interval (see Figure 4.17). The (cyclically extended) OFDM signal will then be multiplied by this window. The signal remains unchanged within $-\Delta + \delta < t < T$, that is, the effective guard interval will be

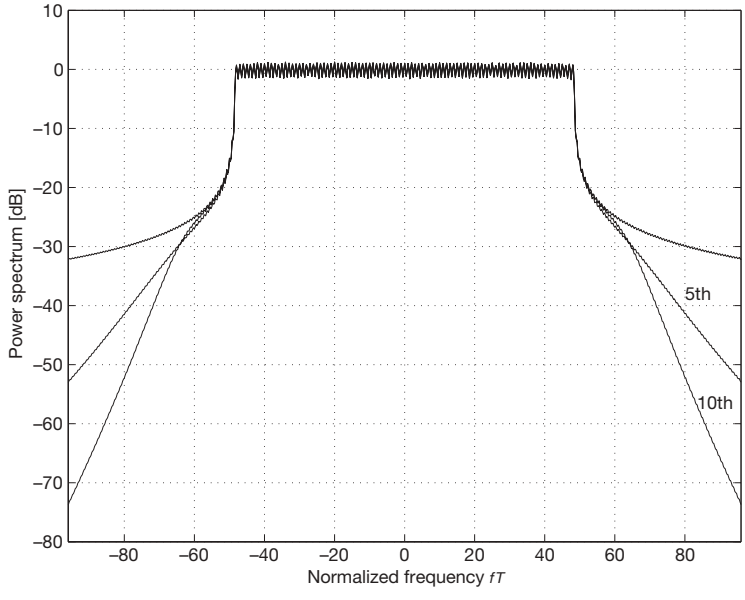

Figure 4.15 OFDM spectrum filtered by a digital Butterworth filter of 5th and 10th order.

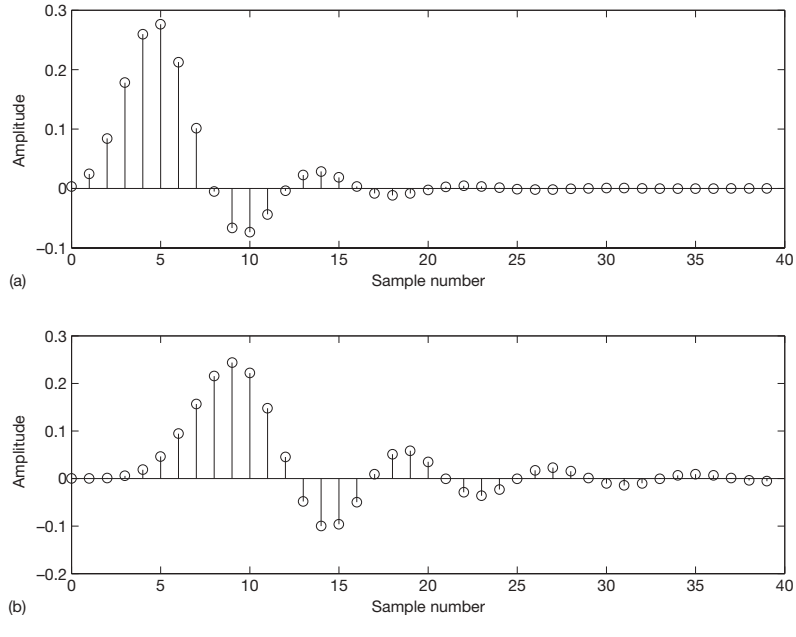

Figure 4.16 Impulse response of the digital Butterworth filter of 5th (a) and 10th (b) order.

Figure 4.17 Smoothing window for the OFDM symbol.

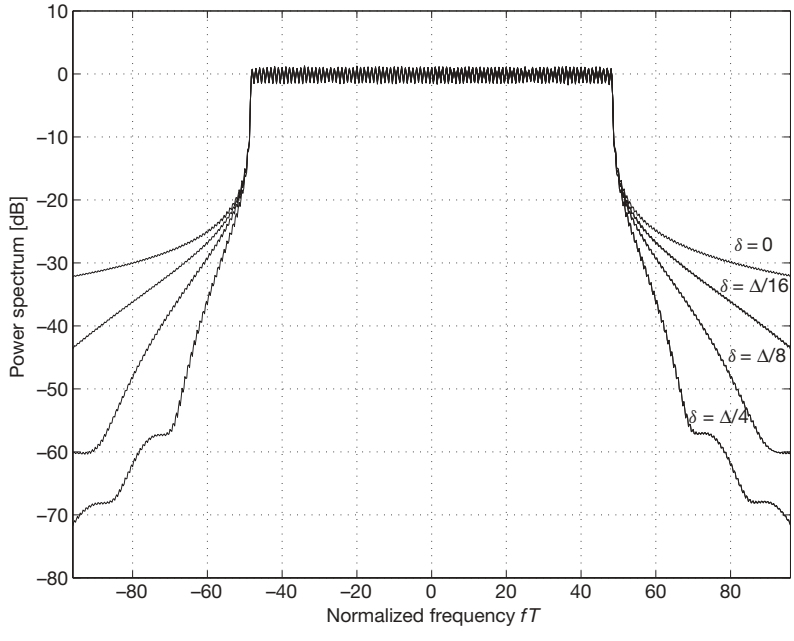

Figure 4.18 OFDM spectrum for a smoothened subcarrier pulse shape.

reduced by δ. We choose a raised-cosine pulse shape (Schmidt 2001). For the digital implementation, the flanks are just the increasing and decreasing flanks of a discrete Hanning window. Figure 4.18 shows the OFDM spectra for $\delta = 0,\ \Delta/16,\ \Delta/8,\ \Delta/4$. The out-of-band power reduction is similar to that of digital filtering.

We finally show the efficiency of the windowing method for an OFDM signal with a high number of carriers. Figure 4.19 shows the OFDM spectra for $K = 1536$ and $\delta = 0,\ \Delta/16,\ \Delta/8,\ \Delta/4$. We note a very steep decay for the out-of-band radiation. Even a small reduction of the guard interval is enough to fulfill the requirements of a broadcasting system[5]. Similar results can be achieved by digital filtering. However, this would require higher-order filters with more computational complexity and a smaller 3 dB bandwidth. Thus, the method of pulse shape smoothing seems to be the better choice.

[5]The DAB system with $K = 1536$ requires a -71 dB attenuation at $fT = 970$ for the most critical cases.

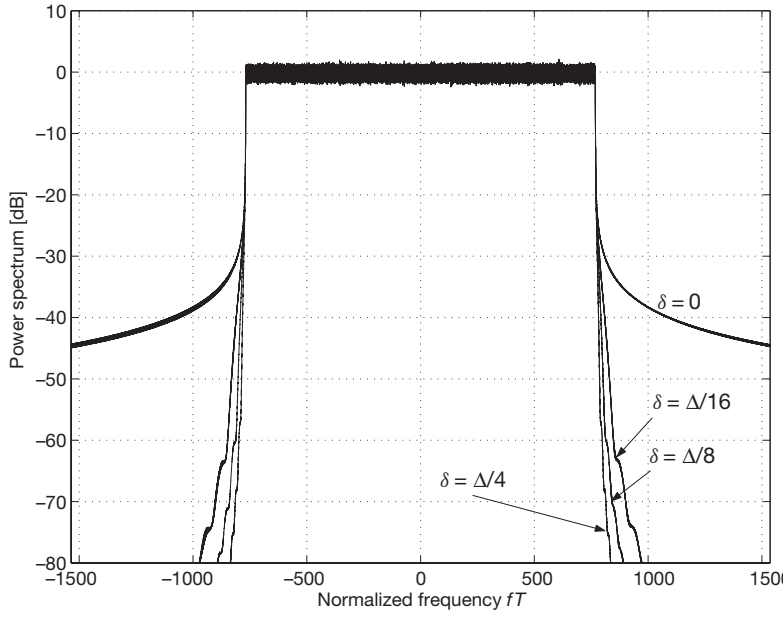

Figure 4.19 OFDM spectrum for a smoothened subcarrier pulse shape ($K = 1536$).

4.2.2 Sensitivity of OFDM signals against nonlinearities

As we have already seen, OFDM signals in the frequency domain look very similar to band-limited white noise. The same is true in the time domain. Figure 4.20 shows the inphase component $I(t) = \Re\{s(t)\}$, the quadrature component $Q(t) = \Im\{s(t)\}$ and the amplitude $|s(t)|$ of an OFDM signal with subcarriers at frequency positions in the complex baseband given by $f_k = k/T$ with $k \in \{0, \pm 1, \pm 2, \ldots, \pm K/2\}$ and $K = 96$ and the guard interval length $\Delta = T/4$. We will further use these OFDM parameters in the following discussion.

Because the inphase and the quadrature component the OFDM are superpositions of many sinoids with random phases, one can argue from the central limit theorem that both are Gaussian random processes. A *normplot* is an appropriate method to test whether the samples of a signal follow Gaussian statistics. To do this, one has to plot the (measured) probability that a sample is smaller than a certain value as a function of that value. The probability values are then scaled in such a way that a Gaussian normal distribution corresponds to a straight line. Figure 4.21 shows such a normplot for the OFDM signal under consideration. We note that the measurements fit quite well to the straight line that corresponds to the Gaussian normal distribution. However, there are deviations for high amplitudes. This is due to the fact that the number of subcarriers is not very high ($K = 96$) and the maximum amplitude of their superposition cannot exceed a certain value. For an increasing number of subcarriers, the measurements follow closely the straight line. For a lower value of K, the agreement becomes poorer. The crest factor $C_s = P_{s,\max}/P_{s,\mathrm{av}}$ is defined as the ratio (usually given in decibels) between the maximum signal power $P_{s,\max}$ and the average signal power $P_{s,\mathrm{av}}$. With $K \to \infty$, the amplitude of an OFDM signal is

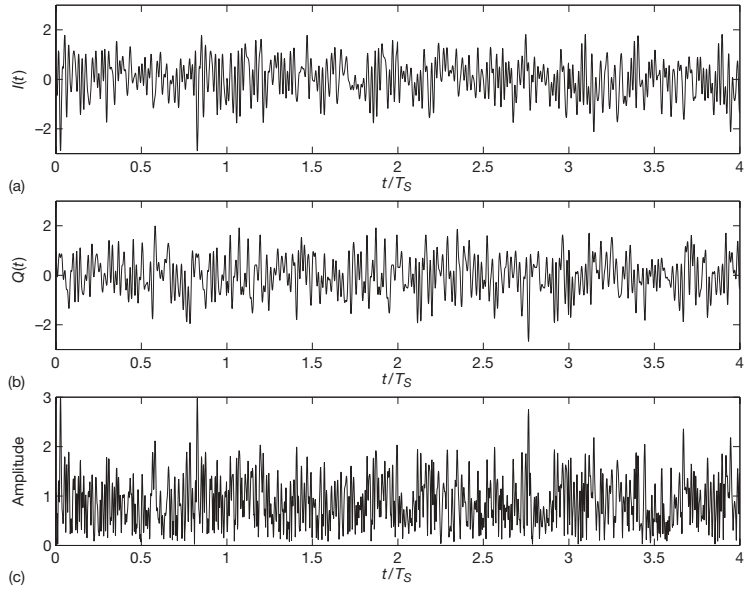

Figure 4.20 The inphase component $I(t)$ (a), the quadrature component $Q(t)$ (b) and the amplitude (c) of an OFDM signal of average power one.

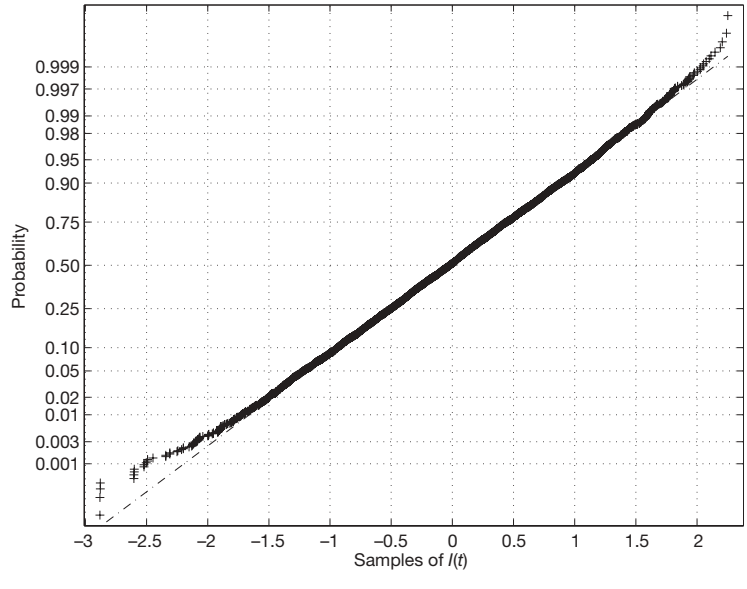

Figure 4.21 Normal probability plot for the inphase component $I(t)$ of an OFDM signal.

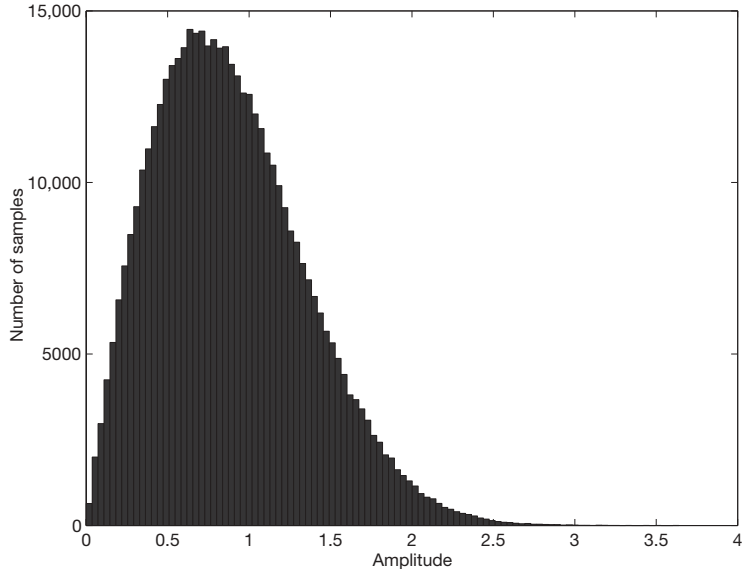

Figure 4.22 Histogram for the amplitude of an OFDM signal.

a Gaussian random variable and the crest factor becomes infinity. Even for a finite (high) number of subcarriers, the crest factor is so high that it does not make sense to use it to characterize the signal. This is because the probability of extremely high-power values decreases exponentially with increasing power.

As discussed in detail in Chapter 3, a normal distribution for the I and Q component of a signal leads to a Rayleigh distribution for the signal amplitude. Figure 4.22 shows the histogram for the amplitude of the OFDM signal under consideration.

We now consider an OFDM complex baseband signal

$$s(t) = a(t)\mathrm{e}^{j\varphi(t)}$$

with amplitude $a(t)$ and phase $\varphi(t)$ that passes a nonlinear amplifier with power saturation as depicted in Figure 4.23. For low values of the input power, the output power grows approximately linear. For intermediate values, the output power falls below that linear growth and it runs into a saturation as the input power grows higher. In addition to that *smooth* nonlinear amplifier, we consider a *clipping* amplifier. This amplifier is linear as long as the input power is smaller than a certain value $P_{\mathrm{in,max}}$ corresponding to the maximum output power $P_{\mathrm{out,max}}$. If the input exceeds $P_{\mathrm{in,max}}$, the output will be *clipped* to $P_{\mathrm{out,max}}$. As depicted in Figure 4.23, for any nonlinear amplifier with power saturation, there is a uniquely defined clipping amplifier with the same linear growth for small input amplitudes and the same saturation (maximum output). For an input signal with average power $P_{s,\mathrm{av}}$, the *input backoff* $IBO = P_{\mathrm{in,max}}/P_{s,\mathrm{av}}$ is defined as the ratio (usually given in decibels) between the power $P_{\mathrm{in,max}}$ and the average signal power $P_{s,\mathrm{av}}$.

The nonlinear amplifier output in the complex baseband model is given by

$$r(t) = F\left(a(t)\right)\mathrm{e}^{j\left(\varphi(t)+\Phi(a(t))\right)}$$

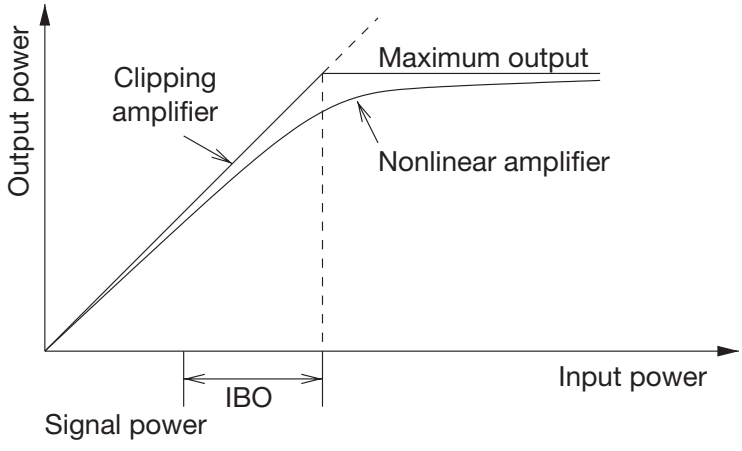

Figure 4.23 Characteristic curves for nonlinear amplifiers with power saturation.

(see (Benedetto and Biglieri 1999)). The real-valued function $F(x)$ is the characteristic curve for the amplitude distortion, and the real-valued function $\Phi(x)$ describes the phase distortion caused by the nonlinear amplifier.

To see how nonlinearities influence an OFDM signal, we consider a very simple characteristic curve $F(x)$ that is approximately linear for small values of x and runs into a saturation for $x \to \infty$. Such a behavior can be modeled by the characteristic curve (normalized to $P_{\text{in,max}} = P_{\text{out,max}} = 1$) given by the function

$$F_{\exp}(x) = 1 - \mathrm{e}^{-x}.$$

For $x \to \infty$, the curve runs exponentially into the saturation $F_{\exp}(x) \to 1$. For small values of x, we can expand into the Taylor series

$$F_{\exp}(x) = x - \frac{1}{2!}x^2 + \frac{1}{3!}x^3 - \frac{1}{4!}x^4 \pm \cdots$$

and observe a linear growth for small values of x. The clipping amplifier is given by the characteristic curve

$$F_{\text{clip}}(x) = \min(x, 1),$$

which is linear for $x < 1$ and equal to 1 for higher values of x. For simplicity, we do not consider phase distortions.

In Figure 4.24, we see an OFDM time signal and the corresponding amplifier output for the smooth nonlinear amplifier corresponding to $F_{\exp}(x)$ and for the clipping amplifier corresponding to $F_{\text{clip}}(x)$ for an IBO of 6 dB. The average OFDM signal power is normalized to one. Thus, an IBO of 6 dB means that all amplitudes with $a(t) > 2$ are clipped in part (c) of that figure.

The nonlinearity severely influences the spectral characteristics of an OFDM signal. As can be seen from the Taylor series for $F_{\exp}(x)$, mixing products of second, third and higher order occur for every subcarrier and for every pair of subcarriers. These mixing products

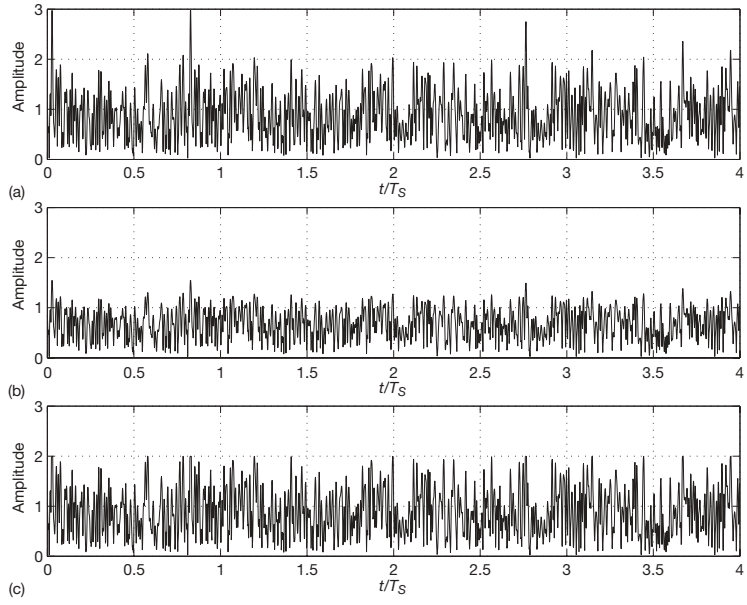

Figure 4.24 Amplitude of an OFDM signal (a) after a smooth nonlinear (b) and a clipping (c) amplifier with IBO = 6 dB.

corrupt the signal inside the main lobe and they will cause out-of-band radiation. This must not be confused with the out-of-band radiation discussed in the preceding subsection, which is caused by the rectangular pulse shape. To distinguish between these two things, we use the spectral smoothing by a raised-cosine window as described in the preceding subsection. We choose $\delta = \Delta/4$ to achieve a very fast decay of the side lobes. Figure 4.25 shows the OFDM signal corrupted by the amplifier corresponding to $F_{\exp}(x)$ for an IBO of 3 dB, 9 dB and 15 dB. As expected, there is a severe out-of-band radiation, and a very high IBO is necessary to reduce this radiation. Note that we have renormalized all the amplifier output signals to the same average power in order to draw all the curves in the same picture. Figure 4.26 shows the OFDM signal corrupted by the amplifier corresponding to $F_{\text{clip}}(x)$ for an IBO of 3 dB, 6 dB and 9 dB. We observe that, compared to the other amplifier, we need much less IBO to reduce the out-of-band radiation.

Inside the main lobe, the useful signal is corrupted by the mixing products between all subcarriers. Simulations of the bit error rate would be necessary to evaluate the performance degradations for a given OFDM system and a given amplifier for the concrete modulation and coding scheme. For a given modulation scheme, the disturbances caused by the nonlinearities can be visualized by the constellation diagram in the signal space. Figure 4.27 shows the constellation of a 16-QAM signal for both amplifiers and the IBO values as given above. For the IBO of 3 dB, the QAM signal is severely distorted for both amplifiers. For the clipping amplifier, the distortion soon becomes smaller as the IBO increases. For the other amplifier, much more IBO is necessary to reduce the disturbance. This is what we may expect by looking at the spectra.

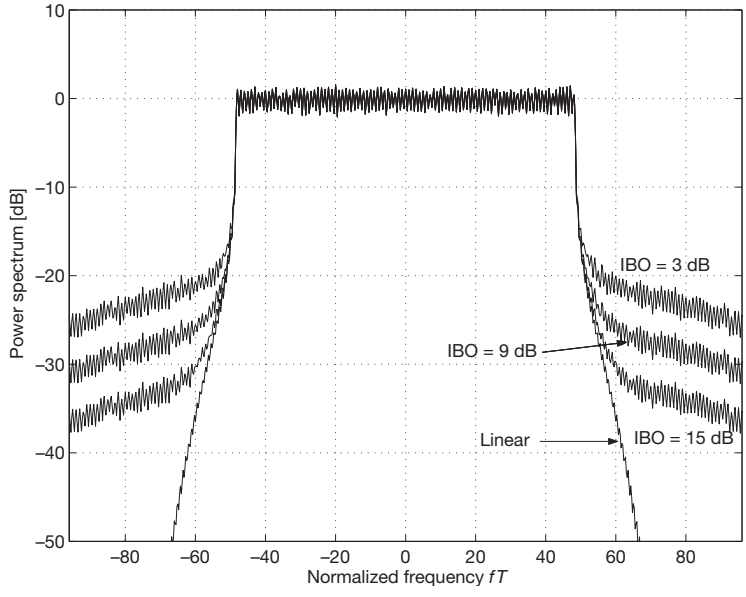

Figure 4.25 Spectrum of an OFDM signal with a (smooth exponential) nonlinear amplifier.

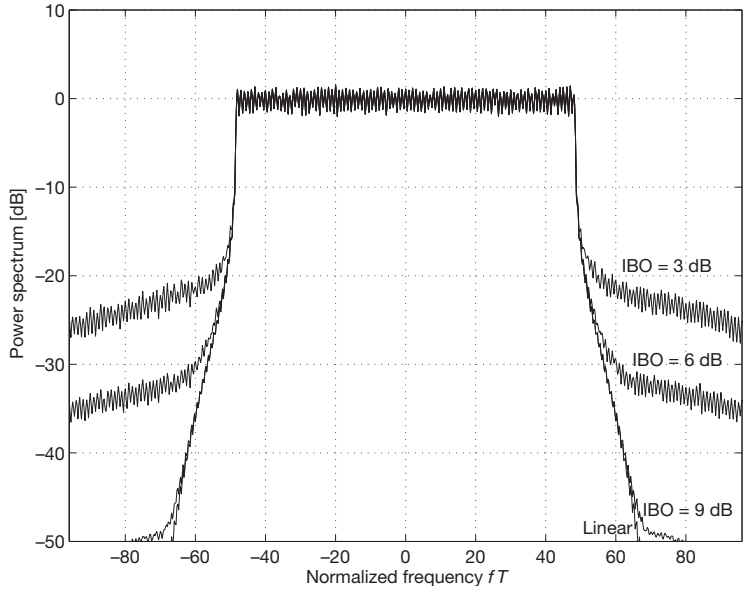

Figure 4.26 Spectrum of an OFDM signal with a (clipping) nonlinear amplifier.

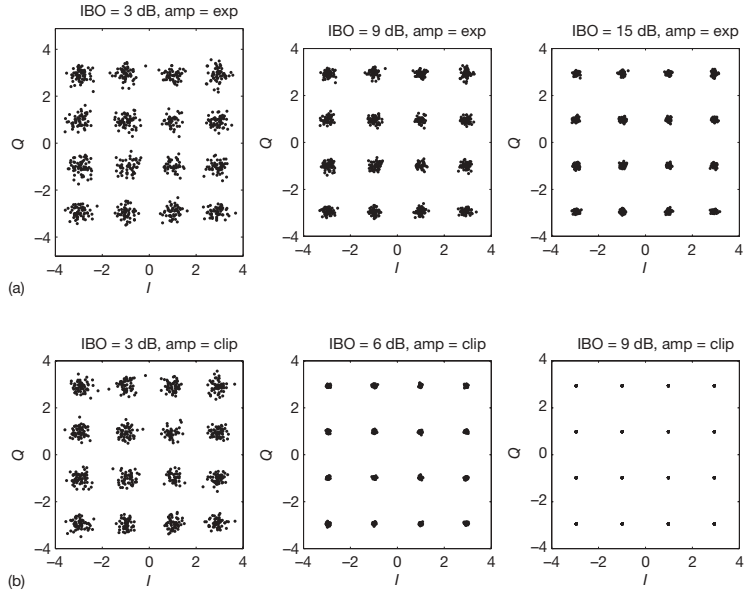

Figure 4.27 The 16-QAM constellation diagram of an OFDM signal with a smooth exponential (a) and a clipping (b) nonlinear amplifier.

Figure 4.27 gives the impression that the QAM symbols are corrupted by an additive noise-like signal. The spectra of Figures 4.25 and 4.26 agree with the picture of an additive *noise floor* that corrupts the signal. At least for the smooth amplifier with a characteristic curve $F_{\exp}(x)$ given by a Taylor series, one can heuristically argue as follows. The quadratic, cubic and higher-order terms cause mixing products of the subcarriers that interfere additively with the useful signal. Each subcarrier is affected by many mixing produces of other subcarriers. Thus, there is an additive disturbance that is the sum of many random variables. By using the central limit theorem, we can argue that this additive disturbance is a Gaussian random variable for the inphase and the quadrature component of the 16-QAM constellation diagram. Figure 4.28 shows the normplots of the error signal (samples of the real and imaginary parts) for the smooth exponential amplifier for the three IBO values.

The samples fit well to the straight line, which confirms the heuristic argument given above. We have also investigated the spectral properties of this interfering signal and found that it shows a white spectrum. Thus, the interference can be modeled as AWGN and can be analyzed by known methods (see Problem 2).

Figure 4.29 shows the normplots of the error signal for the clipping amplifier. Only for 3 dB, the statistics error signal seems to follow a normal distribution. For higher values of the IBO, there are severe deviations.

One can argue that the performance degradations caused by the interference can be neglected if the signal-to-interference ratio (SIR) is significantly higher than the signal-to-noise ratio (SNR). We have calculated the SIR for several values of the IBO. The results are depicted in Figure 4.30 . We find a rapid growth of the SIR as a function of the IBO for the clipping amplifier. For an IBO above approximately 6 dB, the SIR can be

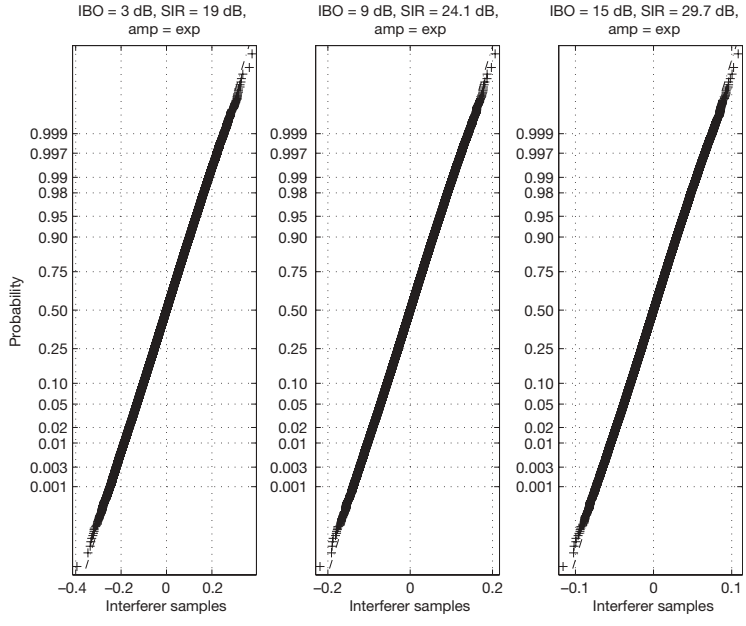

Figure 4.28 Normal probability plot of the 16-QAM error signal for a smooth exponential nonlinear amplifier.

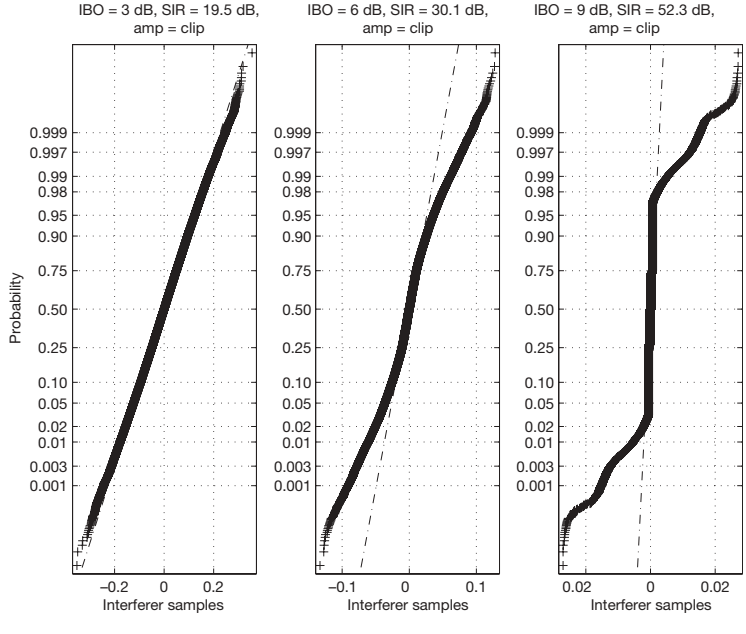

Figure 4.29 Normal probability plot of the 16-QAM error signal for a clipping amplifier.

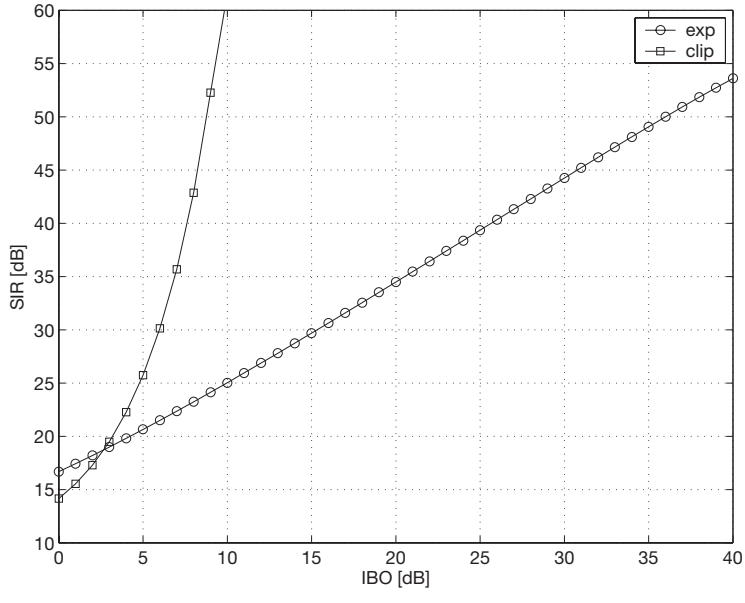

Figure 4.30 The SIR for the 16-QAM symbol for OFDM signal with a smooth exponential and a clipping nonlinear amplifier.

practically neglected. For the smooth exponential amplifier, the SIR increases very slowly as an approximately linear function at IBO values above 10 dB. One must increase the IBO by a factor of 10 for an SIR increase approximately by a factor of 10.

We summarize and add the following remarks:

- OFDM systems are much more sensitive against nonlinearities than single carrier systems. The nonlinearities of a power amplifier degrade the BER (bit error rate) performance and inflate the out-of-band radiation. The performance degradations will typically be the less severe problem because most communication systems work at an SNR well below 20 dB, while the SIR will typically be beyond that value. However, a high IBO value may be necessary to fulfill the requirements of a given spectral mask. As a consequence, the power amplifier will then work with a poor efficiency. In certain cases, it may be necessary to reduce the out-band radiation by using a filter after the power amplifier.

- There are several methods to reduce the crest factor of an OFDM signal by modifying the signal in a certain way (see (Schmidt 2001) and references therein). However, these methods are typically incompatible to existing standards and cannot be applied in those OFDM systems.

- Preferably one should separate the problem of nonlinearities and the OFDM signal processing. This can be done by a predistortion of the signal before amplification.

Analog and digital implementations are possible. After OFDM was chosen as the transmission scheme for several communication standards, there has been a considerable progress in this field (see (Banelli and Baruffa 2001; D'Andrea *et al.* 1996) and references therein).

4.3 Synchronization and Channel Estimation Aspects for OFDM Systems

4.3.1 Time and frequency synchronization for OFDM systems

There are some special aspects that make synchronization for OFDM systems very different from that for single carrier systems. OFDM splits up the data stream into a high number of subcarriers. Each of them has a low data rate and a long symbol duration T_S. This is the original intention for using multicarrier modulation, as it makes the system more robust against echoes. Consequently, the system also becomes more robust against time synchronization errors that can also be absorbed by the guard interval of length $\Delta = T_S - T$. A typical choice is $\Delta = T_S/5 = T/4$ which allows a big symbol timing uncertainty of 20% in case of no physical echoes. In practice, there will appear a superposition of timing uncertainty and physical echoes.

On the other hand, because the subcarrier spacing T^{-1} is typically much smaller than the total bandwidth, frequency synchronization becomes more difficult. Consider, for example, an OFDM system working at the center frequency $f_c = 1500$ MHz with $T = 500$ ms. The ratio between carrier spacing and center frequency is then given by $(f_c T)^{-1} = 1.33 \cdot 10^{-9}$, which is a very high demand for the accuracy of the downconversion to the complex baseband.

Once the correct Fourier analysis window is found by an appropriate time synchronization mechanism and the downconversion is carried out with sufficient accuracy, the OFDM demodulator (implemented by the FFT) produces the noisy receive symbols given by the discrete channel

$$r_{kl} = \sqrt{\frac{T}{T_S}}\, c_{kl} s_{kl} + n_{kl}$$

(see Subsection 4.1.4). The amplitudes and phases of the channel coefficients c_{kl} are still unknown. The knowledge of the channel is not required for systems with differential demodulation. For coherent demodulation, the channel estimation is a different task that has to be done after time and frequency synchronization. In this subsection, we focus our attention on time and frequency synchronization and follow (in parts) the discussion presented by Schmidt (2001). Channel estimation will be discussed in the subsequent subsections.

When speaking of frequency synchronization items for OFDM, there often appears some misunderstanding because for single carrier PSK systems there is a joint frequency and phase synchronization that can be realized, for example, by a squaring loop or a Costas loop (see e.g. (Proakis 2001)). As mentioned above, frequency synchronization and phase estimation are quite different tasks for OFDM systems.

Time synchronization

An obvious way to obtain time synchronization is to introduce a kind of *time stamp* into the seemingly irregular and noise-like OFDM time signal. The EU147 DAB system – which can be regarded as the pioneer OFDM system – uses quite a simple method that even allows for traditional analog techniques to be used for a coarse time synchronization. At the beginning of each transmission frame, the signal will be set to zero for the duration of (approximately) one OFDM symbol. This *null symbol* can be detected by a classical analog envelope detector (which may also be digitally realized) and tells the receiver where the frame and where the first OFDM symbol begin.

A more sophisticated time stamp can be introduced by periodically repeating a certain known OFDM reference symbol of known content. The subcarriers should be modulated with known complex symbols of equal amplitude to have a white frequency spectrum and a δ-type cyclic time autocorrelation function. Thus, as long as the echoes do not exceed the length of the guard interval, the channel impulse response can be measured by cross correlating the received and the transmitted reference symbol.

In the DAB system, the first OFDM symbol after the null symbol is such a reference symbol. It has the normal OFDM symbol duration T_S and is called the *TFPR* (*time-frequency-phase reference*) symbol. It is also used for frequency synchronization (see the following text) and it provides the phase references for the beginning of the differential demodulation. We note that the channel estimate provided by the TFPR symbol is only needed for the positioning of the Fourier analysis window, not for coherent demodulation.

In the wireless LAN systems IEEE 802.11a and HIPERLAN/2, a reference OFDM symbol of length $2T_S$ is used for time synchronization and for the estimation of the channel coefficients c_{kl} that are needed for coherent demodulation. The OFDM subcarriers are modulated with known data. The signal of length T resulting from the Fourier synthesis will then be cyclically extended to twice the length of the other OFDM symbols.

Another smart method to find the time synchronization without any time stamp is based on the guard interval. We note that an OFDM signal with guard interval has a regular structure because the cyclically extended part of the signal occurs twice in every OFDM symbol of duration T_S – this means that the OFDM signal $s(t)$ given has the property

$$s(t) = s(t + T)$$

for $lT_S - \Delta < t < lT_S$ (l integer), that is, the beginning and the end of each OFDM symbol are identical (see Figure 4.31). We may thus correlate $s(t)$ with $s(t + T)$ by using a sliding

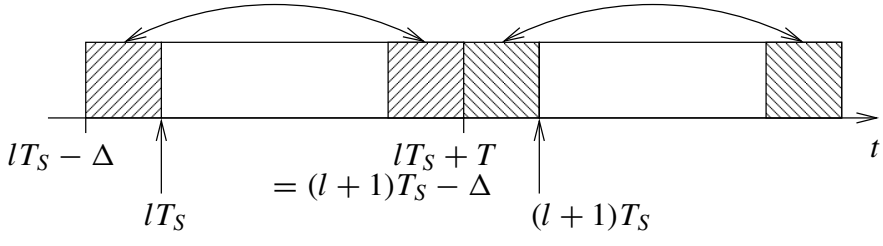

Figure 4.31 Identical parts of the OFDM symbol.

correlation analysis window of length Δ, that is, we calculate the correlator output signal

$$y(t) = \Delta^{-1} \int_{t-\Delta}^{t} \Re\left\{s(\tau)s^*(\tau + T)\right\}\, \mathrm{d}\tau.$$

This correlator output can be considered as a sliding average given by the convolution

$$y(t) = h(t) * x(t).$$

Here,

$$h(t) = \Delta^{-1}\Pi\left(\frac{t}{\Delta} - \frac{1}{2}\right)$$

is the (normalized) rectangle between $t = 0$ and $t = \Delta$, and

$$x(t) = \Re\left\{s(\tau)s^*(\tau + T)\right\}$$

is the function to be averaged. The signal $y(t)$ has peaks at $t = lT_S$, that is, at the beginning of the analysis window for each symbol, (see Figure 4.32(a)). Because of the statistical nature of the OFDM signal, the correlator output is not strictly periodic, but it shows some fluctuations. But it is not necessary to place the analysis window for every OFDM symbol. Only the relative position is relevant and it must be updated from time to time. Thus, we may average over several OFDM symbols to obtain a more regular symbol synchronization signal (see Figure 4.32(b)). This averaging also reduces the impairments due to noise. In a mobile radio environment, the signal in Figure 4.32 is smeared out because of the impulse response of the channel. It is a nontrivial task to find the optimal position of the Fourier analysis window. This may be aided by using the results of the channel estimation.

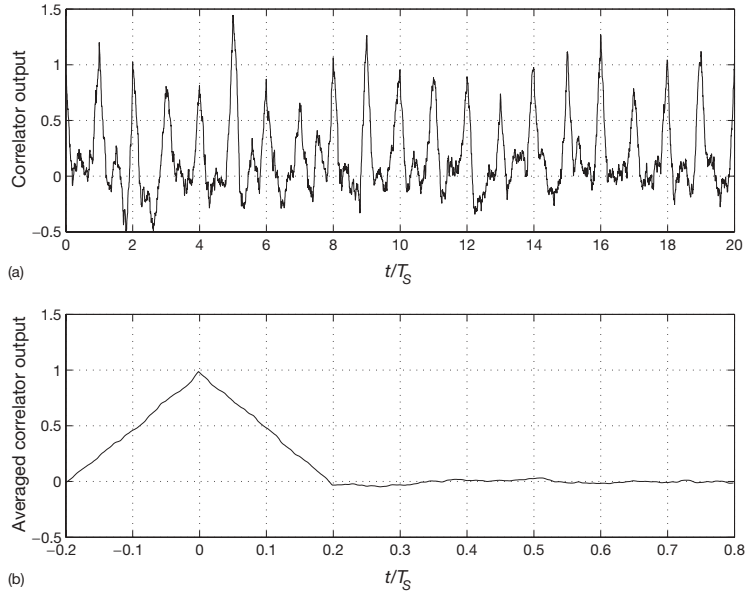

Figure 4.32 The correlator output $y(t)$ (a) and the average of it over 20 OFDM symbols (b).

Frequency synchronization

Because the spacing T^{-1} between adjacent subcarriers is typically very small, accurate frequency synchronization is an important item for OFDM systems. Such a high accuracy can usually not be provided by the local oscillator itself. Standard frequency-tracking mechanisms can be applied if measurements of the frequency deviation δf are available.

First, we want to discuss what happens to an OFDM system if there is a residual frequency offset δf that has not been corrected. There are two effects:

1. The orthogonality between transmit and receive pulses will be corrupted.
2. There is a time-variant phase rotation of the receive symbols.

The latter effect occurs for any digital transmission system, but the first is a special OFDM item that can be understood as follows. Using the notation introduced in Subsection 4.1.4, we write

$$s(t) = \sum_{kl} s_{kl} g'_{kl}(t)$$

for the transmitted OFDM signal that is modulated, for example, with complex QAM symbols s_{kl}. Here, k and l are the time and frequency indices, respectively. We assume a noise-free channel with a time variance that describes the frequency shift. The receive signal is then given by

$$r(t) = \mathrm{e}^{j2\pi\delta f\, t} s(t).$$

To study the first effect, we consider only the first OFDM symbol and drop the corresponding time index $l = 0$. The detector for the subcarrier at frequency $f_k = k/T$ is given by the Fourier analysis operation

$$\mathcal{D}_k[r] = \langle g_k, r\rangle = \int_{-\infty}^{\infty} g_k^*(t) r(t)\,\mathrm{d}t = \sqrt{\frac{1}{T}} \int_0^T \mathrm{e}^{-j2\pi f_k t}\, r(t)\,\mathrm{d}t.$$

Because of the orthogonality

$$\left\langle g_k, g'_{k'}\right\rangle = \sqrt{\frac{T}{T_S}}\,\delta_{kk'}$$

between the transmit and receive base pulses, the Fourier analysis detector recovers the undisturbed QAM symbols from the original transmit symbol, that is,

$$\mathcal{D}_k[s] = s_k.$$

The frequency offset, however, corrupts the orthogonality, leading to the detector output

$$\mathcal{D}_k[r] = \sqrt{\frac{T}{T_S}} \sum_m \gamma_{km}(\delta f)\, s_m$$

with

$$\gamma_{km}(\delta f) = \int_{-\infty}^{\infty} g_k^*(t) g_m(t) \mathrm{e}^{j2\pi\delta f\, t}\,\mathrm{d}t.$$

Typically, for small frequency offsets with $\delta = \delta f \cdot T \ll 1$, the term with $k = m$ dominates the sum, but all the other terms contribute and cause intersymbol interference that must be regarded as an additive disturbance to the QAM symbol.

We now consider an OFDM signal with running time index $l = 0, 1, 2, \ldots$. The frequency shift that is given by the multiplication with $\exp(j2\pi\delta f\, t)$ means that the QAM symbols s_{kl} are rotated by a phase angle $2\pi\delta f \cdot T_S$ between the OFDM symbols with time indices l and $l + 1$. Figure 4.33 shows a 16-QAM constellation affected by that rotation and the additive disturbance. The OFDM parameters are the same as above, and a small frequency offset given by $\delta = \delta f \cdot T = 0.01$ is chosen.

In the discrete channel model, the phase rotation can be regarded as the time variance of the channel, that is, the channel coefficient shows the proportionality

$$c_{kl} \propto \mathrm{e}^{j2\pi\delta f\, T_S l}.$$

In a coherent system with channel estimation, this time variance can be measured and the QAM constellation will be back rotated. Part (a) of Figure 4.34 shows the back-rotated 16-QAM constellation for $\delta = 0.01$, $\delta = 0.02$ and $\delta = 0.05$. The additive disturbances look similar to Gaussian noise. Indeed, a statistical analysis with a normplot fits well to a Gaussian normal distribution (see part (b) of Figure 4.34. One can therefore argue that the frequency is accurate enough if the SIR of the residual additive disturbance (after frequency tracking) is significantly below the SNR where the system is supposed to work. The latter can be obtained from the BER performance curves of the channel coding and modulation scheme.

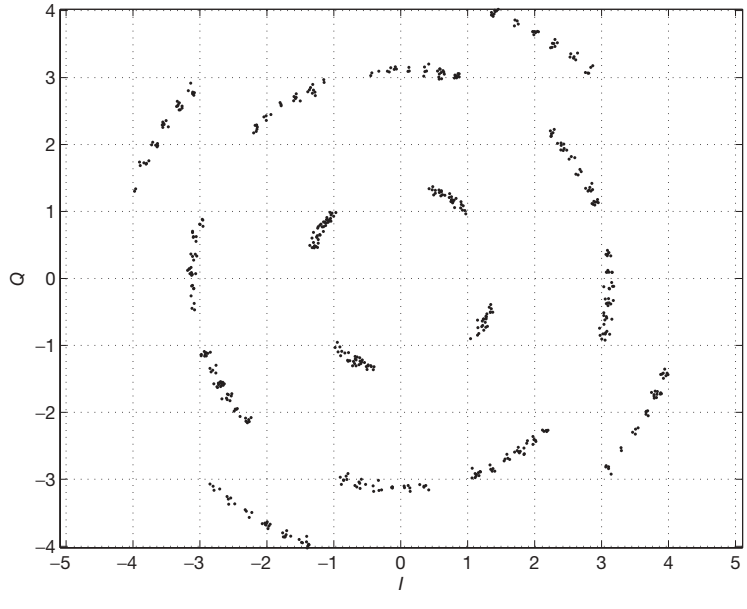

Figure 4.33 16-QAM for OFDM with frequency offset given by $\delta = \delta f \cdot T = 0.01$.

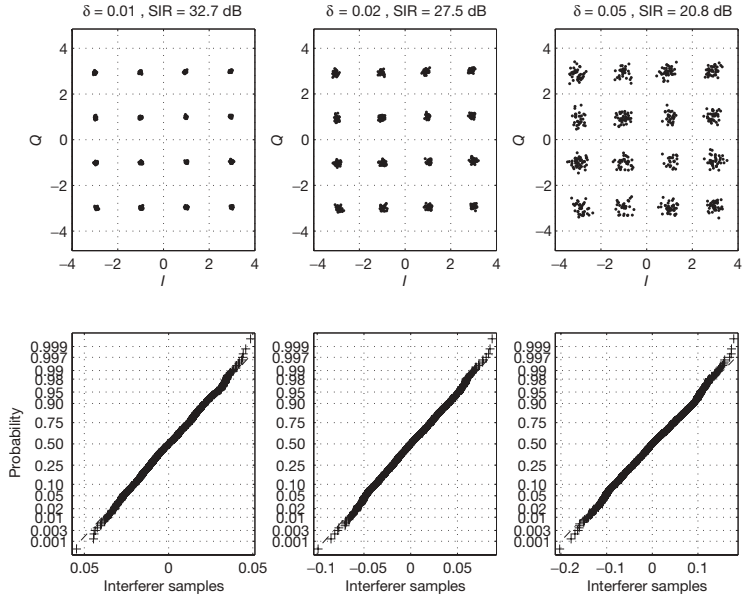

Figure 4.34 16-QAM for OFDM with frequency offset given by $\delta = \delta f \cdot T = 0.01$.

As pointed out above, an estimate for δf can be obtained from the estimated channel coefficients $\hat{c}_{kl}$. This can be done by frequency demodulation and averaging. The frequency demodulation can be implemented as follows. We note that for any complex time signal

$$z(t) = a(t)\mathrm{e}^{j\varphi(t)}$$

with amplitude $a(t)$ and phase $\varphi(t)$, the time derivative of the phase can be calculated as (see Problem 3)

$$\dot{\varphi}(t) = \Im\left\{\frac{\dot{z}(t)}{z(t)}\right\},$$

where the dot denotes the time derivative. The instantaneous frequency modulation (FM) is then given by

$$f_M(t) = \frac{1}{2\pi}\dot{\varphi}(t) = \frac{1}{2\pi}\Im\left\{\frac{\dot{z}(t)}{z(t)}\right\}.$$

For a discrete-time signal $z[n] = z(nt_s)$ that has been obtained by sampling $z(t)$ with the sampling frequency $f_s = t_s^{-1}$, the time discrete FM is

$$f_M[n] = \frac{1}{2\pi t_s}\Im\left\{\frac{z[n] - z[n-1]}{z[n]}\right\}.$$

For an OFDM system with channel estimation as discussed in the next subsection, a noisy estimate $\hat{c}_{kl}$ of the channel coefficient c_{kl} is obtained for every OFDM symbol of duration T_S at a frequency position k. The estimated instantaneous frequency deviation for time index l is then

$$\widehat{\delta f}_{kl} = \frac{1}{2\pi T_S}\Im\left\{\frac{\hat{c}_{kl} - \hat{c}_{k\,l-1}}{\hat{c}_{kl}}\right\}.$$

This noisy instantaneous estimate of the frequency deviation has to be averaged over a sufficiently large number of OFDM symbols and over the frequency index k. This average $\widehat{\delta f}$ may then be used to obtain a frequency-shift-corrected receive signal

$$\hat{r}(t) = \mathrm{e}^{-j2\pi\widehat{\delta f}\,t} r(t).$$

In a typical mobile radio channel with Doppler spread, the time variance of the channel will introduce an additional frequency modulation. The averaging of the FM will place the Doppler spectrum in such a way that its first moment vanishes. In the WSSUS model, the Doppler spectrum is the same for every subcarrier frequency. Thus, an accurate estimate for the frequency offset and for the Doppler spectrum can be obtained from the measurements at a certain number of subcarrier positions (at least one). It is a common method applied in the DVB-T system and the wireless LAN systems IEEE 802.11a and HIPERLAN/2 to use certain subcarriers as *continuous pilots*. These subcarriers that are boosted by a certain factor and carry known data will be used for frequency synchronization and estimation of the Doppler bandwidth $\nu_{\max}$. The latter will be needed for the channel estimation by Wiener filtering, as discussed in the next subsection. The Doppler spectrum can be estimated from the continuous pilots (after frequency-shift correction) by standard power spectral density estimation methods.

Wireless LAN systems require a very fast frequency synchronization at the beginning of every burst. For this purpose, a special OFDM symbol at the beginning of the burst has been defined. In this OFDM symbol, only 12 subcarriers are modulated to serve as a frequency reference.

An accurate frequency synchronization is also necessary for OFDM systems with differential demodulation. The EU147 DAB system uses DQPSK. The first symbol in every frame (after the null symbol) serves as the phase reference for the differential modulation and as a reference for time and frequency synchronization. The complex symbols are built from CAZAC (constant amplitude zero autocorrelation) sequences. They allow a frequency offset estimation by correlating in frequency direction.

4.3.2 OFDM with pilot symbols for channel estimation

Coherent demodulation requires the knowledge of the channel, that is, of the coefficients c_{kl} in the discrete-time model for OFDM transmission in a fading channel. The two-dimensional structure of the OFDM signal makes a two-dimensional pilot grid especially attractive for channel measurement and estimation. An example of such a grid is depicted in Figure 4.35. These pilots are usually called *scattered pilots* to distinguish them from the continuous pilots discussed in the preceding subsection.

At certain positions in time and frequency, the modulation symbols s_{kl} will be replaced by known pilot symbols. At these positions, the channel can be measured. Figure 4.35 shows a rectangular grid with pilot symbols at every third frequency and every fourth time slot. The pilot density is thus 1/12, that is, 1/12 of the whole capacity is used for channel estimation. This lowers not only the data rate, but also the available energy E_b per bit. Both must be taken into account in the evaluation of the spectral and the power efficiency of such a system.

The density of the grid has to be matched to the incoherency of the channel, that is, to the time-frequency fluctuations described by the scattering function. To illustrate this by a

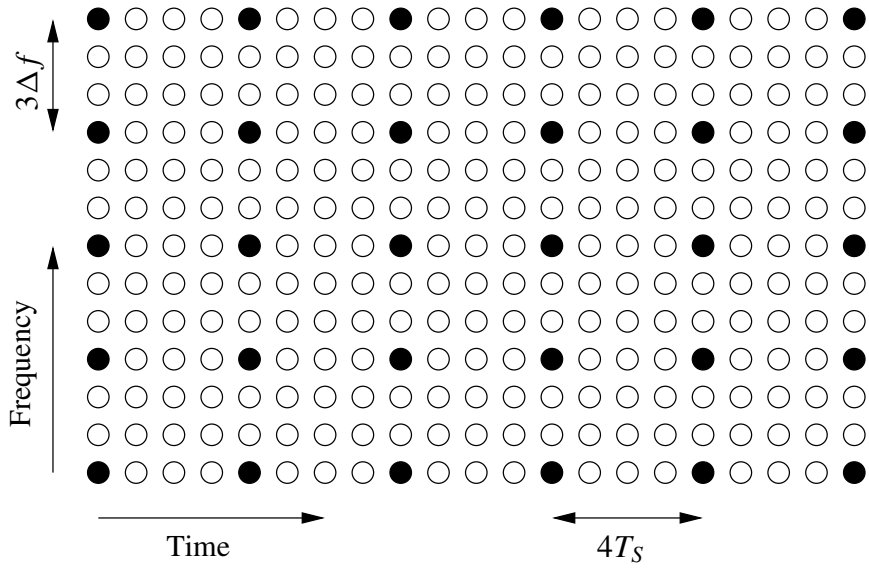

Figure 4.35 Example of a rectangular pilot grid.

numerical example, we consider the grid of Figure 4.35 for an OFDM system with carrier spacing $\Delta f = 1/T = 1$ kHz and symbol duration $T_S = 1250$ µs. At every third frequency, the channel will be measured once in the time $4T_S = 5$ ms, that is, the unknown signal (the time-variant channel) is sampled at the sampling frequency of 200 Hz. For a noise-free channel, we can conclude from the sampling theorem that the signal can be recovered from the samples if the maximum Doppler frequency $\nu_{\max}$ fulfills the condition

$$\nu_{\max} < 100\,\text{Hz}.$$

More generally, for a pilot spacing of $4T_S$, the condition

$$\nu_{\max} T_S < 1/8$$

must be fulfilled.

In frequency direction, the sample spacing is 3 kHz. From the (frequency domain) sampling theorem, we conclude that the delay power spectrum must be inside an interval of the length of 333 µs. Since the guard interval already has the length 250 µs, this condition is automatically fulfilled if we can assume that all the echoes lie within the guard interval. We can now start the interpolation (according to the sampling theorem) either in time or in frequency direction and then calculate the interpolated values for the other direction. Simpler interpolations are possible and may be used in practice for a very coherent channel, for example, linear interpolation or piecewise constant approximation. However, for a really time-variant and frequency-selective channel, these methods are not adequate. For a noisy channel, even the interpolation given by the sampling theorem is not the best choice because the noise is not taken into account. The optimum linear estimator will be derived in the next subsection.

In some systems, the pilot symbols are *boosted*, that is, they are transmitted with a higher energy than the modulation symbols. In that case, a rectangular grid as shown in

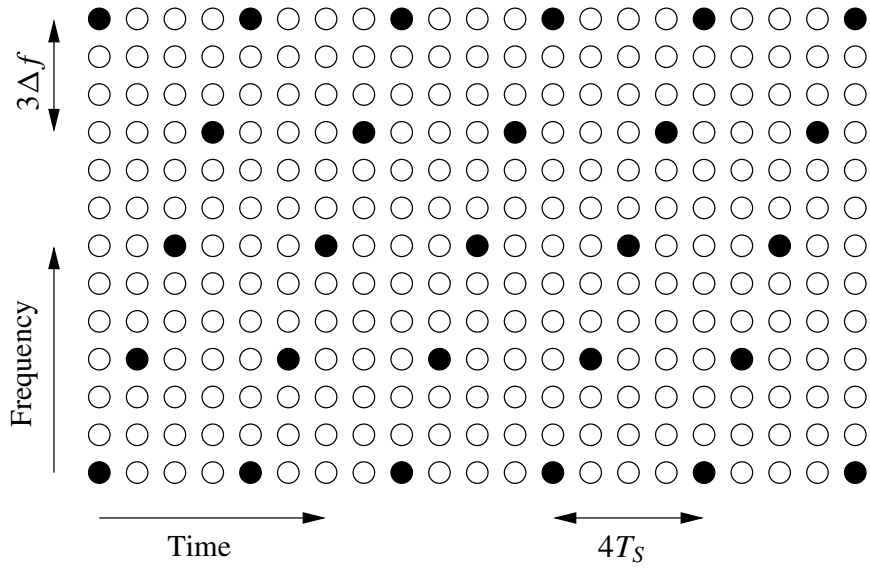

Figure 4.36 Example of a diagonal pilot grid.

Figure 4.35 would cause a higher average power for every fourth OFDM symbol, which is not desirable for reasons of transmitter implementation. In that case, a diagonal grid will be chosen. Figure 4.36 shows such a diagonal grid as it is used for the DVB-T system.

4.3.3 The Wiener estimator

Consider a complex discrete stochastic process with samples y_l that have to be estimated. For our application, we think of the complex fading amplitudes of a discrete channel model. Recall that in Section 4.1.4 we derived a discrete channel model for OFDM that could be written as

$$r_{kl} = \sqrt{\frac{T}{T_S}}\, c_{kl} s_{kl} + n_{kl}.$$

Here, c_{kl} is the complex fading amplitude of the time-frequency discrete channel model with frequency index k and time index l. This is a stochastic process in two dimensions. We may keep either the time index or the frequency index fixed and consider only one dimension. For the treatment of the two-dimensional stochastic process, we may rearrange the numbering similar to a parallel–serial conversion so that one can work with only one index. This makes the formalism more clear. The samples y_l of the process under consideration must be estimated from measurements x_m that are samples of another stochastic process. For our application, these processes are closely related: the x_m are the noisy channel measurements at the pilot positions. We look for a linear estimator, that is, we assume that the estimates $\hat{y}_l$ of the process y_l can be written as

$$\hat{y}_l = \sum_m b_{lm} x_m \tag{4.13}$$

with properly chosen estimator coefficients b_{lm}. The sum can be finite or infinite. To simplify the formalism, we assume that only a finite number of L samples y_l must be estimated from a finite number M of measurements x_m. We may then write the linear estimator as

$$\hat{\mathbf{y}} = \mathbf{B}\mathbf{x} \tag{4.14}$$

with the vectors $\hat{\mathbf{y}} = (\hat{y}_1, \ldots, \hat{y}_L)^T$ and $\mathbf{x} = (x_1, \ldots, x_M)^T$ and the estimator matrix

$$\mathbf{B} = \begin{pmatrix} b_{11} & b_{12} & \cdots & b_{1M} \\ b_{21} & b_{22} & \cdots & b_{2M} \\ \vdots & \vdots & \ddots & \vdots \\ b_{L1} & b_{L2} & \cdots & b_{LM} \end{pmatrix}.$$

Let $e_l = y_l - \hat{y}_l$ be the error of the estimate for the sample number l. The *ansatz* of the Wiener estimator is to minimize the mean square error (MMSE) for each sample, that is,

$$\mathrm{E}\left\{|e_l|^2\right\} = \min.$$

The *orthogonality principle* (or *projection theorem*) of probability theory (Papoulis 1991; Therrien 1992) says that this is equivalent to the orthogonality condition

$$\mathrm{E}\left\{e_l x_m^*\right\} = 0. \tag{4.15}$$

This orthogonality principle becomes intuitively clear and it can easily be visualized by means of the vector space structure of random variables. Then $\mathrm{E}\left\{e_l x_m^*\right\}$ is the scalar product of the random variables (vectors) e_l and x_m, and $\mathrm{E}\{|e_l|^2\} = \mathrm{E}\{|y_l - \hat{y}_l|^2\}$ is the squared distance between the vectors y_l and $\hat{y}_l$. Equation (4.13) says that $\hat{y}_l$ lies in the plane that is spanned by the random variables (vectors) $x_1, \ldots, x_l$. Then, as depicted in Figure 4.37, this distance (length of the error vector) becomes minimal if $\hat{y}_l$ is just the orthogonal projection of y_l on that plane. In that case, $e_l = y_l - \hat{y}_l$ is orthogonal to every vector x_m, that is, Equation (4.15) holds.

It is convenient to write Equation (4.15) in vector notation as

$$\mathrm{E}\left\{\mathbf{e} \cdot \mathbf{x}^\dagger\right\} = 0,$$

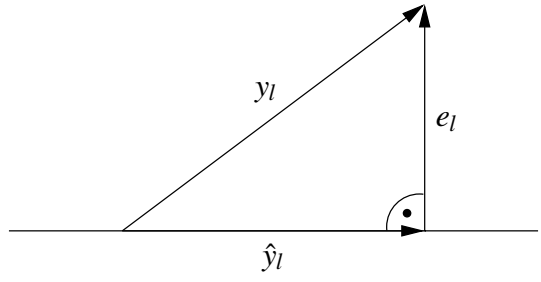

Figure 4.37 Illustration of the orthogonality principle.

that is, the $L \times M$ cross-correlation matrix between the error vector $\mathbf{e} = (e_1, \ldots, e_M)^T$ and the vector of measurements $\mathbf{x} = (x_1, \ldots, x_M)^T$ vanishes. Writing $\mathbf{e} = \mathbf{y} - \hat{\mathbf{y}}$, we obtain

$$\mathrm{E}\left\{(\mathbf{y} - \hat{\mathbf{y}}) \cdot \mathbf{x}^\dagger\right\} = 0,$$

and, employing Equation (4.14)

$$\mathrm{E}\left\{\mathbf{y} \cdot \mathbf{x}^\dagger\right\} = \mathrm{E}\left\{\mathbf{B}\mathbf{x} \cdot \mathbf{x}^\dagger\right\}.$$

This *Wiener–Hopf equation* can be written as

$$\mathbf{R}_{\mathbf{yx}} = \mathbf{B}\mathbf{R}_{\mathbf{xx}}, \tag{4.16}$$

where

$$\mathbf{R}_{\mathbf{xx}} = \mathrm{E}\left\{\mathbf{x} \cdot \mathbf{x}^\dagger\right\} \tag{4.17}$$

denotes the autocorrelation matrix of $\mathbf{x}$ and

$$\mathbf{R}_{\mathbf{yx}} = \mathrm{E}\left\{\mathbf{y} \cdot \mathbf{x}^\dagger\right\} \tag{4.18}$$

the cross-correlation matrix between $\mathbf{y}$ and $\mathbf{x}$. The Wiener–Hopf equation can be solved by matrix inversion, that is,

$$\mathbf{B} = \mathbf{R}_{\mathbf{yx}}\mathbf{R}_{\mathbf{xx}}^{-1}.$$

Estimation error

The estimation error of a linear predictor can be derived as follows. We define a mean square error (MSE) matrix $\mathbf{E}$ by

$$\mathbf{E} = \mathrm{E}\left\{\mathbf{e} \cdot \mathbf{e}^\dagger\right\} = \mathrm{E}\left\{(\mathbf{y} - \hat{\mathbf{y}}) \cdot (\mathbf{y} - \hat{\mathbf{y}})^\dagger\right\}.$$

The diagonal elements $\mathrm{E}\left\{|e_l|^2\right\}$ of that matrix are the MSE for the estimates. For the linear estimator of Equation (4.14), we get

$$\mathbf{E} = \mathrm{E}\left\{(\mathbf{y} - \mathbf{B}\mathbf{x}) \cdot (\mathbf{y} - \mathbf{B}\mathbf{x})^\dagger\right\}$$

and

$$\mathbf{E} = \mathrm{E}\left\{\mathbf{y} \cdot \mathbf{y}^\dagger - \mathbf{B}\mathbf{x} \cdot \mathbf{y}^\dagger - \mathbf{y} \cdot (\mathbf{B}\mathbf{x})^\dagger + \mathbf{B}\mathbf{x} \cdot (\mathbf{B}\mathbf{x})^\dagger\right\}.$$

With Equations (4.17) and (4.18) we get

$$\mathbf{E} = \mathbf{R}_{\mathbf{yy}} - \mathbf{B}\mathbf{R}_{\mathbf{yx}}^\dagger - \left(\mathbf{R}_{\mathbf{yx}} - \mathbf{B}\mathbf{R}_{\mathbf{xx}}\right)\mathbf{B}^\dagger.$$

This is the general expression for any linear estimator $\mathbf{B}$. If $\mathbf{B}$ is the solution of the Wiener–Hopf equation, the expression in parentheses vanishes and we get the MMSE error matrix

$$\mathbf{E} = \mathbf{R}_{\mathbf{yy}} - \mathbf{B}\mathbf{R}_{\mathbf{yx}}^\dagger.$$

4.3.4 Wiener filtering for OFDM

For our application, the stochastic process corresponds to the complex fading amplitudes at certain times and frequencies, that is,

$$y_i = H(f_i, t_i),$$

where $H(f, t)$ is the time-variant channel transfer function, see Section 4.1.4. If only channel estimation in time direction is required (at a given frequency), all the values of f_i are identical. If only channel estimation in frequency direction is required (at a given time), all the values of t_i are identical. But, in general, we have to deal with an arbitrary set of points in the time-frequency plane. The measurements will be taken at some pilot positions given by $\left\{\left(f_{i_m}, t_{i_m}\right)\right\}_{m=1}^{M}$. The measurements x_m are noisy channel samples, that is,

$$x_m = H\left(f_{i_m}, t_{i_m}\right) + n_i,$$

where n_i is complex AWGN with variance $\sigma^2 = E_S/N_0$ and E_S is the energy of the pilot symbols. As discussed in detail in Chapter 2, we assume the WSSUS model for $H(f, t)$ with two-dimensional autocorrelation function

$$\mathrm{E}\left\{H(f, t)H^*(f', t')\right\} = \mathcal{R}(f - f', t - t').$$

We assume that the noise and the fading are statistically independent. Then the matrix elements of $\mathbf{R_{xx}}$ are given by

$$(\mathbf{R_{xx}})_{km} = \mathcal{R}\left(f_{i_k} - f_{i_m}, t_{i_k} - t_{i_m}\right) + \delta_{km}\sigma^2, \tag{4.19}$$

and the matrix elements of $\mathbf{R_{yx}}$ are

$$\left(\mathbf{R_{yx}}\right)_{lm} = \mathcal{R}\left(f_l - f_{i_m}, t_l - t_{i_m}\right). \tag{4.20}$$

Channel estimation in time direction

Consider a fixed carrier of an OFDM signal. In that case, all the frequency samples are equal to the subcarrier frequency f_k and we only have to deal with samples of the multiplicative fading process $c(t) = H(f_k, t)$ for that frequency. This wide-sense stationary process has the autocorrelation function

$$\mathcal{R}(0, t) = \mathcal{R}_c(t),$$

which is given as the inverse Fourier transform of the Doppler spectrum. For the Jakes spectrum, it is given by

$$\mathcal{R}_c(t) = \mathrm{J}_0\left(2\pi\nu_{\max}t\right).$$

For a rectangular Doppler spectrum between $-\nu_{\max}$ and $\nu_{\max}$, it is given by

$$\mathcal{R}_c(t) = \mathrm{sinc}\left(2\nu_{\max}t\right).$$

For some applications, the Gaussian Doppler spectrum

$$\mathcal{S}_c(\nu) = \frac{1}{\sqrt{2\pi\sigma_D^2}}\exp\left(-\frac{1}{2\sigma_D^2}\nu^2\right)$$

of width σ_D is an appropriate model. It has the autocorrelation function

$$\mathcal{R}_c(t) = \exp\left(-\frac{1}{2}(2\pi\sigma_D t)^2\right).$$

The autocorrelation matrix $\mathbf{R_{xx}}$ is given by the elements

$$(\mathbf{R_{xx}})_{km} = \mathcal{R}_c\left(t_{i_k} - t_{i_m}\right) + \delta_{km}\sigma^2.$$

The matrix elements of the cross correlation $\mathbf{R_{yx}}$ are given by

$$\left(\mathbf{R_{yx}}\right)_{lm} = \mathcal{R}\left(t_l - t_{i_m}\right).$$

To give a concrete example, we assume that every fourth symbol in time direction is a pilot symbol, as it is the case for DVB-T for certain subcarrier frequencies. The channel at the positions in between and at the pilot positions itself must be estimated from the channel measurements taken at these pilot positions. In practice, only a finite number of measurements can be used. We illustrate the channel estimation for the case that channel measurements are taken at the five positions $t = -8T_S, -4T_S, 0, +4T_S, +8T_S$ for the estimation at the four positions $t = 0, T_S, 2T_S, 3T_S$. This corresponds to the grid as depicted in Figure 4.35 or Figure 4.36 at a frequency where pilots are located. Note that measurements are taken at five adjacent pilot positions to estimate the channel at four adjacent time slots. One of them is the pilot position in the middle and the other three are those between this pilot and the next one. Obviously, this is a noncausal estimator, that is, a delay has to be taken into account. The measurements are given by the random vector

$$\mathbf{x} = \begin{pmatrix} c(-8T_S) & c(-4T_S) & c(0) & c(4T_S) & c(8T_S) \end{pmatrix}^T + \mathbf{n},$$

where $\mathbf{n}$ is a vector of five AWGN samples, each with variance σ^2. The random vector to be estimated is given by

$$\mathbf{y} = \begin{pmatrix} c(0) & c(T_S) & c(2T_S) & c(3T_S) \end{pmatrix}^T,$$

and the autocorrelation matrix is given by

$$\mathbf{R_{xx}} = \begin{pmatrix} \mathcal{R}_c(0)+\sigma^2 & \mathcal{R}_c(4T_S) & \mathcal{R}_c(8T_S) & \mathcal{R}_c(12T_S) & \mathcal{R}_c(16T_S) \\ \mathcal{R}_c(-4T_S) & \mathcal{R}_c(0)+\sigma^2 & \mathcal{R}_c(4T_S) & \mathcal{R}_c(8T_S) & \mathcal{R}_c(12T_S) \\ \mathcal{R}_c(-8T_S) & \mathcal{R}_c(-4T_S) & \mathcal{R}_c(0)+\sigma^2 & \mathcal{R}_c(4T_S) & \mathcal{R}_c(8T_S) \\ \mathcal{R}_c(-12T_S) & \mathcal{R}_c(-8T_S) & \mathcal{R}_c(-4T_S) & \mathcal{R}_c(0)+\sigma^2 & \mathcal{R}_c(4T_S) \\ \mathcal{R}_c(-16T_S) & \mathcal{R}_c(-12T_S) & \mathcal{R}_c(-8T_S) & \mathcal{R}_c(-4T_S) & \mathcal{R}_c(0)+\sigma^2 \end{pmatrix}.$$

We note that the additive SNR term σ^2 on the diagonal ensures that the matrix is nonsingular. We will see in Subsection 4.4.3 that the eigenvalues of this matrix for $\sigma^2 = 0$ represent the diversity branches of the equivalent independent fading channel. It may happen (and is often the case in practice) that the channel does not have the full diversity degree. This corresponds to a singular matrix. To ensure that $\mathbf{R_{xx}}$ can be inverted, one should always set $\sigma^2 > 0$. In practice, a very rough estimate of the noise is sufficient. For example, one can iteratively improve the noise estimate by comparing the measured channel values at

the pilot position with their estimates. One starts that procedure with some reasonable SNR value, where the system will typically work.

The cross-correlation matrix is given by

$$\mathbf{R_{yx}} = \begin{pmatrix} \mathcal{R}_c(8T_S) & \mathcal{R}_c(4T_S) & \mathcal{R}_c(0) & \mathcal{R}_c(-4T_S) & \mathcal{R}_c(-8T_S) \\ \mathcal{R}_c(9T_S) & \mathcal{R}_c(5T_S) & \mathcal{R}_c(T_S) & \mathcal{R}_c(-3T_S) & \mathcal{R}_c(-7T_S) \\ \mathcal{R}_c(10T_S) & \mathcal{R}_c(6T_S) & \mathcal{R}_c(2T_S) & \mathcal{R}_c(-2T_S) & \mathcal{R}_c(-6T_S) \\ \mathcal{R}_c(11T_S) & \mathcal{R}_c(7T_S) & \mathcal{R}_c(3T_S) & \mathcal{R}_c(-T_S) & \mathcal{R}_c(-5T_S) \end{pmatrix}.$$

The estimator matrix

$$\mathbf{B} = \mathbf{R_{yx}}\mathbf{R_{xx}^{-1}}$$

has the shape

$$\mathbf{B} = \begin{pmatrix} b_{11} & b_{12} & b_{13} & b_{14} & b_{15} \\ b_{21} & b_{22} & b_{23} & b_{24} & b_{25} \\ b_{31} & b_{32} & b_{33} & b_{34} & b_{35} \\ b_{41} & b_{42} & b_{43} & b_{44} & b_{45} \end{pmatrix}.$$

Now, denote the noisy channels measurements by the vector

$$\mathbf{x} = \begin{pmatrix} \tilde{c}(-8T_S) & \tilde{c}(-4T_S) & \tilde{c}(0) & \tilde{c}(4T_S) & \tilde{c}(8T_S) \end{pmatrix}^T$$

and the estimates by the vector

$$\hat{\mathbf{y}} = \begin{pmatrix} \hat{c}(0) & \hat{c}(T_S) & \hat{c}(2T_S) & \hat{c}(3T_S) \end{pmatrix}^T.$$

Then, the estimator is given by

$$\begin{pmatrix} \hat{c}(0) \\ \hat{c}(T_S) \\ \hat{c}(2T_S) \\ \hat{c}(3T_S) \end{pmatrix} = \begin{pmatrix} b_{11} & b_{12} & b_{13} & b_{14} & b_{15} \\ b_{21} & b_{22} & b_{23} & b_{24} & b_{25} \\ b_{31} & b_{32} & b_{33} & b_{34} & b_{35} \\ b_{41} & b_{42} & b_{43} & b_{44} & b_{45} \end{pmatrix} \begin{pmatrix} \tilde{c}(-8T_S) \\ \tilde{c}(-4T_S) \\ \tilde{c}(0) \\ \tilde{c}(4T_S) \\ \tilde{c}(8T_S) \end{pmatrix}.$$

Since the random process $c(t)$ is wide-sense stationary and the pilot positions are periodic with period $4T_S$, any time shift of the whole setup by $4iT_S$, $i = 1, 2, 3, \ldots$ result in the same estimator, that is,

$$\begin{pmatrix} \hat{c}(4iT_S) \\ \hat{c}((4i+1)T_S) \\ \hat{c}((4i+2)T_S) \\ \hat{c}((4i+3)T_S) \end{pmatrix} = \begin{pmatrix} b_{11} & b_{12} & b_{13} & b_{14} & b_{15} \\ b_{21} & b_{22} & b_{23} & b_{24} & b_{25} \\ b_{31} & b_{32} & b_{33} & b_{34} & b_{35} \\ b_{41} & b_{42} & b_{43} & b_{44} & b_{45} \end{pmatrix} \begin{pmatrix} \tilde{c}(4(i-2)T_S) \\ \tilde{c}(4(i-1)T_S) \\ \tilde{c}(4iT_S) \\ \tilde{c}(4(i+1)T_S) \\ \tilde{c}(4(i+2)T_S) \end{pmatrix}.$$

The estimate can now be interpreted as the convolution of the measurements with the left–right flipped columns of the estimator matrix. To see this, we define the four discrete-time signals

$$\hat{c}_l[i] = \hat{c}((4i+l)T_S),\ l = 0, 1, 2, 3$$

for the estimates and the discrete-time signal

$$\tilde{c}[m] = \tilde{c}(4mT_S)$$

for the measurements. We define four impulse responses $b_l[m]$, $l = 0, 1, 2, 3$ of the estimator by rewriting the estimator matrix as

$$\mathbf{B} = \begin{pmatrix} b_0[2] & b_0[1] & b_0[0] & b_0[-1] & b_0[-2] \\ b_1[2] & b_1[1] & b_1[0] & b_1[-1] & b_1[-2] \\ b_2[2] & b_2[1] & b_2[0] & b_2[-1] & b_2[-2] \\ b_3[2] & b_3[1] & b_3[0] & b_3[-1] & b_3[-2] \end{pmatrix}.$$

The estimator can now be written as the noncausal filtering

$$\hat{c}_l[i] = \sum_{m=-2}^{2} b_l[m]\tilde{c}[i-m]$$

of the measurements.

To keep the treatment more easy, we have chosen a small filter with a fixed number of five taps. The generalization to more taps is straightforward. In practice, a figure in the order of 20 taps is a reasonable choice.

Channel estimation in frequency direction

We now consider the time slot of a fixed OFDM symbol. In that case, all the time samples are equal and we only have to deal with frequency samples of the transfer function. This uncorrelated scattering (i.e. frequency-shift invariant) process $H(f)$ has the frequency autocorrelation function

$$\mathcal{R}(f, 0) = \mathcal{R}_H(f),$$

which is given as the Fourier transform of the delay power spectrum. For the exponential delay power spectrum, we have

$$\mathcal{R}_H(f) = \frac{1}{1 + j2\pi f\tau_m}.$$

For a rectangular delay power spectrum between 0 and $\tau_{\max}$, it is given by

$$\mathcal{R}_H(f) = \mathrm{e}^{-j\pi f\tau_{\max}} \cdot \operatorname{sinc}(f\tau_{\max}).$$

The autocorrelation matrix $\mathbf{R_{xx}}$ has the elements

$$(\mathbf{R_{xx}})_{km} = \mathcal{R}_H\left(f_{i_k} - f_{i_m}\right) + \delta_{km}\sigma^2,$$

and the cross-correlation matrix $\mathbf{R_{yx}}$ has the elements

$$\left(\mathbf{R_{yx}}\right)_{lm} = \mathcal{R}_H\left(f_l - f_{i_m}\right).$$

Again, we consider a concrete example that is inspired by the pilot structure of DVB-T. We assume that every third symbol in frequency direction is a pilot symbol. The channel at the positions in between and at the pilot positions itself must be estimated from the channel measurements taken at these pilot positions. We assume that channel measurements are taken at the five positions $f = -6\Delta f, -3\Delta f, 0, +3\Delta f, +6\Delta f$ for the estimation at the four positions $f = 0, \Delta f, 2\Delta f, 3\Delta f$. Here $\Delta f = 1/T$ is the OFDM carrier spacing, and

$f = 0$ corresponds to the center frequency. The measurements are given by the random vector

$$\mathbf{x} = \begin{pmatrix} H(-6\Delta f) & H(-2\Delta f) & H(0) & H(2\Delta f) & H(6\Delta f) \end{pmatrix}^T + \mathbf{n},$$

where $\mathbf{n}$ is a vector of five AWGN samples with variance σ^2. The random vector to be estimated is

$$\mathbf{y} = \begin{pmatrix} H(0) & H(\Delta f) & H(2\Delta f) \end{pmatrix}^T.$$

For the autocorrelation matrix, we have

$$\mathbf{R_{xx}} = \begin{pmatrix} \mathcal{R}_H(0) + \sigma^2 & \mathcal{R}_H(3\Delta f) & \mathcal{R}_H(6\Delta f) & \mathcal{R}_H(9\Delta f) & \mathcal{R}_H(12\Delta f) \\ \mathcal{R}_H(-3\Delta f) & \mathcal{R}_H(0) + \sigma^2 & \mathcal{R}_H(3\Delta f) & \mathcal{R}_H(6\Delta f) & \mathcal{R}_H(9\Delta f) \\ \mathcal{R}_H(-6\Delta f) & \mathcal{R}_H(-3\Delta f) & \mathcal{R}_H(0) + \sigma^2 & \mathcal{R}_H(3\Delta f) & \mathcal{R}_H(6\Delta f) \\ \mathcal{R}_H(-9\Delta f) & \mathcal{R}_H(-6\Delta f) & \mathcal{R}_H(-3\Delta f) & \mathcal{R}_H(0) + \sigma^2 & \mathcal{R}_H(3\Delta f) \\ \mathcal{R}_H(-12\Delta f) & \mathcal{R}_H(-9\Delta f) & \mathcal{R}_H(-6\Delta f) & \mathcal{R}_H(-3\Delta f) & \mathcal{R}_H(0) + \sigma^2 \end{pmatrix},$$

and the cross-correlation matrix is given by

$$\mathbf{R_{yx}} = \begin{pmatrix} \mathcal{R}_H(6\Delta f) & \mathcal{R}_H(3\Delta f) & \mathcal{R}_H(0) & \mathcal{R}_H(-3\Delta f) & \mathcal{R}_H(-6\Delta f) \\ \mathcal{R}_H(7\Delta f) & \mathcal{R}_H(4\Delta f) & \mathcal{R}_H(\Delta f) & \mathcal{R}_H(-2\Delta f) & \mathcal{R}_H(-5\Delta f) \\ \mathcal{R}_H(8\Delta f) & \mathcal{R}_H(5\Delta f) & \mathcal{R}_H(2\Delta f) & \mathcal{R}_H(-\Delta f) & \mathcal{R}_H(-4\Delta f) \end{pmatrix}.$$

The estimator matrix

$$\mathbf{B} = \mathbf{R_{yx}} \mathbf{R_{xx}^{-1}}$$

has the shape

$$\mathbf{B} = \begin{pmatrix} b_{11} & b_{12} & b_{13} & b_{14} & b_{15} \\ b_{21} & b_{22} & b_{23} & b_{24} & b_{25} \\ b_{31} & b_{32} & b_{33} & b_{34} & b_{35} \end{pmatrix}.$$

Now, denote the noisy channel measurements by the vector

$$\mathbf{x} = \begin{pmatrix} \tilde{H}(-6\Delta f) & \tilde{H}(-3\Delta f) & \tilde{H}(0) & \tilde{H}(3\Delta f) & \tilde{H}(6\Delta f) \end{pmatrix}^T$$

and the estimates by the vector

$$\hat{\mathbf{y}} = \begin{pmatrix} \hat{H}(0) & \hat{H}(\Delta f) & \hat{H}(2\Delta f) \end{pmatrix}^T.$$

Then, the estimator is given by

$$\begin{pmatrix} \hat{H}(0) \\ \hat{H}(\Delta f) \\ \hat{H}(2\Delta f) \end{pmatrix} = \begin{pmatrix} b_{11} & b_{12} & b_{13} & b_{14} & b_{15} \\ b_{21} & b_{22} & b_{23} & b_{24} & b_{25} \\ b_{31} & b_{32} & b_{33} & b_{34} & b_{35} \end{pmatrix} \begin{pmatrix} \tilde{H}(-6\Delta f) \\ \tilde{H}(-3\Delta f) \\ \tilde{H}(0) \\ \tilde{H}(3\Delta f) \\ \tilde{H}(6\Delta f) \end{pmatrix}.$$

Since the random process $H(f)$ is *uncorrelated scattering* (i.e. wide-sense stationary in frequency direction) and the pilot positions are periodic with period $3\Delta f$, any frequency shift by $3i/T$, $i = 0, \pm 1, \pm 2, \ldots$ of the whole setup will result into the same estimator.

Then, we can use the same arguments as for the estimation in time direction to show that the estimate can be interpreted as the convolution of the measurements with the left–right flipped columns of the estimator matrix. We define the three (frequency-) discrete signals

$$\hat{H}_l[i] = \hat{H}\left((3i + l)\,\Delta f\right),\ l = 0, 1, 2$$

for the estimates and the discrete signal

$$\tilde{H}[m] = \tilde{H}\left(3mT_S\right)$$

for the measurements. We define three impulse responses $b_l[m]$, $(l = 0, 1, 2)$ of the estimator by rewriting the estimator matrix as

$$\mathbf{B} = \begin{pmatrix} b_0[2] & b_0[1] & b_0[0] & b_0[-1] & b_0[-2] \\ b_1[2] & b_1[1] & b_1[0] & b_1[-1] & b_1[-2] \\ b_2[2] & b_2[1] & b_2[0] & b_2[-1] & b_2[-2] \end{pmatrix}.$$

The estimator can now be written as the noncausal filtering

$$\hat{H}_l[i] = \sum_{m=-2}^{2} b_l[m]\tilde{H}[i - m]$$

of the measurements.

Even though this filtering in the frequency domain is formally the same as filtering in the time domain, there is an essential difference in practice. One can easily think of an infinite time duration of the transmission, but the frequency domain is always hard limited by the signal bandwidth, corresponding to a finite number of OFDM subcarriers. This number may be quite small (approximately 50 for WLAN systems or approximately 200 for DRM) or large (more than 6000 for the 8K mode for DVB-T). In any case, there will be edge effects. At both edges, there are some measurements not available because there are no pilots outside the band. If one ignores these terms in the sum, it will severely degrade the performance. This is especially severe for a low number of carriers. For WLAN systems and a filter of approximately length 10, the channel estimation would be correct for only approximately 40 subcarriers. Especially for higher-level QAM modulation, this results in an unacceptable error, even for a high number of subcarriers. To cope with this, the estimator must be modified at the edges. It is not a convolution there, but a matrix estimator that makes use of, for example, the 20 closest available pilots.

In contrast to time domain estimation, the estimation in frequency domain is always a problem with a finite number of measurements and a finite number of estimates. It is therefore worth considering the use of the full matrix estimator to solve this problem. This needs more processor power, but it provides us with the optimal MMSE estimate for the given number of measurements that are available.

In that case, the matrix elements of $\mathbf{R_{xx}}$ are calculated for all pairs of pilot positions f_{i_k}, f_{i_m} as

$$(\mathbf{R_{xx}})_{km} = \mathcal{R}_H\left(f_{i_k} - f_{i_m}\right) + \delta_{km}\sigma^2$$

and the matrix elements of $\mathbf{R_{yx}}$ as

$$\left(\mathbf{R_{yx}}\right)_{lm} = \mathcal{R}_H\left(f_l - f_{i_m}\right),$$

where the f_l are the positions of the estimates. The estimator matrix

$$\mathbf{B} = \mathbf{R}_{\mathbf{yx}}\mathbf{R}_{\mathbf{xx}}^{-1}$$

then has as much columns as there are pilot positions and as many rows as there are estimate positions.

Channel estimation in time and frequency direction

In most situations, a channel estimation has to be performed both in time and frequency direction. In that case, the full autocorrelation matrix according to Equation (4.19) and the cross correlation according to Equation (4.20) must be calculated. The pilot positions $\left(f_{i_k}, t_{i_k}\right)$ are arbitrary. Typically, they are positioned on some grid. Figure 4.35 shows such a rectangular grid corresponding to the above examples for time and frequency.

The pilot positions are numbered in some order. In most typical channel models, the scattering function and thus the two-dimensional autocorrelation function factorizes to

$$\mathcal{R}(f,t) = \mathcal{R}_H(f)\mathcal{R}_c(t).$$

From this, the estimator matrix **B** can be calculated. The estimation is time- and frequency-shift invariant because of the WSSUS property. As a consequence, the estimation can be written as a two-dimensional convolution. Of course, the edges of the frequency have to be taken into account as discussed above.

Instead of that rather involved 2-D filtering one can perform a suboptimal 1-D × 1-D filtering without losing significantly in performance (Hoeher 1991; Hoeher *et al.* 1997). One may first perform a 1-D channel estimation, for example, in frequency direction (with the method described above) at those time slots where the pilots are located. After that, at these time slots, there is a channel estimate available for every frequency. Now a 1-D channel estimation in time direction can be performed and an estimate for all time-frequency positions is available. One can also first do a 1-D channel estimation in time direction and then in frequency direction. The order can be shown to be arbitrary due to linearity of the estimation and due to the fact that the rectangular constellation is the Cartesian product of two one-dimensional ones.

We finally note that in practical systems as DVB-T and DRM a diagonal grid has been chosen rather than a rectangular one. The procedure is similar, but the order of channel estimation is no longer arbitrary.

4.4 Interleaving and Channel Diversity for OFDM Systems

4.4.1 Requirements of the mobile radio channel

As already discussed in Chapter 3, channel coding is one important method to introduce diversity into the mobile radio transmission. To achieve the full diversity gain of the code, the transmitted bits must be affected by independent fading. Independent or uncorrelated fading amplitudes[6] can only be realized by a physical separation of the parts of the signal corresponding to the different bits. Bits that are closely related by the code should not be

[6]Here we do not distinguish between uncorrelated and independent, keeping in mind that we will later focus on the case where both are the same.

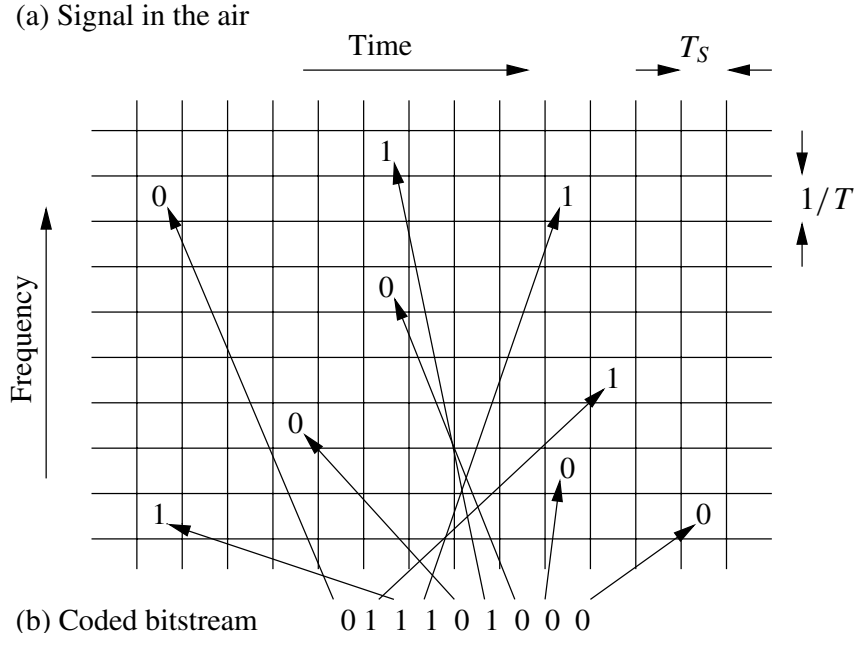

Figure 4.38 Time and frequency interleaving for OFDM with symbol duration T_S and Fourier analysis window T.

transmitted at closely related locations of the channel. For a block code, bits are closely related by the code if they are part of the same code word. For a convolutional code, they are closely related unless there are many constraint lengths between them. For a moving receiver (or transmitter), the separation of closely related bits can be realized in the physical dimension of time. This separation is called *time interleaving*. Obviously, one must wait some time until all closely related bits are received and can be decoded. Thus, time interleaving introduces a *decoding delay*.

For multicarrier transmission, there is an obvious additional way to realize a physical separation in frequency direction. This is called *frequency interleaving*. Thus, as depicted in Figure 4.38, multicarrier transmission provides us with two degrees of freedom to separate the information in the physical transmission channel: time and frequency. The physical reasons that cause decorrelation in time and in frequency direction are independent, so that multicarrier transmission with time *and* frequency interleaving is a very powerful technique for mobile radio transmission systems.

The decorrelation in time has its origin in the time variance of the channel due to the Doppler spread that is caused by multipath reception for a moving vehicle. It can equivalently be interpreted as caused by the motion of a vehicle through a spatial interference pattern. The spatial correlation length is $x_{\text{corr}} = \lambda$, where $\lambda = c/f_0$ is the wavelength, c is the velocity of light and f_0 is the radio frequency. The corresponding correlation time is $t_{\text{corr}} = x_{\text{corr}}/v = \nu_{\max}^{-1}$, where v is the vehicle speed and

$$\nu_{\max} = \frac{v}{c} f_0$$

is the maximum Doppler frequency. The correlation time is then given by

$$t_{\text{corr}} = \frac{c}{f_0 v} \approx \frac{1080 \text{ MHz}}{f_0} \frac{\text{km/h}}{v} \text{ seconds.}$$

The time separation of closely related bits should be significantly larger that this correlation time. We give a numerical example.

Example 7 (Time interleaving for DAB) *The European DAB system has been introduced in many regions in Europe and in Canada. It uses Band III (174–240 MHz) and L-band (1452–1492 MHz) frequencies. In many European regions, the TV channel 12 (223–230 MHz) has been allocated for DAB. For* $f_0 = 225$ *MHz and* $v = 100$ *km/h, the above formula yields a correlation time* $t_{\text{corr}} = 48$ *ms. We will later see that the DAB time interleaver separates two adjacent encoded bits by exactly 24 ms, that is, twice the correlation time. Thus, for Band III transmission and typical vehicle speeds, time interleaving alone does, by far, not guarantee a sufficient statistical independence of the fading amplitude of closely related bits. In the DAB system – as in many other communication systems – a trade-off has to be made between the requirements of channel coding (leading to a huge interleaver) and the restrictions of decoding delay given by the application. For multicarrier systems as DAB, the frequency interleaving is an appropriate method to come out of this dilemma.*

The decorrelation in frequency direction has its origin in the frequency selectivity of the channel due to the different travel times caused by the multipath reception. The frequency correlation length f_{corr} – or coherence bandwidth – as introduced in Chapter 2 is given by $f_{\text{corr}} = \tau_m^{-1}$, where τ_m is the delay spread of the channel. An electromagnetic wave travels 300 m in 1 µs. Thus, in an environment with path differences of a few hundred meters, the system bandwidth should be significantly greater than 1 MHz to achieve an efficient frequency interleaving.

4.4.2 Time and frequency interleavers

Interleaving can be implemented by different techniques. A *block interleaver* always takes a *block* of K coded symbols[7] of the data stream and changes the order of symbols within this block. After this permutation, the symbols are sent to the channel. At the receiver, the permutation is inverted. A *convolutional interleaver* – similar to a convolutional code – has no block-oriented structure and acts on the flowing symbol stream. Frequency interleavers are typically block interleavers as there is a block structure involved by the number of subcarriers. Convolutional interleavers are often regarded as the best choice for the time interleaver as they have desirable properties concerning decoding delay.

Block interleavers

The simplest way to implement a block interleaver is to apply a pseudorandom permutation to each block of K encoded symbols. Owing to the random nature of the interleaver, this, by construction, does not guarantee any minimum separation of symbols on the channel.

[7] This can be encoded bits or bytes (for RS codes) or even complex modulation symbols.

However, any randomly chosen permutation can easily be analyzed numerically and its performance for a given transmission system can be evaluated by simulations.

A matrix block interleaver offers a more constructive approach. We take a block of $K = N \cdot B$ symbols and write them row-wise into an $N \times B$ matrix. Then we read them out column-wise and send them to the channel. Take, as an example, $N = 12$, $B = 4$, and $K = 48$. We write the 48 symbols $a_0, a_1, a_2, \ldots, a_{48}$ row-wise into a 12×4 matrix as

$$\text{r} \downarrow \begin{pmatrix} a_0 & a_1 & a_2 & a_3 \\ a_4 & a_5 & a_6 & a_7 \\ a_8 & a_9 & a_{10} & a_{11} \\ a_{12} & a_{13} & a_{14} & a_{15} \\ \vdots & \vdots & \vdots & \vdots \\ a_{44} & a_{45} & a_{46} & a_{47} \\ & \text{w} & \rightarrow & \end{pmatrix}$$

and read them out column-wise. The bit stream on the channel is then given by

$$(a_0, a_4, a_8, a_{12}, a_{16}, a_{20}, a_{24}, \ldots, a_{44}\, a_1, a_5, \ldots, a_{39}, a_{43}, a_{47}).$$

At the receiver, the deinterleaver writes column-wise into the same matrix and reads out row-wise.

Let us call each matrix row a *subblock*. Assume that the symbols of each subblock are closely related, but symbols of different subblocks are unrelated because each subblock is a code word. We may think, for example, of a WH(4, 2, 2) code and write each code word of length $B = 4$ into a row. Then, on the channel, any two bits of the same code word are separated on the channel by at least $N = 12$ symbol positions. To extend this example further, we think of OFDM transmission with $K = 48$ subcarriers with carrier spacing T^{-1}. We choose BPSK modulation and map the symbols in the above order on these carriers. Then each two bits of the same code word are separated in the frequency dimension by $12/T$[8]. Thus, for two symbols of the same subblock, this matrix block interleaver guarantees a separation in frequency by $N \cdot T^{-1}$ when used as frequency interleaver for OFDM, or in time by $N \cdot T_S$ when used as a time interleaver. The deinterleaver at the receiver simply writes column-wise into the matrix and reads out row-wise. The matrix at the (de) interleaver can be implemented by a RAM.

Let us summarize. We call each matrix column a *frame*. A frame is a sequence of N adjacent symbols on the channel. The $N \times B$ matrix block interleaver with frame length N and subblock length B has the following properties:

1. All symbols of one subblock of length B are transmitted in different frames.
2. If one frame of length N is completely corrupted by an error burst, this will only affect one symbol in each subblock of length B.
3. The overall decoding delay (interleaver plus deinterleaver together) is $2BN$ symbol clocks.

[8]For QPSK transmission, half of the code words are mapped on the inphase and the other half on the quadrature component. We may thus simply double the matrix in horizontal direction. The left part will then be mapped on the inphase, the right on the quadrature component.

We note that, by construction, such a matrix block interleaver guarantees a certain physical separation. However, the very regular structure of this interleaver may sometimes lead to unwanted properties.

Convolutional interleavers

It is possible to construct a convolutional interleaver with the same two first properties as above but only half the decoding delay of the corresponding block interleaver. Because decoding delay is a critical item for most communication systems, convolutional interleavers are often preferred in practical systems.

We consider a serial symbol stream $a_0, a_1, a_2, \ldots$. With this symbol stream we do a serial-to-parallel (S/P) conversion that results in a stream of subblocks of B parallel symbols. Let $i = 0, 1, 2, \ldots, B-1$ denote the position of each symbol of a subblock. Then the symbol with position i in a subblock is delayed by $i \cdot M$ parallel symbol clocks, where M is a certain integer number that must be chosen to adjust the interleaver properties. After that delay, the parallel symbol stream will be P/S converted and then transmitted (see Figure 4.39).

For a better understanding of the properties of the convolutional interleaver, we may think that M subblocks of length B are grouped together to a *data frame* of length $N = B \cdot M$. The interleaver output will be grouped into *transmission frames* of the same structure, but, by the action of the interleaver, the symbols are transmitted in different frames. Since the serial symbol clock and the parallel symbol clock are related by the factor B, the symbol with position i in each subblock will be delayed by $i \cdot N$ serial symbol clocks, that is, by i frames, thereby retaining the relative position within a frame.

The deinterleaver at the receiver has the same structure as the interleaver, but the symbol with position $i = 0, 1, 2, \ldots, B-1$ in a subblock will be delayed by $(B - i - 1) \cdot M$ parallel symbol clocks (see Figure 4.40).

It is evident from both figures that the deinterleaver inverts the operation of the interleaver, thereby introducing an overall decoding delay of $(B-1) \cdot N$ symbol clocks, that is, $B-1$ frames.

The action of an (N, B) convolutional interleaver can be visualized as shown in Figure 4.41 for $N = 12$ and $B = 4$. As depicted in part (a) of the figure, we arrange

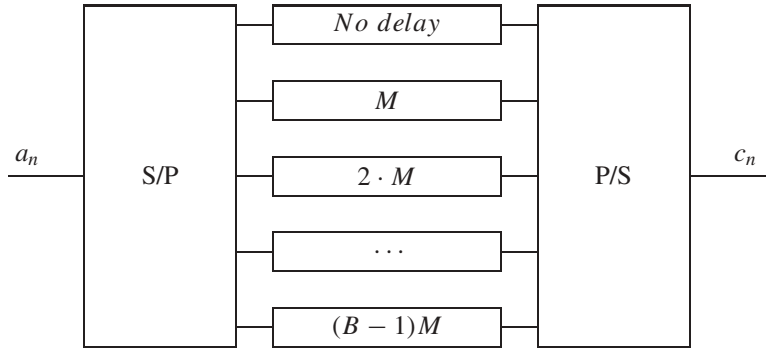

Figure 4.39 Block diagram for the convolutional interleaver.

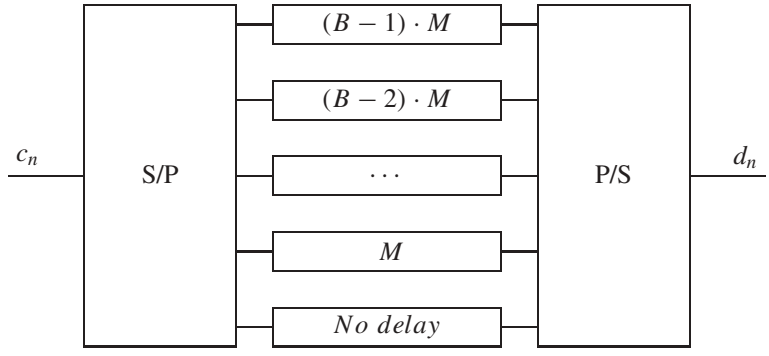

Figure 4.40 Block diagram for the convolutional deinterleaver.

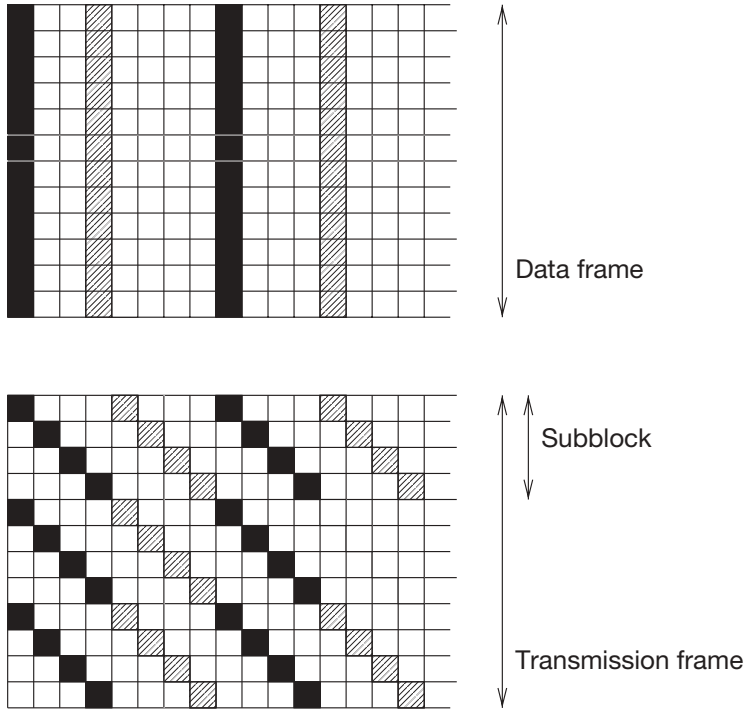

Figure 4.41 The action of a convolutional interleaver.

the sequence of frames as the columns of a matrix. If we read out this matrix column-wise, adjacent positions in the same row will be read out with a time difference of one frame duration, that is, N symbol clocks. We may thus realize the actions of the interleaver by shifting the row of position number i in the subblock to the right by i horizontal positions (see part (b) of the figure). Obviously, the B bits within the same subblock will be shifted

to B different columns that correspond to different transmission frames when we read out the matrix. We summarize the properties of a (N, B) convolutional interleaver.

1. All symbols of one subblock of length B are transmitted in different frames.
2. If one transmission frame of length N is completely corrupted by an error burst, this affects only one symbol in each subblock of length B in the data frame.
3. If one subblock of length B inside a transmission frame of length N is completely corrupted by an error burst, this will only affect one symbol in a data frame of length N.
4. The overall decoding delay (interleaver plus deinterleaver together) is $(B-1)\cdot N$ symbol clocks.

The first two properties are clear from the above discussion. They are identical to the first two properties of the $N \times B$ matrix block interleaver. The third property has no such correspondence. It is clear from the figure and it can be understood from the fact that one can interchange the interleaver and the deinterleaver without altering the properties. Using this argument, the third property immediately follows from the first one.

Figures 4.39 and 4.40 correspond to a shift register implementation of the delays. However, Figure 4.41 suggests a matrix representation realized by a RAM. This will be favorable for implementation.

To do so, we need a matrix with N rows. For a moment, we allow the matrix to have an infinite number of columns. The interleaver can then be implemented by diagonal writing for each subblock. For $N = 12$, $B = 4$, $M = 3$, we write the matrix

$$\left(\begin{array}{cccc|cccc} a_0 & a_{12} & a_{24} & a_{36} & a_{48} & a_{60} & a_{72} & \cdots \\ \cdot & a_1 & a_{13} & a_{25} & a_{37} & a_{49} & a_{61} & \cdots \\ \cdot & \cdot & a_2 & a_{14} & a_{26} & a_{38} & a_{50} & \cdots \\ \cdot & \cdot & \cdot & a_3 & a_{15} & a_{27} & a_{39} & \cdots \\ a_4 & a_{16} & a_{28} & a_{40} & a_{52} & a_{64} & a_{76} & \cdots \\ \cdot & a_5 & a_{17} & a_{29} & a_{41} & a_{53} & a_{65} & \cdots \\ \cdot & \cdot & a_6 & a_{18} & a_{30} & a_{42} & a_{54} & \cdots \\ \cdot & \cdot & \cdot & a_7 & a_{19} & a_{31} & a_{43} & \cdots \\ a_8 & a_{20} & a_{32} & a_{44} & a_{56} & a_{68} & a_{80} & \cdots \\ \cdot & a_9 & a_{21} & a_{33} & a_{45} & a_{57} & a_{69} & \cdots \\ \cdot & \cdot & a_{10} & a_{22} & a_{34} & a_{46} & a_{58} & \cdots \\ \cdot & \cdot & \cdot & a_{11} & a_{23} & a_{35} & a_{47} & \cdots \end{array}\right)$$

and then read it out column-wise. At the receiver, the deinterleaver has the same structure, but the write and read operations are interchanged. The matrix will be initialized with dummy symbols. Because of the diagonal writing, there will be some dummy symbols left at the beginning of the matrix. A real RAM is not a matrix with an infinite number of rows, but this is not necessary. At positions where the data are read out, new data can be written. It is easy to see that a matrix with B columns is sufficient. The RAM can then be addressed cyclically. All data in the right part of the matrix above can be written into the left part as the symbols there have already been read out.

4.4.3 The diversity spectrum of a wideband multicarrier channel

In this subsection, we address the question how much interleaving is necessary to have enough statistical independence for the channel code to work. We further present a method to analyze the correlations of a wideband channel with interleaving. In particular, we discuss the question how much bandwidth is needed to allow the channel code to exploit its diversity degree that is given by the Hamming distance d_H (or free distance d_{free}).

To start with a simple example, we first consider a transmission channel given by four frequencies f_1, f_2, f_3, f_4 that are sufficiently separated so that their Rayleigh fading amplitudes can be regarded as independent. We encode a bit stream by a repetition code of rate $R_c = 1/4$ with Hamming distance $d_H = 4$ and transmit each of the four bits in a code word on another frequency, where we may use, for example, BPSK modulation. Of course, this is nothing else but simple frequency diversity, but we regard it as RP(4, 1, 4) coding with frequency interleaving and multicarrier transmission. The pairwise error probability (PEP) that the code word (0000) is transmitted but the receiver decides for (1111), decreases asymptotically as

$$P_{\text{err}} \sim \left(\frac{E_b}{N_0}\right)^{-L} \tag{4.21}$$

with $L = d_H = 4$. We now consider the same transmission setup with the Walsh–Hadamard code of length 4, rate $R_c = 1/2$ and Hamming distance $d_H = 2$. The decay of the PEP for each error event is given by the power law of Equation (4.21) with $L = d_H = 2$. We may say that the channel has a diversity degree of four – because of the four independently fading subcarriers – and the two codes have diversity degrees (i.e. Hamming distance d_H) four and two, respectively. We are interested in the question whether a fading channel provides enough diversity so that the code can exploit its full diversity, that is, Equation (4.21) holds with $L = d_H$. It is obvious that the channel diversity must not be smaller than d_H. However, equality of both diversity degrees typically does not guarantee that the diversity of the code can be fully exploited, as it can easily be seen by the example of the WH(4, 2, 2) code whose code words are given by the rows of the matrix

$$\begin{pmatrix} 0 & 0 & 0 & 0 \\ 0 & 1 & 0 & 1 \\ 0 & 0 & 1 & 1 \\ 0 & 1 & 1 & 0 \end{pmatrix}.$$

If we use only the frequencies f_1, f_2 and transmit the bits numbers 1 and 3 on f_1 and the bits numbers 2 and 4 on f_2, we have different power laws for different error events. Let (0000) be the transmitted code word. The power law for probability that the receiver decides for (0101) is given by Equation (4.21) with $L = 1$, because the two bits in which the code words differ are transmitted on the same frequency. This is not the case for the other two error events corresponding to the code words (0011) and (0110) for which the power law with $L = 2$ holds.

An obviously sufficient condition for a (block) code to exploit its full diversity is to transmit each bit of a code word at another frequency, for example, if the diversity degree of the channel is at least the length of the code. The condition is not necessary. One can easily see that three frequencies would be sufficient for the WH(4, 2, 2) code. For a convolutional

code, a detailed analysis is more difficult because the number of possible error events is infinite and their length is growing to infinity. However, one should intuitively expect that the diversity degree of the code will be exploited if the diversity degree of the channel significantly exceeds the free distance d_{free}.

We add the following remarks:

- The two example codes we have chosen are quite weak so they will not be used in practice. Indeed, they have no coding gain in an AWGN channel because $d_H R_c = 1$ in either case.

- A transmission channel that splits up into a given number of K independently fading channels ($K = 4$ in the above example) is called a *block fading* channel. It is of practical relevance, for example, for frequency hopping systems, where K different frequencies are used subsequently during different time slots. The question, what number of K must be chosen to allow the code to exploit its diversity is of great practical relevance. For the simple convolutional code with memory 2, the most probable error event corresponds to the code word (111011000...). We conclude that we should hop at least between six different frequencies for that code.

Up to now, we have considered independently fading (sub) carrier frequencies. In practice, the fading of adjacent subcarriers in a multicarrier system is highly correlated. Take as an example an OFDM system with the (typical) ratio $T/\Delta = 4$ between the Fourier analysis window and the guard interval. Since Δ must be chosen to be larger than the maximum path delay, the delay spread τ_m should be significantly smaller than Δ. We take as an example $\tau_m = \Delta/5$, which is already quite a frequency-selective channel. We then have $T = 20\,\tau_m$. For this figure, the frequency correlation length (or coherency bandwidth) $f_{\text{corr}} = \tau_m^{-1}$ exceeds the frequency separation T^{-1} of the subcarriers by a factor of 20, which means that up to 20 neighboring subcarriers are highly correlated. The number of subcarriers in an OFDM system must therefore significantly exceed this number to guarantee some decorrelation that is necessary to exploit the frequency diversity in a channel coded and frequency-interleaved OFDM system. Only in that case we may legitimately call this a wideband system from the physical system point of view. A proper code design needs some information on the diversity that can be provided by the channel. In a real multicarrier system, there are always significant correlations. It is therefore desirable to find a quantity to characterize the diversity of a correlated fading channel.

In the following discussion, we will present a method to characterize the diversity of a wideband channel with correlated fading. We consider a set of channel samples

$$c_i = H(f_i, t_i),\ i = 1, \ldots, K$$

in the time-frequency plane. We assume a WSSUS Rayleigh process with average power $\mathrm{E}\left\{|c_i|^2\right\} = 1$. Thus, the channel samples c_i are zero mean complex Gaussian random variables that can be completely characterized by their autocorrelation properties. Writing the channel samples as a channel vector $\mathbf{c} = (c_1, \ldots, c_K)^T$, the autocorrelation matrix is

$$\mathbf{R} = \mathrm{E}\left\{\mathbf{c}\mathbf{c}^{\dagger}\right\}$$

with elements $R_{ik} = \mathrm{E}\left\{c_i c_k^*\right\}$ given by

$$R_{ik} = \mathcal{R}(f_i - f_k, t_i - t_k),$$

where $\mathcal{R}(f,t)$ is the two-dimensional autocorrelation function of the GWSSUS process $H(f,t)$. Since $\mathcal{R}(f,t) = \mathcal{R}^*(-f,-t)$, the matrix $\mathbf{R}$ is Hermitian. From matrix theory, we know that every Hermitian matrix can be transformed to a diagonal matrix: there exists a unitary matrix $\mathbf{U}$ (i.e. $\mathbf{U}^{-1} = \mathbf{U}^\dagger$) such that

$$\mathbf{U}\mathbf{R}\mathbf{U}^\dagger = \mathbf{D},$$

where $\mathbf{D} = \mathrm{diag}(\lambda_1, \ldots, \lambda_K)$ is the diagonal matrix of the eigenvalues of $\mathbf{R}$. We may write this as

$$\mathrm{E}\left\{\mathbf{U}\mathbf{c}(\mathbf{U}\mathbf{c})^\dagger\right\} = \mathbf{D}$$

and set

$$\mathbf{b} = \mathbf{U}\mathbf{c}.$$

This is a vector of mean zero Gaussian random variables with the diagonal autocorrelation matrix $\mathbf{D}$, that is, the coefficients of $\mathbf{b} = (b_1, \ldots, b_K)^T$ are uncorrelated

$$\mathrm{E}\left\{b_i b_k^*\right\} = \lambda_i \delta_{ik}$$

and, because they are Gaussian, even independent. We may regard this unitarily transformed channel vector as the *equivalent independently fading channel*. To explain this name, we consider as a simple example the multicarrier BPSK modulation with a K-fold repetition code, that is, the same BPSK symbol $s \in \left\{\pm\sqrt{E_S}\right\}$ will be transmitted at K different positions in the time-frequency plane. This is again simple frequency diversity combined with time diversity, but with correlated fading amplitudes. We recall from subsection 2.4.6 that the conditional PEP is given by

$$P(s \mapsto \tilde{s}|\mathbf{c}) = \frac{1}{2}\mathrm{erfc}\left(\sqrt{\frac{E_S}{N_0}\sum_{i=1}^{K}|c_i|^2}\right).$$

Because the matrix $\mathbf{U}$ is unitary, it leaves the vector norm invariant, that is,

$$\|\mathbf{b}\|^2 = \|\mathbf{U}\mathbf{c}\|^2 = \|\mathbf{c}\|^2$$

or

$$\sum_{i=1}^{K}|b_i|^2 = \sum_{i=1}^{K}|c_i|^2.$$

This means that the transfer power of the equivalent channel is the same. $P(s \mapsto \tilde{s}|\mathbf{c})$ can then be expressed as

$$P(s \mapsto \tilde{s}|\mathbf{c}) = P(s \mapsto \tilde{s}|\mathbf{U}^{-1}\mathbf{b}) = \frac{1}{2}\mathrm{erfc}\left(\sqrt{\frac{E_S}{N_0}\sum_{i=1}^{K}|b_i|^2}\right).$$

Since the transformed fading amplitudes b_i are independent, we can apply the same method as in Subsection 2.4.6 to perform the average for

$$P(s \mapsto \tilde{s}) = \mathrm{E}\left\{P(s \mapsto \tilde{s}|\mathbf{U}^{-1}\mathbf{b})\right\}$$

and eventually obtain the expression

$$P(s \mapsto \tilde{s}) = \frac{1}{\pi} \int_0^{\pi/2} \prod_{i=1}^{L} \frac{1}{1 + \frac{\lambda_i}{\sin^2 \theta} \frac{E_S}{N_0}} \, \mathrm{d}\theta.$$

Using $E_b = K E_S$, we obtain the tight Chernoff-like bound

$$P(s \mapsto \tilde{s}) \leq \frac{1}{2} \prod_{i=1}^{K} \frac{1}{1 + \frac{\lambda_i}{K} \frac{E_b}{N_0}}. \tag{4.22}$$

For independent fading, we have $\lambda_i = 1$ for all values of i and we obtain the power law of Equation (4.21) with $L = K$. For correlated fading they are different, but because of

$$\mathrm{E}\left\{ \sum_{i=1}^{K} |b_i|^2 \right\} = \mathrm{E}\left\{ \sum_{i=1}^{K} |c_i|^2 \right\},$$

their sum

$$\sum_{i=1}^{K} \lambda_i = K$$

is always the same. Even though – in case that $\lambda_i \neq 0$ for all i – Equation (4.22) will asymptotically approach the power law of Equation (4.21) with $L = K$ for large E_b/N_0, many of the eigenvalues may be very small so that they will not contribute significantly to the product for relevant values of E_b/N_0. Only those eigenvalues λ_i of significant size contribute, but there is no natural threshold. The diversity that can be achieved by the channel is thus characterized by the whole eigenvalue spectrum $\{\lambda_i\}_{i=1}^{K}$ of the autocorrelation matrix of the fading. We thus call it the *diversity branch spectrum* of the channel.

For the following numerical example, we restrict ourselves to the frequency direction and assume an exponential delay power spectrum

$$S_D(\tau) = \frac{1}{\tau_m} \mathrm{e}^{-\tau/\tau_m} \epsilon(\tau),$$

where τ_m is the mean delay and $\epsilon(\tau)$ is the Heaviside function. The corresponding frequency autocorrelation function is given by

$$\mathcal{R}_f(f) = \frac{1}{1 + j2\pi f \tau_m}.$$

Figure 4.42 shows the first 16 eigenvalues for $K = 64$ and different values of the bandwidth B. We define a *normalized* bandwidth $X = B\tau_m$. We have assumed that the BPSK symbols are equally frequency spaced over the bandwidth. We see that for a small bandwidth (e.g. $X = 1$ corresponding to 1 MHz for $\tau = 1$ µs), the equivalent independent fading channel has only a low number of diversity branches of significant power. We found that the *diversity branch spectrum* as shown in Figure 4.42 is nearly independent of K if K is significantly greater than X. It is therefore a very useful quantity to characterize the diversity that can be provided by the channel. A look at the eigenvalues gives a first glimpse at how many diversity branches of the equivalent independent fading channel contribute

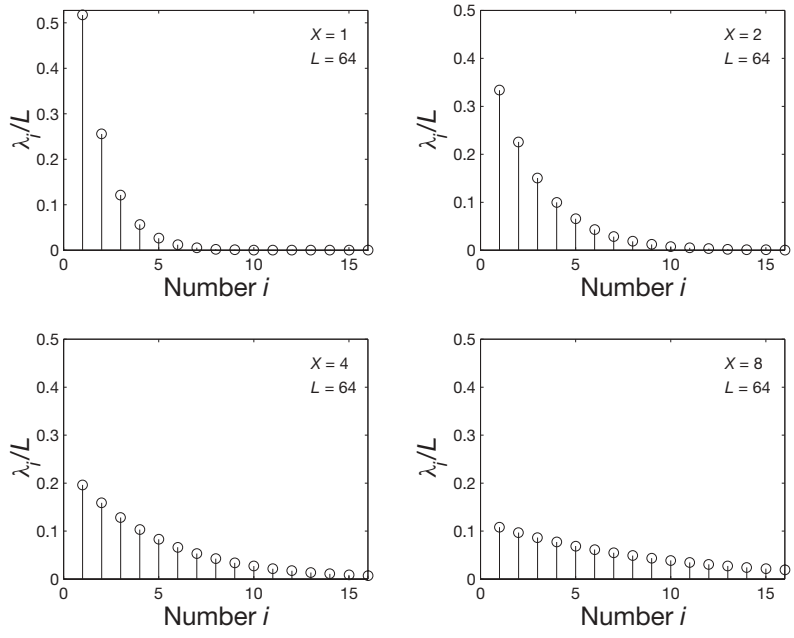

Figure 4.42 Diversity branches of the equivalent independent fading channel and normalized bandwidth $X = B\tau_m = 1, 2, 4, 8$.

significantly to the transmission. It finds its reflection in the performance curves. Figure 4.43 shows the pairwise (=bit) error probability for $K = 32$ and $X = B\tau_m = 0.5, 1, 2, 4, 8, 16$. The high diversity degree of the repetition code ($K = 32$) can show a high diversity gain if the equivalent channel has enough independent diversity branches of significant power. This is the case for $X = 16$, but not for $X = 1$ or $X = 2$. For low X, a lower repetition rate K would have been sufficient.

Figure 4.44 shows the bit error probability for $K = 10$ and the same values of X. For low X, the curves of Figure 4.43 and 4.44 are nearly identical. For higher X, the curves of Figure 4.44 run into a saturation that is given by the performance curve of the independent Rayleigh fading. For $X = 8$, this limit is practically achieved. There is still a gap of nearly 2 dB in the AWGN limit at the bit error rate of 10^{-4}.

For BPSK and any linear code, the probability for an error event corresponding to a Hamming distance d is given by

$$P_d = \frac{1}{\pi} \int_0^{\pi/2} \prod_{i=1}^{d} \frac{1}{1 + \frac{\lambda_i}{\sin^2\theta} \frac{E_S}{N_0}} \, \mathrm{d}\theta, \tag{4.23}$$

which can be upper bounded by

$$P_d \leq \frac{1}{2} \prod_{i=1}^{d} \frac{1}{1 + \lambda_i \frac{E_S}{N_0}}.$$

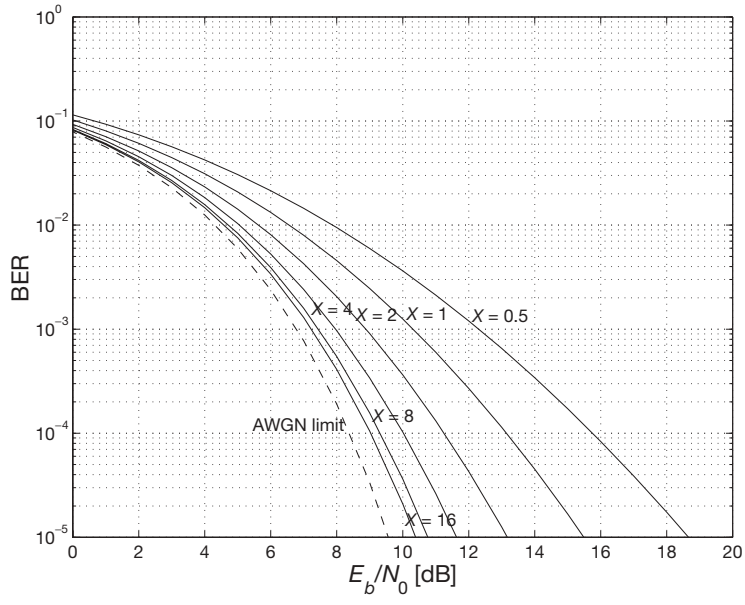

Figure 4.43 Bit error probabilities for 32-fold repetition diversity with $X = 0.5$, 1, 2, 4, 8, 16.

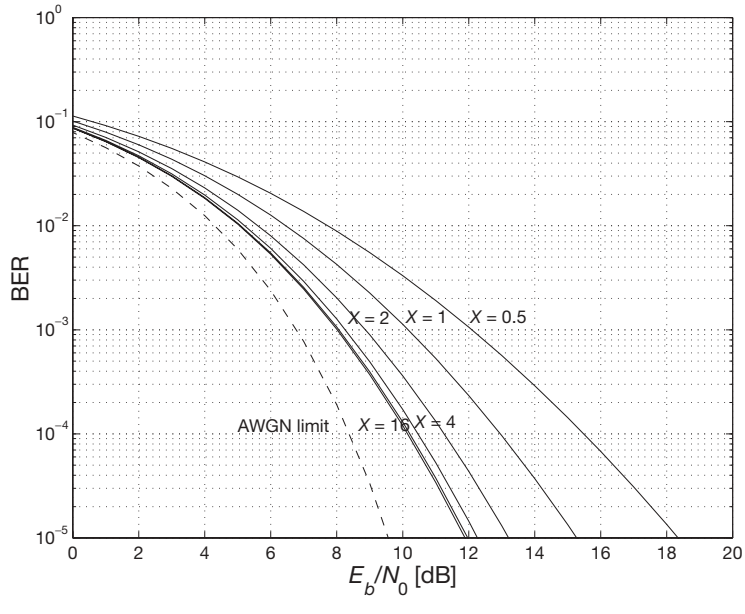

Figure 4.44 Bit error probabilities for 10-fold repetition diversity with $X = 0.5$, 1, 2, 4, 8, 16.

For the region of reasonable E_S/N_0, those factors with $\lambda_i \ll 1$ do not contribute significantly to the product. Thus, it is not possible to obtain tight union bounds like

$$P_d \leq \sum_{d=d_{\text{free}}}^{\infty} c_d P_d$$

because P_d does not decrease as $(E_S/N_0)^{-d}$ if d is greater than the diversity degree of the channel, that is, the number of significant eigenvalues λ_i. The c_d values grow with d and thus the union bound will typically diverge.

However, the diversity branch spectrum may serve as a good indicator of whether the time-frequency interleaving for a coded OFDM system is sufficient. Consider for example a system with a convolutional code[9] with free distance $d_{\text{free}} = 10$ like the popular NASA code $(133,\ 171)_{\text{oct}}$. The probability for the most likely error event is given by Equation (4.23) with $d = d_{\text{free}} = 10$. This probability will decrease as $(E_S/N_0)^{-10}$ only if the 10 eigenvalues λ_i, $i = 1, \ldots, 10$ are of significant size. Let us consider an OFDM system with a pseudorandom time-frequency interleaver over the time T_{frame} of one frame and over a bandwidth B. We consider a GWSSUS model scattering function given by

$$S(\tau, \nu) = S_{\text{Delay}}(\tau) S_{\text{Doppler}}(\nu)$$

as a product of a delay power spectrum $S_{\text{Delay}}(\tau)$ and a Doppler spectrum $S_{\text{Doppler}}(\nu)$. As a consequence, the time-frequency autocorrelation function also factorizes into

$$\mathcal{R}(f, t) = \mathcal{R}_f(f)\mathcal{R}_t(t).$$

We assume an exponential power delay spectrum with delay time constant τ_m that has a frequency autocorrelation function

$$\mathcal{R}_f(f) = \frac{1}{1 + j2\pi f \tau_m}$$

and an isotropic Doppler spectrum (Jakes spectrum) with a maximum Doppler frequency $\nu_{\max}$ that has a time autocorrelation function given by

$$\mathcal{R}_t(t) = \mathrm{J}_0\left(2\pi \nu_{\max} t\right).$$

The correlation lengths in frequency and time are given by $f_{\text{corr}} = \tau_m^{-1}$ and $t_{\text{corr}} = \nu_{\max}^{-1}$, respectively.

The $d_{\text{free}} = 10$ time-frequency positions (t_i, f_i) of the BPSK symbols corresponding to the most likely error event are spread randomly over the time T_{frame} and the bandwidth B. Thus, the diversity branch spectrum is a random vector. To eliminate this randomness, we average over an ensemble of 100 such vectors, which turns out to be enough for a stable result. To justify this procedure, we recall that error probabilities are averaged quantities.

Figure 4.45 shows the diversity branch spectrum $\{\lambda_i\}_{i=1}^{10}$ for frequency interleaving only (i.e. $T_{\text{frame}}/t_{\text{corr}} = 0$) and values $B/f_{\text{corr}} = 1, 2, 4, 8, 16, 32$ for the normalized bandwidth. It can be seen that even for $B/f_{\text{corr}} = 32$, the full diversity is not reached because the size

[9] Similar considerations apply for linear block codes.

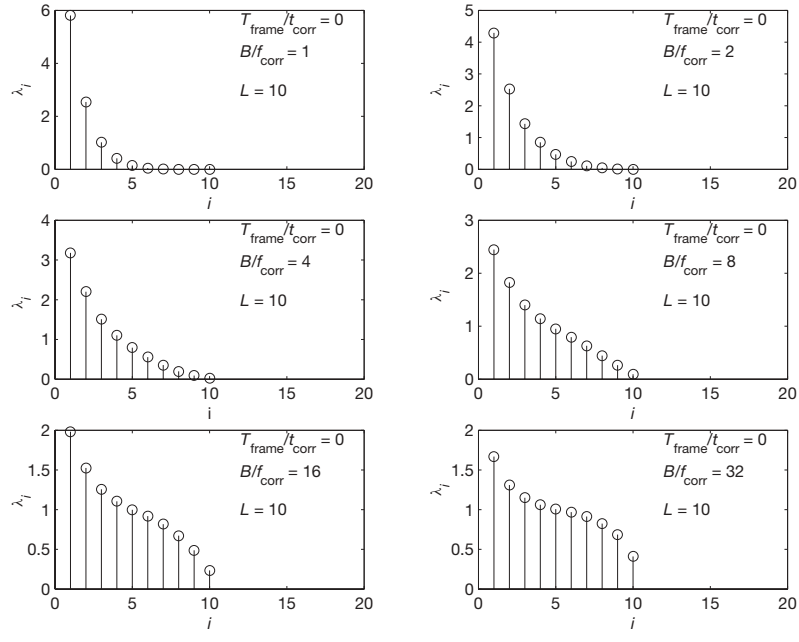

Figure 4.45 Diversity branch spectrum for $d = 10$ and frequency interleaving only.

of normalized eigenvalues is very different and the greatest values dominate the product. As shown in Figure 4.46, the same is true if only time interleaving is applied. The figure shows the spectra for time interleaving over a normalized length of $T_{\text{frame}}/t_{\text{corr}} = 1, 2, 4, 8, 16, 32$. Note that, due to the different autocorrelation in time and frequency domain, both diversity branch spectra show a different shape. Figure 4.47 shows the diversity branch spectrum for combined frequency-time interleaving. It can be seen that both mechanisms help each other, and for a wideband system with long time interleaving, all eigenvalues contribute to the product. However, the interleaving can be considered to be ideal only if all eigenvalues are of nearly the same size. As shown in Figure 4.48, a huge time-frequency interleaver is necessary to achieve this.

We may say that an OFDM system is a *wideband system* if the system bandwidth B is large enough compared to f_{corr} so that the frequency interleaver works properly. For a well-designed OFDM system, the guard interval length Δ must be matched to the maximum echo length. Assume, for example, a channel with $\tau_m = \Delta/5$ and a guard interval of length $\Delta = T/4$. Using $B = K/T$, where K is the number of carriers and T is the Fourier analysis window length, we obtain the relation

$$K = 20B\tau_m.$$

With a look at the figures we may speak of a wideband system, for example, for $B/f_{\text{corr}} = B\tau_m = 32$, which leads to $K = 640$. There may of course occur flat fading channels with $\tau_m \ll \Delta$, where the frequency interleaving fails to work. But we may conclude that an OFDM system may be called a *wideband* system relative to the channel parameters only

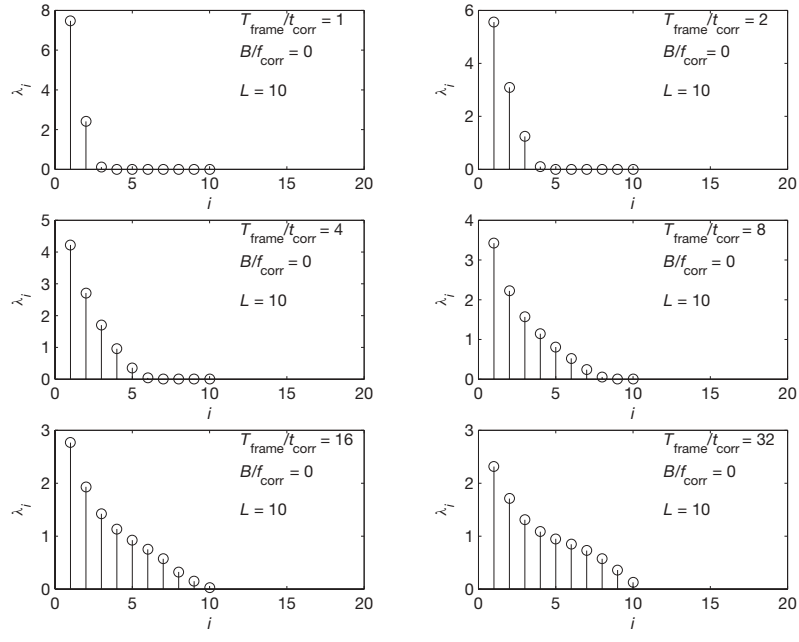

Figure 4.46 Diversity branch spectrum for $d = 10$ and time interleaving only.

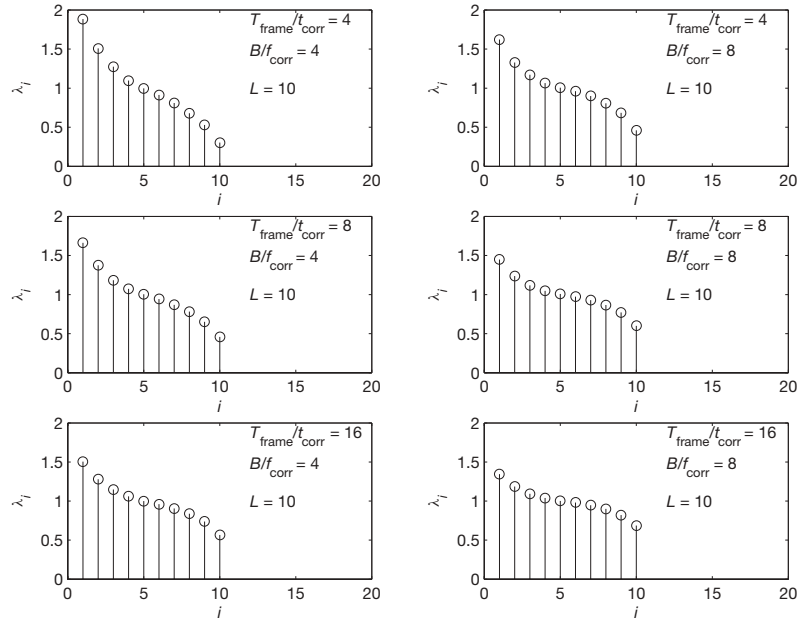

Figure 4.47 Diversity branch spectrum for $d = 10$ for moderate time-frequency interleaving.

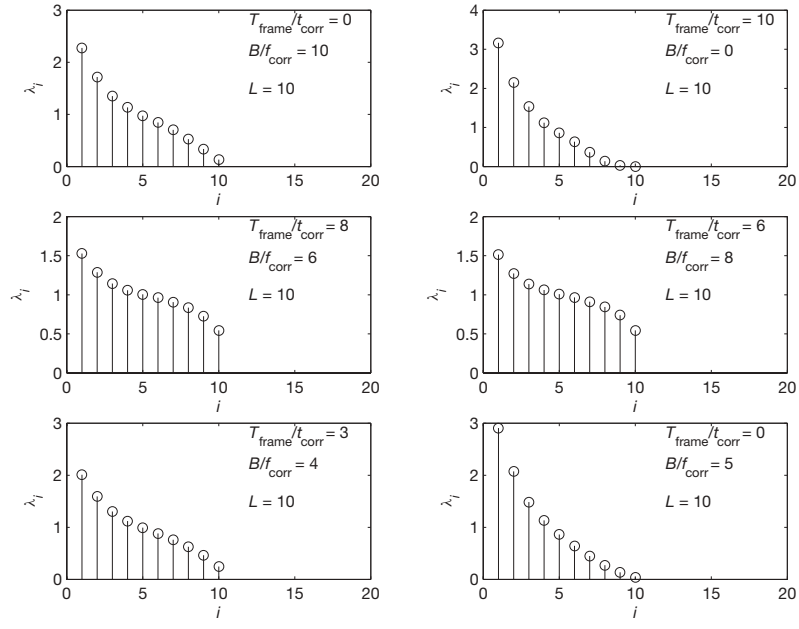

Figure 4.48 Diversity branch spectrum for $d = 10$ and small and huge time-frequency interleavers.

if at least several hundred subcarriers are used. This is the case for the digital audio and video broadcasting systems DAB and DVB-T. It is not the case for the WLAN systems IEEE 802.11a and HIPERLAN/2 with only 48 carriers.

Time interleaving alone is often not able to provide the system with sufficient diversity. A certain vehicle speed can, typically, not be guaranteed in practice. For the DAB system working at 225 MHz, a vehicle speed of 48 km/h leads to a Doppler frequency that is as low as 10 Hz. For such a Doppler frequency, sufficient time interleaving alone would lead to a delay of several seconds, which is not tolerable in practice. It is an attractive feature of OFDM that the time and frequency mechanisms together may often lead to a good interleaving. However, there will always be situations where the correlations of the channel must be taken into account.

4.5 Modulation and Channel Coding for OFDM Systems

4.5.1 OFDM systems with convolutional coding and QPSK

In this subsection, we present theoretical performance curves for OFDM systems with QPSK modulation, both with differential and coherent demodulation. These curves are of great relevance for the performance analysis of existing practical systems. Fortunately, most practical OFDM systems use essentially the same convolutional code, at least for the inner code. And most of these systems use QPSK modulation, at least as one of several possible

options. DAB always uses differential QPSK, and DVB-T as well as the WLAN systems (IEEE 802.11a and HIPERLAN/2) use QAM, where QPSK is a special case. These WLAN systems also have the option to use BPSK. The performance curves for coherent BPSK are the same as those for QPSK when plotted as a function of E_b/N_0. When plotted as a function of *SNR*, there is a gap of 3.01 dB between the BPSK and the QPSK curves. The performance of higher-level QAM will be discussed in a subsequent subsection.

The channel coding of all the above-mentioned systems is based on the so-called NASA planetary standard, the rate 1/2, memory 6 convolutional code with generator polynomials $(133,\ 171)_{\text{oct}}$, that is,

$$\mathbf{g}(D) = \begin{pmatrix} 1 + D^2 + D^3 + D^5 + D^6 \\ 1 + D + D^2 + D^3 + D^6 \end{pmatrix}.$$

This code can be punctured to get higher code rates. For the DAB system, lower code rates are needed, for example, to protect the most sensitive bits in the audio frame, and two additional generator polynomials are introduced. The generator polynomials of this code $R_c = 1/4$ are given by $(133,\ 171,\ 145,\ 133)_{\text{oct}}$, that is,

$$\mathbf{g}(D) = \begin{pmatrix} 1 + D^2 + D^3 + D^5 + D^6 \\ 1 + D + D^2 + D^3 + D^6 \\ 1 + D + D^4 + D^6 \\ 1 + D^2 + D^3 + D^5 + D^6 \end{pmatrix}.$$

This encoder is depicted in Figure 4.49. The shift register is drawn twice to make it easier to survey the picture. For DVB-T and the wireless LAN systems, only the part of the code corresponding to the upper shift register is used.

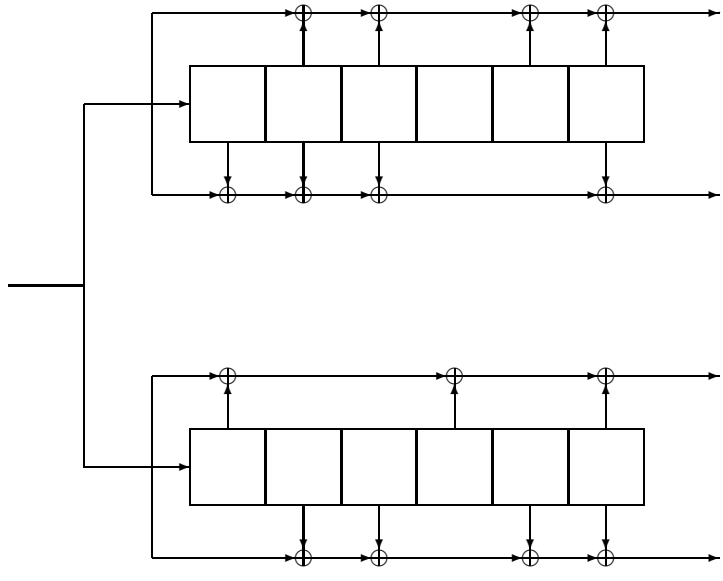

Figure 4.49 The DAB convolutional encoder.

The bit error rates for a convolutional code can be upper bounded by the union bound

$$P_d \leq \sum_{d=d_{\text{free}}}^{\infty} c_d P_d. \tag{4.24}$$

Here, P_d is the PEP for d-fold diversity as given by the expressions in Subsection 2.4.6. The coefficient c_d is the error coefficient corresponding to all the error events with Hamming distance d. We note that c_d depends only on the code, while P_d depends only on the modulation scheme and the channel. The union bound given in Equation (4.24) is valid for any channel. For an AWGN channel, the error event probability is simply given by

$$P_d = \frac{1}{2}\text{erfc}\left(\sqrt{d\frac{E_S}{N_0}}\right),$$

where $E_S = |s|^2$ is the energy of the PSK symbol s. For the independently fading Rayleigh channel, the expressions for the error event probabilities P_d were discussed in Subsection 2.4.6. All the curves asymptotically decay as

$$P_d \sim \left(\frac{E_S}{N_0}\right)^{-d}.$$

The union bound is also valid for the correlated fading channel, but it does not tightly bound the bit error rate. It may even diverge. This is because the degree of the channel diversity is limited and the pairwise error probabilities for diversity run into a saturation for $d \to \infty$, while the coefficients c_d grow monotonically.

The c_d values can be obtained by the analysis of the state diagram of the code. In Hagenauer's paper about RCPC (rate compatible punctured convolutional) codes (Hagenauer 1988), these values have been tabulated for punctured codes of rate $R_c = 8/N$ with $N \in \{9, 10, 11, \ldots, 24\}$. These punctured codes have been implemented in the DAB system. In the other systems, some different code rates are used. However, their performance can be estimated from the closest code rates of that paper. We now discuss the performance of these codes for (D)QPSK in a Rayleigh fading channel.

First we consider DQPSK and an ideally interleaved Rayleigh fading channel with the isotropic Doppler spectrum of maximum Doppler frequency $\nu_{\max}$. The P_d values depend on the product $\nu_{\max} T_S$. High values of this product cause a loss of coherency between adjacent symbols, which degrades the performance of differential modulation. We first consider the ideal case $\nu_{\max} T_S = 0$. In practice, this is of course a contradiction to the assumption of ideal interleaving. But we may think of a very huge (time and frequency) interleaver and the limit of very low vehicle speed. Figure 4.50 shows the union bounds of the performance curves in that case for several code rates. We have plotted the bit error probabilities as a function of the *SNR*, not as a function of E_b/N_0. The latter is better suited to compare the power efficiencies, but for practical planning aspects the *SNR* is the relevant physical quantity. Both are related by

$$SNR = \frac{T}{T_S} R_c \log_2(M) \frac{E_b}{N_0}$$

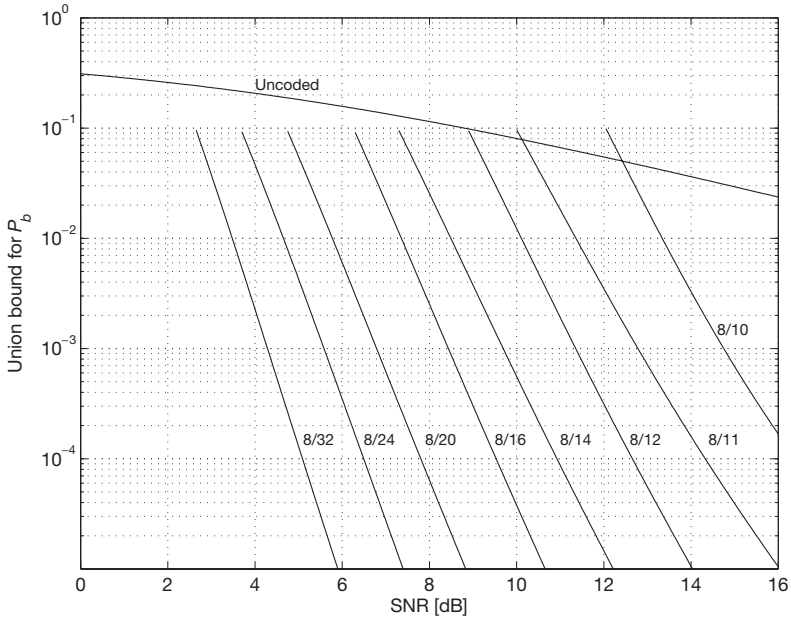

Figure 4.50 Union Bounds for the bit error probability for DQPSK and $\nu_{\max} T_S = 0$ for $R_c = 8/10,\ 8/11,\ 8/12,\ 8/14,\ 8/16,\ 8/20,\ 8/24,\ 8/32$.

with $M = 4$ for (D)QPSK. Another reason to plot the different performance curves together as a function of the SNR is that different parts of the data stream may be protected by different code rates as it is the case for the DAB system discussed in Subsection 4.6.1. Here, all parts of the signal are affected by the same SNR. For example, the curves of Figure 4.50 are the basis for the design of the unequal error protection (UEP) scheme of the DAB audio frame, where the most important header bits are better protected than the audio scale factors that are better protected than the audio samples. For more details, see (Hoeg and Lauterbach 2003; Hoeher *et al.* 1991). The curves show that there is a high degree of flexibility to choose the appropriate error protection level for different applications. Note that there are still intermediate code rates in between that have been omitted in order not to overload the picture. Figure 4.51 shows the union bounds for the performance curves for the same codes, but with a higher Doppler frequency corresponding to $\nu_{\max} T_S = 0.02$. For the DAB system (Transmission Mode I) with $T_S \approx 1250$ µs working at 225 MHz, this corresponds to a moderate vehicle speed of approximately 80 km/h. One can see that the curves become less steep, and *flatten out*. This effect is greater for the weak codes, and it is nearly neglectible for the strong codes. In any case, this degradation is still small. Figure 4.52 shows the union bounds for the performance curves for the same codes, but with a higher Doppler frequency corresponding to $\nu_{\max} T_S = 0.05$. For the DAB system (Transmission Mode I) with $T_S \approx 1250$ µs working at 225 MHz, this corresponds to a high vehicle speed of approximately 190 km/h. The curves flatten out significantly; the loss is approximately 1.5 dB at $P_b = 10^{-4}$ for $R_c = 8/16$, and it is more than 3 dB for $R_c = 8/12$.

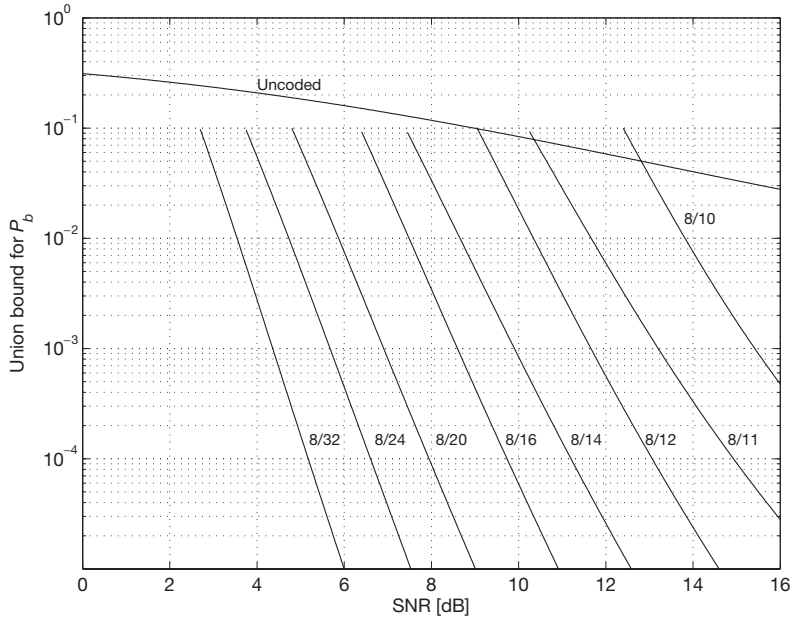

Figure 4.51 Union Bounds for the bit error probability for DQPSK and $\nu_{\max} T_S = 0.02$ for $R_c = 8/10,\ 8/11,\ 8/12,\ 8/14,\ 8/16,\ 8/20,\ 8/24,\ 8/32$.

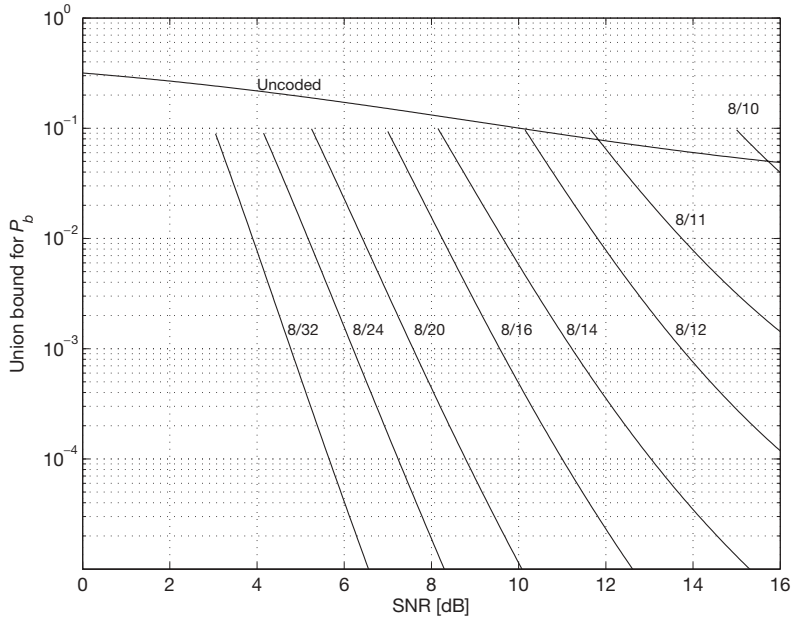

Figure 4.52 Union Bounds for the bit error probability for DQPSK and $\nu_{\max} T_S = 0.05$ for $R_c = 8/10,\ 8/11,\ 8/12,\ 8/14,\ 8/16,\ 8/20,\ 8/24,\ 8/32$.

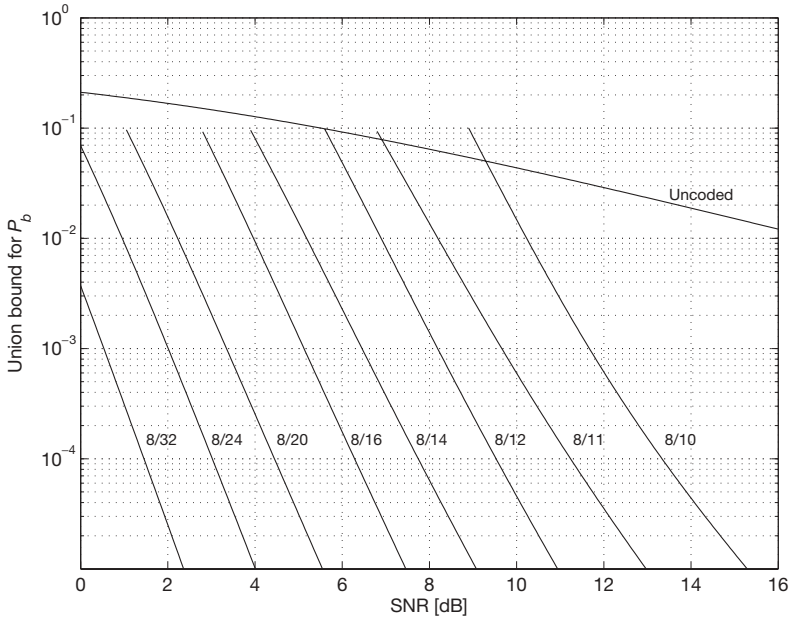

Figure 4.53 Union Bounds for the bit error probability for QPSK and $R_c = 8/10$, 8/11, 8/12, 8/14, 8/16, 8/20, 8/24, 8/32.

As long as the interleaving is sufficient, all these curves fit quite well to computer simulations. We will show some DQPSK performance curves for simulations of the DAB system in a subsequent section. One must keep in mind that high Doppler frequencies also effect the orthogonality of the subcarriers, which will cause additional degradations. However, this effect turns out to be significantly smaller than the DQPSK coherency loss for each single subcarrier.

Figure 4.53 shows the union bounds of the performance curves for QPSK and the same code rates. QPSK is not affected directly by the Doppler spread. However, the loss of orthogonality will also degrade QPSK. In practice, the most significant loss due to high Doppler frequencies turns out to be due to degradations in the channel estimation. In fact, it was generally believed for many years that for this reason, in practice, coherent QPSK is not really superior to differential QPSK, because this channel estimation loss approximately compensates the gain. In a subsequent section, we will discuss this item and we will show that this is not true.

4.5.2 OFDM systems with convolutional coding and M^2-QAM

In this subsection, we analyze the performance of OFDM systems with M^2-QAM modulation, as it is used for DVB-T as well as the WLAN systems IEEE 802.11a and HIPERLAN/2. The channel coding of these systems is based on the same coding scheme as discussed in the preceding subsection.